UNIVERSITÄT DER BUNDESWEHR MÜNCHEN
Fakultät für Elektrotechnik und Informationstechnik

Performance and reliability of micropump based liquid dosing systems

Christoph Werner Jenke

Vollständiger Abdruck der von der Fakultät für Elektrotechnik und Informationstechnik der Universität der Bundeswehr München zur Erlangung des akademischen Grades eines

Doktor-Ingenieurs

genehmigten Dissertation.

Gutachter/Gutachterin:
1. Prof. Dr. rer. nat. Christoph Kutter
2. Prof. Dr.-Ing. Roland Zengerle
3. Prof. Dr. rer. nat. Georg Düsberg

Die Dissertation wurde am 08.05.2018 bei der Universität der Bundeswehr München eingereicht und durch die Fakultät für Elektrotechnik und Informationstechnik am 13.06.2018 angenommen. Die mündliche Prüfung fand am 23.11.2018 statt.

Abstract

Micropump based liquid dosing systems have the potential to enable many application scenarios. For example, their small size can realize implants and the ability to accurately dose small volume enables drug delivery as well as analytical devices. Their low energy demands can lead to stand-alone dosing systems. However, the wide range of use cases demands for quite different sets of performance and reliability requirements that are often challenging to meet. Due to an evolving pump design, existing dynamic models, like for the actuator motion or the flow rate determination, became more and more inaccurate and little is understood about flow stability and failure mechanisms. The goal of this work is to facilitate the efficient and accurate design of micropump systems by providing models, methods and standard procedures for performance and reliability.

The performance behavior of micropump systems was investigated, as it is the key to an accurate design and constitutes the foundations to estimate the reliability characteristics. Therefore, the effect of system parameters and driving signal on the flow rate, liquid pressure ability, gas pressure ability for bubble tolerance as well as self-priming ability, energetic conversion efficiency, size and costs was evaluated. Analytical and numerical models were developed to simulate and optimize the static and dynamic behavior of actuator, valves and the whole micropump, embedded in a system environment. It was found that limitations of the flow rate mainly originate from viscous squeeze film damping, cavitation and valve efficiency. The design is restricted by prevailing stresses in the actuator diaphragm and its manufacturing method, available piezo ceramic properties, the valve sealing lip, the pump chamber height and pressure smoothing characteristics of the fluidic path.

Reliability describes the ability to keep performance values within accuracy limits over a lifetime within a failure probability. The core task of a dosing system can be reduced to providing a flow rate over a time period. Both, inherent influences, like cavitation, actuator fatigue and valve sticking, as well as external influences, such as temperature, pressure and particle laden flow, affect the flow stability and were investigated. The required conditions and impact of each effect were identified and are described together with critical failure mechanisms. To avoid or reduce the impact of these influences, guidelines are given to adjust the architecture, pump design, manufacturing methods as well as operating conditions. The results show that cavitation, valve sticking as well as temperature and pressure variations are most critical for the short term flow stability, but are fully reversible effects. In contrast, actuator fatigue and particle laden flow usually alter the flow rate performance of the system irreversibly.

A procedure to define the system architecture is proposed that starts with selecting the required functional components and is followed by their individual design, the specification of operating strategies and the implementation of system integration. Within this framework, matching solutions can be achieved with open-loop and closed-loop flow control. Based on the analysis of competing design directions, a process was developed to balance different goals for open-loop flow control. If no match can be found, but performance requirements alone can be met, closed-loop flow control can be implemented with direct or indirect flow sensing. Flow control modes, sensing technologies and suitable system setups were investigated to combine micropumps and flow sensors. Thermal calorimeter and differential pressure based flow sensors showed acceptable accuracy in measuring the highly pulsatile micropump flow in single stroke mode.

To conclude, this work is able to expand the potential field of applications by providing insights, models and procedures for an accurate application specific design of micropump based liquid dosing systems.

Zusammenfassung

Mikropumpen basierte Flüssigkeits-Dosiersysteme haben das Potential viele Anwendungen zu ermöglichen. Durch ihre geringe Größe können beispielsweise Implantate realisiert werden. Ihre Fähigkeit geringe Flüssigkeitsmengen genau zu dosieren ermöglicht neue Analysegeräte oder Systeme für die Medikamentenverabreichung. Durch die relativ geringe Leistungsaufnahme sind energieautarken Dosiersysteme umsetzbar. Allerdings führt das breite Anwendungsspektrum auch zu stark unterschiedlichen und teilweise schwer erreichbaren Anforderungen an Leistung und Zuverlässigkeit. Existierende dynamische Modelle, etwa für die Aktorbewegung oder Flussratenbestimmung, wurden durch die stetige Weiterentwicklung der Mikropumpen zunehmend ungeeignet. Außerdem ist bisher wenig über die Flussstabilität und Fehlereffekte entsprechender Systeme bekannt. Ziel dieser Arbeit ist es eine effiziente und genaue Auslegung von Mikropumpsystemen durch die Entwicklung von Modellen und Methoden zu ermöglichen, die das ganzheitliche System mit Leistungs- und Zuverlässigkeitsmerkmalen berücksichtigt.

Das Verständnis des Leistungsverhaltens von Mikropumpsystemen ist der Schlüssel zu einer genauen Auslegung und liefert außerdem die Grundlage zur Abschätzung des Zuverlässigkeitsverhaltens. Deswegen wurden der Einfluss der Systemparameter und des Ansteuersignals auf die Flussrate, Flüssigkeits-Druckfähigkeit, Gasdruckfähigkeit für Blasentoleranz und Selbstansaugfähigkeit, Wirkungsgrad, Größe und Kosten untersucht. Analytische und numerische Modelle wurden entwickelt um das statische und dynamische Verhalten des Aktors, der Ventile, sowie des gesamten Mikropumpensystems beschreiben und optimieren zu können. Es wurde herausgefunden, dass die Flussrate hauptsächlich durch viskose Dämpfung, Kavitation und Ventileffizienz begrenzt wird. Die Auslegungsmöglichkeiten werden durch die design- und herstellbedingte mechanische Stabilität der Aktormembran, die Materialeigenschaften der Piezokeramiken, die Ventildichtlippen, die Pumpkammerhöhe, sowie die Dämpfungseigenschaften des fluidischen Pfades begrenzt.

Die Zuverlässigkeit beschreibt die Fähigkeit eines Systems Leistungskennwerte über eine Lebensdauer und innerhalb einer Ausfallwahrscheinlichkeit im Rahmen der Genauigkeitsgrenzen zu halten. Die Kernaufgabe jedes Dosiersystems kann darauf reduziert werden, eine Flussrate über einen bestimmen Zeitraum zur Verfügung zu stellen. Sowohl inhärente Einflüsse, wie Kavitation, Aktorermüdung oder Ventilsticking, als auch externe Einflüsse, wie Temperatur, Druck oder Partikel, haben einen Einfluss auf die Flussgenauigkeit und wurden daher untersucht. Zu den jeweiligen Effekten wurden die erforderlichen Bedingungen, die quantitative Auswirkung und die daraus resultierenden kritischen Fehlermechanismen identifiziert und beschrieben. Um die Einflüsse zu minimieren oder gar ganz zu verhindern werden Richtlinien bezüglich Systemarchitektur, Pumpenauslegung, Herstellprozessen und Betriebsbedingungen vorgeschlagen. Die Ergebnisse zeigen, dass Kavitation und Ventilsticking, aber auch Temperatur- und Druckschwankungen die kurzfristige Flussstabilität am meisten beeinträchtigen, jedoch voll reversibel sind. Im Gegensatz dazu verändern Aktorermüdung und Partikel-beladene Flüssigkeiten die Flussrate meist nachhaltig und irreversibel.

Die vorgeschlagene Herangehensweise zur Festlegung der Systemarchitektur berücksichtigt die Auswahl der relevanten funktionalen Komponenten, deren individuelle Auslegung, die Spezifikation der Betriebsstrategien und die Umsetzung der Systemintegration. Innerhalb dieses Konzeptes wird näher auf die beiden Lösungsansätze eines gesteuerten bzw. eines geregelten Systems eingegangen. Ausgehend von einer Analyse der teils konkurrierenden Auslegungsrichtungen wurde ein Prozess entwickelt, um verschiedene

Zielkennwerte miteinander abzustimmen und so gesteuerte Systeme zu ermöglichen. Falls dieser Prozess zu keinem Ergebnis führt, jedoch die Leistungswerte erreichbar sind, können geregelte Systeme mit Hilfe direkter oder indirekter Flussmessung umgesetzt werden. Verschiedene Flussregelmodi, mögliche Flussmesstechnologien und geeignete Systemkonzepte wurden dafür untersucht. Hierbei wiesen differenzdrucksensorbasierte und thermische Flusssensoren akzeptable Messgenauigkeiten beim Umgang mit hoch pulsatilem Mikropumpenfluss im Einzelhubmodus auf.
Insgesamt liefert diese Arbeit die Grundlagen für eine zielgerichtete und genaue Auslegung von Mikropumpsystemen in Form von Erkenntnissen, Modellen und Vorgehensweisen und ist damit in der Lage neue mögliche Anwendungsfelder zu erschließen.

Contents

1 Introduction

Micro dosing systems dispense liquids and gases in the range of micro liter to milliliter within minutes, feature a compact system size smaller than a few cubic centimeter or contain components with functional dimensions in the micron range [1, 2]. This definition contains a broad spectrum of systems, which can focus on different aspects of micron dimensions in dosing systems.

Liquid micro dosing applications

The potential fields of applications are vast (examples in Figure 1.1). From the number of reported applications, the most relevant field is in the health sector, from research and analytical devices to drug delivery (Figure 1.1) [3], but many others, like cooling and fuel cells, were reported [2]. Micropumping is required in most parts of microfluidics and is an enabler for many applications. Currently, the by far biggest market of microfluidics is pharmaceutical and life science research, followed by clinical and veterinary diagnostics, analytical devices, point-of-care diagnostics and drug delivery [4]. Industrial, environmental and micro reaction technology are yet minor markets. However, after more than 30 years of micropump research, only few of the potential innovations were realized in products. One of the main reasons is because of the challenging requirements of performance and reliability and the difficulty to meet all of them in the still maturing multidisciplinary field of liquid micro dosing systems.

In micropump based liquid dosing systems usually a stream is produced, in order to move liquid from one point to another. Depending on the application, different kinds of liquids have to be pumped: water, drugs, analytical chemicals, disinfectants, lubricants, nutrient solutions, fuels, paints or solvents. This includes high variations in liquid properties. Besides the direct effect of liquids like drugs or solvents, moving a liquid can generate several useful effects: cooling, heating, pressure regulation, wetting, irrigation, cleaning, air humidity, air scent or coloring. The variety of possibilities allows to address many potential needs in a multitude of industry sectors (Figure 1.1).

In the medical field, the advantage of compact systems can be used for portable drug delivery systems or implants. In the case of portable systems, insulin delivery for diabetes therapy is one of the most famous applications [5, 6, 7, 2]. Furthermore, a portable systems enables continuous and locally highly concentrated dosing of cytostatic agents for tumor therapy [8]. Examples for implants are painkiller dosing systems [9], artificial sphincter systems [10] or intraocular pressure regulation for glaucoma and phthisis [11]. Numerous applications in biological and chemical analytical systems require micropumps for lab automation or more accurate dosing [2, 12, 13]. Here, micro dosing enables portable micro total analysis systems and lab-on-chip systems and allows for the reduction of sample and reagent quantities or enables quicker assays with less manual intervention [2, 14, 15, 16]. For lab automation, dosing robots can provide high dosing accuracy together with compact integration of parallel systems [17, 18].

Besides the major fields of drug delivery and analysis systems, other interesting use cases can be found (Figure 1.1). Using microfluidics for synthetic chemistry, allows for automated mixing and the extraction of intermediate reaction chemicals which would not be possible on a macroscopic scale [19]. Micropumps are also used for fuel supply in fuel cells [20, 21]. In the electronics sector, micropumps enable compact chip cooling systems for heat dissipation, one of the biggest limitations for microelectronic chips [22, 23].

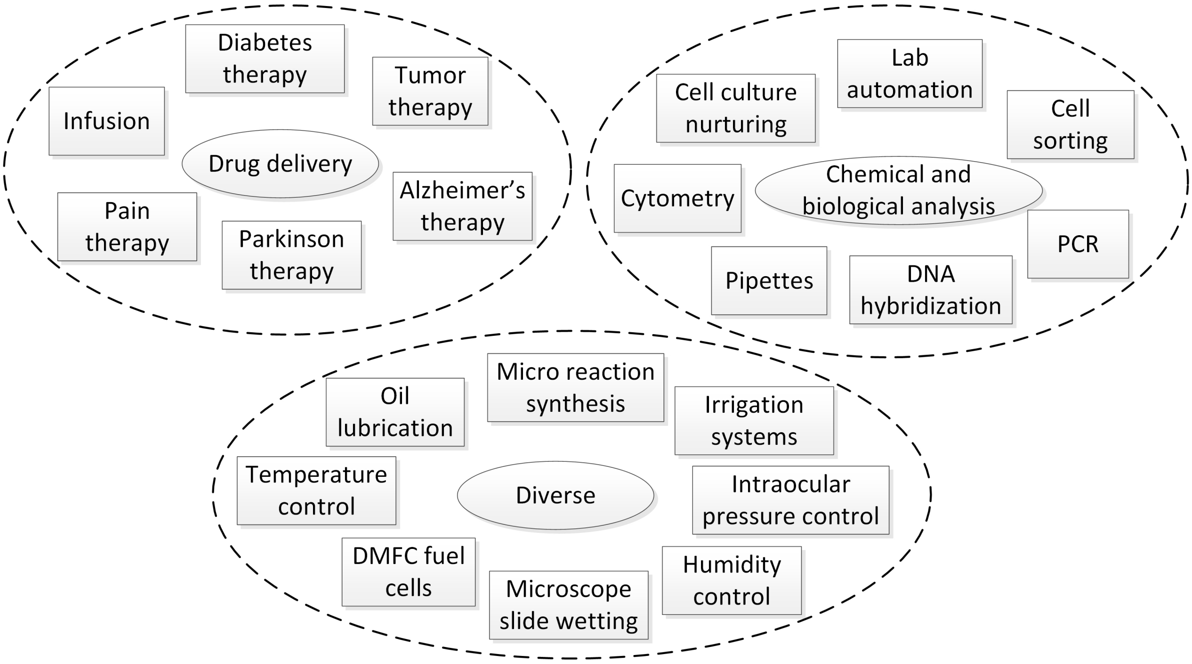

Figure 1.1: Fields of micro dosing applications.

Challenges

From the multitude of potential applications, quite different and tough requirements regarding flow rate, accuracy, energy efficiency, lifetime or costs arise. In addition, only few use cases, like diabetes therapy feature high quantities and a big market volume. But, especially for micro technical fabrication technologies, research and development are connected with high costs, while providing the potential of low production price per piece at high quantities. Thus, the development and production infrastructure is too expansive for many applications. The development of new systems, though, is not only expensive due to the production technology, but because of the challenging requirements and partially insufficiently understood design coherences.

In medical applications, usually reliability, size and applied voltage levels, power consumption, costs and biocompatibility are common constraints [2]. Flow accuracy is very important, as most drugs are only effective if kept within a narrow accuracy range [3]. Below that range, the drug has limited effectiveness and exceeding the limit is often harmful or even lethal [24]. The accuracy needs to be maintained for liquids with different or changing properties, like pH, viscosity, viscoelasticity, temperature as well as the presence of particles [2]. The applied voltage is an important factor for many actuation principles, like piezoelectric or electrostatic, but has to be limited for safety reasons, if operated in proximity to humans or as implants [3]. For portable systems like fuel cell energy conversion, the minimization of size and weight is desired [20]. Because of the low dosing volumes and suitable actuation mechanisms, small micro dosing systems can be realized, but further integration of microsystems is challenging. In the case of microelectronic chips, a small surface exhibits a high heat generation. In order to dissipate the heat, a flow rate of more than 10ml/min may be required for efficient cooling [25, 26]. While the flow rate specification is already challenging for micropumps, it is accompanied by a high flow resistance due to narrow micro channels for enhanced heat conduction. These are merely a few examples of complex applications with challenging requirements or competing design directions. As a result, the design process requires many cost-intensive iterations or no solution can be found, due to inaccurate models.

Value proposition of micro diaphragm pump based liquid dosing systems

One of the main advantages, while designing micro diaphragm pumps is their high adaptability to different requirements. Huge trade-offs between fluidic and electric performance, passive performance requirements, like size, costs or safety and the reliability aspects accuracy and lifetime under the influence of widely varying external conditions can be implemented. This regards both the micropump design, but also the applied driving signal. With an established platform for microfluidic systems, standard components can be selected to complement different types of dosing systems.

A large flow rate range can be achieved, including a low minimum flow rate with reasonable accuracy and high variability of flow rate by adapting the frequency or with drawbacks also the voltage levels [2]. Furthermore, pressure ability levels of up to the magnitude of MPa are possible. The electromechanic conversion efficiency for piezoelectric actuation can be up to 10-30% [2], but strongly depends on the diaphragm radius and the working pressure. While this represents a good efficiency compared to many other actuation principles, even higher efficiencies can be obtained for driving the diaphragm with an magnetic DC motor [27]. System sizes of less than one cubic centimeter can be achieved with micro diaphragm pumps [28], but miniaturization through system integration still offers huge potential. It often depends mainly on packaging requirements like hermeticity with conducts, electronics or reservoir. In most cases the micropump defines the system size more via necessary electronics for the operating signal and voltages, than by its own size. A suitable measure for performance per size is the self-pumping frequency [29, 2].

Due to the multidisciplinarity and complexity of micro dosing systems, many failure probabilities arise. In addition, many external or inherent influences change the system performance. Issues can be caused, but are not limited to the two phase boundary between liquids and gases, particles, changing liquid properties like viscosity or density, mechanically moving parts or electronic components with high voltages. On the upside, single crystal materials like silicon, provide an ideal elastic behavior within its yield strength. This allows for a long-term use over billions of cycles without failure. As little standards are available for microfluidic devices, yet, and the involved fabrication processes are often complex, the development of liquid micro dosing systems is often expensive. With a platform strategy, though, development risks and costs can be reduced significantly. The manufacturing prize is only an issue in the beginning of production, where time intensive steps have to be automated. Another aspect for many biological, chemical and medical systems is material biocompatibility and chemical resistance. Fortunately, the materials used for micro fabrication often provide desirable characteristics. The currently mostly employed materials are polymers, glass, silicon and metal, in order of decreasing share [4].

Conclusion

With the overview over the most relevant fields of applications for liquid dosing systems, the resulting challenges for the development and the pros and cons of micro diaphragm pump based dosing systems: what are the inhibitions against the realization of more applications? The realization of some use cases may have failed due to production costs or size constraints. While other promising applications, like insulin delivery with a huge market potential, probably did not show up, yet, because of challenging requirements regarding flow accuracy at fluidic and electric performance. Furthermore, many developments were reported as promising and realization was expected, but were not continued, which indicates high development costs. As Nisar et al. [3] pointed out in 2008, the "overall commercialization of MEMS micropumps in drug delivery and biomedical application is still in its beginning" ([3], pp. 939) and "to find a micropump suitable for a particular application is a challenge and this will continue to motivate researchers to work on developing micropumps and incorporating them in practical drug delivery and biomedical systems" ([3], pp. 939). 10 years later, these conclusions are still valid, even though considerable progress has been made for different pumping technologies. The reasons are multiple requirements of performance and reliability on the one side and a complex system behavior with many potential disturbance variables on the other side.

In order to increase the addressable field of applications, the obstacles and limitations have to be identified and solved. This thesis shows and expands the current possibilities and limitations in the design of micropump based dosing systems. Therefore, a requirements based generic design approach is developed to allow for an application specific system design. That includes the system architecture, special focus on performance and reliability of micropump systems, as well as closed-loop control solutions for accurate dosing.

For a detailed understanding of micro diaphragm pump alternatives, its state of the art is reviewed briefly, followed by the deployed micropump technology from the Fraunhofer Research Institution for Microsystems and Solid State Technologies EMFT. Subsequently a general overview of potential liquid micro dosing system concepts is given. The chapter is concluded by the detailed research goal and an overview over the contributions and structure of the whole thesis.

1.1 Micro diaphragm pumps - state of the art

The numerous micropump technologies are extensively described by Laser and Santiago [2], Nisar et al. [3] and Iverson and Garimella [27]. However, the most common type is the micro diaphragm pump, due to its broad applicability to all kinds of fluids [27]. The pumps utilized for the investigations are piezoelectrically driven micro diaphragm pumps with passive flap valves (see section 1.2). But, most results of this thesis are applicable to all micro diaphragm pump based dosing systems.

The development of micropumps started with Smits, who first patented his invention in 1984 [30] and described its working principle in 1989 [31], after the first micropump publication from van Lintel in 1987 [32]. Since then, a huge research field emerged. In the beginning the focus was mainly on different actuation and valve principles (Figure 1.2) and appropriate models to optimize their fluidic performance, especially the flow rate [27, 33, 34]. Soon, it was obvious that the pump performance is affected by many influences. Since the late 1990s more focus has therefore been put on the reliability of micropumps, including self-priming ability and bubble tolerance [35] or pressure independence within a limited operating range [36, 37]. Several micropumps have been commercialized, starting with the company thinXXS.

While many micro actuation techniques for diaphragm pumps were investigated, only few are frequently used nowadays. Relevant selection criteria for the actuation principle include the conversion efficiency, important for portable devices, the force generation and reaction time for a high frequency dependent flow rate or the voltage levels for electronics size and safety aspects. The actuation principles were summarized several times[2, 38, 3]. In this work, a brief overview of the most important characteristics is given for the selection of actuation principles (Figure 1.2).

The most common principle is piezoelectric actuation. Due to its high force generation and fast mechanical response, driving frequencies of several kHz are possible [38]. Drawbacks are the high voltages

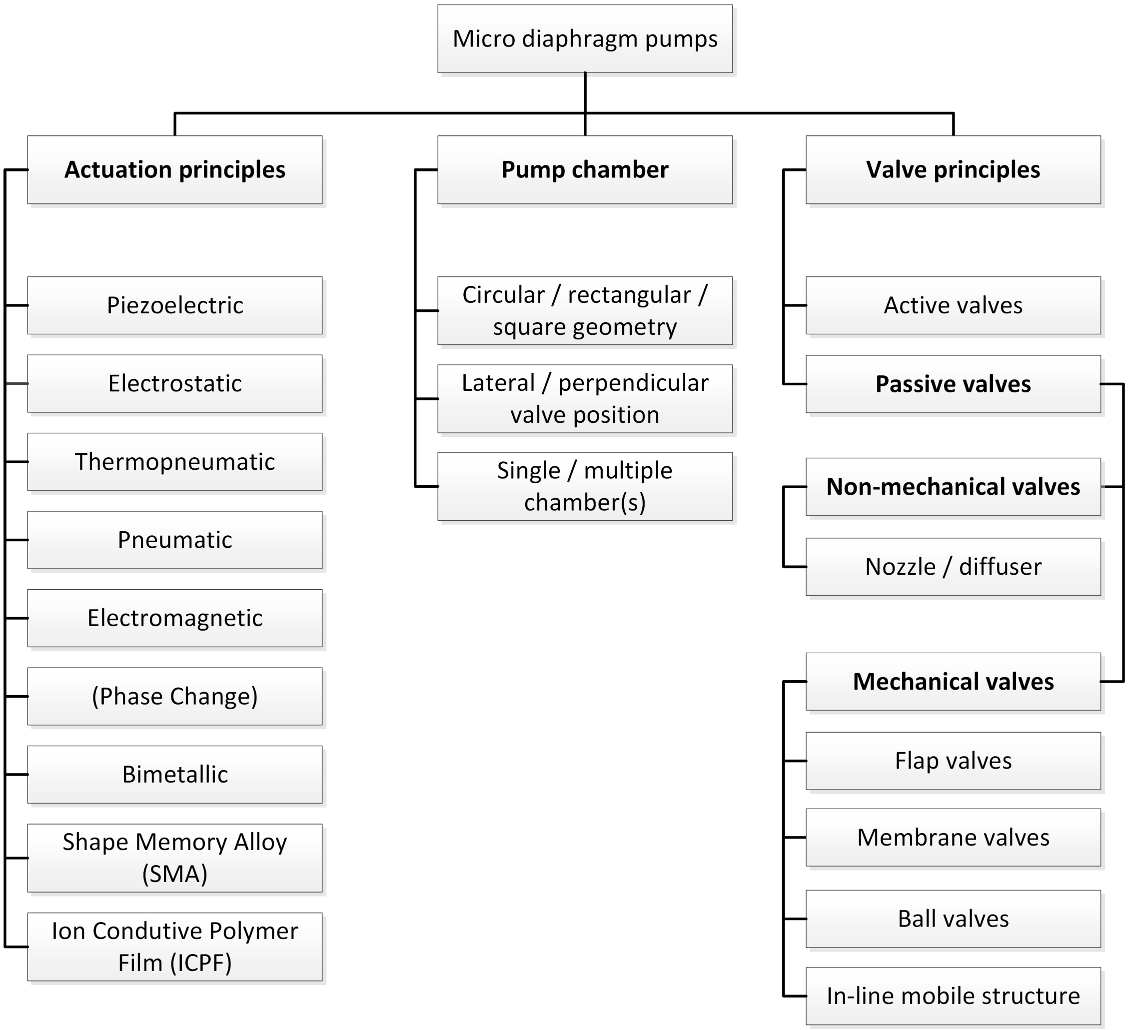

Figure 1.2: Overview of micro diaphragm pumps.

for single layer piezos and the adhesion process to attach the piezo to the diaphragm. To counter the disadvantages, lead free piezo ceramics [39], low voltage multilayer piezos [40] and coatings to increase the breakdown voltage were evaluated. The electrostatic actuation also provides high forces and fast mechanical response times at high voltages, which leads to driving frequencies in the range of kHz [41, 42]. Though, according to the parallel plate approximation of Coulomb's law, the force decreases with the electrode distance d_e by d_e^{-2} [3]. That limits the achievable electrostatically generated stroke volume and flow rate compared to the piezoelectric principle with effectively constant electrode distance. However, it provides a better energy efficiency and is compatible to the semiconductor fabrication processes.

Thermopneumatic actuation heats up gas in a confined space and the resulting pressure pushes a diaphragm [43]. In the cooling phase, the gas contracts and pulls the diaphragm inwards. The cooling process is slower than the heating process and displays the main limitation of the driving frequency, which is usually below 10-50 Hz. The same pneumatic principle can be used by directly applying and subsequently venting the space above the diaphragm, but requires an external pressure source, which is not reasonably miniaturizable. Alternatively a phase-change actuation can produce a bubble in a liquid

with a heater that increases the pressure in a confined chamber [44]. However, these principles provide poor efficiency and are usually not suitable for portable systems.
Electromagnetic actuation usually includes a permanent magnet, which is attached to the diaphragm and driven by an external coil with relatively low voltages [45]. While the large actuation forces are maintained over a longer distance to the coil than for electrostatic actuation, downscaling is more difficult [3].
Other rarely used actuation principles are shape memory alloy [46], bimetallic [47] or ion conductive polymer film [48]. These principles, also have their advantages for niche applications, but are less suitable for reliable long-term operation in combination with high performance.
Valves are as important for micropumps as the actuation itself, because they define which proportion of the moved liquid is actually redirected successfully from inlet to outlet. Oh and Ahn [49] provide the most focused overview of active and passive valves principles and implementations, besides other more general reviews that include valve technologies [50, 51].
The two passive valve categories (Figure 1.2), mechanical and non-mechanical both provide unique characteristics. Mechanical valves in the form of flap, membrane, ball or other moving parts and geometry principles usually exhibit high flow redirection efficiency [49]. However, the moving elements are sensitive to particles that can get clamped and reduce the valve efficiency. The non-mechanical valves effectively exhibit the contrary behavior, with lower redirection efficiency but high particle tolerance. Only clogging of large or adhering particles are failures that can affect both principles.
Active valves on the other hand only occasionally provide real benefits in micropumps and are usually implemented according to the peristaltic driving principle [31]. These benefits can be a reduced leakage due to pressurized valve closure or bi-directionality. The latter can alternatively be achieved by special pump design and driving signal or with an additional pump. On the downside, additional control logic and energy is required to drive the valves.
The pump chamber (Figure 1.2), which is connecting the actuation unit with the valve, was reduced more and more in order to achieve self-priming ability and bubble tolerance even at challenging conditions, like excess outlet pressure [8]. To still use the full displacement volume, the actuator can be predisplaced during the manufacturing process, which shifts the idle state, also referred to as zero-position at zero voltage, away from the pump chamber boundary [52]. Another way of using the full stroke, while minimizing dead volume is by changing the pump chamber boundary to match the displacement curve of the actuator [53]. Other than this aspect and square or circular geometries, the pump chamber structure has seen little innovation. Inlet and outlet are usually either located laterally at the outer chamber rim or placed perpendicularly and close to the center of the flat chamber.
The operating signal provides further options for micropump manipulation. One full cycle of reciprocating pumps starts with the supply mode, where liquid is sucked into the chamber and is followed by the pump mode, where the liquid is pushed out through the outlet. Depending on the frequency dependent displacement reduction and valve efficiency, the flow rate first increases linearly with the frequency, then turns concave and reaches its peak flow at its so called peak frequency. If the actuation frequency is further raised and is located in the range of the valve resonance frequency, a reverse pumping effect can be provoked [54]. If the actuator is driven in its own resonance frequency, the pump can reach a high flow rate [55], but leaves little space for variability and can damage the actuator due to high bending stresses.
Another option to modify the pump performance and reliability aspects is by changing the duty cycle of supply and pump mode. This means, the time share of each cycle is not distributed evenly between supply and pump, but one receives a larger share and potentially also a different driving signal [56, 43].

Of course, the shape and voltage levels can be adjusted arbitrarily to reduce other unwanted effects and reinforce desired ones.
Given the micropump itself, it is still a long way from a complete system, but it represents the actuating core component. As such, the micropump is responsible for the conversion of usually electric energy to fluidic performance. Though, the surrounding components are significantly influencing the fluidic performance over their network of inertances, capacitances and resistances. Further developments of micro diaphragm pump technology will probably regard further miniaturization, integration and cost reduction and hopefully also in improving reliability and introducing standards for interconnecting microfluidic devices. Before reviewing the state of the art of micro dosing system principles, the utilized EMFT silicon pump technology is described briefly.

1.2 Fraunhofer EMFT silicon micropump technology

The silicon based EMFT micropump technology is a piezoelectrically driven diaphragm with passive flap valves (Figure 1.3). In this combination, the micropumps feature high fluidic and electric performance and efficiency with good adaptability of different goals and towards increased reliability. The design parameters of the most important designs with actuator, chamber and valve geometry can be seen in Table 1.1. The tested design space is much larger, but these two specialized pumps are able to address a wide spectrum of performance and reliability requirements.
Especially in the manufacturing technology of silicon wafer stack structuring and assembly and the adhering of the piezo with epoxy resin are difficult and critical processes. Predeflected actuators [52] together with shallow fabricated pump chamber heights are used to increase the compression ratio and thereby the gas pressure ability of the pumps. Thereby, the Fraunhofer pumps achieve self-priming ability and bubble tolerance even at challenging outlet pressure conditions. However, by decreasing pump chamber heights, the influence of viscous squeeze film damping on dynamic motion and thereby frequency dependent flow rate became increasingly stronger [11]. Despite high actuation forces and deformation velocity, the actuator no longer overshoots but gets over-critically damped. The investigation and modeling of this effect and its consequences on the frequency dependent flow rate and flow stability is part of this thesis.

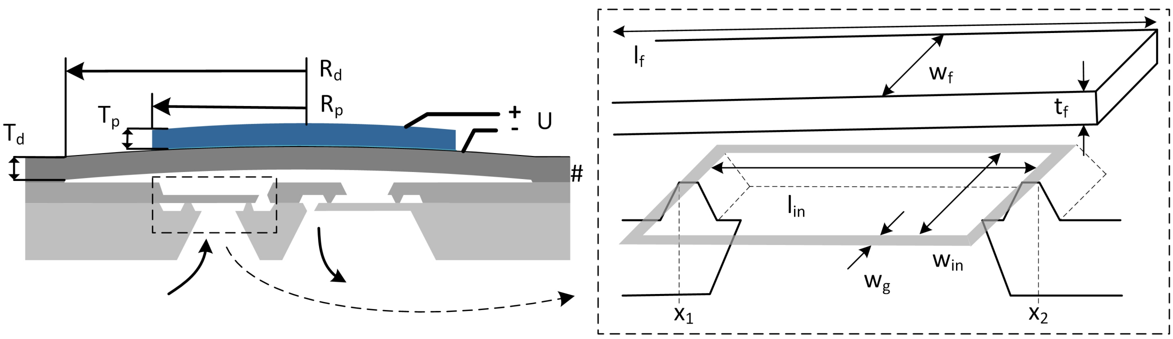

Figure 1.3: Micropump cross-section with actuator (left) and valve (right) dimensions.

Parameter	MIKROAUG (reference)	TUDOS
Diaphragm radius R_d	3.15 mm	3.15 mm
Diaphragm thickness T_d	40 µm	120 µm
Piezo radius R_p	2.8 mm	2.8 mm
Piezo thickness T_p	150 µm	190 µm
Piezo material	PIC255	PIC151
Maximum voltage levels $U_n \| U_p$	-60|+300 V	-76|+380 V
Fabricated pump chamber height h_{pch}	3 µm	1/3/5 µm
Valve flap length l_f	800 µm	800 µm
Valve flap width w_f	480 µm	480 µm
Valve flap thickness t_f	15 µm	15 µm
Square valve inlet width w_i	380 µm	380 µm
Valve sealing lip width w_s	6 µm	6 µm

Table 1.1: Fraunhofer pump designs called MIKROAUG (reference pump) and TUDOS, parameters according to Figure 1.3.

1.3 Micropump based liquid dosing systems - state of the art

The variety of implementation concepts for liquid handling systems is huge. To provide a short overview of how to set up system architecture, the known possibilities of micropump based liquid dosing systems are reviewed (Figure 1.4).

With increasing interest and research on the topic, soon a variety of published microfluidic devices, like pumps and valves, accumulated. Shoji and Esashi [50] summarized the possibilities of micro flow devices in an early stage of the field in 1994. With increasing maturity of the field, the awareness of the advantages of micro dosing for drug delivery became more and more apparent. Therefore, Tsai and Sue [57] outlined the use of MEMS components for building drug delivery systems. Nisar et al. [3] provided an excellent overview over different micropump principles and their value proposition compared to each other in order to build micropump based systems for drug delivery and biomedical applications. In the same year, 2008, Iverson and Garimella [27] not only gave an extensive overview over pump principles and characteristics, but connected these to the large field of potential application and provided micropump selection guidelines. While the state of the art in section 1.1 only covers micro diaphragm pumps, these overviews help to select the best micro pumping principle for an use case.

A system needs certain core components to reliably deliver the required flow rate within accuracy and lifetime (Figure 1.4). The compilation of suitable components is further described in section 2.2. Here, important new ideas for these components are described. The pump as the beating heart of a dosing system (Figure 1.4) can be set up in various configurations, like simply in serial or parallel connection or in specialized structures, like a double actuator in one chamber or one actuator for two chambers [58, 59]. To allow bi-directional pumping, either two parallel pumps can be placed in opposite directions [60], or a bi-directional pump with peristaltic principle can be used [31] or valve phase-shift can be exploited [54]. With a network of active or passive valves, the control and switching of fluidic paths allows for a flexible and compact system design [61, 62].

In order to receive information about important system parameters for safety measures or closed-loop control, sensors can be implemented (Figure 1.4) [63, 64, 8]. The task of the dosing system is primarily to deliver a certain flow rate or volume in a period. The flow can either directly be measured with a flow sensor or indirect correlations can be drawn, for example from a temperature sensor (section 5.2).

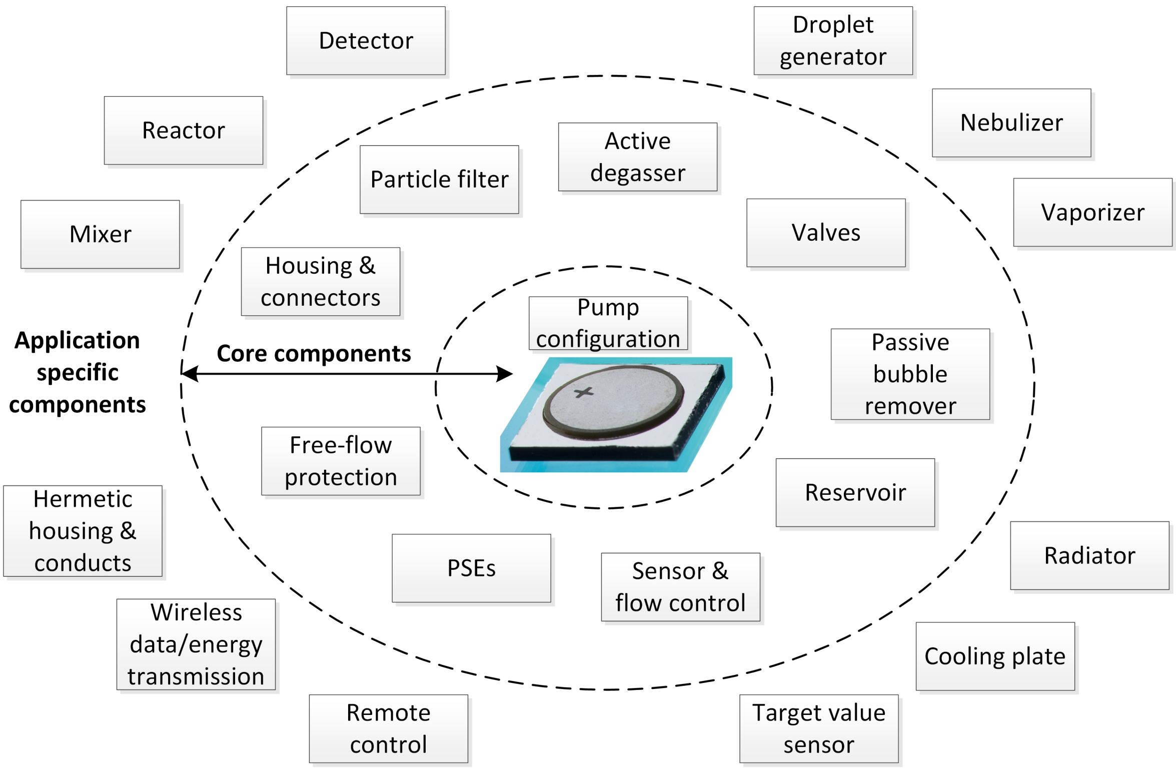

Figure 1.4: Relevant components for micropump systems.

Though, for drug delivery systems, like insulin therapy, the glucose level should be monitored with a sensor and if possible, insulin can indirectly be controlled over the target value glucose [65, 7]. In combination with flow sensors, pressure smoothing elements (PSEs) can be of importance to increase sensor accuracy (section 5.2). Though, they also affect pump performance, as they can decouple the masses before and behind the PSE and both decrease and increase flow rate performance [66].
In some use cases, the flow rate drop, caused by bubbles is tolerable. In others, like intravenous infusion, bubbles have to prevented or removed before leaving the system. Standard hydrophobic membrane based passive bubble removers can be used for bubble extraction. A hydrophobic passivated venting whole allows bubbles to be removed while preventing liquid from leaking [67, 68]. While a passive bubble remover works with the pressured outlet path, an active degasser can not only remove bubbles faster, but degases the liquid and can be placed in-line of the inlet path. Degassing is needed for high flow stability or applications like dialysis or DMFC fuel cells [69, 70]. A good method for micro degassers is to combine venting holes with piezo generated vibrations to produce gas bubbles that can be exhausted [69]. A larger implementation method are standard micro degassing chambers, where gas is exhausted through a gas permeable tube or membrane by applying suction pressure.
Particle filters are also important components (Figure 1.4) and are usually built as membrane or sintered filters [71, 72]. Implementing a sensing element to monitor the clogging extent gives valuable information about system performance or for filter exchange scheduling [73]. Integrating a safety filter into micropumps provides a reliability increase, as particles can originate from fabrication, assembly, handling or during normal operation [74, 75, 5].
In order to prevent inlet pressure from causing free-flow through the pump with forward valve directions,

a free-flow protection valve can be implemented (Figure 1.4) [76, 77]. The reservoir plays a decisive role for the system size, as the magnitude of dosing volume can easily exceed the volume of the system itself. Refill ports are an option to reduce reservoir volume, but come along with additional challenges like inlet pressure caused free-flow or high pressure from syringes [78]. The reservoir itself can also be equipped with a sensor to monitor the flow via the reservoir fill level [8]. For a reliable and unobstructed operation, the fluidic connectors and lines are crucial and therefore part of the core components. Besides the relatively large medical standard Luer and silicon tubes, LEE and HPCL connectors and capillaries provide less space requirement and lower gas permeability, but are usually more expensive. Alternative connection methods provide even less space and are important for integrated systems [55, 8].
On top of the basic system concept options and core components, additional aspects of system architecture have to be considered, when it comes to specific use cases (Figure 1.4). For human or veterinary drug delivery to some parts of the body, biological barriers against drug penetration exist, like for eyes, ears or the brain [79]. This circumstance often requires device implantation or local attachment. Other examples for positioning constraints are the local delivering of high drug concentrations at tumors [8] or swallowing a microtechnical system pill for gastro-intestinal monitoring or drug release [80]. Where portability and local attachment is required, the size plays an important part for patient convenience and safety. If implanted, even higher size constraints may be given [10, 11], while requiring hermeticity of housing and conducts, a refill port, wireless transmission of energy and data and a remote control unit. In biological and chemical analysis or synthesis systems, bi-directional pumping is often required for sampling and washing. Another concept is to pump air in order to move liquid, like in an air buffer pipette. The goal of both concepts is to avoid contamination of subsequent samples. Micro mixers and reactors are often integrated in analysis systems for time dependent processes and adjustable sampling [81]. PCR within microfluidic chips is of rising importance and requires pumps, valves and mixers in different configurations [61]. For this field of use platform strategies can be especially helpful [17]. For cooling applications, heat radiators and cooling plates are required in a closed system [23]. Many other components are conceivable for the whole range of applications.

1.4 Research goal and outline of contributions

Problem statement
In order the enable many of the potential applications, each set of requirements has to be brought together with the large design space of micropump based liquid dosing systems in an efficient way. In the state of the art (section 1.3) many different solutions were developed for individual use cases. However, a generic approach to system design is still missing. For the latter, accurate models are required to simulate the system behavior. Existing quasi-static models of actuator and valve deformation can be used. However, recent developments towards lower pump chamber heights increased gas pressure ability, but also introduced a viscous squeeze film effect. This significantly changed pump dynamics and made existing models inaccurate. Though, such a model is crucial, not only for performance design, but also to determine the influence of disturbance values on flow stability.

Research goal
The research goal of this thesis is to investigate performance and reliability characteristics of micropump based liquid dosing systems and to identify main influencing parameters. In addition, models are to be

developed and combined to be able to simulate the system's behavior in a large design space. On a system level, guidelines need to be established to facilitate the definition and implementation of appropriate system architectures. Based on the gained insights, the potential and the limitations of open- or closed-loop flow control should be evaluated to provide efficient solutions for new applications.

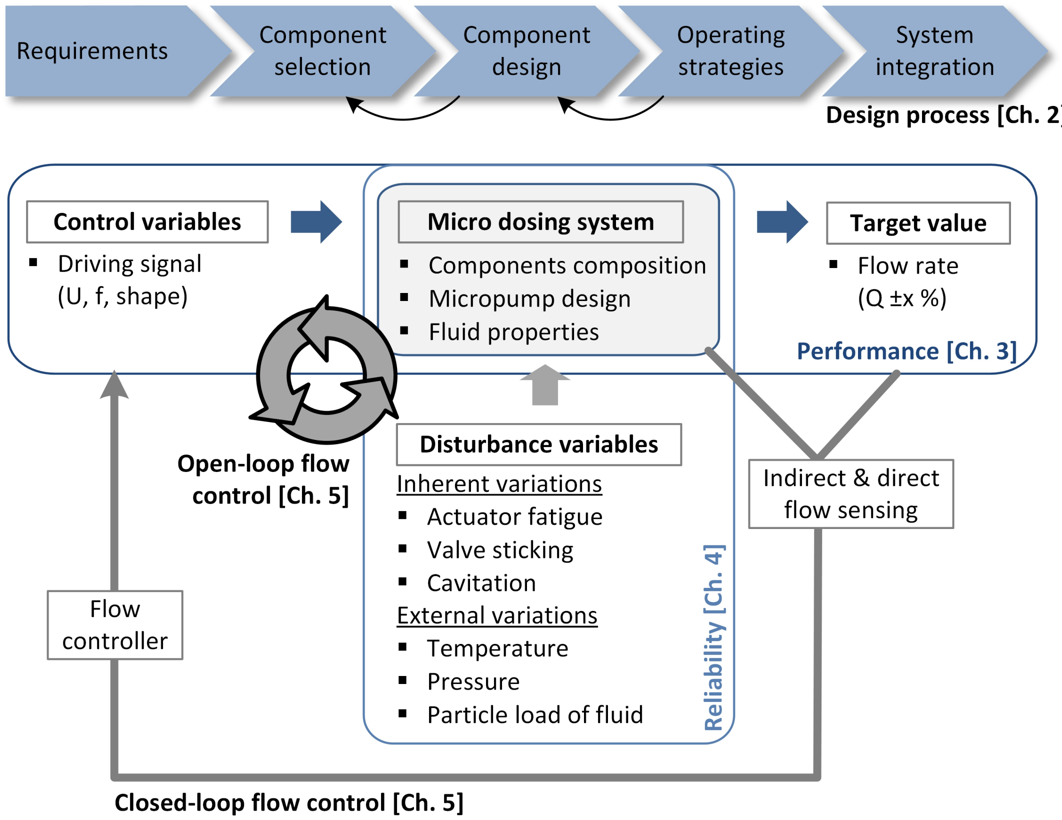

Figure 1.5: Outline of the thesis.

Outline of contributions

The content of the thesis in outlined in Figure 1.5. In Chapter 2, a system level design process is proposed, to determine the right system architecture for each intended use case. Within a generic micropump system, Chapters 3 and 4 describe the behavior of performance and reliability. Based on the system behavior, two flow control solution concepts are provided in Chapter 5. First, a design balancing process is proposed for open-loop flow control. Subsequently, indirect and direct flow sensing is evaluated in the context of closed-loop flow control.

In Chapter 2 (Figure 1.5), the most relevant aspects of system architecture are addressed. Typical requirements of liquid dosing systems are presented. Each application specific set of demands is the basis for selecting the right functional components for a reliable operation. Therefore, an overview of suitable components, their working principles and employment possibilities is given. The design of each component has to be conducted with proposed potential operating strategies in mind. To complete the system, its integration can follow different optimization directions that bear a variety of described challenges.

In Chapter 3 (Figure 1.5), the performance behavior of micropumps, embedded in liquid dosing systems, is described. The static performance of piezoelectric diaphragm actuators was evaluated for different optimization goals, clarifying the limitations of this technology. The same was done for micro flap valves with the help of a novel parametrized fluid-structure-interaction model to accurately simulate the flow through new valve designs. On a micropump level, the gas pressure ability was evaluated theoretically and experimentally, regarding the issue of gas leakage. By investigating the flow rate influencing effects of liquid micropump systems, the major loss effects were identified and a single stroke based flow rate model is proposed. This pump level model is build upon novel dynamic actuator models that are able to simulate the transient actuator course during resistive squeeze film damping and under the effect of cavitation.

In Chapter 4 (Figure 1.5), the reliability of micropump based systems is covered. The core task of all dosing applications can be reduced to provide a flow rate within an accuracy band over a lifetime within a certain failure probability. A multitude of external and internal disturbance variables influence the flow stability and can lead to failures. Most relevant internal variations originate in actuator fatigue, valve sticking and cavitation, while main external factors are temperature, pressure and particle laden flow. The working principles and main dependencies of these disturbance variables were worked out. The effect of internal and external variations on the flow rate was estimated with the models from the performance chapter and measured, where possible. A proposed adaption of certain design parameters, allows to minimize certain influences, usually at the cost of performance.

In Chapter 5 (Figure 1.5), the potential and limitations of open- and closed-loop flow control solutions are evaluated. As competing design directions exist between performance and reliability, a balancing process is proposed. For a improved understanding of coherences, an overview of the most influential parameters was given for each characteristic. For when closed-loop flow control is required, due to safety or flow stability reasons, indirect and direct flow control was evaluated. In closed-loop control the design can focus on performance, but sensor velocity, robustness and integration aspects are challenging.

For an efficient design process, performance and reliability behavior of micropump dosing systems were investigated as well as accurate models developed and integrated into a system design process. Thereby, this dissertation aims to demonstrate the current possibilities and limitations in the design of micropump based dosing systems.

2 System architecture of micro dosing systems

The system architecture provides the foundation and framework to build application-specific systems. While various dosing system architectures were published (section 1.3), a generic process of how to set up micropump based dosing systems is still missing. Therefore, a high-level approach is proposed that includes the most relevant aspects of building application-specific micropump dosing systems.

This process starts with the demands of an application (Figure 2.1). In order to meet all requirements the system architecture has to be defined accordingly in four major steps. First, the functional components need to be chosen. Second, the core fluidic components are designed regarding all performance and reliability aspects. Third, the operating strategies define the conditions in which the system is operating. Last, the challenges of the system integration are addressed. The design process, however, is not always compellingly linear, especially if the trade-off between performance and reliability reaches its limitations. Then, a balance of component selection, component design and the limitation of operating conditions may be necessary. With this target-oriented process, new micropump systems can be designed accurately and efficiently.

The structure of this chapter follows the individual process steps and starts with an overview of typical requirements (section 2.1). Subsequently, the alternatives of functional components are described (section 2.2) and the rough interdependencies of designing the core components are mentioned (section 2.3). What follows are the choices of operating strategies (section 2.4) and the challenges of system integration (section 2.5).

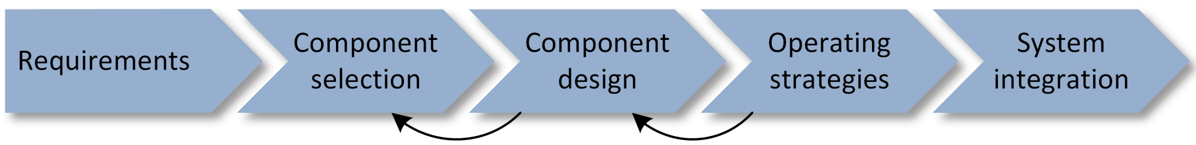

Figure 2.1: Requirements based process for micro dosing system design.

2.1 Requirements of micro dosing systems

Requirements are the system-level characteristics that enable the right behavior for an application. The characteristics can be achieved by an appropriate design of all system parameters. Requirements can be divided in two categories: performance and reliability. Performance requirements describe the desired functions. Reliability assesses the stability of performance or functions, which includes the accuracy and lifetime with a defined failure probability. The allowed failure probability within the specified lifetime is usually defined for the overall system function and therefore leads to a failure probability budget for each performance aspect. This means, in order to describe a system function, performance and reliability aspects have to be mentioned together. For example, a system might require a constant flow rate of

100 µl/min within an accuracy of ±20 % and a lifetime of 10000 h at a failure probability of less than 1 %. Furthermore, the demanded reliability may as well include a tolerance against a certain magnitude of environmental influences. This usually aggravates the difficulty to reach the reliability requirements. For micro dosing systems, the flow rate is often the single most important target requirement and its reliability demands affects subordinate aspects. For example, its total accuracy budget determines the allowed individual influence budget for each external influence. Once the flow rate leaves its accuracy boundaries it is classified as a failure, regardless whether the failure is just temporary or irreversible.

An overview of the most important requirements of micro dosing systems is given in Table 2.1. It is complemented by a short definition, the unit and a typical range for each requirement. The performance requirements are further grouped in fluidic performance, electric performance, outlet flow properties and passive requirements. The reliability requirements can be summarized in the two aspects accuracy and lifetime, but also address the influence of external parameters. The optimization direction of performance and reliability goals is often opposite to each other. Therefore a clear definition of the required values helps to realize an use case.

	Requirement	**Definition [unit]**	**Typical range**
Performance requirements	<u>Fluidic performance</u>		
	Flow rate range	Volume/period [µl/min]	0-2000 µl/min
	Liquid pressure ability	Actuator pressure [kPa]	100-1000 kPa
	Gas pressure ability	µP suction|excess pressure [kPa]	<-70|<+100 kPa
	Self-priming ability	Ability at max. pressure [yes/no]	y <70 kPa
	Leakage flow rate	Volume/period/pressure [µl*min^{-1}kPa^{-1}]	<0.02 µl*min^{-1}kPa^{-1}
	Free-flow rate	Volume/period/pressure [µl*min^{-1}kPa^{-1}]	<10 µl*min^{-1}kPa^{-1}
	<u>Electric performance</u>		
	Power consumption	Current at voltage [mW]	30-100 mW @3.3 V
	Battery runtime	Uptime [h]	<100 h/(1000 mAh @3.3 V)
	<u>Outlet flow properties</u>		
	Pulsatiliy	Deviation of target flow rate [%]	0-200 %
	Purity	Concentration of particles [vol-%]	<1 ‰
	Dead time	Time of no liquid [s]	0-100 s
	<u>Passive</u>		
	Size	Integrated system volume [cm³]	1-100 ml
	Noise emission	Acoustic pressure [dB]	<50 dB
	Costs	Manufacturing costs/unit [€]	1-1000 €
	Safety	Severity x Occurance x Detection [/]	
	Usability / Compatibility	Customer demands	
	Liquid	Application demands	
Reliability requirements	Accuracy	Deviation of target value, within defined period [%]	<±20 %
	Lifetime	Time for performance value to stay within acc-limits [h] at failure probability [%]	100-20000 h | <1 %
	<u>Tolerance to variations of external influences</u>		
	Temperature	Liquid|ambient temperature [°C]	0-50 °C
	Pressure	Inlet|outlet|ambient pressure [kPa]	<±10|<±50|<±5 kPa
	Vibrations	Frequency [kHz] and acceleration[g]	<10 kHz | <10 g
	Particle laden flow	Size and concentration [µm|vol%]	0-10 µm|<1 ‰
	Bubbles	Volume [µl]	1-100 µl
	EMV	DIN standard compliance	

Reliability of performance = Stability of performance
=> <u>Performance</u> value within <u>accuracy</u> over <u>life-time</u> within <u>failure probability</u>

Table 2.1: Performance and reliability requirements for micro dosing systems.

2.2 Functional components for dosing systems

Every micropump based fluidic system requires the a driving unit, consisting of a micropump and the driving electronics (Figure 2.2 - green). The passive fluidic path reaches from the reservoir, the inlet path, the micropump and the outlet path to the system outlet (Figure 2.2 - arrow and gray elements). A housing facilitates the fluidic connection and may have integrated additional components, like filters or a free flow protection. To ensure continuously reliable operation, additional elements can be added to the system (Figure 2.2 - blue). The integration of sensors allows for monitoring or closed-loop control of the system (Figure 2.2 - orange).
Depending on the requirements of an application, different combinations of components have to be chosen. Foreknowledge on the effects and conditions that influence the system behavior is needed for the selection. This may result in a different choice of components after the first iteration of designing the components and determining appropriate operating strategies. For an understanding of the component functions, each one of them is explained.

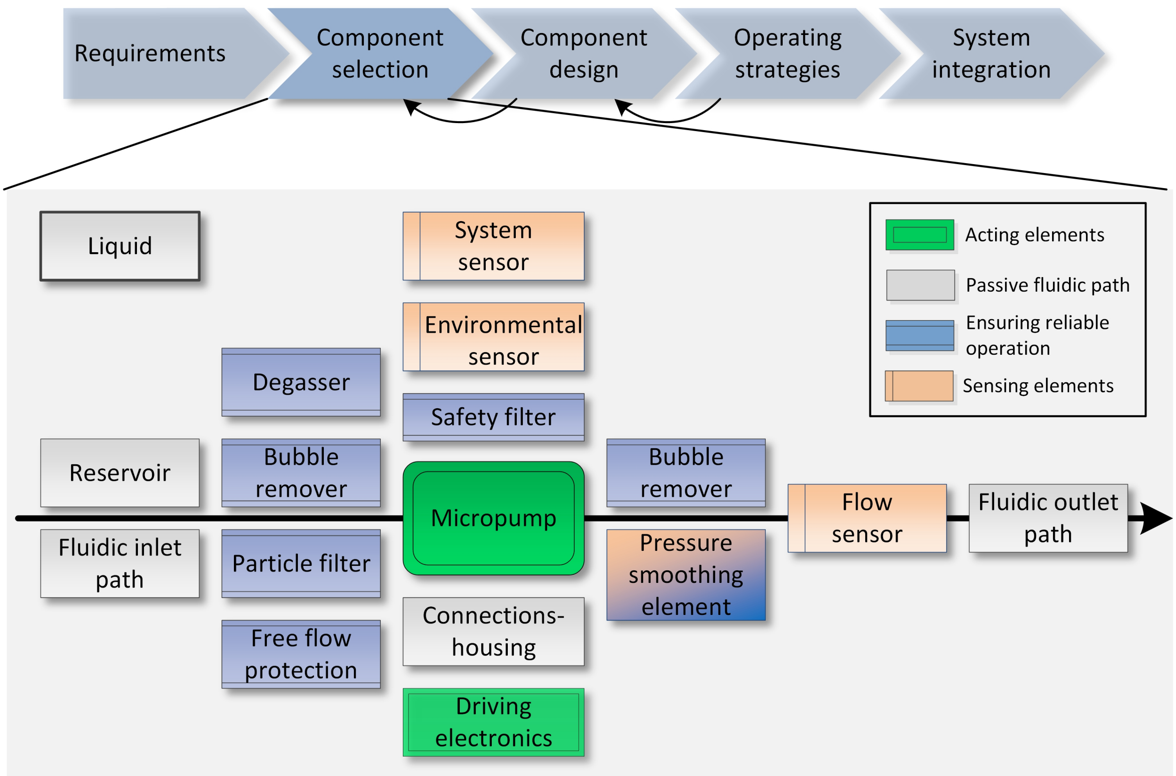

Figure 2.2: Components for micro dosing systems.

Liquid

The pumping liquid depends on the application and can be for instance a solvent, a lubricant, a drug or a body liquid. They come along with different properties like viscosity, heat capacity or mechanical and chemical stability. All these aspects have to be considered in the choice and design of the components.

Micropump

The micropump is the core component of the micro dosing system. It is responsible for moving the liquid from the reservoir to the system outlet and is driven by the electronics. As discussed in the state of the art of micropumps (section 1.1), piezoelectrically driven micro diaphragm pumps with passive flap valves are used due to their high pressure ability and flow rate efficiency and variability. Resistances, capacitances and inertances in the fluidic paths directly influence the micropump behavior and thus the flow rate. Therefore, the main emphasis of dosing system design is put on the micropump behavior itself.

Driving electronics

Driving electronics provide the signal for the micropump and thereby define the performance of the system. However, the allowed driving signal is limited by the design parameters of the micropump. Important aspects of the signal are the output quality compared to the desired signal shape, the voltage levels and the frequency range, together with a duty cycle variation. The latter determines the available time for supply and pump mode within one cycle. Usually, a low voltage direct current is used to generate an alternating high voltage signal. This increase of voltage levels is one of main limitations of the electric-electric energy conversion efficiency. Another is the conceded space for the electronic circuit.

Degasser

A degasser is mandatory if flow stability and high performance is required. Due to its gas permeable membrane it is able to actively remove bubbles from the liquid stream and reduce the concentration of solved gas in the liquid. If placed in-line between reservoir and micropump, it prevents bubbles from remaining in the fluidic path after the filling process. Thereby, the flow performance can reach its designed maximum. At cavitation conditions (section 3.4), degassed water reduces the chance for stable cavitation, where a stable bubble emerges from the solved gas. This increases flow stability and allows to operate the pump with higher voltage levels or frequency. If stable cavitation occurs nevertheless, bubbles get absorbed faster than without a degasser. As a result, if the fluidic outlet path is long enough, no bubble remover is necessary for applications that prohibit the outflow of gas. However, degassing chambers, which are currently available, require a vacuum pressure supply and are therefore not yet miniaturized or autonomous.

Bubble remover

A bubble remover can be built in the same way as a degasser, where bubbles can leave the fluidic path over a hydrophobic and gas permeable membrane or tube. The distinction is that a bubble remover can only be placed behind the micropump as it only works the available pressure difference from liquid to environment to separate the bubbles.

Safety and particle filter

Safety and particle filter in principle share the same function. Though, they are designed for different purposes. The particle filter is the, usually exchangeable, primary filter that retains large amounts of particles. The secondary safety filter, in contrast, is permanently attached to the micropump inlet to prevent randomly appearing particles from entering the pump. These random particles can originate from handling and assembly, standard operation or during the exchange of the primary filter. The design of pore size, filter area and material depends on the micropump particle tolerance (subsection 4.2.3) and the used liquid. Sensors for clogging grade detection [73] enable an automated maintenance notification to exchange the particle filter.

Free-flow protection

Free-flow is flow through the pump, which appears due to a positive pressure difference between inlet and outlet. If this kind of flow has to be prevented during normal operation, two options arise. The first is to make sure that there is no positive pressure difference. The second is to include a free-flow protection. A simple implementation as a free-flow protection valve was invented that prevents excess inlet pressure from causing free-flow, as the valve only opens if the micropump generates suction pressure [76, 77]. If the free-flow only needs to be prevented during standby, an active switching valve displays an alternative.

Pressure smoothing element

Pressure smoothing elements (PSEs) damp pulsatile flow. As the micropump generates highly pulsatile flow, these elements are important for two cases. First, if a continuous flow is required at the outlet, the flow needs to be smoothed. Or second, if a sensor is used that is not fast enough to accurately measure a quickly changing pulsatile flow (section 5.2), smoothing the flow enables the sensor to operate in an accurate mode. Every tube displays a capacitance and PSE, but a miniaturized integration of micropump, PSE and sensor is still a major challenge.

Flow sensor

A flow sensor directly measures the target value of a dosing system. This information can either be used for safety, so that the system knows when a failure occurs, or it can be used for closed-loop flow control to keep the flow rate in the allowed accuracy band. Many sensing principles are feasible and were implemented (review in section 5.2) and the right one has to be chosen for each application. They differ from each other in terms of measurement principle, measurement velocity, pulsatile and quasi-static accuracy, size or electronic readout ability.

System sensor

System parameters can provide valuable insights on the performance and state of the system. Most important are the transient actuator displacement relative to the pump chamber boundary and the valve bending. Piezo self-sensing can deliver information about the deformation and the flow due to pressure feedback on the piezo. This information is valuable to detect any abnormal deviations or even deduce changes of flow rate. However, compared to the flow sensor additional inaccuracy and uncertainty remains.

Environmental sensor

Environmental sensors can measure all aspects of external influences. This includes fluid properties like particle or bubble concentration, fluid temperature, surrounding air temperature or pressure at inlet, outlet and of the surrounding air. All these parameters can have an impact on the system performance. If an application merely faces variations of single influences, the implementation of an environmental sensor can be sufficient to keep the flow rate within accuracy limitations via closed-loop control. As environmental sensors are often cheaper than flow sensors, such a choice can be beneficial.

2.3 Component design

The design of individual components cannot be carried out isolated from each other, because their interaction is too strong. The fluidic core components of a micro dosing system are the micropump together with the driving unit and the whole passive fluidic path within a certain system architecture. Additional components like filters, sensors or PSEs change the fluidic characteristics of the path. The fluidic paths exhibit networks of resistances, inertances and capacitances, analogous to an electrical circuit. These characteristics of the fluidic paths influence the micropump and therefore the system behavior together with the fluid properties like viscosity or density. The system behavior leads to the principal target value flow rate and can be adjusted with the control variables (Figure 2.3). The selection and design of components, together with the driving signal determine the performance behavior, which is covered in chapter 3.

The performance is influenced by disturbance variables of internal or external origin that change the conditions for the dosing system (Figure 2.3). This ultimately produces variations of flow rate, affecting the reliability of the system (chapter 4). Components like a particle filter can be selected and designed with respect to the micropump to increase reliability.

In order to build systems that fulfill both performance and reliability requirements, two strategies are presented in chapter 5. The first approach is to balance all involved parameters to meet the goals over a guided design process and with the help of models. The second is to select sensors and provide the conditions to implement an accurate closed-loop flow control. The design of components therefore also depends on the choice of this implementation strategy.

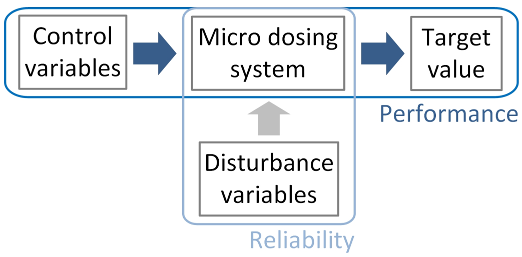

Figure 2.3: Micro dosing system behavior.

2.4 Operating strategies

Operating strategies can be employed to ensure that the system reaches its theoretical performance or is able to maintain a stable performance. On the one hand, employing these strategies may add effort or limit the range of use of the system, on the other hand it may reduce costs or enable an application at all. Therefore, operating strategies are not always recommended to be applied. They include methods to apply before and after operation or to adjust environmental conditions (Figure 2.4).

Gas priming

After filling of the fluidic path from reservoir to system outlet, entrapped bubbles may remain behind. These bubbles work as capacitances, which affect the system performance. Any change of bubble size or detaching and flushing out has an impact on the flow rate while operating. To avoid remaining bubbles in the fluidic path, a method was developed to prime the fluidic path prior to filling with a special gas that easily dissolves in the liquid [82]. The effect of gas bubbles on the flow rate and its prevention is further explained in section 3.4 and section 5.2. A different approach to prevent bubbles in the fluidic path is by employing an in-line degasser, as described in section 2.2.

Prefiltration

Particles may influence the dynamic micropump behavior and cause flow rate changes. Up to a certain level, micropump design together with particle filters can deal with this issue. For some applications the pumping of particles is necessary, for instance pumping protein based drugs. However, if particles in a liquid are not of functional use, prefiltration of the liquid solution should be considered. The filtering process can be conducted with high efficiency due to large filters, high pressure and with smaller filter pore sizes than feasible at an in-line filter. Prefiltration would also avoid the implementation of a particle filter and frequent exchanges due to clogging, which lowers the system and maintenance costs. However, a safety filter right in front of the micropump is still recommended to prevent critical particles from handling, assembly and operation from entering the pump.

Sterile operation

Bacteria and fungi have little requirements to grow in a humid or liquid environment, but can clog a system. They only need an energy source, like light or heat, and little nutrition. These prerequisites can often be found in fluidic systems and has therefore to be dealt with by different approaches. First, the micro dosing system should be sterile from the beginning. This can be done by an autoclave or by rinsing the system with a 70 % ethanol / 30 % water solution for 30 min. Nutritious remains can be solved with acetone, followed by fast drying isopropanol rinse. Furthermore, the liquid should not be exposed to light or heat, which however is difficult to follow as most lab equipment is made out of glass. Though, applying sterilization and using sterile liquids is sufficient for most cases. A cycling liquid, where outlet flow reenters the inlet reservoir, should be avoided, as contamination is more likely to be spread. Adding a herbicide is theoretically a valid approach for testing purpose, but can not be applied in many applications. Drying the system before storage also reduces the chance of biological growth.

Stand-by flow resistance

In standby mode of the system a pressure difference between inlet and outlet leads to free-flow or leakage flow. By leaving the actuator at the lower turning point (positive voltage level) in standby, the flow resistance increases and both free-flow and leakage flow are reduced.

Acclimatizing

Temperature variations change the flow rate significantly (subsection 4.2.1). By using the system in a acclimatized environment or naturally lower temperature variations, the possible flow rate changes can be reduced as well. This limits the range of use or increases the effort for acclimatizing, but may keep the flow accuracy in an acceptable range. Compared to the solid micropump body, housing and capillaries, the liquid usually has the highest impact on the flow rate. Therefore, acclimatizing the liquid only will significantly contribute to flow stability.

Pressure level manipulation
Pressure levels at inlet, outlet and at the actuator surface have a significant effect on pump performance, which can be utilized. If a high flow rate and only a limited variability is required, an excess pressure at the inlet can shift the flow rate by a base free-flow. If, on the other hand, a high free-flow protection is needed, a suction pressure at the inlet compared to the outlet prevents free-flow. A pressure variation at the actuator surface is able to shift the zero-position compared to the pump chamber boundary.

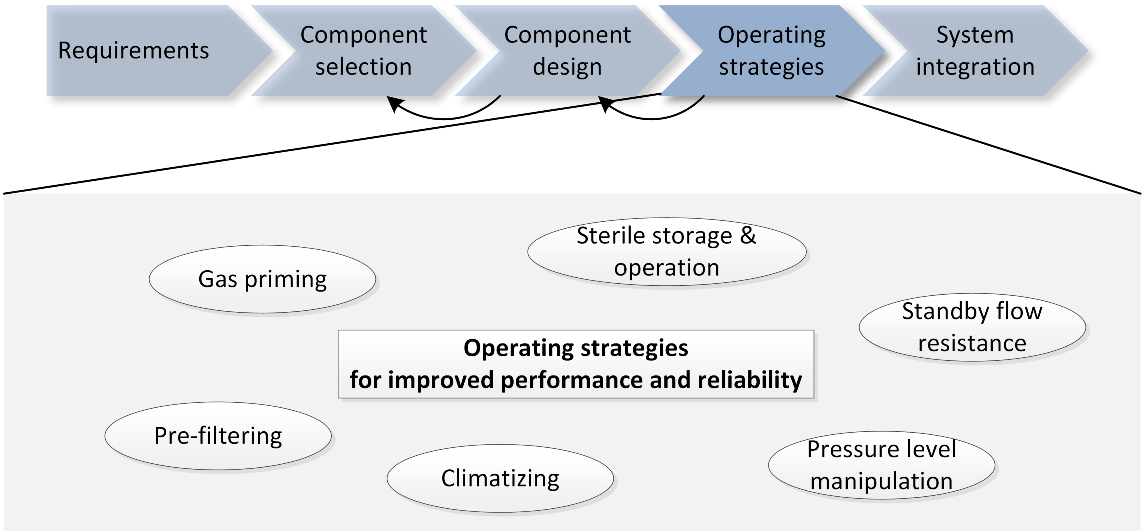

Figure 2.4: Operating strategies.

2.5 System integration

Once the components are selected and defined and the system function can be guaranteed, the system integration holds additional challenges. The goal of system integration is to deliver reliable and safe fluidic, electric and mechanic interfaces, a cheap producibility, the required size or adequate noise levels. System integration of microsystems itself is an own research discipline and not the focus of this work. The system integration aspects mentioned here cannot satisfy the demands for this complex topic, but aims for a description of the challenges that arise from the specific functional needs of micro dosing systems (Figure 2.5).

Electronics integration
The driving electronics play a significant role for dosing systems and feature certain choices and challenges regarding its integration level. The most obvious and important aspect is the electronics size. Compared to the micropump itself, the driving electronics usually takes up its multiple size and mainly depend on the signal quality (boost converter principle vs. power amplifier), voltage levels (voltage height vs. component volume), the desired efficiency (minimum setup vs. energy recuperation at boost converter principle) and the integration level (discrete circuit vs. ASIC). As the micropump is made of silicon and manufactured with semiconductor MEMS processes, a certain manufacturing compatibility exists for

pump and CMOS processes based electronic circuits or sensors. This would allow for a highly integrated package of pump, ASIC and sensors.

Electronics protection

Electronic circuits are sensible to various environmental influences like liquids (water, oil), microbes, temperature or dielectric property changing influences that can cause short-circuits. Protecting the driving and sensor electronics from humidity and other environmental influences increases their reliability. Molding of electronic components is a standard procedure that can help to decrease the electronics failure probability to an acceptable level. This is especially important for implanted systems, where the device is surrounded by liquid and highest reliability requirements are necessary. Though, for a long term implantation, a hermetic housing might be required to prevent dangerous substances to damage the electronics.

Hermeticity

Hermeticity not only keeps substances that affect the reliability from entering the system, but also prevents hazardous substances from leaving the system. Hermetic housings can often be seen at implants using titanium for additional biocompatibility. Only metals provide a proper hermeticity for thicknesses down to several hundred micrometers and for years of employment. However, the difficulty is to get electric signals and energy through the metal housing. The standard approach is to use a pin surrounded by a ceramic layer to separate the electric line from the conducting metal housing. Unfortunately, this technology still requires a lot of space (several mm in diameter), which makes it large compared to other system parts like the micropump or even the driving electronics.

Sensor integration

Sensors can be useful to measure system parameters, environmental parameters or the target parameter flow rate. Most important for a purposeful deployment is their placement location, the right and sufficient operating range and the influence of external influences. For example, the location of pressure or temperature sensors is crucial for the right adjustment of pump performance (subsection 4.2.1 and 4.2.2). The most useful system parameter to measure is the transient displacement, as many insights can be derived from this information (section 3.4). Piezo self-sensing is a concept that would allow to gain senor data without additional sensors, only by adding evaluation electronics. For the integration of a flow sensor, the pulsatility of the flow plays a significant role for the versatility of the sensor and the validity of its signal (section 5.2). For a compact integration of the flow sensor, a pressure smoothing element might be necessary to damp the highly pulsatile flow of the micropump.

Pulsatility damping

The reciprocating micropump exhibits a highly pulsatile flow. There are two cases, where a damping of the pulsatile flow is necessary (section 5.2). First, if the employed flow sensor is not fast enough to measure the transient flow pulse. Second, if the applications requires a continuous flow at the outlet. A soft tube of some cm in length already provides a significantly smoothed flow, but there may be space limitations. In the case of a flow sensor, it is best to place it as close to the pump outlet as possible. Elastic element like diaphragms or soft tubes can be used as pressure smoothing elements (PSEs) (section 5.2) and damp the pulsatile flow. However, an aligned design of PSEs and a compact integration together with a sensor is a challenge.

Fluidic connections

Fluidic connections can be found along the whole fluidic path, i.e. connecting to the reservoir, the pump inlet and outlet and all components with direct liquid contact. These connections all have to be air tight, withstand certain stresses, be manufacturable and some need to be easily exchangeable. One of the most critical connections is at the pump interface itself. A very smooth silicon surface with little space between inlet and outlet has to be connected to the inlet and outlet path. This is usually done by a pump housing but two main concepts are competing, clamping and adhering. Clamping provides the possibility of removing and exchanging the pump for test purposes. However, it consumes more space and the pump performance reduces with increasing clamping force, as the remaining pump chamber height decreases. The issue at hand is that the tightness of the fluidic connection increases with the contact pressure and has to exceed a certain level in any case. Another challenge of clamping is the air tightness of the sealing to the housing, as it is difficult to produce a low surface roughness with the micromachining process of plastic housings. Thus, either the air tightness suffers or the housing costs increase and a performance reduction takes place in any case.
On the other hand, adhering the pump to the fluidic paths renders it impossible to remove and a pump from the housing without damage and reuse it. Depending on the adhesive, it may degas while hardening and chemicals may stick to critical surfaces like the valve contact area, which influences the flow stability (subsection 4.1.2). To find the right adhesive for specific material combinations can therefore be difficult and to develop a reliable adhering process is challenging and increases the development effort. Though, if these aspects are under control, many advantages arise from adhering the pump. No performance drop is expected, as no torsional stress reduce the remaining pump chamber height. The fluidic connections can be implemented in a more compact way, as no space for the sealing and clamping is required. Once a robust adhering process is set up, the assembly is easier and contains less parts, which also reduces manufacturing costs.

Miniaturization

A compact system size is a main advantages of micro dosing systems. Therefore, the miniaturization of the system size is one of the critical design directions and a challenge for the system integration. The micropump size itself mainly depends on the required performance. Though, compared to other system components, it often only takes up a small portion of the system volume. As described, the driving and control electronics feature one of the highest miniaturization potentials that come along with reduced signal quality, voltage height, efficiency and quantity dependent costs. The fluidic path itself can be miniaturized pretty well, if adhering is used. Only the reservoir size is fixed due to the required volume at adequate refill-intervals. A hermetic package housing increases in size with the number of feedthrough connections needed for data or energy transmission. Additional components like sensors, a degasser and bubble remover, filters or free-flow protection are mostly not yet available in a miniaturized shape and can add to the system size significantly.

Free-flow protection

A method to reduce or stop free-flow is the implementation of a safety valve. In theory, only a thin layer is necessary to implement this safety valve [77]. Though, from experience, the realization of the desired mechanical properties is quite difficult and does not always cover all pressure regions equally.

Electric safety

The system integration of a dosing system involves the electric safety for humans and the environment. Piezoelectrically driven system often come along with high voltages and temporarily high currents. In order to protect humans that interact with the system from being injured, any charge dissipation over the human body need to be prevented. In an explosive environment, sparks inside the system should either be prevented or flame propagation need to be stopped at the system boundary through lamellae. Besides specific isolation of charge carriers, well known electronic components like Zener-, suppressor or Schottky-diodes, pull-down resistors or current limitations can be implemented to ensure electric safety.

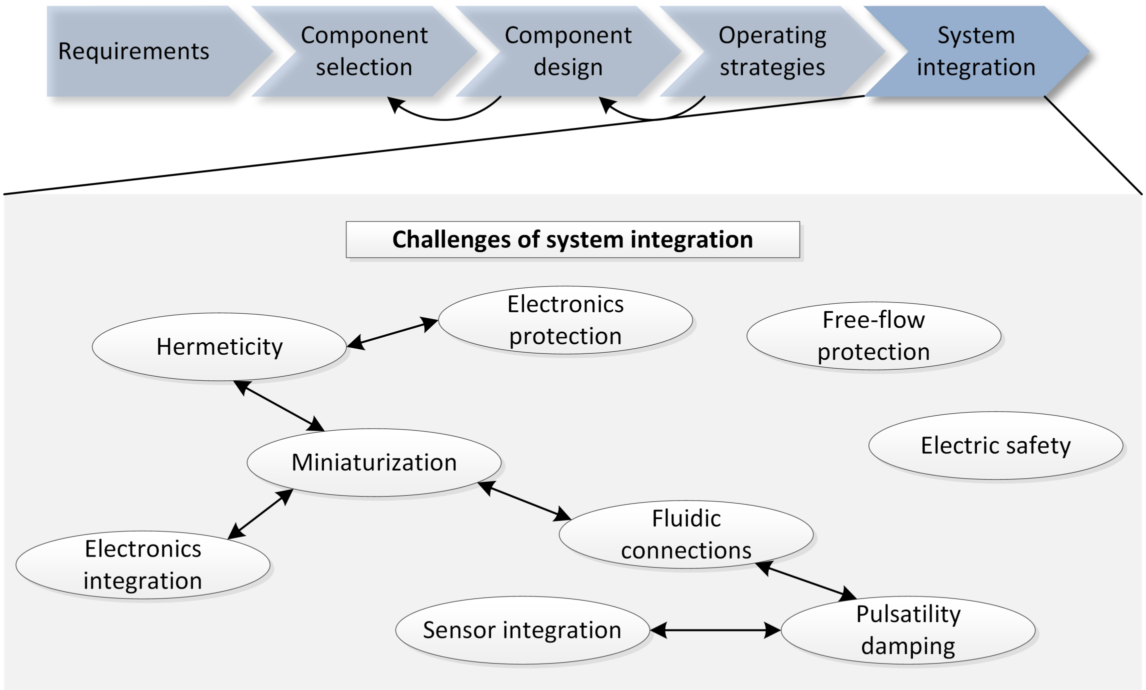

Figure 2.5: System integration challenges.

3 Performance behavior of micropump systems

Performance is understood as the functional characteristics of a system. For dosing systems this applies for the conversion of electrical energy to fluid flow and pressure. The resulting key performance indicators of liquid dosing systems are summarized in Table 2.1. For an efficient and accurate design, the behavior of micropump systems needs be comprehended and models are required for simulations. While good quasi-static models exist for actuator and valve deformation, appropriate dynamic models for actuator and pump, quasi-static models for valve flow as well as gas pressure ability are still missing and had to be developed. Together, they were used to evaluate the performance of micropump systems.
Piezoelectric diaphragm actuator with passive flap valves were employed for their high pressure ability and flow conversion efficiency. The system performance of the piezoelectric driven micropump based dosing systems depends on the control signal of the actuator and is passively influenced by the chamber, the valve, the fluidic path and environmental conditions (Figure 3.1). The design dependencies and limitations of piezoelectric actuators was investigated with measurements and simulations. The big signal behavior of silicon diaphragm actuators was identified, stress limitations were evaluated and the influence of geometric design on displacement volume at working pressure, maximum pressure ability, as well as conversion efficiency and cost aspects were investigated. For the flap valve, a parametrized fluid-structure-interaction (FSI) FEM-model was developed, validated with measurements and compared to available analytical models. Quasi-static models for excess and suction gas pressure abilities were established and compared to the measurement based practical influence of gas leakage. Optimization potential for design and operating conditions was worked out. For liquid micropump systems, the major flow rate influencing effects were identified (Figure 3.1), being liquid resistive damping, cavitation based gaseous capacitive damping and reactive valve volumes. Applicable analytical and numerical models were combined to a semi-empirical single-stroke based micropump model that is able to accurately simulate the frequency dependent flow rate performance.
Regarding the structure of this chapter, it starts with the piezoelectric actuator (section 3.1), is followed by the flap valve (section 3.2) and the gas pressure ability (section 3.3) and is concluded by the flow rate influencing effects of liquid micropump systems (section 3.4).

3.1 Piezoelectric diaphragm actuator

Compared to other driving principles, piezo ceramics feature high forces at low deformations. Laminating a piezo layer on a passive plate enables the conversion and leveraging of the piezo generated lateral force into a vertical deflection (Figure 3.2). As Herz et. al [34] showed, the deflection can be further increased by adding a lateral constraint to the plate, as achieved by clamping the diaphragm at the outer rim or by attaching the actuator with surrounding diaphragm material to a pump body as done for micropumps. An analytical model, developed by Prasad et. al [83] and extended by Herz et. al [34] provides a well matching description of actuator deformation at a working pressure and will be detailed in the state of

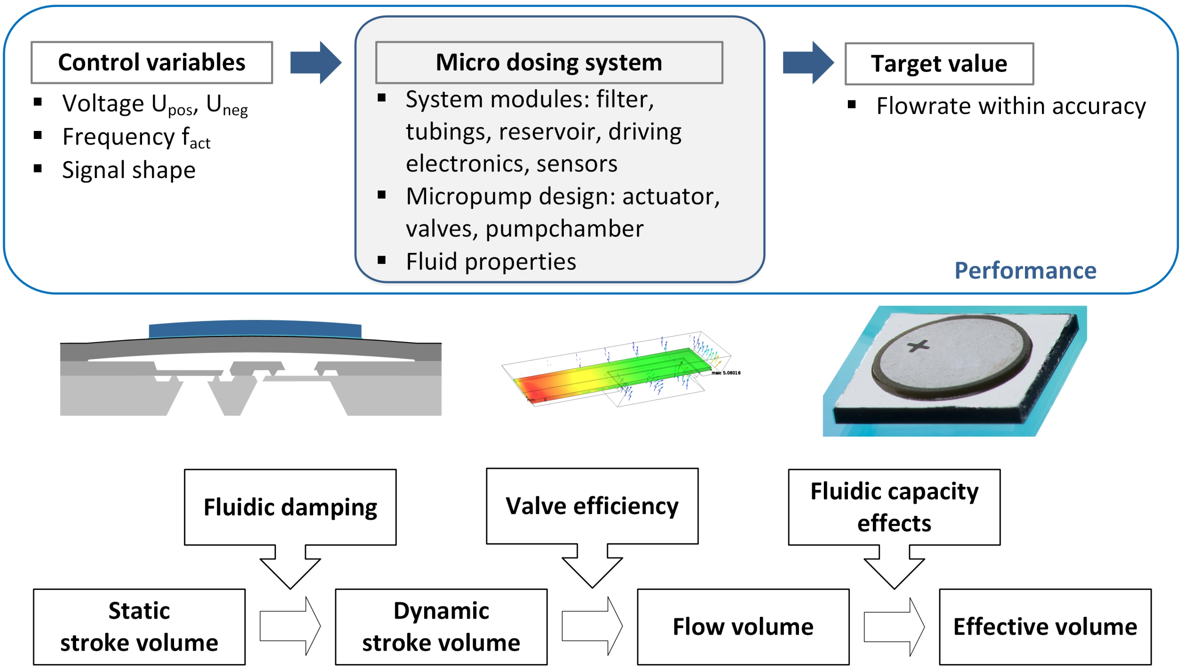

Figure 3.1: Performance aspects of micropump dosing systems.

the art. The model was applied to optimize the displacement volume at a certain working pressure for steel-based pumps and to give guidelines for the actuator design. However, the model holds the potential to also optimize further performance aspects including limitations for stroke volume optimization, the blocking pressure and the electric-mechanic conversion efficiency. Taking micropump as a whole with chamber and valves into account, the model can be extended for considerations regarding flow rate and gas pressure, as well as reliability aspects like pressure sensitivity, temperature sensitivity and bubble tolerance.

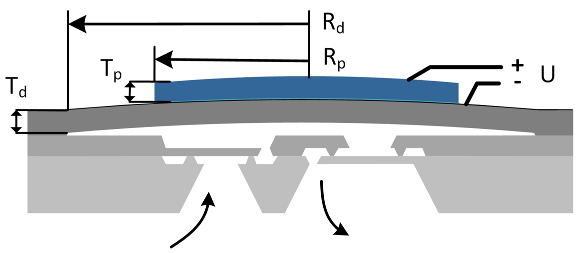

Figure 3.2: Micropump cross-section with main geometric actuator parameters: diaphragm thickness T_d, diaphragm radius R_d, piezo thickness T_p, piezo radius R_p, voltage U.

State of the art

The type of actuator used for this work (EMFT micropumps - section 1.2) is a circular axisymmetric piezoelectric unimorph, where the piezo ceramic is attached to a silicon diaphragm with two-component epoxy resin adhesive. The analytical model was mainly developed by Prasad [84, 83] and is based on Kirchhoff's thin plate theory and Timoshenko's Classic Laminated Plate Theory (CLPT) [85]. To apply CLPT the following assumptions need to be satisfied [34, 66]:

1. Materials are linearly elastic and transversely isotropic.
2. Each layer has uniform thickness.
3. Layers are ideally bonded.
4. Plates are thin and transverse deflections are small compared to the plate thickness.

A detailed derivation of the fundamental equations for circular unimorphs was described by Deshpande and Saggere [86]. Herz et. al. enhanced the model by separating the effect of pressure p with fluidic capacitance C_p and electric field E_z with volumetric–electrical coupling coefficient C_E to calculate the displacement volume V_{disp} [34]:

$$V_{disp} = C_E E_z + C_p p \tag{3.1}$$

The model includes a uniformly distributed pressure load at the pump side. Assumptions made in the model are a fixed condition at the clamped edge, a uniform distribution of electric potential and a perfect bond of piezo and diaphragm. The layers of epoxy resin and electrodes were neglected as they are thin compared to the piezo and diaphragm, unlike in the model of Deshpande and Saggere [86]. Due to a similar Poisson's ratios ν of silicon (~0.27) and piezo ceramic (~0.34), the ratio was set to be equal to strongly simplify the model. Analytical predictions of the displacement were validated both with FEM and experimentally by Prasad and Herz, as well as by other authors that used the CLPT model to find relations of geometry or material properties for their optimization purposes [83, 34, 86, 87, 88].
Herz et. al showed, that the ideal actuator features an infinitesimally thin diaphragm with a piezo radius reaching the diaphragm radius [34], i.e. the actuator is only attached to a circular supporting edge. As a direct circular line attachment of the piezo is not feasible, a diaphragm layer is always required. Though, minimum membrane thickness and ratio of piezo to diaphragm radius are limited by (1) the maximum yield strength in the outer rim of the diaphragm, (2) the positioning tolerances while mounting the piezo disc and (3) excess adhesive from the mounting process. Therefore two optimization procedures were proposed [34]. First, for given diaphragm thickness and radius, only the optimum piezo geometry has to be determined. Or, second, for given diaphragm and piezo radius, only the thicknesses of both parts have to be determined .

Research goal

For silicon micropumps these two optimization procedures stay valid. However, applicability of the model has to be validated for the different materials of diaphragm and piezo. Furthermore, the statements regarding the influence of stress that limit the design space need to be investigated. Even though the diaphragm radius is included as a variable in the model, its influence on pump performance has not been evaluated, yet. As it defines major pump performance parameters, the limitations concerning the optimization of the stroke volume need to be given. Besides the stroke volume limitations, the blocking pressure and the electric-mechanic conversion efficiency are important requirements for micro dosing systems and the model is used to evaluate these.

Methods

The analytical model exists in the program 'Wolfram Mathematica' and core equations for line displacement, displacement volume and internal stresses are used for further evaluations and process automation. For both measurements and simulations, a MIKROAUG micropump was used as reference (section 1.2). The center displacement of the actuator was calculated from the measured line displacement of the actuator at different voltages. A profilometer from FRT (appendix A) was used with an accuracy of +-0.1 µm and a range of 300 µm in combination with a xy-table. The pressure was varied in the pump chamber with the external pressure controller Mensor CPC3000 (appendix A).

Results

Model validation for silicon actuator With changing materials and different elastic behavior of silicon compared to steel diaphragms, the model predictions need to validated. The model gives two key parameters for the displacement volume, the volumetric–electrical coupling coefficient C_E and the fluidic capacitance C_p. Here, C_E describes the constant of linear displacement for applying an electric field of E_z. For the reference MIKROAUG pump with a piezo thickness T_p of 150 µm, the voltage ($U = E_z T_p$) can be varied between E_{neg} =-60 V and E_{pos} =+300 V (equivalent to notation 'n60p300' and '-60|+300 V') for allowed electric fields of -0.4 kV/mm and +2 kV/mm. The resulting center displacement of the actuator (Figure 3.3) is subject to a hysteresis effect and a big signal behavior due to the piezo characteristics [89]. The kink of the center displacement can be explained with the actuator touching the pump chamber boundary. While the model assumes a linear dependency, a square correction has to be added to fit the real displacement (Figure 3.4):

$$z_A = C_E E_z + \delta_E E_z^2 \tag{3.2}$$

The volumetric–electrical coupling coefficient C_E, calculated from the model gives 6.12 $\frac{\mu\text{m}\cdot\text{mm}}{\text{kV}}$ and describes the initial inclination well. Using that value together with the square correction factor δ_E of 0.675 $\frac{\mu\text{m}\cdot\text{mm}^2}{\text{kV}^2}$ a well matching description for the whole electric field range is reached.

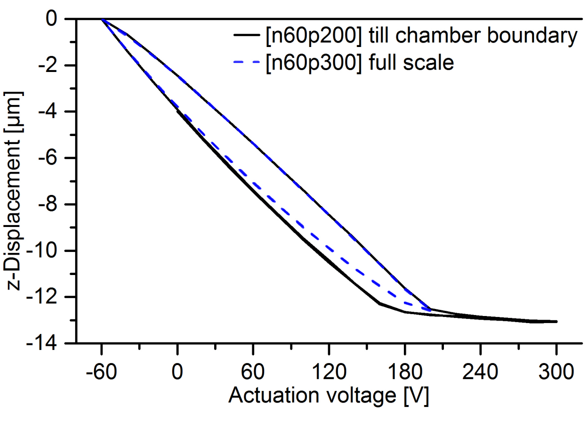

Figure 3.3: Measured center displacement of the MIKROAUG reference pump over actuation voltage to reach the chamber boundary (-60 V to +200 V) and full scale (-60 V to +300 V).

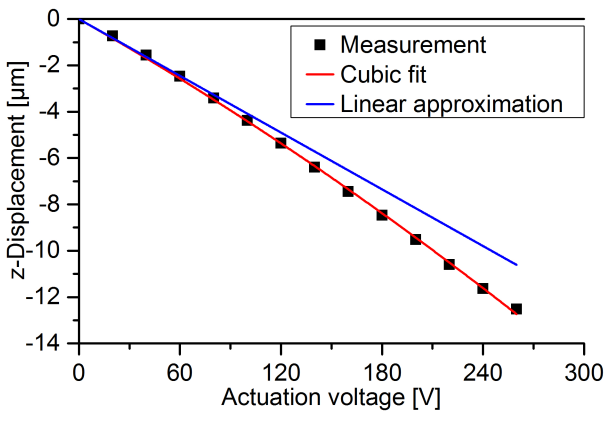

Figure 3.4: Measured big signal displacement over voltage with linear approximation of standard model and cubic big signal fit correction.

For the evaluation of C_p, the pressure was varied in steps from 0 kPa down to -88 kPa with respect to ambient pressure (Figure 3.5). To avoid the influence of piezo hysteresis on the measurements, the full voltage cycle was always carried out twice. The resulting change of actuator displacement against applied pressure was evaluated with respect to the pump chamber boundary and shows a linear dependency over pressure (Figure 3.6). While the model calculates a C_p of 0.072 µm/kPa, the measurement exhibits 0.078 µm/kPa. A potential pressure hysteresis of the actuator was evaluated as well, but lead to no significantly measurable hysteresis behavior for a sensor accuracy of +-0.1 µm. As the measurements show, the independence of C_E and C_p is given , but a cubic big signal correction needs to be applied to calculate the right center displacement values.

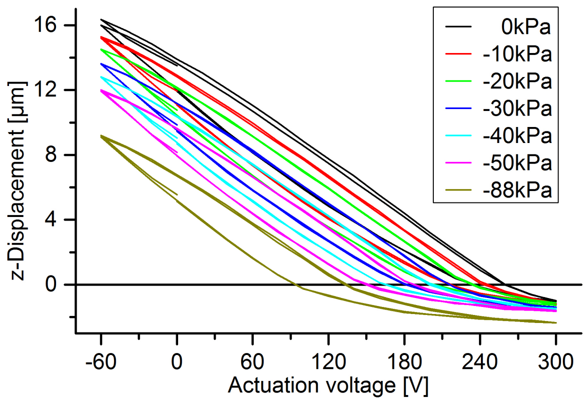

Figure 3.5: Center displacement (C_E) for varying applied suction pressure levels.

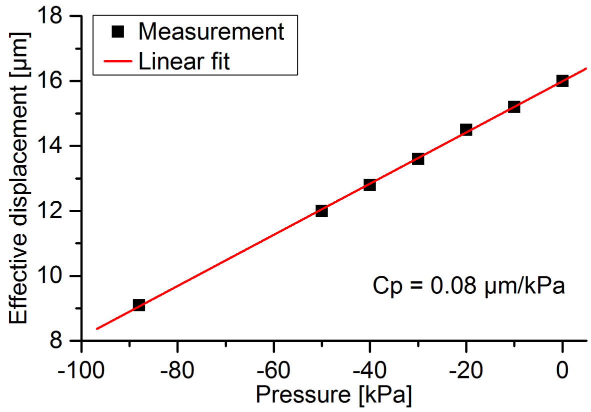

Figure 3.6: Actuator pressure sensitivity (C_p) of center displacement.

With the basic model validated for silicon actuators, the line displacement of measurement and simulation was compared (Figure 3.7), while the simulated maximum displacement was corrected with the big signal correction. Measurement and simulation show good accordance, with deviations in the range of the sensor accuracy (appendix A). Integrating the simulated line displacement gives the displacement volume (Figure 3.8).

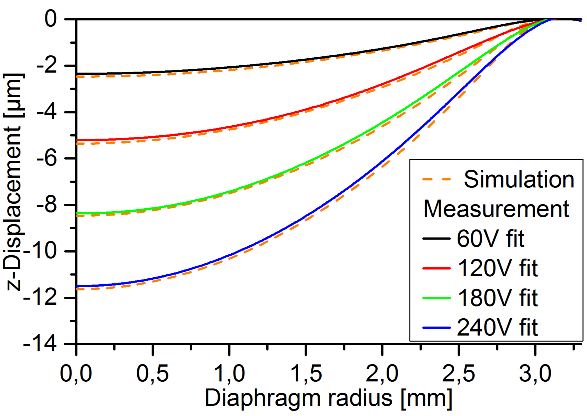

Figure 3.7: Comparison of measured line displacement its and big signal corrected simulation for voltage differences of 60/120/180/240 V.

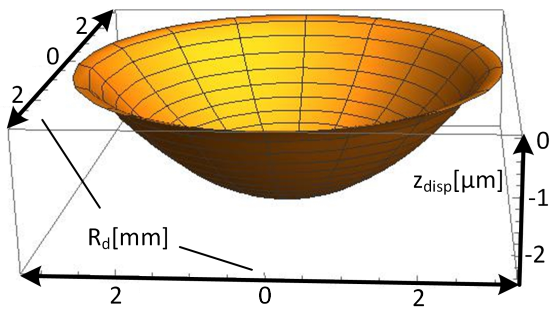

Figure 3.8: Simulated 3D displacement by rotation of the line displacement, enabling the calculation of the displacement volume.

Stress limitations As piezo ceramics feature high forces that have to be transmitted by thin silicon diaphragms, the issue of stress related ruptures may arise. For current micropump designs (compare to 1.2) no systematic diaphragm failures were observed if operated at specified conditions. However, the whole design space covers regions of higher stresses that may exceed the yield strength of piezo or silicon. To evaluate the existing safety margin under practical conditions, intentional ruptures of micropump actuators were provoked by leaving the specified electric field levels. In order to understand the critical regions of the actuator, both the internal stresses of the rupture condition and subsequently varying design parameters were simulated with the actuator model.

Out of five micropump actuators, two ruptures of the diaphragm occurred at the outer rim while increasing the electric field to -1.2|+6 kV/mm at a 10 µm-predeflected MIKROAUG actuator, which corresponds to effectively -2.2|+5 kV/mm for a non-predeflected actuator. The internal stresses of this pump design and operating conditions were simulated in radial and circular directions from the actuator model. The simulations confirmed that the critical highest tensile stresses appear at the outer rim in radial direction. For a negative electric field, the diaphragm is subject to compression, only the upward bending leads to tensile stresses up to 0.05 GPa, with the highest value at the bottom side of the diaphragm. For a positive electric field, the diaphragm is subject to tension, which is increased at the upper side due to downward bending and usually features the highest tensile stresses of up to 0.5 GPa. The influence of bending curvature is usually higher than from the general compression and tension stresses from the piezo ceramic, but downward bending is limited to the pump chamber boundary. Even though the yield strength of monocrystalline silicon is at 7 GPa, in reality, defects and microcracks from wafer processing lead to lower effective yield strengths. Especially the grinding process of the top diaphragm side leaves microscopically observable microcracks behind. Internal stresses towards upper and lower actuator position are within the same order of magnitude for the predeflected actuator, but the effectively higher positive electric field, together with the processed top surface makes a diaphragm rupture more likely in the lower turning point.

The MIKROAUG pump was used as starting point for the simulations and piezo radius, piezo thickness and diaphragm thickness were varied. From the rupture evaluation it is clear that the most critical tensile stresses occur at the outer rim of the diaphragm in radial direction and the highest values are reached at the maximum positive electric field of 2 kV/mm, even for a predeflected actuator. Therefore, simulations feature the radial stresses of the outer diaphragm annulus at 2 kV/mm electric field. In the first simulation, the piezo radius Rp was varied between 2.7-3.1 mm, while keeping the diaphragm radius constant (Figure 3.9). The resulting stresses increase drastically with increasing piezo radius, and reach critical values (0.5 GPa) at a ratio of 98 %. In the second simulation, the diaphragm thickness was varied between 10-150 µm, keeping the radii of diaphragm and piezo constant (Figure 3.10). Here stresses slowly increase until 70 µm and decrease for higher thicknesses. The decreasing tensile stresses at thinner diaphragms can be explained by a decreasing influence of the bending curvature due to a very elastic outer diaphragm rim. However, this design direction leads to an increased local fluidic capacitance of the actuator. In the third simulation, the piezo thickness was varied between 50-300 µm, while keeping all other parameters constant (Figure 3.11). Even though thicker piezo ceramic discs provide higher forces, they do not lead to higher tensile stresses, as the bending is reduced due to the increased actuator stiffness.

It can be concluded that bending leads to much higher critical tensile stresses than pure tension due to lateral piezo deformation. Though, internal stresses should not become a problem for the diaphragm

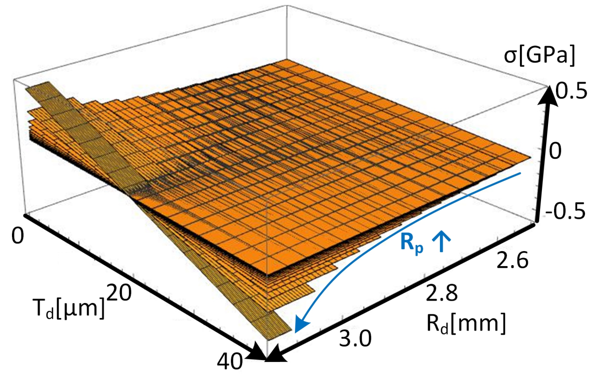

Figure 3.9: Internal stress of outer diaphragm rim over diaphragm thickness T_d at variable piezo radius R_p (2.7-3.1 mm) and constant diaphragm radius R_d.

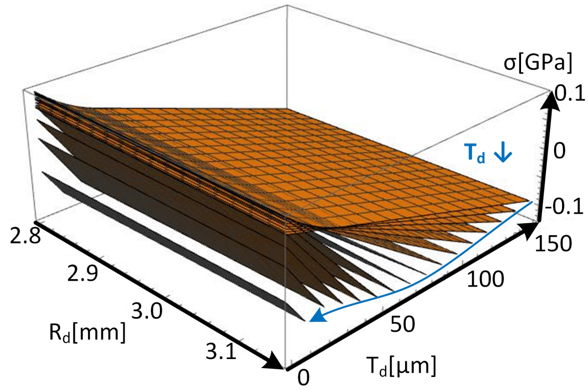

Figure 3.10: Internal stress of outer diaphragm rim over diaphragm thickness T_d at variable diaphragm thickness T_d (10-150 µm).

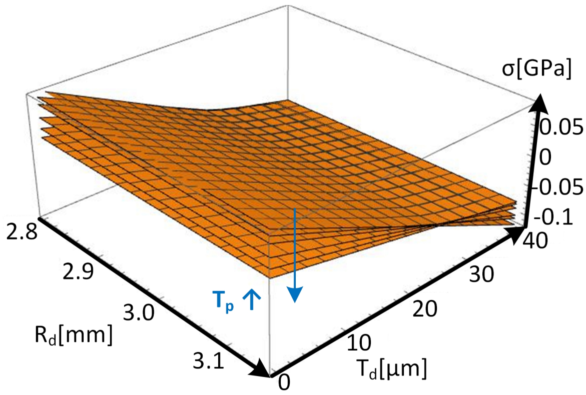

Figure 3.11: Internal stress of outer diaphragm rim over diaphragm thickness T_d at variable piezo thickness T_p (50-300 µm).

if operated under standard conditions of the electric field of -0.4|+2 kV/mm. However, if the desired actuator efficiency of the actuator rises, the stresses may exceed practical yield strengths of grinded silicon diaphragms. Regarding the piezo ceramic, cracks were observed under strong bending, but are of highly spread statistic distribution and will be further discussed in the reliability section 4.1.1.

Standard optimization procedure The standard actuator optimization procedure for silicon pumps starts with defining the pump size with diaphragm radius R_d and the outer surface to reliably attach the diaphragm to the pump body, considering the governing positioning tolerances. The diaphragm radius defines the order of magnitude for the displacement volume, which is proportional to R_d^4 (Figure 3.12 - black). With linearly increasing working pressure of 20 kPa steps, the displacement volume decreases exponentially (Figure 3.12). The optimization towards maximum displacement leads to increased piezo thicknesses with rising working pressure and diaphragm radius (Figure 3.13). The diaphragm thickness was kept constant at 40 µm. The value of diaphragm thickness T_d was chosen, because for grinded and etched silicon wafers a practical lower limit of currently ~40 µm leads to reliable operations. Again, optimizing for displacement volume and comparing the liquid pressure ability to the displacement volume, reveals the opposing design direction regarding the diaphragm radius (Figure 3.14). Regarding the fluidic performance, a larger diaphragm radius is always preferable (Figure 3.15). However, the maximum displacement volume for a new actuator design needs to be chosen carefully, because it not only affects the maximum flow rate and the minimally available single stroke volume at constant voltage levels, but also strongly influences pump costs, energy efficiency and system size at pump and electronics. In order to understand the influences of diaphragm thickness and piezo geometry on the different optimization goals, they are evaluated individually.

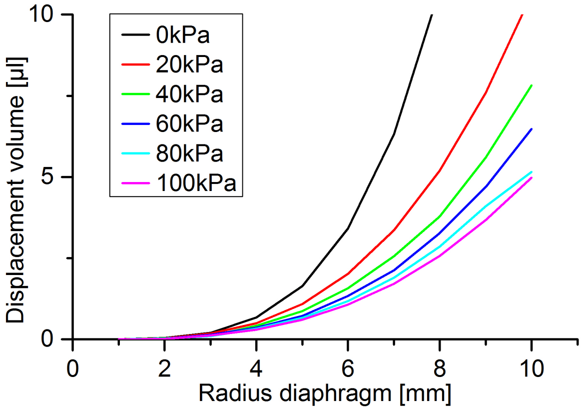

Figure 3.12: Simulation of optimized displacement volume at different outlet working pressure levels.

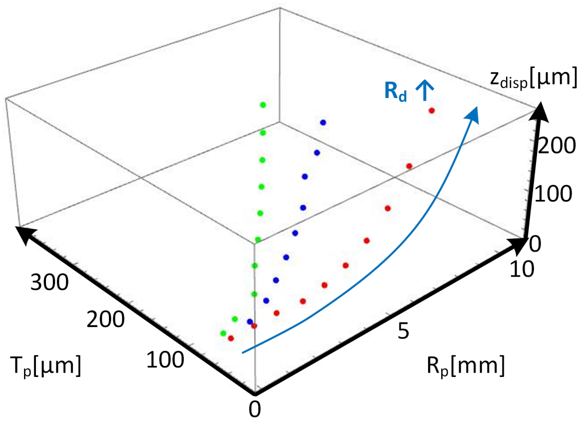

Figure 3.13: Simulation of optimized displacement at piezo radius and piezo thickness for different outlet pressure levels (red 0 kPa, blue 20 kPa, green 40 kPa).

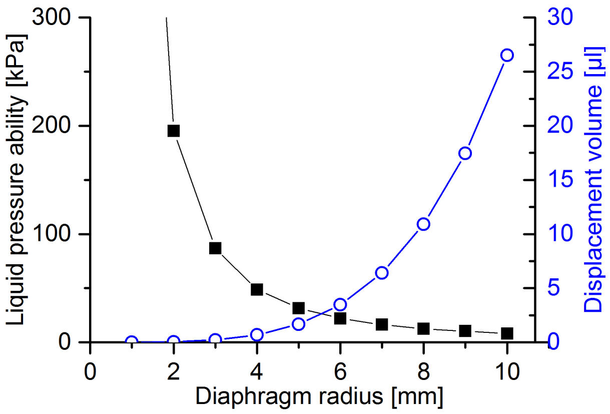

Figure 3.14: Simulation of optimized liquid pressure ability and displacement volume for increasing diaphragm radius (outlet pressure 0 kPa).

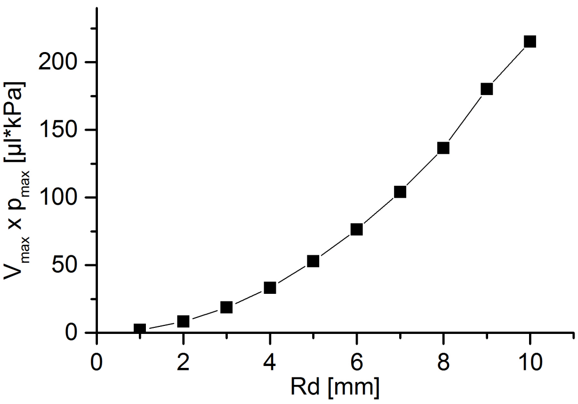

Figure 3.15: Multiplication product of simulated liquid pressure ability and displacement volume for rising diaphragm radius (optimized for displacement volume, outlet pressure 0 kPa).

Displacement volume at working pressure As long as there is a known constant or average working pressure, it needs to be considered while optimizing the displacement volume. Optimizing the piezo geometry for the MIKROAUG diaphragm dimensions of $R_d = 3.15$mm and $T_d = 40$µm towards maximum displacement volume gives $R_p = 2.77\,\mathrm{mm}$ and $T_p = 76.8\,\mu\mathrm{m}$ with a ratio of $R_p/R_d = 87.9\,\%$ (Figure 3.16). For higher piezo radii, the volume increases very fast. If tolerances of piezo or positioning are in a critical range, the piezo radius should be chosen smaller, to give a higher error margin in the direction of lower volume change. Varying the diaphragm thickness shows that, the maximum volume is proportional to $\sim T_d^x$ and should therefore be minimized (Figure 3.17).

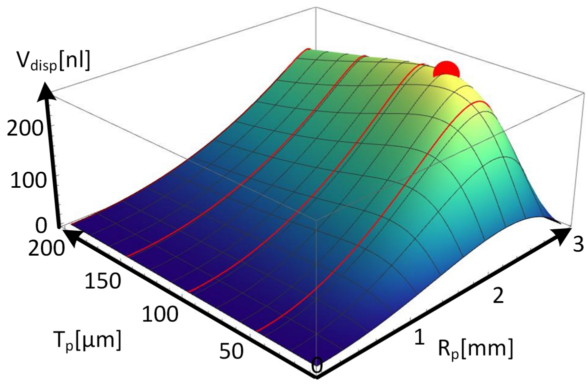

Figure 3.16: Displacement volume with respect to piezo thickness and radius at constant diaphragm geometry (red lines - indication of 50 µm piezo thickness steps, red point - highest volume).

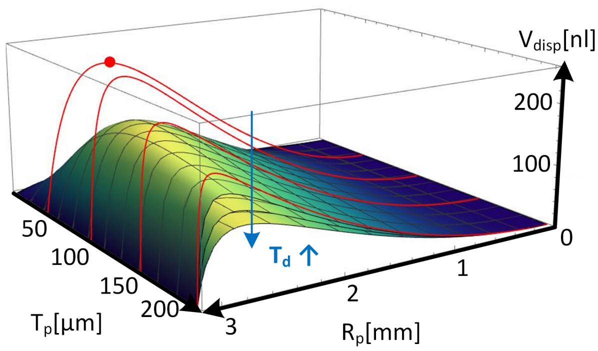

Figure 3.17: Displacement volume with respect to piezo thickness and radius for increasing diaphragm thicknesses (40(red lines)/60/80/100 µm) at constant diaphragm radius (red lines - indication of 50 µm piezo thickness steps, red point - highest volume).

Pressure ability / blocking pressure The maximum pressure ability gives the blocking pressure where no displacement volume can be generated due to an applied counter pressure at the outlet. Plotting the maximum pressure ability with respect to the piezo geometry at otherwise constant diaphragm geometry (MIKROAUG diaphragm dimensions of R_d=3.15 mm and T_d=40 µm) shows the highest values for increasing piezo thicknesses in general and keeping the piezo radius converging towards the diaphragm radius (Figure 3.18). As evaluated under 'stress limitations', an increasing piezo radius towards the diaphragm radius may results in critical stresses. In addition positioning tolerances of the piezo discs may aggravate the issue. Both factors are important to consider for the design choice. With rising diaphragm thicknesses, the pressure ability also increases (Figure 3.19). Though, it is noteworthy that the increase of pressure ability is decaying with increasing T_d (Figure 3.20), i.e., it is more efficient to increase piezo thickness than diaphragm thickness.

Efficiency For a balanced actuator design, not only fluidic, but also electric characteristics are important. Especially the power consumption is critical for many implants, running on a battery. Therefore, the conversion efficiency of electric energy to fluidic work was investigated. The energy of a circular capacitor as displayed by the piezo electrodes is given by:

$$W_C = \frac{1}{2}CU^2 \tag{3.3}$$

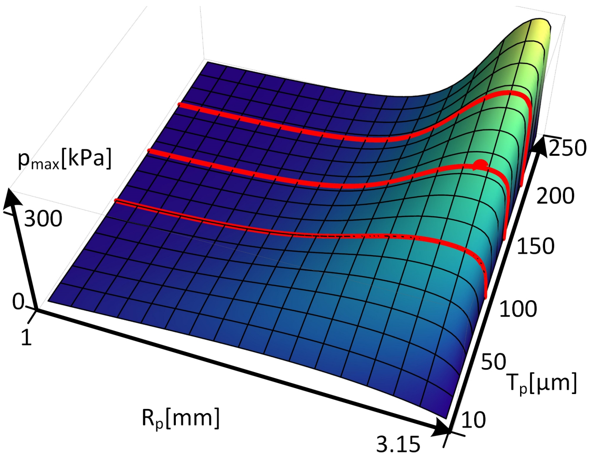

Figure 3.18: Pressure ability with respect to piezo thickness and radius at fixed diaphragm geometry: R_d=3.15 mm, T_d=40 µm (red lines - indicating 100/150/200 µm piezo thickness.

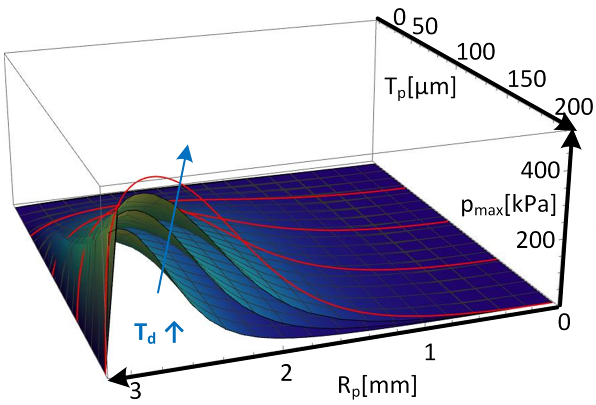

Figure 3.19: Pressure ability with respect to piezo thickness and radius for increasing diaphragm thickness (40/60/80/100(red lines) µm).

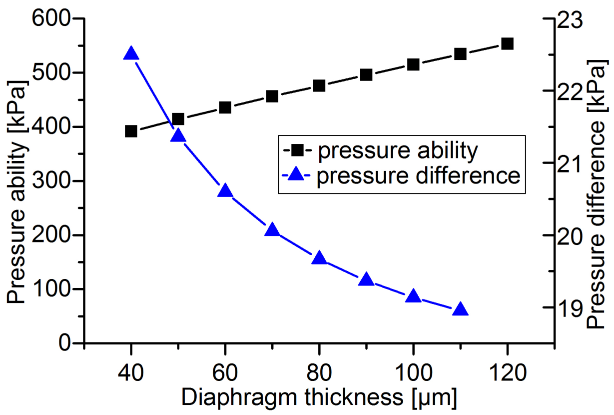

Figure 3.20: Pressure ability and pressure difference increment between each step over diaphragm thickness.

Here, the capacitance C of the capacitor is:

$$C = \varepsilon_0 \varepsilon_r \frac{A_e}{T_p} \tag{3.4}$$

, where $\varepsilon_0 = 8.85 \times 10^{-12}\,\frac{\mathrm{As}}{\mathrm{Vm}}$ is the vacuum permittivity, ε_r is the material permittivity, A_e is the electrode area and T_p is the piezo thickness. Combined with the applied voltage U:

$$U = E_z T_p \tag{3.5}$$

the energy stored in the capacitor equals:

$$W_C = \frac{1}{2} \varepsilon_0 \varepsilon_r R_p^2 \pi T_p (E_{pos}^2 + E_{neg}^2) \tag{3.6}$$

On the other hand, the fluidic work is defined by the multiplication of working pressure and displaced volume:

$$W_f = p_w V_{disp} \tag{3.7}$$

The optimization directions are either the piezo geometry or the electric field levels. From Equ. 3.1, the linear dependence of displacement volume with respect to the electric field strength is known. With the square dependence of the charging energy (Equ. 3.6) versus the electric field strength, it is obvious that the efficiency would benefit from a minimization of the electric field, though, limiting the displacement volume and pressure ability of the actuator. A minimization of R_p and T_p leads to minimized energy, whereas the displacement volume reveals a different maximum (Figure 3.21). Comparing the electric energy of charging the piezo capacitor and the fluidic work performed gives the electric-fluidic conversion efficiency:

$$\eta_{ef} = \frac{W_f}{W_C} \tag{3.8}$$

For rising working pressures of 10/60/110 kPa, the efficiency increases from 6 % up to 9.5 % (Figure 3.22). With a working pressure of zero, no effective fluidic work is calculated, as it only temporarily encounters a transient pressure. However, the desired function of delivering a liquid is still provided for. In this case a modified volume conversion efficiency should be calculated, including only the displacement volume instead of the fluidic work:

$$\eta_{eV} = \frac{V_{disp}}{W_C} \tag{3.9}$$

At 0 kPa counter pressure, the volume conversion efficiency (Figure 3.23) favors an increase of piezo radius over the increase of piezo thickness, as the reduction of efficiency is considerably smaller.

Costs Another aspect of actuator design are the costs of the piezo ceramic, as it has a significant share compared to the silicon pump body. Besides the processing technology, the amount of material volume has the largest impact on piezo costs. Comparing the volume or fluidic work to the piezo volume, gives the same design guidelines as for the standard conversion efficiency, because the volume of the ceramic gives $V_p = R_p^2 \pi T_p$, hence the same piezo geometry dependence as for the electric energy, which is required to charge the capacitor. Only the absolute values differ.

For the silicon pump body, the main influence on costs is the required lateral area as it determines the amount of chips per wafer and thus the efficiency of parallel wafer batch processing. The diaphragm radius R_d together with the surface that attaches the actuator to the pump body defines the area for each pump chip. While the required displacement volume implicitly defines the diaphragm radius, it is more important to optimize and tailor the actuator to the applications needs, than to minimize costs.

Discussion

In the presented work, various goals of piezoelectric actuators are evaluated that lead to different optimization directions of piezo and diaphragm geometry. The application determines the emphasis of the actuator design, which is why no clear design guidelines can be given. The standard procedure of actuator design starts with the predefined parameters and the remaining aspects can be optimized towards displacement volume as well as maximum pressure ability. Limiting aspects are usually maximum voltages,

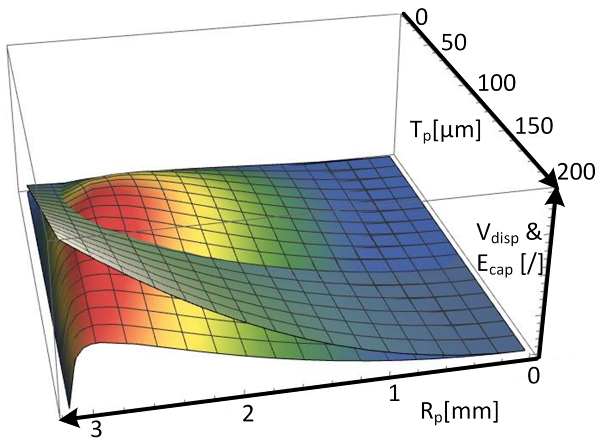

Figure 3.21: Comparison of simulated (dimensionless) displacement volume (blue-yellow-red) and capacitor charging energy (blue-green) with respect to piezo thickness and radius at -0.4|+2 kV/mm electric field strength.

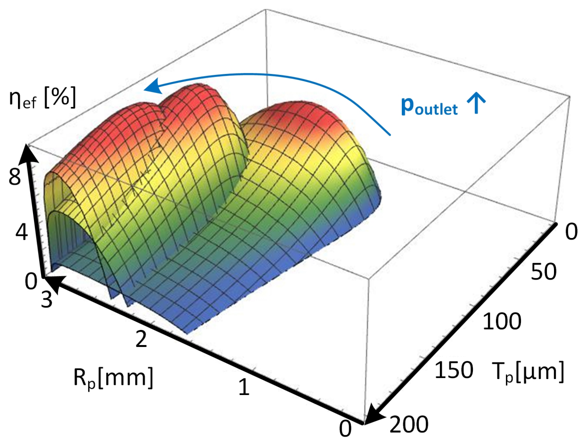

Figure 3.22: Electric-fluidic conversion efficiency with respect to piezo geometry (R_p, T_p) at increasing outlet working pressure levels (10/60/110 kPa).

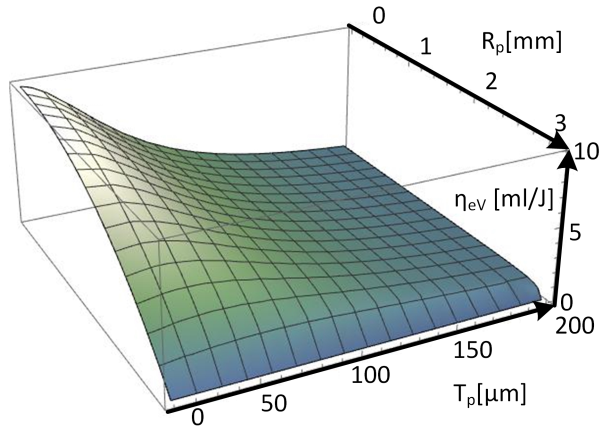

Figure 3.23: Volume conversion efficiency over piezo thickness and radius at 0 kPa.

maximum electric field strengths, power consumption or size and cost constraints.

The actuator model, developed by Herz et al. [34], provides the foundation for most of the evaluations in this section. The model accuracy was evaluated by comparison to measurements and FEM simulations [34]. The predicted center deflection of the analytical model matches the measurements well and only starts to significantly stay below for deflections of more than 50 µm for a 12.5 mm radius of a brass diaphragm. This affects the deformation at applying pressure as well as electric field. The deviations can be explained by leaving the conditions for CLPT, where transverse deflections are small compared to plate thickness. In addition, Herz et al. mentioned increasing deviations of more than 7 % for working pressures of lower than 50 kPa, while comparing optimized stroke volumes of analytical model and FEM simulations. They were explained by the effect of non-linear material behavior. The evaluation of model accuracy mainly focused on a large design space of different geometries and material parameters, together with the optimization of stroke volume at a constant working pressure.

As the materials and dimensions of the investigated micropumps are different, the model was reevaluated by comparing the simulations of line displacement, center displacement, volumetric–electrical coupling coefficient C_E and fluidic capacitance C_p to measurements. A square fit based big signal correction was introduced to describe the center displacement for increasing electric field strength. Together with the big signal correction, very good agreements of simulations and measurements were reached for a working pressure of 0 kPa. A sole optimization of stroke volume at working pressure is not expedient for many applications. Therefore, the model was utilized to evaluate the most relevant aspects of geometric actuator design.

First, the critical tensile stress in radial direction was investigated for different geometries of the circular actuator. While no issues emerged in the experimentally tested design space, ruptures can be provoked by leaving the specified electric field levels and generating critical stress levels (0.5 GPa). Simulations revealed the main dependencies and directions of increased stresses. Even though, the theoretical yield strength of monocrystalline silicon (7 GPa) is not exceeded, microcracks from fabrication processes, like grinding, can reduce the practical yield strength by a order of magnitude and thereby reach critical stress levels.

The proposed standard optimization procedure has to start with the diaphragm radius. It provides the highest influence for defining displacement volume and pressure ability and has to match the application needs. These characteristics and the dependency of working pressure on optimum piezo geometry were simulated to provide a well matching starting point for the actuator design. From there, additional design choices can be made.

Subsequently, the individual key performance indicators were investigated, being displacement volume, pressure ability, conversion efficiency and costs. The connections between these performance goals and diaphragm thickness, piezo thickness, piezo radius and additional aspects were visualized and explained. It can be stated that the diaphragm thickness should be chosen as thin as possible for higher displacement volume and efficiency. To keep a high displacement volume, but increase maximum pressure ability, the piezo is to be made thicker, while keeping a slowly rising ratio of piezo to diaphragm thickness of about 80-90 %. Addressing the conversion efficiency of the actuator, the presence of working pressure is an important factor. For a working pressure above 0 kPa, the simulations reveal a small design space of significant conversion efficiency of up to 8 % for 110 kPa, otherwise it is close to zero. If no working pressure, but only transient pressure due to fluidic resistance, is present, the calculation of standard conversion efficiency provides no useful information. Therefore, a volumetric conversion efficiency was introduced to connect energy consumption to displacement volume. The latter leads to the same design direction as the influence of piezo geometry on costs. For silicon batch fabrication, the piezo is often the single most expensive part. To reduce its costs by reducing piezo volume can be a desired optimization direction, if other performance requirements can easily be matched.

Conclusion

In literature, so far, only center displacement or displacement volume at working pressure was optimized for piezo actuators. However, additional performance goals are required for applications. These can be a blocking pressure to remove, for instance venous obstructions at the outlet, specific voltage levels, electric-fluidic conversion efficiency to minimize power consumption of systems running on battery, or size and cost aspects regarding the dimension of the diaphragm or the volume of the piezo ceramic. The given basic design guidelines for each performance aspect facilitates an application-specific design. However, usually, a multitude of these requirements with different priorities have to be addressed with the actuator design. In addition, once combining the actuator with the pump body, including pump chamber and valve, further and higher-level aspects such as flow rate and gas pressure ability have to be considered. On a system level, system efficiency including the electronics for signal generation, usually between 20-80 %, have to be taken into account as well. Besides performance, use of the model will also be made to evaluate reliability aspects like pressure and temperature sensitivity and particle tolerance.

3.2 Micro flap valve

Besides the actuator, the valves are the main performance determining units inside a micropump. They are responsible for redirecting the flow from the inlet to the outlet. Flap valves (Figure 3.24) are chosen for their diode-like behavior, leading to superior redirection efficiency compared to other non-mechanical or diaphragm valves [49]. This work describes the main performance influencing aspects for stand-alone micro flap valves, which are flow resistance, fracture stress limitations, leakage, reactive valve volume and dead volume. Furthermore, the results will help to investigate reliability aspects of the flap valve such as sticking tolerance and particle tolerance (section 4). For this, a new parametrized fluid-structure-interaction (FSI) model was developed to enable an accurate design in a large space. For validation, the results were compared to existing analytical models and experiments. Design guidelines for application specific performance goals of the flap valve are given.

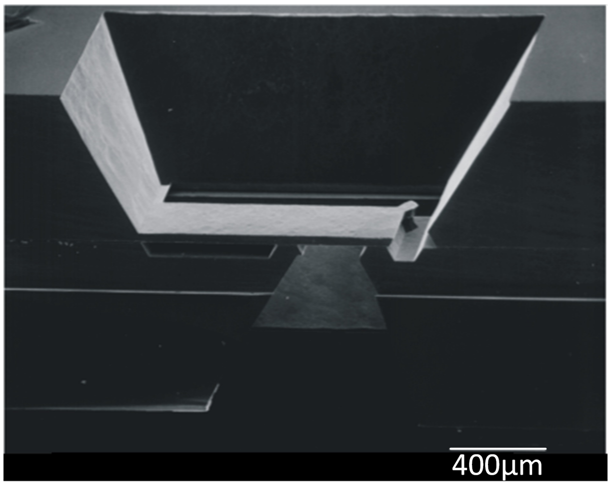

Figure 3.24: Fraunhofer silicon micro flap valve.

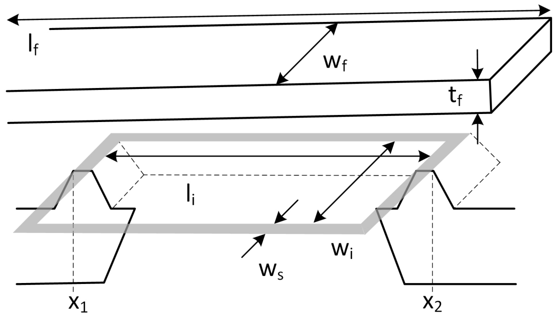

Figure 3.25: Key variables of valve geometry: flap length l_f, flap width w_f, flap thickness t_f, inlet beginning position x_1, inlet end position x_2, inlet length l_i, inlet width w_i, sealing lip gap width w_s.

State of the art

Bending Ulrich and Zengerle provided a comprehensive description of the flap valve behavior by comparing analytical models with FEM simulations and partly measurement data [90]. An accurate bending model, describing the deflection of the cantilever under pressure is based on the equation [90]:

$$\ddot{z}[x] = \frac{-M[x]}{E\, I_y} \tag{3.10}$$

with the torque $M[x]$, the Young's modulus E and the axial area moment of inertia I_y to bend the cantilever around the y-axis, which results in displacement in z-direction. The torque can be calculated with the flap length l_f and the width of the pressure application area w_i by integrating over the pressure distribution $p[x]$ [90]:

$$M[x] = \int_0^{l_f} p[x]\, w_{in} dx \tag{3.11}$$

The area moment of inertia is defined by:

$$I_y = \frac{w_f\, t_f^3}{12} \tag{3.12}$$

with the flap width w_f and the flap thickness t_f.
The pressure distribution under the flap can be approximated as constant and only present at the area within the inlet (Figure 3.25), as the main pressure drop occurs at the gap between flap and sealing lip. A good agreement between analytical model and measurement is reached describing the deflection in steady state at a certain applied hydrostatic pressure [90, 91]. However, at increasing pressure the deflection becomes non-linear, because the diffuser part of the sealing under the flap produces a negative pressure, not accounted for in the model [90].

Flow The known flow models for micro flap valves are the analytical models of gap and orifice flow from Richter [92] and the more accurate semi-empiric model from Ulrich and Zengerle [90] which combines both flow types. The gap volume flow is based on the wall friction of laminar flow with a liquid of dynamic viscosity μ in a channel of width w_c, height z_c and length l_c, described by the law of Hagen-Poiseuille [92]:

$$q = \triangle p \frac{w_c\, z_c[x]^3}{12\mu\, l_c} \tag{3.13}$$

For flap deflections larger than the gap width w_g, the Bernoulli equation is valid and the flow q is dominated by fluid inertia [90]:

$$\triangle p = \alpha_f \frac{\rho}{2} v^2, \text{ with } v = \left(\frac{q}{A_o}\right) \tag{3.14}$$

with the orifice area A_o, the density ρ and the flow profile based flow coefficient α_f. Ulrich and Zengerle separated the areas underneath the flap and assuming inertia dominated flow (Equ. 3.14) for all parts except for friction dominated flow in the sealing lip gap (Equ. 3.13), as it displays the by far narrowest element and features a rectangular shape. Additionally, a loss coefficient was introduced to describe the pressure drop due to fluid friction. However, the loss coefficient had to be determined with a FEM simulation. This semi-empirical model is the the best fitting analytical model known. Though, at an applied pressure of 20 kPa, deviations of up to 30 % are observed.
The best accordance of measurement and simulation was reached by running a 3D FEM simulation coupling the flap deflection and the liquid and solving it iteratively [90]. However, computational performance and automatic coupling possibilities were still quite limited back then, where the work was formed.

Herz and Horsch followed these insights and set up a coupled iterative 3D simulation to determine the flow through their specific valve geometry [66, 91].

Research goal

In order to utilize flap valves in micropumps, various performance and reliability design aspects have to be considered, which are the forward flow, reverse leakage, reactive valve volume, stress limitations and valve dead volume or particle and sticking tolerance. For this kind of optimization, an accurate model describing the valve behavior in a large design space is required.

As there is currently no analytical model available or envisioned to describe the flow of a flap valve directly, a FEM simulation with coupled fluid-structure interaction (FSI) that is solved iteratively, is the method of choice, as explained in the state of the art. While former models in ANSYS required manual coupling, COMSOL offers directly coupled FSI simulations, which is easier to set up and to obtain converged solutions. Therefore, a model should be set up in COMSOL that allows for a large design space of flap valve geometries. To realize the large design space, the model needs to be parametrized for the relevant geometries of the cantilever flap and the inlet pressure application area together with the sealing lip geometry. Considering the various optimization goals, design guidelines and opposing directions need to be pointed out.

Methods

The 3D FSI-FEM model was set up with COMSOL 4.3a. A stationary study together with a fully coupled linear solver was chosen. The number of elements vary, depending on the geometry, but converging solutions for the reference valve were obtained with 48000 elements. Predefined material properties of silicon and water and incompressible flow were selected. The mesh was formed of tetrahedral elements of normal size ate critical structures and extremely coarse size at the surrounding liquid at a hyperelastic mesh smoothing type. The studies were set to a relative tolerance of 10^{-4} or 0.01 %.

In order to be able to evaluate a valve design towards the various parameters, the 3D FSI-FEM model in COMSOL is parametrized. The parametrization allows for a fast adaption of valve geometry and evaluation of flow, bending, stresses and dead volume. The key geometric parameters of cantilever flap dimensions, pressure application area and sealing lip width (Figure 3.25) can be varied, and the remaining geometric parameters to describe the valve in total are adapted automatically. One issue for this kind of simulation is the aspect ratio of the sealing lip gap to the total valve dimensions. To find solutions for the simulation the mesh needs to be of element sizes in the magnitude of the smallest dimensions, in this case several µm. However, total dimensions of several mm cause the number of elements and the solution time to grow too high. Therefore, the mesh had to be configured accordingly with small element sizes in the are of the sealing lip gap and with growing element sizes leading away from it (Figure 3.26). With this setup the simulation can start right after manipulating the geometry and a parameter study can be performed easily in various desired design directions.

Measurement data was obtained by using a pressure controller to apply gas pressure on a liquid reservoir followed by a Coriolis flow sensor. First the resistance of the setup $R_{ref,setup}$ was measured, then a single independent valve was connected between reservoir and flow sensor in forward and reverse direction. The effective flow q_v through the valve was calculated with the applied pressure of the setup $p_{v,setup}$ and the measured flow of the setup $q_{v,setup}$:

$$q_v = p_{v,setup} \left(\frac{p_{v,setup}}{q_{v,setup}} - R_{ref,setup} \right)^{-1} \tag{3.15}$$

The bending model was implemented in Mathematica 10.0, the reference code for the deflection is based on the implementation of Horsch and Herz [66, 91].

Results

A parametric study was performed with the 3D FSI-FEM model, changing either flow or pressure conditions at the inlet. To validate the FEM model, it is compared to analytical models and measurements. First, the pressure distribution along the flap valve was investigated. Due to the highest flow resistance at the narrow gap of the sealing lip, this is the realm of the main pressure drop. The simulations (Figure 3.27) show the main pressure drop for pressure differences up to 9.7 kPa at exactly this position. For higher pressures and different valve diffuser geometries, a negative pressure was observed behind the sealing lip underneath the flap [90], leading to reduced deformation compared to the simplified analytical model that assumes, the inlet pressure applies uniformly and only within the sealing area.

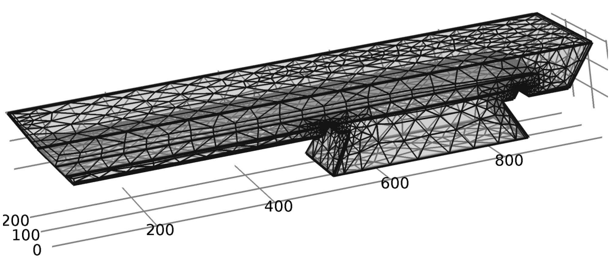

Figure 3.26: Meshing for parametrized FSI model with finer structured mesh around the sealing lip gap area.

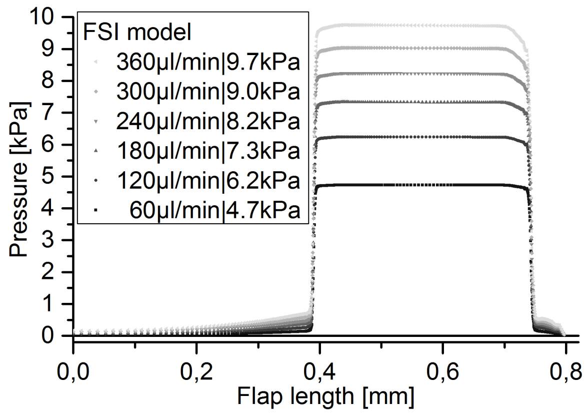

Figure 3.27: Pressure distribution over flap length for different static flow rates.

The flap deflection of the FSI model was verified by comparing it to the analytical model for two reasons, (1) because the bending model is close to reality and was validated before [90], and (2) because it is difficult to measure the flap deflection in water optically. Comparing the measurements to air would be feasible, but might display a different pressure distribution underneath the flap. For varying flow rates of 60-360µl/min through the valve and pressures between 4.7-9.7kPa, the analytical model and the FSI model agree very well, as expected (Figure 3.28).

The static flow through the valve from the FSI model was compared to measurements and simplified gap (Equ. 3.13) and orifice (Equ. 3.14) flow (Figure 3.29). While FSI results show very good agreement with the measurements, the gap and orifice flow both show a strong flow overestimation. In the real valve, beside the laminar friction losses in the sealing lip gap, there are additional friction losses due to vortexes in the diffuser part, which is why real flow is lower [90]. The undesired influence of negative pressure areas due to friction losses can be optimized with the help of evaluating the three dimensional flow field of the FSI model (Figure 3.30).

The stress in the flap can be evaluated with the FSI model as well (Figure 3.30), showing the highest stresses in the area close to the fixation. In the reference valve design, stresses are not an issue, but in former valve designs with longer flaps and higher flows, occasional fractures of the flap close to the fixation were observed. However no reliable experimental data existed or was obtained.

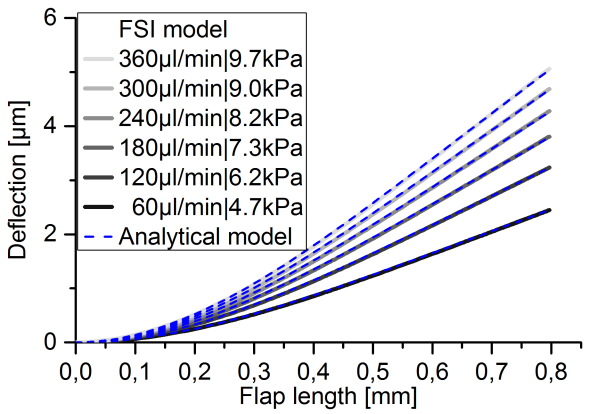

Figure 3.28: Comparison of FSI simulation and analytical model of flap deflection over flap length for different pressure levels.

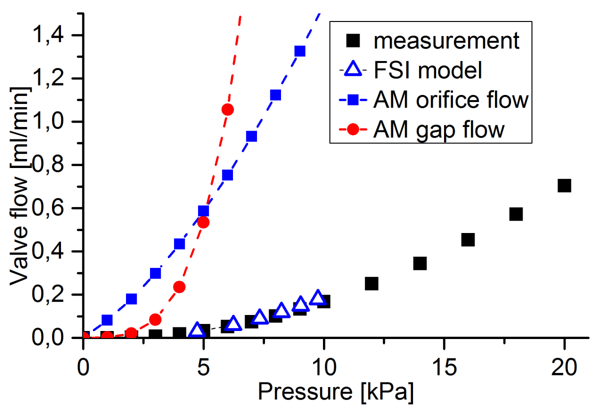

Figure 3.29: Comparison of flow through a flap valve between measurement, FSI model, analytical orifice model and analytical gap model.

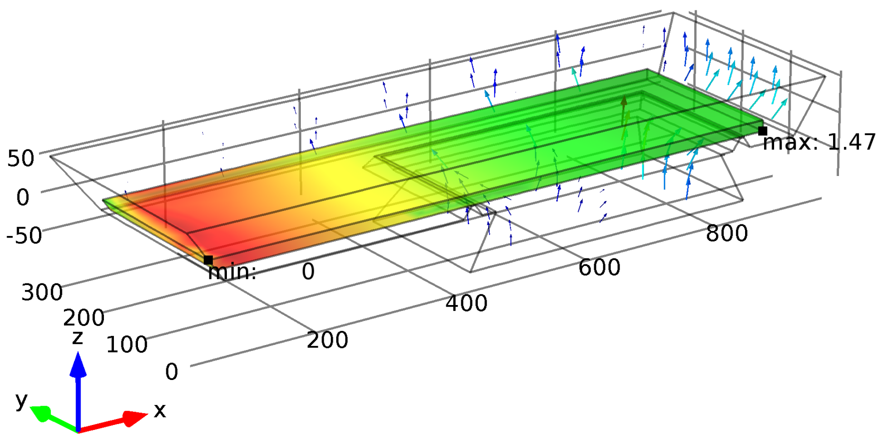

Figure 3.30: Typical evaluation example of flap stresses (red-yellow-green) and flow profile (arrows) for the 3D FSI model.

With the validated model, the different optimization directions and their major influences can be explained. One of the relevant aspects of a valve is the forward flow at a certain pressure. This resistance should usually be as low as possible for higher fluidic performance. The biggest influences on the pressure drop and hence the flow are (1) the bending of the flap and (2) the geometry of the sealing with its gap and diffuser. Bending per pressure can be increased by reducing flap thickness, lengthening the flap and

extending the pressure application area. The losses can be reduced by shortening the sealing lip width or changing the diffuser geometry.
With changing deflection, the cross sectional area for the flow A_{flow} changes accordingly:

$$A_{flow} = w_i(z[x_1] + z[x_2]) + \int_{x_1}^{x_2} z[x]dx \tag{3.16}$$

The pressure application area A_{pa} is:

$$A_{pa} = (x_2 - x_1)\, w_i \tag{3.17}$$

However, with increased flap deflection per pressure, the maximum tensile stress rises in the flap close to its fixation (Figure 3.30). Therefore, forward valve resistance and bending stresses have to be balanced for a safe operation. The flap faces periodic pressure pulses within a micropump and external pressure changes may even add up and lead to critical fracture stress. An additional safety margin needs to be added in such cases. One option to reduce maximum bending is by adding a stopper element, so that the flap is inhibited from bending over a defined boundary. This stopping element could be the actuator diaphragm itself.
Another important performance parameter for valves is the reactive volume capacitance, which results from the closing of a valve. The flap pushes fluid in the backward direction while closing. Additional dynamic leakage may occur. The reactive valve volume C_{flap} mainly depends on the flap deflection and the pressure application area and is defined as the volume beneath the flap and the sealing lip:

$$C_{flap} = w_i \int_{x_1}^{x_2} z[x]dx \tag{3.18}$$

While the valve in reverse direction is closed, static leakage may occur through an initial fabrication based slit at low pressures, and due to surface roughness and uneven deformation of the flap closing the square sealing. While a circular sealing would reduce the slits at flap deformation, the used pressure application area would diminish. To assess the single valve redirection efficiency, the common ratio of forward flow to reverse flow can be used [66, pp. 71].
Besides fluid flow, the dead volume of the valve is a main performance limiting aspect. The flap surrounding volume has no function besides providing a flow channel to the pump chamber. It reduces the gas pressure ability of a micropump and therefore impacts the bubble tolerance and self-priming ability. This volume can easily be extracted from the FSI model. The major influence is the volume in which the flap moves. Theoretically, the inlet valve needs no space above, except for fabrication reasons, as it could move in the space of the moving actuator diaphragm. The dead volume of the outlet valve depends mainly on the pressure application area, which has to be considered for self-priming ability and bubble tolerance, when changing this area.
Certain reliability aspects like particle tolerance and sticking tolerance can be evaluated with this model as well, and is done for in chapter 4.

Discussion

With the parametrized model many different performance and reliability aspects can be evaluated. Unfortunately, many aspects exhibit contradicting optimization directions. Therefore, it is not possible to

give clear overall design directions. However, an application specific design can be carried out. Here, whenever a requirement is predefined, it can be used as a starting point to limit some parameters and find a good balancing trade off for the rest.
In Table 3.1 an overview of the influence of increasing (arrow up) valve parameters on key valve characteristics (effect direction indicated by arrows) is given. Thereby, the necessary design changes for desired optimization directions can be preassessed. For these considerations, the position of the pressure application area is assumed to stay closest to the end of the flap.

Per pressure:	**Deflection**	**Forward flow**	**Reverse leakage**	**Stress**	**Reactive volume**	**Dead volume**
Flap thickness ↑	↓	↓	↓	↓	↓	↓
Flap length ↑	↑	↑	→	↑	↑	↑
Flap width ↑	→	↑	↑	→	↑	↑
Inlet area↑	↑	↑	↑	↑	↑	↑
Sealing lip width ↑	→	↓	↓	→	→	→

Table 3.1: Influence of increasing (arrow up) valve parameter (left column) on valve characteristics (top), indicated by arrows for the direction of effect.

To additionally reduce reverse leakage, the geometry of the sealing can be changed to circular. However, this would require a process change from KOH etching to DRIE etching with further implications on the overall process flow. Furthermore, the lower the frequency and the slower the actuator movement, the higher is the reverse leakage due to time and pressure.
Another constraining aspect is the grinding process of the valve wafer as it leads to microcracks. This currently limits the upper valve wafer to thicknesses of more than 50 µm, even though flap deflections design would allow for a thinner processing. Using DOI wafers would be a solution to this thickness limitation, but would as well change the whole process flow and may require a different wafer bonding process.
As mentioned, in the reference valve design, stresses are not an issue. The theoretical yield strength is 7 GPa, but depending on the fabrication, the real fracture stress can be considerably lower, like 1/100 as for the grinded actuator diaphragm. Though, as the flap is only KOH-etched, no grinding related microcracks occur, which should lead to a practical yield strength closer to the theoretical 7 GPa.

Conclusion

Like for the actuator, the relatively simple flap valve features many important characteristics that have to be addressed, when incorporated into micropumps. The proposed optimization directions lead to revealed partially contradicting design directions. Therefore, the existing constraints from the requirement have to be addressed first and the other aspects can subsequently be optimized and balanced. The developed parametrized FSI model provides an easy and fast evaluation method to investigate different design changes in parametric studies. The limitations and opposing design guidelines were given and discussed. In addition the foundation for the evaluation of the reliability aspects, like particle tolerance and sticking tolerance is provided (chapter 4).

3.3 Gas pressure limitations of micropumps

This section is connected to section 3.1 and section 3.2 and continues the evaluation of the actuator and the valve in the context of the whole micropump. Adding the dead volume of pump chamber and valves allows for the investigation of gas pressures. The gas pressure ability is important for the micropump requirements self-priming ability and bubble tolerance.
The equations to calculate micropump gas pressures were developed. Based on these equations and together with actuator and valve models, pump design dependent simulations of excess and suction pressure are shown. Experimental investigations are compared to the simulations to reveal the actual influence of gas leakage at different driving signal conditions.

State of the art
Gas pressure ability is separated into excess and suction pressure. The pressure ability determines the self-priming ability, being the ability to independently fill the fluidic path with liquid, and the bubble tolerance, being the capability to have a bubble pass the pump. For bubble tolerance and self-priming ability, the micropump suction and excess pressure needs to exceed threshold pressures of valves as well as of in-/outlet ports. While for self-priming ability, air leakage at the outlet valve is a critical factor, capillary forces at a wetted valve can be a critical aspect for bubble tolerance [35, 92]. Exceeding beyond bubble tolerance, bubble independence, as defined by Richter et al. [35], means a constant volumetric flow rate even at a bubble passing through the pump. This can be achieved by driving the pump in a low frequency, where all pressure differences are eventually equalized at the end of pump and supply mode. However, with volumetric pumping, a dead time would still occur, where gas would exit the outlet instead of liquid. Even a bubble remover behind the pump would only remove the gas, but would not change the dead time. These aspects have to be considered if stable or continuous dosing is required.
The exactly required gas pressure ability to achieve self-priming ability and bubble tolerance under varying conditions is not yet understood or emphasis of this work. Therefore, the focus was put on the quantifiable excess and suction pressure as a measure for comparison of pump performance.

Research goal
The goal is to be able to estimate excess and suction gas pressure of the micropump. Therefore, analytical equations together with input from actuator and valve model are needed to simulate the pressure ability. Experiments have to be carried out to help understand deviations to simulated values.

Methods
The simulations are carried out with Wolfram Mathematica 10.0, as for the actuator model. The 3D FSI-FEM valve model in COMSOL 4.3a provided values of the valve dead volume.
For the experimental investigations, a Honeywell 26PCCFA6D pressure sensor (A) was connected to the otherwise sealed pump inlet. The pump was driven by a frequency generator and voltage amplifier (A).

Results

Theory The theoretically achievable gas pressure is limited by the displacement volume at a certain working pressure (Equ. 3.1) and the dead volume, which is defined by the pump chamber and valves (Figure 3.31).
The maximum suction pressure, declared in relation to ambient pressure, is:

$$p_{min,air} = p_{out}\left(\frac{V_{start}}{V_{end}}\right)^{\kappa} = p_{out}\left(\frac{V_{dead,valves} + V_{dead,chamber}[p_{out}, U_{pos}]}{V_{dead,valves} + V_{dead,chamber}[p_{out}] + V_{disp}[p_{min,air}, \triangle U]}\right)^{\kappa} \tag{3.19}$$

with outlet pressure p_{out}, inlet pressure p_{in}, dead volume of valves $V_{dead,valves}$ and chamber $V_{dead,chamber}$, displacement volume V_{disp} and the isentropic exponent κ, which is 1 for isothermal expansion and 1.402 for adiabatic expansion. The displacement volume V_{disp} depends on the voltage levels and the pressure the diaphragm is facing. For a temporarily closed inlet the maximum suction pressure $p_{min,air}$ is directly reached. For a sealed chamber at the inlet, the inlet pressure p_{in} will reach $p_{min,air}$ in equilibrium.
Accordingly, the excess pressure is defined by:

$$p_{max,air} = p_{in}\left(\frac{V_{start}}{V_{end}}\right)^{\kappa} = p_{in}\left(\frac{V_{dead,valves} + V_{dead,chamber}[p_{max,air}, U_{pos}] + V_{disp}[p_{max,air}, \triangle U]}{V_{dead,valves} + V_{dead,chamber}[p_{max,air}]}\right)^{\kappa} \tag{3.20}$$

A adiabatic expansion with an isentropic exponent of 1.402 is assumed for the simulations, as the change happens too fast for a significant heat exchange between gas volume and pump body.

Simulation of theoretical gas pressures Applying actuator and valve models to calculate the required parameters allow for a theoretical calculation and optimization of gas pressures. The valve dead volume can be extracted from the 3D FSI valve model. The inlet valve with its large flap area exhibits a dead volume of 29.4 nl at 70 µm wafer thickness. The dead volume of the outlet valve is with 10.5 nl only about a third of the inlet dead volume, as the valve sealing with its pressure application area requires a smaller inlet for the reference valve. The actuator model provides the displacement volume at the adjusted electric field levels of -0.4|2 kV/mm and the maximum gas pressures. An iterative numeric evaluation of the recursive Equ. 3.19 and 3.20 has to be applied with a chosen maximum number of 200 iterations. Thereby, the suction (Figure 3.32) and excess (Figure 3.33) gas pressures can be calculated for arbitrary piezo geometry and reference pump diaphragm dimensions (Equ. 1.1). Comparing excess and suction gas pressures show a stagnating suction pressure and a yet continuously increasing excess pressure for increasing piezo thickness (Figure 3.34). With increasing diaphragm thickness from 40 µm to 80 µm to 120 µm a decrease in suction pressure can be observed (Figure 3.35). To understand the influence of diaphragm radius, the suction gas pressure was evaluated varying the R_d between 3-5 mm (Figure 3.36). Here the piezo thickness was chosen to be 200 µm to be comparable to the other evaluations, while keeping T_d at 40 µm. An increase of gas pressure with rising diaphragm radii can be observed.

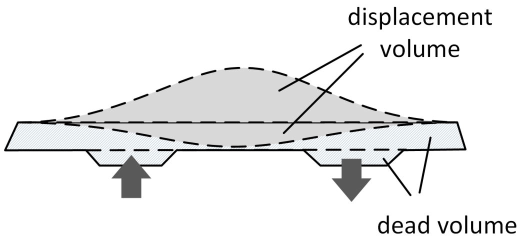

Figure 3.31: Displacement volume and dead volume (from pump chamber and valves).

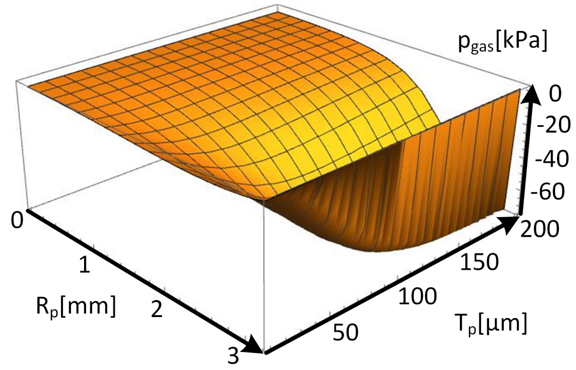

Figure 3.32: Suction pressure over piezo radius and thickness at constant diaphragm geometry (T_d=40 µm, R_d=3.15 µm).

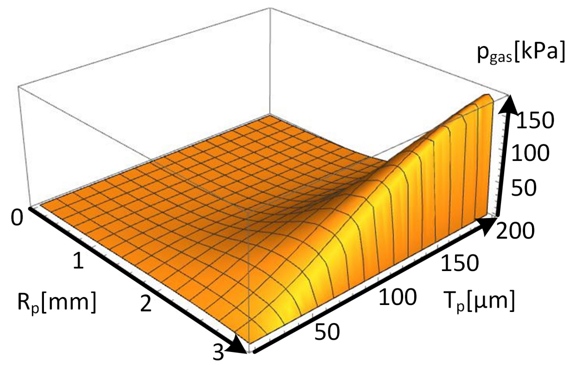

Figure 3.33: Excess pressure over piezo radius and thickness at constant diaphragm geometry (T_d=40 µm, R_d=3.15 µm).

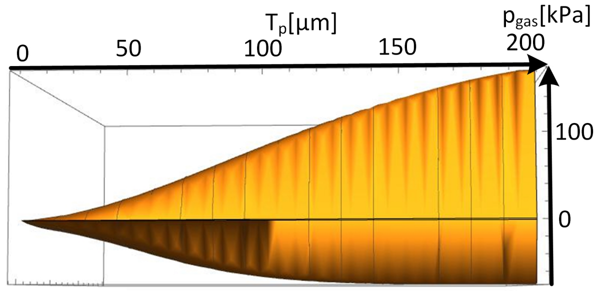

Figure 3.34: Comparison of suction and excess pressure over piezo thickness at constant diaphragm geometry (T_d=40 µm, R_d=3.15 µm.

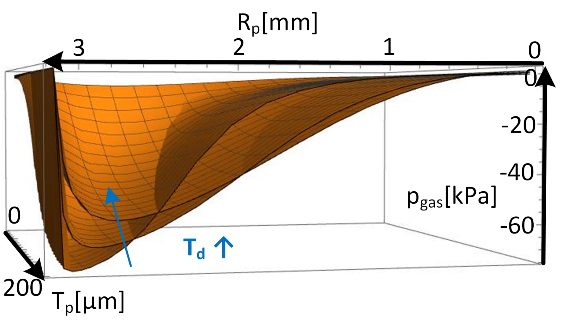

Figure 3.35: Suction pressure over piezo radius and thickness at diaphragm thickness variation (40/80/120 µm) and constant diaphragm radius (3.15 µm).

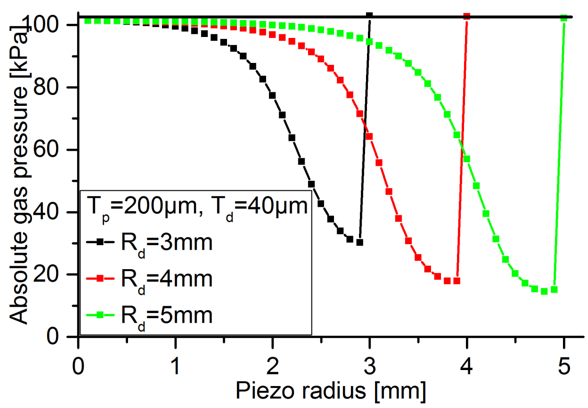

Figure 3.36: Piezo radius dependent suction pressure (absolute pressure scale) for three different diaphragm radii (3/4/5 mm).

Experimental investigation of suction gas pressure In order to validate the calculated theoretic suction gas pressure, a pressure sensor was attached to the inlet and sealed air tight. While the simulations of the reference pump where conducted with the electric field levels of -0.4|+2 kV/mm to evaluate maximum performance, the measurements of the reference pump could only be done with -0.4|+1.5 kV/mm, because the actuator would touch the pump chamber boundary otherwise. Therefore, the achievable theoretic suction gas pressure for a maximum electric field of 1.5 kV/mm was calculated and is 38.8 kPa absolute pressure compared to 29.2 kPa for 2 kV/mm. The pressure sensor attachment features a dead volume of roughly 50 µl, which has to be evacuated before the maximum suction pressure can be reached. For a sine driving signal the suction pressure was measured for frequencies up to 1 kHz (Figure 3.37) and shows the lowest pressure of 53.9 kPa at 1kHz. For a rectangular driving signal the suction pressure was measured for frequencies up to 4 kHz (Figure 3.38) and features its minimum pressure of 43.3 kPa at 1kHz. Besides the gas pressure, the frequency dependent gas flow rate was measured for both signals (Figures 3.37 & 3.38).

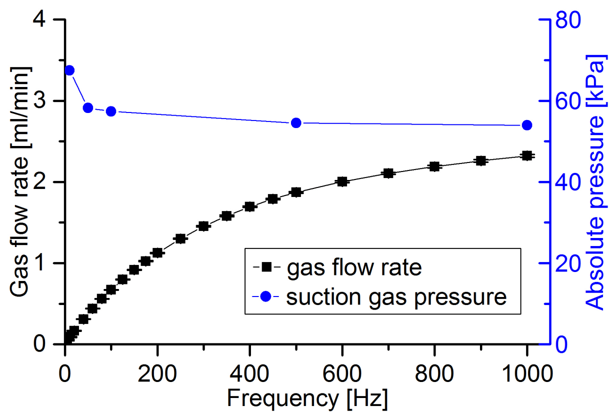

Figure 3.37: Gas flow rate (black) and equilibrium absolute pressure (blue) for a sine signal with frequencies up to 1 kHz (-0.4|+1.5 kV/mm).

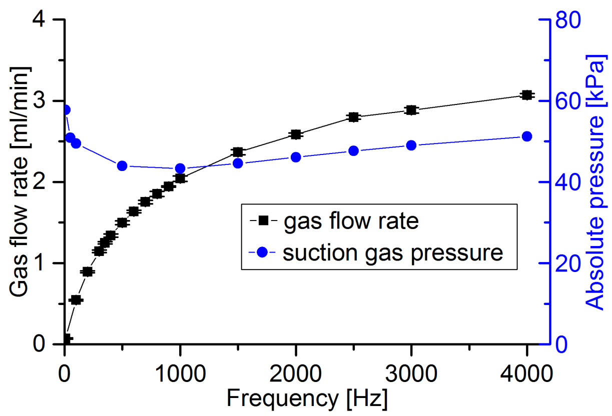

Figure 3.38: Gas flow rate (black) and equilibrium absolute pressure for a rectangular signal with frequencies up to 4 kHz (-0.4|+1.5 kV/mm).

Discussion

The highest measured suction pressure is 93 % of the theoretically calculated gas pressure. From the frequency dependency of the gas pressure it is evident, that gas leakage must occur. Leakage emerges from pressure sensor attachment into the pump chamber, whenever the rough vacuum pressure is below the pump chamber pressure (Figure 3.39). Additional leakage from the outlet into pump chamber appears in the supply mode. The leakage reduces the effectively moved gas volume from pressure sensor chamber for a full pump cycle and also reduces the pressure peak inside the micropump. For driving frequencies of 1 kHz there seems to be a optimum ratio between effective gas evacuation and leakage. Besides leakage, additional factors explain the differences between theory and measurements. First, the dynamic displacement at 1 kHz is much lower than the static displacement for the calculation. This frequency dependent displacement reduction is evaluated and explained thoroughly for liquids in section 3.4. Second, the position of the lower actuator turning point is not right at the pump chamber boundary, which reduces the effective compression ratio and therefore the achievable gas pressure. Third, the isentropic exponent might be lower than 1.402 as some heat exchange might take place.

If the maximum gas pressure ability is to be reached, these additional aspects have to be addressed. This can be done by first evaluating the dynamic displacement at 1 kHz, then fabricate a new pump and set the predeflection to the value that the lower turning point of the actuator is just about to touch the pump chamber boundary. A more elaborate way to adjust the relative diaphragm position is by changing the pressure above the actuator, to reach the same state, as the relative displacement is more or less unaffected by this change.
A optimization of relative positioning of actuator to the chamber boundary would also be desirable for maximum bubble tolerance. If a bubble enters the chamber, the resistive damping decreases, which leads to higher relative displacement. The highest bubble tolerance can be achieved, when the actuator is just about to touch the chamber boundary, while facing bubble resistance instead of liquid resistance. Now the optimum gas pressure ability is reached and the bubble is put through the pump the fastest way possible. If a bubble detection is implemented, then the frequency can also be increased in the time of a bubble residing in the pump chamber.
For the fastest way to reach the minimum pressure, a higher frequency can be chosen first to increase flow and therefore evacuation speed and subsequently change to lower frequencies down to the optimum frequency (1 kHz for pump in Figure 3.38) to reach the best gas pressure. The same applies for the fastest self-priming characteristic.

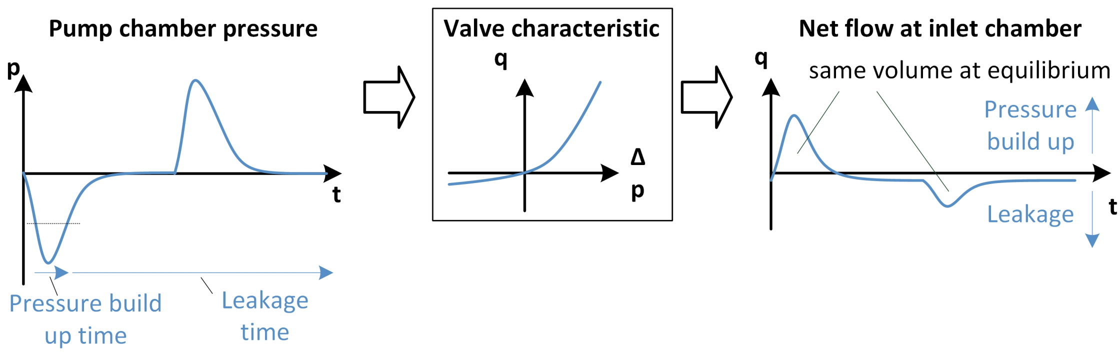

Figure 3.39: Principle of suction pressure equilibrium (pressure build up vs. leakage) for a confined chamber attached to the inlet.

Conclusion

Combining the static models of actuator and valve enable the prediction of theoretical suction and excess gas pressures. Theoretic calculation of gas pressures, model calculations for different actuator geometries and experimental validation was performed. Not considering the influence of frequency dependent leakage and a reduced compression ratio at a dynamically moving actuator, still 93 % of the predicted value of suction pressure can be reached. This delivers a good method to predict gas pressures. Furthermore design guidelines to optimize time dependent pressure build up are given, which facilitates application specific optimization of self-priming ability and bubble tolerance.

3.4 Flow rate influencing effects of micropumps

This section explains the influencing effects on the flow rate of micropumps for liquids and is the content of a submitted Journal paper [93]. Therefore, the structure follows the Journal structure.

Current micropump technology features bubble tolerance and self-priming ability, achieved with high pressure ability at shallow pump chambers for low dead volume and high compression ratio. Though, the pump dynamics are strongly affected by a pump chamber height dependent viscous squeeze film damping. Therefore, all major flow influencing effects were investigated for micro diaphragm pumps, being liquid resistive damping, cavitation based gaseous capacitive damping and reactive valve volumes. Analytical models were developed that are able to describe and predict the transient actuator displacement, derive the frequency dependent displacement and estimate the valve loss effect in order to determine the flow rate performance of micropumps. In addition, a new oscillator model is able to simulate the inception of cavitation and the time course of both actuator and liquid. The individual effect models were combined into a single-cycle based, frequency dependent, flow rate model, validated for frequencies of up to 100 Hz. Compared to the maximum achievable flow rate, the liquid resistive damping reduces dynamic stroke volume and is responsible for a reduction of 23-57 % at 100 Hz. Valve induced flow losses reduce the effectively redirected volume towards the outlet. The effect is enhanced by the strong damping, but also feeds back on the actuator by reducing initial damping significantly. Reactive valve volumes amount for 6.2-12.4 % flow rate reduction at 100 Hz. Full cavitation, generated at the supply mode and affecting the pump mode, can cause gas bubble generation and lead to a drop of flow rate down to 65 % at 80 Hz. By placing an in-line degasser the flow stability was improved to ±2.2 % over 10 h. After reducing the frequency to 20 Hz, cavitation only affected the supply mode and in combination with a degasser a flow stability of ±0.15 % over 2 h was achieved. By reducing voltage levels, cavitation was avoided completely, featuring a stability of ±0.08 %. The understanding of the flow rate limiting effects enables the application specific design to meet all performance and reliability requirements for micropump based liquid dosing systems.

State of the art

The application range of microfluidic systems featuring micropumps stretches from micro analyzing systems over oil lubrication to medical devices, either pumping drugs or body liquids [94, 95, 96]. The task is always to pump a certain volume within a period of time or to maintain a certain flow rate. The main requirements for these applications are self-priming ability and bubble tolerance for easy setup initiation and robust operation [35]. Furthermore, high accuracy of stable flow rates or of certain volumes in combination with a high lifetime is desired for a safe operation, especially at dosing of highly concentrated drugs [94, 97]. On system level, sensor-enabled closed-loop control can be used to tackle safety and accuracy requirements [98], but system costs go up due to the additional component. For implantable systems, size and energy efficiency are additional constraints [11]. Last but not least, low fabrication costs are necessary to address certain markets, for example disposable medical devices [94]. As every application is different, pump and system models are necessary to target the individual requirements.

All these requirements led to certain characteristics of micro diaphragm pumps. For the actuator usually a circular piezoelectric bimorph is used due to the piezo's superior force generation. For flow redirection either valveless nozzle-diffuser geometries are chosen for their superior particle tolerance or mechanical flap or diaphragm valves are used for their superior flow redirection efficiency. Another important re-

quirement is bubble tolerance. However, it is not clearly defined in literature. While it usually only describes the fact that a bubble can pass the pump, it should be defined together with a maximum back pressure as a more robust criterion. To increase self-priming ability and bubble tolerance, the pump chamber height became very low to reduce dead volume in combination with a predeflected actuator [52]. However, a shallow pump chamber of a few microns leads to strong viscous friction due to a squeeze film effect [99, 100]. Because of this strong resistive damping the pump dynamics changed significantly, leading to altered flow rate influencing and limiting effects. This made existing models inaccurate in describing piezoelectrically driven diaphragm pumps with mechanical valves and low chamber heights.
Recent efforts to analytically model the dynamic behavior of circular unimorph actuators and investigate the influences of micropump flow rate addressed some of the current issues. An accurate, physical design dependent, 3D model to predict the vibration and resonance frequency of clamped actuators in air was developed by Gomes [101]. He et al. [102] presented a 3D model that is able to predict the displacement amplitude for a sine wave driven actuator at liquid pressure load. A suitable model to describe the performance of a planar valveless micropump by means of 3D fluid-diaphragm coupling was published by Dinh and Ogami [103]. It includes the effects of fluid inertia and squeeze film by iteratively solving pressure conditions, the Reynolds equation for damping influence and the coupling equation. Singh et al. [104] developed a model to predict the natural frequency and flow rate performance of a planar valveless micropump, based on the force balance between actuator and fluid pressures at inlet and outlet valves. Additional numerical and experimental investigations provide understanding on the influence of chamber height, voltage and frequency on the net flow rate.

Research goal and outline

The research goal is to describe all major flow rate influencing effects of current micro diaphragm pumps in a single stroke based way. In addition, the coupling of effects and the conditions for a stable flow rate were investigated. Understanding the dynamic behavior of the micropump and providing appropriate models for pump design not only helps to increase performance of micropumps, but also to improve reliability in long-term operation.
This paper first gives a short overview of the main influencing effects and subsequently describes the influences of actuator, gas capacitances and valves in detail. Then the combined influences and additional design considerations are described, followed by the conclusion of the work.

Overview of influences

The logic path to describe the influences on the flow rate of reciprocating pumps starts at the pressure generating actuator that moves fluid according to existing resistances. In the supply mode the actuator builds up a negative pressure compared to ambient pressure, sucking the liquid through the inlet valve and is followed by the pump mode, where excess pressure pushes the liquid through the outlet valve. According to Zengerle and Richter [33] the maximum achievable flow rate depends on the stroke volume and frequency and is limited by:

$$Q = f\,V_{stroke} \tag{3.21}$$

Compared to the static stroke volume, squeeze film damping at low chamber height causes an overdamped actuator and a strong time delay compared to the actuation signal [100] in the dynamic mode (Figure

3.40). That leads to a highly frequency dependent dynamic stroke volume. Gaseous capacitive damping effects due to bubbles or cavitation can further reduce the actually flown volume in and out of the pump chamber. The effective volume flown at the outlet is determined by the valve efficiency and depends on valve volume losses at static valve resistances and dynamic effects [33]. Reactive valve volumes also reduce pump chamber resistance for the moving actuator until the valve in reverse direction closes.

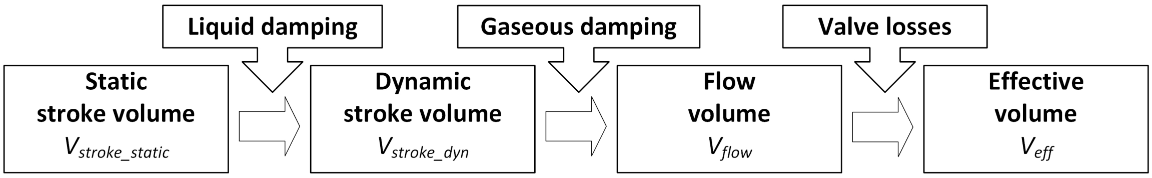

Figure 3.40: Flow rate influencing effects.

The Fraunhofer EMFT fabricated piezoelectrically driven silicon micro diaphragm pump (Figure 3.41 – photo and crosssection) is implemented in a measurement setup, comprising various sensing and control technologies (Figure 3.41 – setup drawing). Additional information on the equipment and guidelines for a correct setup can be found in [98]. With one exception, the reference pump (Figure 1.1) is used in all measurements and for simulations. The TUDOS pump with higher pressure ability is only used for the measurement in Figure 3.50. The valves are equal for both pump types.

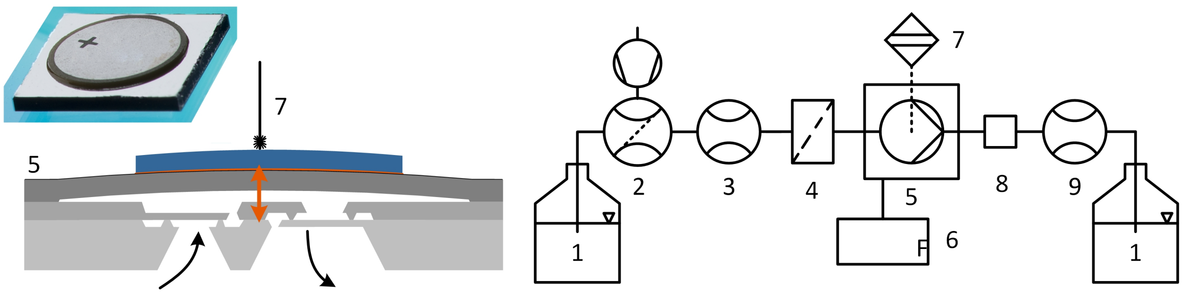

Figure 3.41: Real micropump, its cross-section and the measurement setup: (1) reservoirs (2) degasser (3) differential pressure based (DPB) flow sensor (4) filter (5) micropump (6) arbitrary wave form generator with amplifier (7) displacement sensor (8) pressure smoothing element(PSE) (9) Coriolis flow sensor.

Actuator influence

Static displacement Displacement volumes of piezoelectric diaphragm actuators mainly depend on the applied voltage (Figure 3.42), described by a peak-to-peak notation 'n60p300' with indication of negative (n) and positive (p) voltage levels. The actuator deformation is determined by geometry and material properties of the diaphragm and the laminated piezo disc. An analytical model to predict the static deformation curve, the resulting displacement volume and the pressure ability was developed by Prasad et al. [83] and was extended by Herz et al. [34]. It does not include the nonlinear effects of the piezo characteristics, comprising mainly the big signal behavior, the electric field hysteresis (Figure 3.42), and the pressure hysteresis [34, 89]. Assuming an overdamped actuator the flow rate at quasi static displacement [34] gives:

$$Q_{max} = f\, V_{stroke,static} = f\,(C_p\, p + C_E\, E_z) \tag{3.22}$$

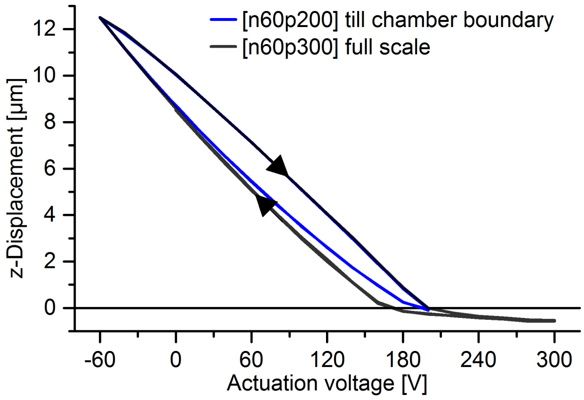

Figure 3.42: Measured center displacement, from -60 V to full scale (+300 V) and till chamber boundary (+200 V).

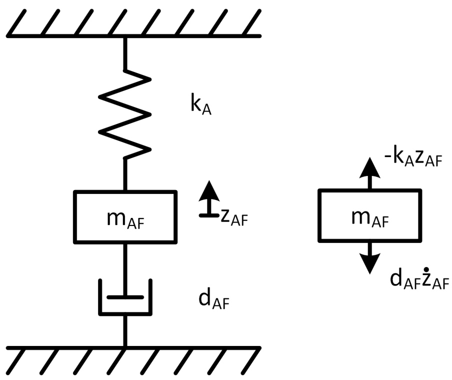

Figure 3.43: Combined mass (actuator & fluid) oscillator model (CMM).

Dynamic displacement Due to low chamber heights of current micropump technology, squeeze film damping became the dominant effect of actuator dynamics [100]. With decreasing distance of actuator to the pump chamber boundary (PCB) the resistive damping increases cubically. Thus, if the actuator diaphragm is actuated close to the pump chamber bottom, the relative displacement becomes highly frequency dependent. To describe the transient course of displacement at these dynamic conditions, an analytical model was developed containing the forces, masses and damping effects occurring during pumping and leading to the equation of motion (Figure 3.43). Not considering the presence of fluidic gas capacities like bubbles or cavitation inside the pump chamber, a simple damped one mass oscillator is suitable to describe the dynamics of the actuator. Furthermore, the damping influence can be studied and a fit curve option is provided to predict frequency dependent displacement (subsequent paragraph 'frequency dependent displacement').
With the sum of actuator and liquid masses m_{AF}, the center diaphragm displacement z_{AF}, its generated force corresponding to the spring constant k_A and the viscous friction based resistive damping factor d_{AF}, the summarized basic differential equation is:

$$m_{AF}\ddot{z}_{AF} + d_{AF}\dot{z}_{AF} + k_A z_{AF} = 0 \tag{3.23}$$

Constant damping
The standard approach $z = A\, e^{\lambda t}$ leads to the solution for high damping with a Lehr's damping ratio $D_L = \frac{d_{AF}}{2\sqrt{m_{AF} k_A}} > 1$:

$$z_{AF}[t] = A_1 e^{\lambda_1 t} + A_2 e^{\lambda_2 t} \tag{3.24}$$

With the eigenvalues $\lambda_{1,2}$ depending on the angular frequency $\omega_0 = \sqrt{\frac{k_A}{m_{AF}}}$:

$$\lambda_{1,2} = -D_L\omega_0 \pm \omega_0\sqrt{D_L^2 - 1} \tag{3.25}$$

And the constants $A_{1,2}$ that can be determined by respecting the initial conditions of the center displacement z:

$$z([t = 0] = z_0 \tag{3.26}$$

$$\dot{z}[t = 0] = 0 \tag{3.27}$$

which express an initial internal stress of the actuator in the moment after the charging of the piezo capacitance. The model gives the final equation of motion:

$$z_{AF}[t] = z_0 \frac{\lambda_2}{\lambda_2 - \lambda_1} e^{\lambda_1 t} - z_0 \frac{\lambda_1}{\lambda_2 - \lambda_1} e^{\lambda_2 t} \tag{3.28}$$

For the application of the model the unknown coefficients of the Equation of motion 3.28 have to be determined. Neglecting the electrode and adhesive layer between piezo (p) and diaphragm (d), the mass m_{AF} is the sum of the diaphragm actuator m_A and the fluid m_F that has to be moved during supply or pump mode:

$$m_{AF} = m_A + m_F = (A_p T_p \rho_{PZT} + A_d T_d \rho_{silicon}) + r_{tube}^2 \pi l_{tube} \rho_{water} \tag{3.29}$$

, with the piezo (p) and diaphragm (d) areas A_p and A_d, thicknesses T_p and T_d, the tube radius r_{tube}, length l_{tube} and densities ρ_{PZT} and $\rho_{silicon}$ and ρ_{water}. The driving force generated by the piezo is represented by the spring. That analogy fits very well, as the force of the diaphragm actuator decreases linearly with the movement of the center displacement [34]. The spring constant is:

$$k_A = \frac{F_{max}[\triangle U]}{\triangle z[\triangle U]} = \frac{p_{max}[\triangle U]\, A_d}{z_0} \tag{3.30}$$

The initial maximum force $F_{max}[\triangle U]$ is equal to the maximum outlet pressure ability $p_{max}[\triangle U]$ of the actuator and can be calculated with the mentioned static displacement model [83, 34] as well as the initial displacement z_0, which equals the static displacement $\triangle z[\triangle U]$ at equal peak-to-peak voltage. The remaining unknown variable of the system is the damping coefficient, which corresponds to the viscous friction based resistive damping. The damping originates mainly from the pump chamber, but the flow is also affected by the resistance of valve and fluidic path or elastic components ahead of or after the pump that induce capacitive damping [98]. With a shallow pump chamber, the resistance becomes strongly height dependent, thus a constant damping cannot be assumed anymore.

Pump chamber height dependent damping

The new approach accounts for cubically increasing resistance with $z_{AF} \to 0$, by describing the damping factor with:

$$d_{AF} = \frac{d_{amp}}{(z_{AF} + d_{shift})^{d_{exp}}} \tag{3.31}$$

While d_{amp} and d_{exp} describe the height of the damping factor, d_{shift} stands for the distance of the remaining pump chamber height (RPCH).

With the RPCH dependent damping factor, an analytical description of the solution is not possible anymore and the actuator motion has to be evaluated numerically. The calculation of the absolute values of pump internal resistances is complex and has both geometric and fluid dynamic influences. Therefore, the model is used to fit the damping value to different measurements of dynamic displacement curves. Hence, the influence of damping on the pump dynamics are revealed, the model can be validated and model based curve descriptions can be implemented for further simulations. Comparing the step responses of the measured transient displacements with the simulations (Figure 3.44), a good agreement can be reached.

The remaining fitting errors can be attributed to actuator creep, internal damping and reactive valve volumes, which all have an effect on the dynamic motion. According to the piezo supplier, a creep-effect starts from 0.1 s in an fluidically undamped case and amounts for 1 % strain per time decade (0.1-1.0 s) [105]:

$$\triangle z_{creep}(t) = 0.01\, z[0.1[s]]\, log_{10}(10t/[s]) \tag{3.32}$$

However, for the entire actuator compound, internal damping contributes to the effective time dependent creep behavior. Measured in a rough vacuum of 12 kPa, the actuator creep amounts for 4-6 % per time decade and starts as early as 2 ms. At a prolonged actuator movement due to damping or creep a reactive flow occurs at the valve, further investigated in the paragraph 'reactive valve volume influence', but has only little effect at low frequencies of below 10 Hz. After subtracting these time dependent displacement influences, the pure RPCH dependent damping can be evaluated (Figure 3.45).

The calculated natural or resonance frequency is ~131 kHz in vacuum and ~23.7 kHz in combination with the liquid, while applied driving frequencies in this work are below 100 Hz. The rectangular driving signal applied to the fast piezo ceramic could theoretically cause an overshoot oscillation, but the high, squeeze film induced, resistive damping leads to an overdamped case and prevents any overshoot. For an accurate description, of frequency limitations, a so called 'cutoff frequency' is introduced [98], which indicates the end of motion within sensor accuracy of ±0.1 µm. The 'damping cutoff frequency' denotes the critical frequency below which all resistive and capacitive damping influences vanished.

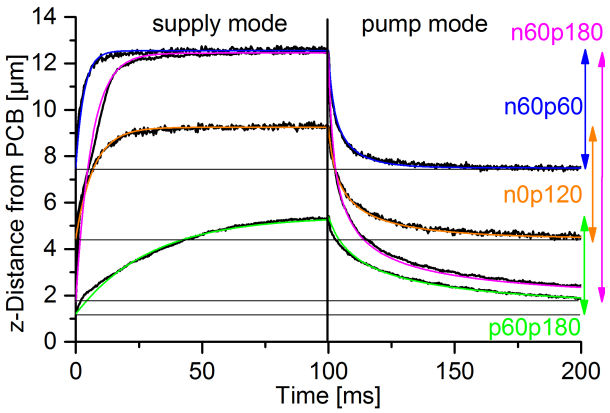

Figure 3.44: Measured and simulated transient displacement curves with first 100 ms of 1 Hz supply and pump mode for different peak-to-peak voltages and chamber distances.

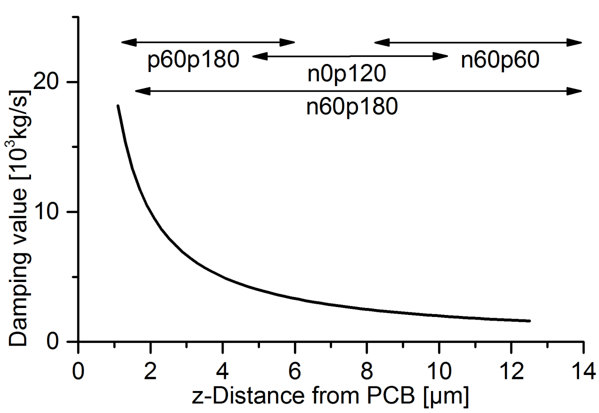

Figure 3.45: Pure resistive damping depending on the remaining pump chamber height.

Frequency dependent displacement Because of the strong damping, the relative displacement drops quickly with increasing frequencies (Figure 3.46). At dominant viscous friction and a z-dependent actuator force, the displacement curves of higher frequencies are a part of the low frequency curve (Figure 3.47), as the conditions for the motion are the same. Increasing the frequency shortens the time for supply and pump stroke. The displacement reduction takes place from both ends of starting and final position (Figure 3.47) until an equilibrium between pump and supply is reached.

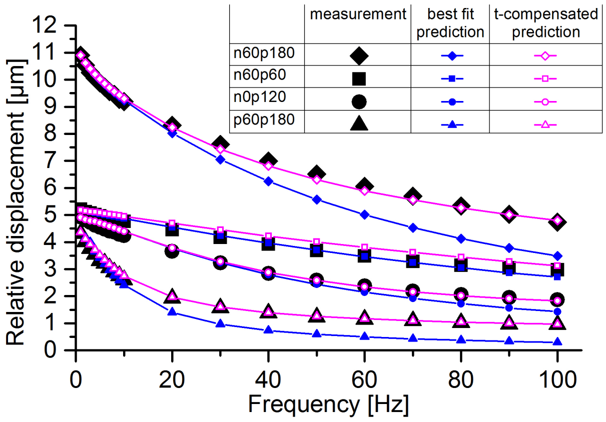

Figure 3.46: Frequency dependent displacement reduction for different voltage levels.

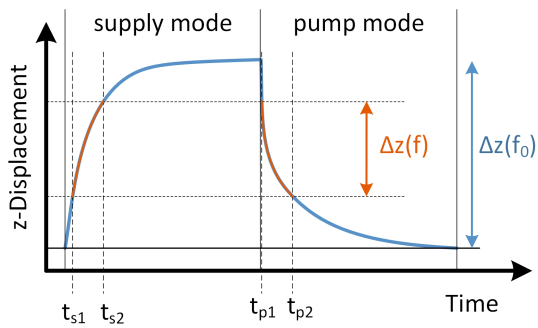

Figure 3.47: Principle of frequency dependent displacement adaption.

That mechanism can be translated into an equation system, where the frequency dependent displacement can be calculated by just having single displacement curves $z_p[t]$ of pump and $z_s[t]$ of supply mode of one low frequency either from measurement or dynamic simulation. The duty cycle is 0.5, which corresponds to an equal time distribution between supply and pump mode. The times t_{p1}, t_{p2}, t_{s1}, t_{s2} (Figure 3.47) determine the resulting frequency-dependent relative displacement. The equations for the solution are:

$$I)\, z_p[t_{p1}] = z_s[t_{s2}] \tag{3.33}$$

$$II)\, z_p[t_{p2}] = z_s[t_{s1}] \tag{3.34}$$

$$III)\, t_{s2} - t_{s1} = (2f)^{-1} \tag{3.35}$$

$$IV)\, t_{p2} - t_{p1} = (2f)^{-1} \tag{3.36}$$

To solve the equation system, a mathematical description of the displacement curves is needed. Suitable functions are either the constant damping model 3.28, suitable at high RPCHs, or the Hill fit function f_H:

$$f_H[t] = A\frac{t^n}{k^n + t^n} \tag{3.37}$$

For relatively high lowest RPCHs a good agreement of predicted displacement values with the measurements is achieved (Figure 3.46 - blue). With decreasing distance to the PCB, the stronger damping leads to an initial reactive flow at the valve for the subsequent mode (paragraph 'reactive valve volume influence'). With the temporary dual pump chamber access, the resistance drops and accelerates the actuator. This acceleration corresponds to a effectively higher time for the displacement and can be calculated as followed:

$$t_{acc} = t[z_{closure}] - t_{closure} = t\left(z([t] + \frac{C_{flap}}{v_d}\right) - t_{closure} \tag{3.38}$$

The time $t_{closure}$, for the flap to reach the valve seat, is indirectly proportional to the applied voltage difference and the flap resonance frequency and ~1 ms for ΔU=120 V and ~0.5 ms for ΔU=240 V. C_{flap}, the flap capacitance (Equ. 3.71), and v_d, the stroke volume per center displacement (Equ. 3.44), define the additional displacement that the actuator has covered until the valve closes. The effect on the resulting acceleration time though is mainly determined by the displacement course, as a more flat curve will result in much higher acceleration times. By adding this acceleration time to the respective Equations 3.35 and 3.36, a new equilibrium of supply and pump displacement is found, reaffecting the calculation of the acceleration time. The time-compensated displacement prediction now fits very well for involved lower RPCHs (Figure 3.46). As the dynamic displacement of supply and pump stroke follow a different curve, an optimization of the relative displacement can be performed by splitting the available time at a frequency with a duty cycle unequal to 0.5. The adapted equation system for the duty cycle optimization is:

$$I)\; z_p[t_{p1}] = z_s[t_{s2}] \tag{3.39}$$

$$II)\; z_p[t_{p2}] = z_s[t_{s1}] \tag{3.40}$$

$$III)\; t_{p2} - t_{p1} + t_{s2} - t_{s1} = f^{-1} \tag{3.41}$$

$$IV)\; \frac{d(\triangle z[f])}{dt} ! = 0 \tag{3.42}$$

Flow rate influence of actuation To estimate the influence of the actuator motion on the frequency dependent flow rate, the displacement volume for different frequencies according to the method explained in [98] is needed. Therefore, the surface line of the static pump actuator is measured from a to b at two voltages and the difference calculated. The stroke volume is thus:

$$V_{stroke}[\triangle U] = \pi \int_a^b x\, y[x]\, dx \tag{3.43}$$

The stroke volume per center displacement for the reference pump is:

$$v_d = \frac{V_{stroke}[\triangle U]}{z_{stroke}[\triangle U]} = 13.6 \frac{nl}{\mu m} \tag{3.44}$$

The frequency dependent stroke volume is received by:

$$V_{stroke,static} \rightarrow V_{stroke,dyn}[f] = \triangle z[f] v_d = \frac{\triangle z[f]}{z_0} V_{stroke,static} = \mu_{disp} V_{stroke,static} \tag{3.45}$$

and subsequently the predicted flow rate values by:

$$Q_{max} = f\, V_{stroke,dyn}[f] \tag{3.46}$$

For equal voltage levels that feature almost equal relative displacement (Figure 3.42), but are positioned with different RPCHs, the actuation is the main flow rate limiting effect (Figure 3.48 - black). Comparing the actuator influence with the flow rate measurement, a remaining gap of similar magnitude is apparent (Figure 3.48 – black vs. red). Avoiding gas capacitance, as for these measurements, the valve losses are responsible for the remaining gap (paragraph 'valve influence').

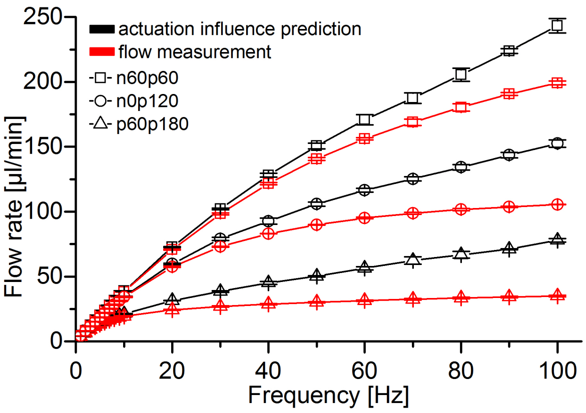

Figure 3.48: Frequency dependent flow rate compared to the actuator influence prediction for three voltage levels.

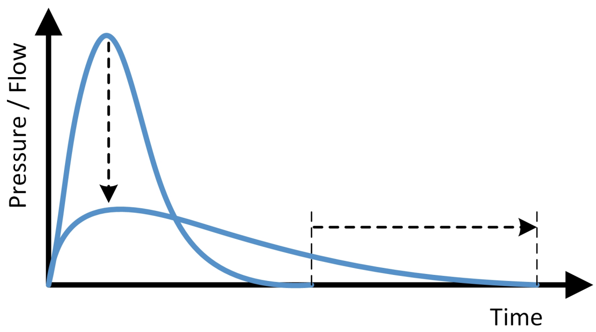

Figure 3.49: Delay of flow through fluidic damping for the same volume.

Gas capacitance influence

Influence and prevention of bubbles The dynamic displacement volume defines the volume that is moved by the actuator. But capacitances lower and therefore delay pressure and flow pulses by storing liquid under pressure (Figure 3.49), called capacitive damping. As a consequence, the liquid actually crossing the micropump boundary will be even more time dependent and thus more frequency dependent. Capacitances can be elastic elements or of gaseous nature. As described by Richter et al. [35], a capacitance inside the pump chamber leads to a damped inlet and outlet flow and should be minimized to optimize pump performance. A capacitance outside of the pump in the fluidic path decouples the masses ahead of and behind the capacitance. That leads to less inertia and flow resistance for the micropump actuator but reduces stroke due to a higher counter pressure. Depending on the system characteristics that effect can decrease or increase flow rate or it can be used to smooth pulsatile flow [66].
In micro diaphragm pumps, the diaphragm stiffness defines its capacitive influence and has to be accounted for. Valve deformation has less influence [33] and plays no significant role in the used pump due to a small and stiff flap valve. Here, the focus is on the fluidic behavior of bubbles and cavitation, which both represent gas capacitances. Gas bubbles can first remain in the fluidic path after filling, second

can be brought into the fluidic path and pump by the delivered liquid or from air leakages or third can originate from gas solved in the liquid.

Current micropumps feature self-priming ability and bubble tolerance due to a high compression ratio even at challenging conditions. However, the flow rate will still drop significantly once a bubble enters the pump and a dead-time with no liquid flowing occurs once the bubble exits the system. Additionally, occurrence and influence of bubbles can hardly be predicted or controlled. If a very precise and stable dosing is required, no macroscopically visible bubbles can be allowed within the fluidic path. To meet this requirement, first the pumped liquid needs to be bubble free or a bubble remover has to be placed in-line of the inlet path. To prevent gas from remaining after filling, two methods are known. One is using a gas with high solubility in water [82], where for example carbon dioxide was used to prime the fluidic path. Afterwards, the path was filled with water, in which the carbon dioxide was able to dissolve entirely, leaving no gaseous bubbles behind. The second method employs an in-line degasser, also known as deaerator, close to the pump inlet. The time scale for dissolving micro liter sized macrobubbles in liquid depends mainly on the solubility of the gas-liquid combination and the gas partial pressure in the liquid [106]. While macrobubbles have to avoided for reliable operation, microbubbles (micron-sized bubbles) are a different case: "In water, microbubbles of air seem to persist almost indefinitely and are almost impossible to remove completely." [107]. This means, entrained gas is most likely to remain at solid boundaries, suspended particles or floating freely [107], which renders the possibility of cavitation at vapor pressure [106].

Cavitation Cavitation is long known to be a performance constraint for micropumps [108, 109]. For valveless diffuser pumps cavitation predominantly starts at the center displacement [97]. Experimental investigations showed more clearly the different phases of cavitation and its effect on the flow [110, 111]. The consecutive phases can be separated into incipient cavitation, where it first occurs, partial cavitation with the effect limited to the supply mode and full cavitation that also affects the pump mode [110]. The basic approach to deal with cavitation is to prevent it from occurring by keeping the pump chamber pressure above the vapor pressure [109, 112]. Eames et al. developed a 1-D model for harmonic actuation to determine the limitation criterion for cavitation [112]. According to Schweitzer and Szebehely all cavitation starts with microscopic amounts of entrained gas sch[106]. Once the pressure falls below the vapor pressure, vapor evolution into the microbubble occurs leading to bubble growth [106]. If gas is solved in the liquid, it comes out of solution and into the growing cavitation bubble. After the collapse a small gas bubble is left behind [107]. This is called soft or stable cavitation.

The goal is to find the limitations of flow rate and flow stability for micro diaphragm pumps. Therefore, the dynamic conditions for cavitation were investigated with measurement and by developing a separated masses model (SMM) to compare actuation and liquid flow.

In order to clearly show the effects of cavitation, a pump actuator with high pressure ability was chosen (Table - 1.1 TUDOS), driven by a rectangular signal to achieve the highest pressure and flow. This pump type was only used to compare the supply mode time course of the displacement and the corresponding flow ahead of the pump (Figure 3.50). The flow is measured after a short capillary, imposing a small elastic capacitive damping and leading to a flow delay (compare to [98]). The high voltage level of the rectangular signal is fixed to 250 V for this pump, nearly touching the chamber boundary. The low voltage level was varied, for decreasing low voltage levels the displacement and pressure ability rises. With the pressure ability rising high enough to get below vapor pressure, cavitation occurs right after switching of the displacement and starts at voltage levels p150p250, where the first kink in displacement curve can be observed (Figure 3.50). Once the actuator reaches a position, where the pressure ability falls below the vapor pressure, the displacement is slowed drastically. After full implosion of the cavitation bubbles, the liquid reattaches to the diaphragm and the actuator reaches its static position according to the dynamic damping model from paragraph 'actuator influence'. The impact of the imploding cavitation bubble can be seen at the curvy flow within the first 100ms after reaching its peak (Figure 3.50 - flow).

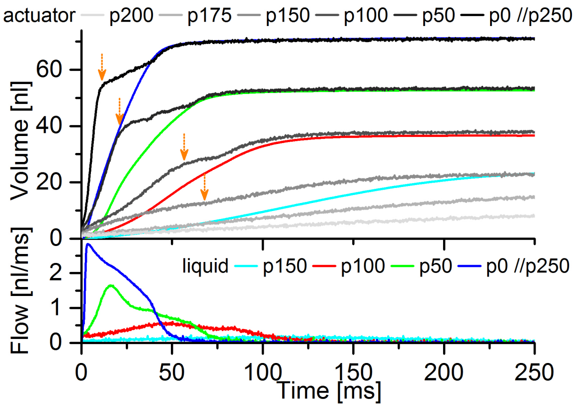

Figure 3.50: Comparison of actuator and liquid measurements at the pump inlet for decreasing lower voltage level (upper fixed to p250), orange arrows indicate end of cavitation ability.

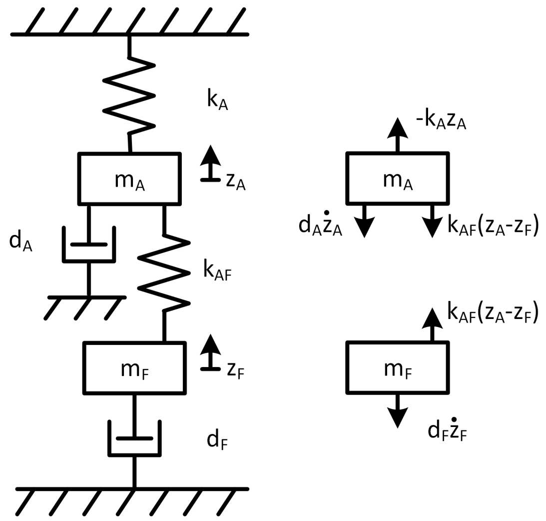

Figure 3.51: Separated masses oscillator model (SMM).

Returning to the reference pump type with less pressure ability, the cavitation effect can also be observed, but the influence on the flow is smaller. In order to understand the physical conditions for cavitation inside the pump, a model was developed, where actuator mass and liquid mass are separated (Figure 3.51). Additionally, this SMM is able to describe the dynamic motion of actuator and liquid across all three phases of cavitation-affected conditions: 1) from starting supply mode till cavitation inception, 2) from cavitation inception and bubble growth till collapse 3) from bubble collapse till reaching the static position or mode switching.

The model in Figure 3.51 gives a new system of basic differential equations, where the masses of actuator m_A and fluid m_F, their positions z_A and z_F, with first ($\dot{z}$) and second ($\ddot{z}$) derivatives, internal actuator damping d_A and fluidic resistive damping d_F are separated, but connected by the pressure with k_{AF}:

$$m_{AF}\ddot{z}_A + d_A\dot{z}_A + (k_A + k_{AF})z_A - k_{AF}z_F = 0 \tag{3.47}$$

$$m_F\ddot{z}_F + d_F\dot{z}_F + k_{AF}z_F - k_{AF}z_A = 0 \tag{3.48}$$

In matrix notation:

$$\underbrace{\begin{bmatrix} m_A & 0 \\ 0 & m_F \end{bmatrix}}_{M}\underbrace{\begin{bmatrix} \ddot{z}_A \\ \ddot{z}_F \end{bmatrix}}_{\ddot{z}} + \underbrace{\begin{bmatrix} d_A & 0 \\ 0 & d_F \end{bmatrix}}_{D}\underbrace{\begin{bmatrix} \dot{z}_A \\ \dot{z}_F \end{bmatrix}}_{\dot{z}} + \underbrace{\begin{bmatrix} k_A + k_{AF} & -k_{AF} \\ -k_{AF} & k_{AF} \end{bmatrix}}_{K}\underbrace{\begin{bmatrix} z_A \\ z_F \end{bmatrix}}_{z} = \underbrace{\begin{bmatrix} 0 \\ 0 \end{bmatrix}}_{0} \tag{3.49}$$

The approach $z = G\,\hat{z}\,e^{\lambda t}$ leads to the characteristic eigenvalue polynomial:

$$\left(\lambda^2 M + \lambda D + K\right)\hat{z} = 0 \tag{3.50}$$

Assuming an overdamped case four negative solutions for the eigenvalue λ are received:

$$\lambda_1 = a,\ \lambda_2 = b,\ \lambda_3 = c,\ \lambda_4 = d \tag{3.51}$$

and the corresponding normalized eigenvectors $\hat{z}_i$:

$$\hat{z}_1 = \begin{pmatrix} 1 \\ f \end{pmatrix},\ \hat{z}_2 = \begin{pmatrix} 1 \\ g \end{pmatrix},\ \hat{z}_3 = \begin{pmatrix} 1 \\ h \end{pmatrix},\ \hat{z}_4 = \begin{pmatrix} 1 \\ j \end{pmatrix} \tag{3.52}$$

Thus, with constants G_i and time t, $z[t]$ turns into:

$$z[t] = \sum_{i=1}^{4} G_i \hat{z}_i e^{\lambda_i t} \tag{3.53}$$

Following:

$$z[t] = \begin{pmatrix} z_A \\ z_F \end{pmatrix} = \begin{pmatrix} G_1 e^{at} + G_2 e^{bt} + G_3 e^{ct} + G_4 e^{dt} \\ G_1 f\, e^{at} + G_2 g\, e^{bt} + G_3 h\, e^{ct} + G_4 j\, e^{dt} \end{pmatrix} \tag{3.54}$$

Following:

$$z[t] = \underbrace{\begin{bmatrix} e^{at} & e^{bt} & e^{ct} & e^{dt} \\ f\, e^{at} & g\, e^{bt} & h\, e^{ct} & j\, e^{dt} \end{bmatrix}}_{M_{coeff}} \begin{bmatrix} G_1 \\ G_2 \\ G_3 \\ G_4 \end{bmatrix} \tag{3.55}$$

The constants G_{1-4} can be determined by taking the initial conditions of each cavitation phase into account and start with:

$$z[t = 0] = z_0 \tag{3.56}$$

$$\dot{z}[t = 0] = 0 \tag{3.57}$$

$$\begin{bmatrix} z_0 \\ z_0 \\ 0 \\ 0 \end{bmatrix} = \begin{bmatrix} M_{coeff}[t = 0] \\ \dot{M}_{coeff}[t = 0] \end{bmatrix} \begin{bmatrix} G_1 \\ G_2 \\ G_3 \\ G_4 \end{bmatrix} \rightarrow \begin{bmatrix} G_1 \\ G_2 \\ G_3 \\ G_4 \end{bmatrix} = \begin{bmatrix} M_{coeff}[t = 0] \\ \dot{M}_{coeff}[t = 0] \end{bmatrix}^{-1} \begin{bmatrix} z_0 \\ z_0 \\ 0 \\ 0 \end{bmatrix} \tag{3.58}$$

The masses of actuator and liquid and actuator spring constant are calculated as in 3.29 and 3.30. The spring constant coupling the actuator with the liquid can be determined over the isothermal compressibility c_L of the liquid [113]. The liquid volume $V_{expanded}$, affected by the expansion due to a pressure below ambient pressure, is mainly the pump chamber volume, as the main pressure drop occurs here and outside of the pump a capacitance damps the flow. Therefore, k_{AF} is:

$$k_{AF} = \frac{p_{max} A_d}{p_{max} c_L V_{expanded}/v_d} = \frac{A_d v_d}{c_L V_{expanded}} = 3.1\times10^9 \frac{N}{m} \tag{3.59}$$

In reality the constant is less due to elasticity of the surrounding pump material. But even a k_{AF} that is two orders of magnitude lower does not change the resulting conditions for cavitation inception noticeably. However due to the lateral pressure drop inside the pump chamber, the force distribution of both sides of the spring is uneven. The average pressure pulling the diaphragm down in only about 75 % of the pressure with which the liquid is pulled in as the lowest pressure is reached at the pump center [97], close to valve inlet. In order to derive the internal actuator damping coefficient $d_A = 100$ kg/s from the combined mass model (CMM) experimentally, a vacuum pressure of -50 kPa was applied below the diaphragm to get rid of most fluid masses. The RPCH depending damping values d_F for the liquid can be obtained from the CMM with low voltage levels, where no cavitation occurs. Due to the complex solution of this model it can only be evaluated numerically. To separate the three phases, the actuator-liquid coupling constant k_{AF} has to be switched once the vapor pressure is reached, indicated in Figure 3.52. After cavitation inception, k_{AF} is governed by the expansion of a vapor bubble with a value below $10^3 \frac{N}{m}$. Due to the high viscous damping of the actuator, the model is very robust concerning the inception of cavitation, but coincidentally strongly influences the time course of actuator and fluid. Plotting the course of actuation and liquid with the model for the reference pump, the cavitation takes place for voltage levels n60p180 (Figure 3.53 - hatched area) and the predicted actuation course follows the measurements.

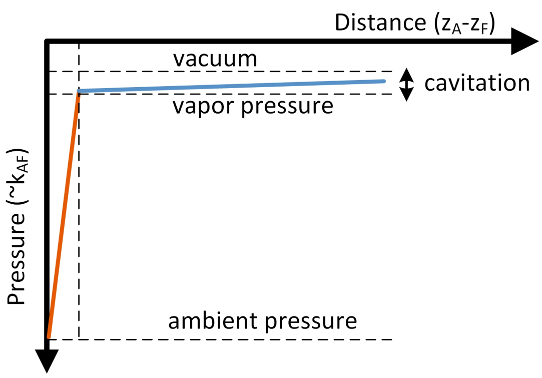

Figure 3.52: Influence of the distance between actuator and liquid on the pump chamber pressure.

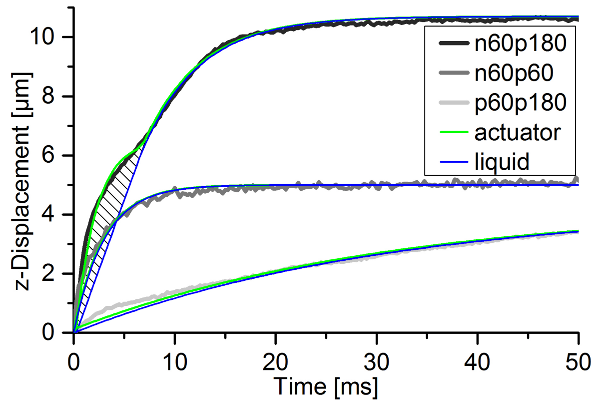

Figure 3.53: Movement of measured displacement (grayscale) compared to model prediction of actuator (green) and liquid (blue) inside the pump chamber.

Flow rate influence of gas capacitances If full cavitation is occurring and the pump mode is also affected by remaining cavitation bubbles, then the actually flown volume into the pump is reduced by the factor σ_{cav} compared to the dynamic displacement volume:

$$V_{stroke,dyn}[f] \rightarrow V_{flow}[f] = \sigma_{cav} V_{stroke,dyn}[f] \tag{3.60}$$

Neither a reduction if flow volume nor conditions featuring damage, as described by Opitz et al. [110] for partial cavitation, are desired. However, driving pumps in partial and full cavitation, no cavitation damage was observed. This may be due to the high resistive damping that slows the liquid and the collapsing of the cavitation bubble, again reducing involved pressure peaks directly and due to gas bubble formation at soft cavitation. A bubble generation effect can be observed (Figure 3.54) by driving the pump within cavitation pressure ability and frequency within full cavitation. Without a degasser (Figure 3.54 - left), the flow is first reduced at the time of generation and pushing the bubble out of the pump (~1 min) and second once reaching the mass flow sensor. With a degasser at 12 kPa absolute pressure and a dwelling time within minutes, the water is not fully degassed. Negative flow jumps still occur, but are less and generated bubbles are reabsorbed quickly and never reach the sensor. The mode of partial cavitation, meaning any cavitation bubble is fully collapsed before mode switching, can be used to enhance the flow rate per cycle. Reducing the frequency to 20 Hz, the flow is affected by partial cavitation and reaches high stability (Figure 3.55). Though, the cavitation effect is a rather statistically distributed mechanism and depends on many factors like number of nuclei available and therefore depends on its history. Reducing the voltage levels can prevent cavitation from happening at all (Figure 3.53) and also features a stable flow (Figure 3.55) without limitation on part of the frequency.

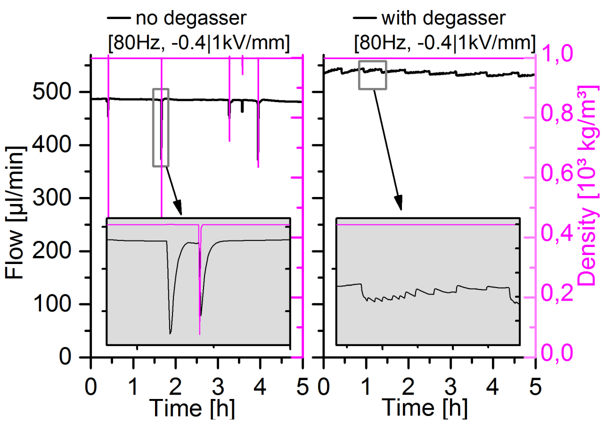

Figure 3.54: Impaired flow stability due to cavitation, with and without a degasser.

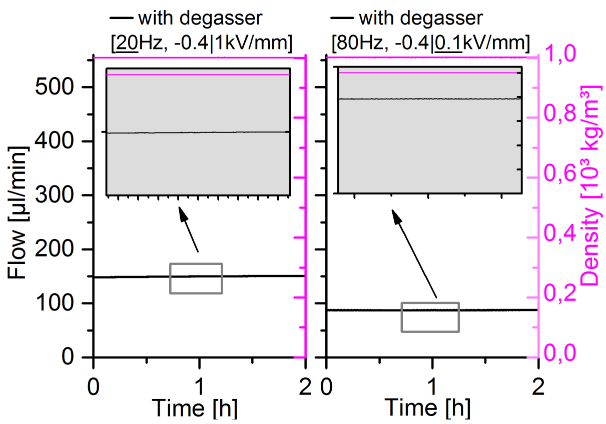

Figure 3.55: Stable flow conditions are reached by either reducing the frequency or the operating voltages.

Valve influence

Valve efficiency With the actually flown liquid in and out of the pump, the remaining flow rate determining factor is the flow redirection efficiency of the valves. First, a general overview for valve efficiency influence is given. Then, the main loss effect due to flap capacitance in combination with a rectangular driving signal is described. Third, the influence of valve efficiency on the effective flow rate is integrated into the model.

In an equilibrium state, the actually flown volumes in and out of the pump are even:

$$\stackrel{EQM}{\Longrightarrow} \; V_{flow} = V_{flow,in} = V_{flow,out} \tag{3.61}$$

Each volume can be separated into effective flow volume and flow losses (Table 3.2):

$$\begin{aligned} & & Effective\ flow\ volume & & & Flow\ losses & \\ V_{flow,in} &= & V_{in,inlet} & & + & V_{in,outlet} & \quad (3.62) \\ V_{flow,out} &= & V_{out,outlet} & & + & V_{out,inlet} & \quad (3.63) \end{aligned}$$

Table 3.2: Effective flow volume and valve losses.

While the overall flown volume is already known, the main interest lies in the loss effects, that reduce the effective flow. There are three known effects that can be divided into two phases for mechanical check valves (Table 3.3). In phase (1) the valve in reverse direction is still deflected, in phase (2) it is closed.

$$\begin{array}{lccccc} & \begin{matrix} Phase\ (1) \\ reactive\ valve\ volume \end{matrix} & & \begin{matrix} Phase\ (1) \\ phase\ shift\ leakage \end{matrix} & & \begin{matrix} Phase\ (2) \\ static\ \ resistance\ leakage \end{matrix} \\ V_{in,outlet} = & V_{flap,cap}^{(1)\,in} & + & V_{phaseshift}^{(1)\,in} & + & V_{R,fl}^{(2)\,in} \\ V_{out,inlet} = & V_{flap,cap}^{(1)\,out} & + & V_{phaseshift}^{(1)\,out} & + & V_{R,fl}^{(2)\,out} \end{array} \quad \begin{matrix} \\ (3.64) \\ (3.65) \end{matrix}$$

Table 3.3: Loss effects of valves in micropumps with deflected (Phase 1) and closed (Phase 2) reverse valve.

The sum of possible loss influences is therefore:

$$\sum V_{losses} = V_{flap,cap}^{(1)\,in} + V_{flap,cap}^{(1)\,out} + V_{phaseshift}^{(1)\,in} + V_{phaseshift}^{(1)\,out} + V_{R,fl}^{(2)\,in} + V_{R,fl}^{(2)\,out} \quad (3.66)$$

The resulting valve efficiency with a maximum value of 1 is the effective volume divided by the flow volume:

$$\eta_{valve} = \frac{V_{flow} - \sum V_{losses}}{V_{flow}} \quad (3.67)$$

The leakage volume $V_{R,fl}^{(2)}$ due to static resistance leakage in phase 2 depends on the resistance ratio between forward ($R_{v,fw}$) and reverse ($R_{v,rv}$) valve direction at the remaining liquid volume with the sum of losses of phase 1 $V_{losses}^{(1)}$:

$$V_{R,fl}^{(2)} = \frac{R_{v,fw}}{R_{v,fw} + R_{v,rv}} \left(V_{flow}[f] - V_{losses}^{(1)} \right) \quad (3.68)$$

The reactive valve volume can affect both valves, but in a different manner [33]. It charges in phase (2), but only leads to losses in phase (1). First, valve deformation occurs for the valve in reverse direction that acts as a capacitance inside the pump chamber. Second, there is the valve capacitance, which denotes the displacement of the volume beyond the flap of the open valve in forward direction that works as reactive volume if the mode of the pump is switched. Zengerle and Richter [33] stated, that valve capacitance does not influence the flow rate at 'low frequencies', meaning below the cutoff frequency. However, for current highly damped micropumps the damping cutoff frequency decreases below 1-10 Hz not even including the creep effect. Thus this effect becomes the main valve induced loss influence at frequencies lower than 100 Hz. While the valve movement behaves quasi-statically and is governed by the liquid flow the reactive valve volume is the main loss effect. Only by increasing the driving frequency to the order of magnitude of the resonance frequency, a dynamic valve movement, based on the inertia of the flap and its surrounding liquid, leads to a real valve phase shift [90]. If no particles keep the reverse valve open, static resistance leakage is negligible due to small valve gaps (Figure 3.56).

Flow rate influence of reactive valve volume Ulrich and Zengerle [90] showed, that their flap valve (length: 1700 µm, width: 1000 µm, thickness: 15 µm) has a resonance frequency of 1200 Hz in water and acts quasi-statically up to frequencies of 200 Hz. As the used valve features a length of 800 µm and a width of 480 µm its resonance frequency would be higher and the applied driving frequencies only go up to 100 Hz. However, with the rectangular driving signal the highest actuator induced excitation frequency is ~23 kHz. Though, the flap will stabilize into quasi-static behavior soon given the time of at least 5 ms for frequencies below 100 Hz and a flap resonance frequency of higher than 1.2 kHz. Therefore, quasi-static behavior right before mode switching and no significant influence of dynamic phase shift leakage below 100 Hz were assumed.
The reactive valve volume originates from the forward flap capacitance at the last flow q_{last} through the valve before switching modes:

$$V^{(1)}_{flap,cap} \propto C_{flap}[q_{last}] \tag{3.69}$$

For a valve with flap width w_f, length l_f, thickness t_f and Young's modulus Y_f and a square valve seat with a length l_s of 380 µm and a width w_s of 6 µm, hydrostatic pressure is applied at the valve seat, corresponding to flap lengths from x_1 and x_2. According to Ulrich and Zengerle, the main pressure drop occurs at the valve seat [90]. A very accurate model was set up by Horsch to describe the flap deflection between x_1 and x_2 [91]:

$$z[x] = \beta \bigtriangleup p \, \frac{\left(x^4 - 4xx_1^3 + x_1^4 - 4x^3x_2 + 6x^2x_2^2\right) l_s}{2\, Y_f \, t_f^3 w_f} \tag{3.70}$$

For compensation of high deflections of several 100 µm and a reduced displacement due to negative pressure behind the valve seat at the diffuser element Horsch introduced a scaling factor β [91]. Compared to the 3D-FSI validation β=1, as the flap does not overextend the valve seat as much and deflections stay below 100 µm. The reactive valve volume for a deflected valve, with unrestricted inlet and outlet corresponds to the volume beneath flap and valve seat plane. For the calculation of a flow dependent reactive volume, the valve flow characteristic is needed. As the analytical models available cannot provide an accurate fit of the flow, a measurement is used, where flow is measured over hydrostatic pressure (Figure 3.56). The same Hill-fit in Equation 3.37 that is able to describe the actuator displacements can be used as a mathematical description to receive $\bigtriangleup p[q]$. The flow dependent reactive valve volume $C_{flap}[q]$ is obtained by combining Equations 3.70 with $\bigtriangleup p[q]$ and integrating over the relevant area:

$$C_{flap}[q] = w_s \int_{x_1}^{x_2} z[x]dx \tag{3.71}$$

For the quasi-static flap movement, the reactive volume depends on the last flow in the moment before switching. With no gas capacitance involved, this last flow can be derived from the dynamic displacement curves of the actuator:

$$q_{last}[t_{s2}||t_{p2}] = \frac{dz(t_{s2}||t_{p2})}{dt} v_d \tag{3.72}$$

Multiplying the capacitance volume with the frequency gives the frequency dependent flow reduction gives:

$$V^{(1)}_{flap,cap}[f] = \gamma_{dyn}\, f\, C_{flap}[q_{last}[f]] \tag{3.73}$$

, where a constant multiplier γ_{dyn} is needed to describe the dynamic leakage influence for the closing valve. Subtracting the measured flow from the calculated dynamic displacement flow 3.46 leaves us with the estimation of the remaining valve influence (Figure 3.57). While calculated reactive flap volume (3.73, $\gamma_{dyn} = 1$) only explains up to 8µl/min (Figure 3.57), a factor γ_{dyn} between 7-10 leads to a very good agreement of measurement and model based valve influence estimations (Figure 3.57). The dynamic leakage flowing through the reverse valve in the closing period is much higher than just the reactive valve volume, but reliably follows the course of it, as a more deflected valve enables increased dynamic leakage. The closer the switching positions are to the PCB, the lower is the pressure difference at the valve. Thus, valve closing is delayed and dynamic leakage increased, leading to the differences in γ_{dyn}.
With valve loss effects, the flow volume V_{flow} is transformed to the effective volume V_{eff} with the efficiency η_{valve}:

$$V_{flow}[f] \rightarrow V_{eff}[f] = \eta_{valve}[f]\, V_{flow}[f] \tag{3.74}$$

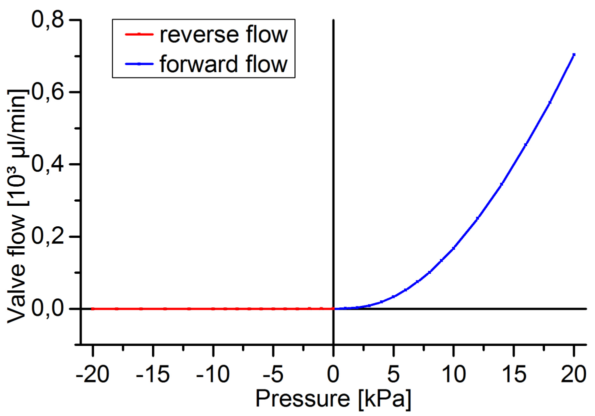

Figure 3.56: Measured pressure-flow valve characteristic in forward and reverse (<0.36 µl/min) direction.

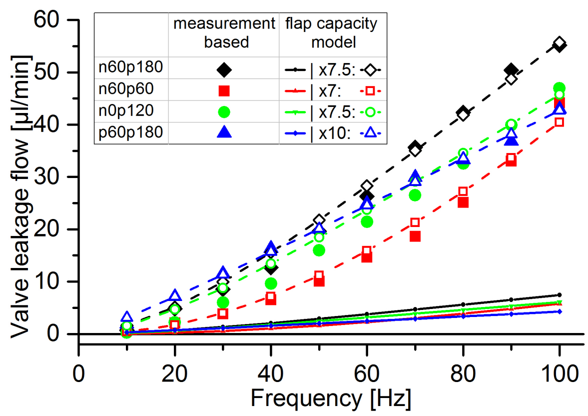

Figure 3.57: Measured valve influence and prediction of reactive flap capacitance losses.

Combined influences discussion

The three major flow influencing effects for self-priming, bubble tolerant micro diaphragm pumps are liquid resistive damping, gaseous capacitive damping and reactive valve volumes. They mainly affect maximum pump performance, but depending on the driving conditions also flow stability. The combination of all major flow rate influencing effects describe the maximum flow rate by multiplying the driving frequency times the frequency dependent effective volume:

$$Q_{max} = f\, \eta_{valve} \sigma_{cav} \mu_{disp} V_{stroke,static} = f\, V_{eff}[f] \tag{3.75}$$

The model is able to describe and predict the transient actuator displacement, derive the frequency dependent displacement and estimate the valve loss effect in order to determine the flow rate performance of the micropump. In addition, the inception of cavitation and time course of the actuator can be simulated, which is important for pump performance and flow stability.

One of the limitations of the CMM actuator model is that the determined RPCH dependent damping value is only valid for the presented pump chamber geometry. Even though the cubic damping function would persist, different chamber radii or inlet/outlet positions would change the absolute resistance values. However, the damping function of new geometries can be evaluated with the presented method. The model accuracy is also limited by the assumed instantaneous full force generation of the piezo compared to a slower process in reality due to delayed switching of piezo domains. The resulting creep displacement has therefore to be added to the pure damping curve to get the most accurate curve description. The frequency dependent displacement prediction model only considers resistive damping influence and is limited by the quality of the curve description. If the pump mode is switched with a still moving actuator, the time-compensated version of the displacement prediction model, which includes the valve reactive volume, has to be used for accurate simulations. The flow rate influence of the reactive valve model itself faces an prediction inaccuracy of $\pm 15\,\%$, due to transient pressure profile and amplitude, but is able to describe the frequency dependence very well. The cavitation model is very robust regarding the inception of cavitation at high viscous damping, but bubble growth and size at stable cavitation is harder to predict with many dependencies like the amount of solved gas or pressure distribution.

Performance wise, a piezoelectrically driven stiff diaphragm together with a shallow pump chamber enables a high compression ratio together with a high pressure ability. However, it was found that one of the most critical parameters in pump design is the remaining pump chamber height (RPCH), being the lower turning point just before switching to the supply mode. Decreasing the RPCH increases the gas pressure ability and therefore self-priming ability and bubble tolerance. But the low chamber height also leads to a squeeze film effect resulting in strong viscous damping and limiting the flow rate. On the one hand, the resistance in combination with a pressure ability above 97 kPa reinforces the tendency for cavitation, which limits the flow in the supply mode. On the other hand, the damped flow reduces the effectively redirected flow due to a reactive flap capacitance volume, if driven with a rectangular signal. This valve loss effect also feeds back to actuator, by significantly reducing the resistance until the reverse valve is closed. The higher the maximum performance, the smaller and more cost efficient the system can be made. The highest flow efficiency tends toward low voltages and low frequencies.

The flow stability is mainly influenced by the effect of cavitation. The rectangular actuation signal with a duty cycle of 0.5 features the highest pressure peak for the outlet and the highest flow at the peak flow frequency, but promotes cavitation in the supply mode. To shift the inception point of cavitation the supply signal shape can be smoothed, while keeping the rectangular signal for the pump mode and changing the duty cycle to give the supply mode additional time [56]. However, this limits the maximum driving frequency. The inception point can be further pushed to higher actuation pressure abilities by reducing inlet resistance, primarily by changing pump chamber geometry or by reducing valve forward resistance. Additionally, a capacitance right in front of the inlet can decouple inlet masses and lead to faster inlet flow. Last but not least, excess inlet pressure together with a free flow inhibiting valve [77] can shift the inception point. If only moderate flow stability ($\pm 10\,\%$) is required, the pump can be driven with a duty cycle optimized rectangular signal, maximum allowed electric field and frequency and in configuration with a degasser. Then, the pump may produce bubbles, but those will be resolved before leaving the system (Figure 3.54).

Conclusion

All major effects, influencing the flow rate of micro diaphragm pumps were described. For current bubble tolerant micropumps with high fluidic performance, analytical models were presented for the main three influences, resistive damping, cavitation related capacitive damping and reactive valve volumes. The individual effect models were combined into a single-cycle based frequency dependent flow rate model. Ultimately, guidelines for an optimization of maximum flow rate, energy efficiency, performance per size and flow stability were given.

With shallow pump chambers, in order to increase bubble tolerance, a high fluidic resistance was introduced. This leads to strong viscous damping, and displays the largest flow limiting effect for micro diaphragm pumps. To quantify this limitation the static displacement volume of a 1 Hz actuation is extrapolated linearly for increasing frequency. The resulting displacement volume per time is compared to the actually achieved value at 100 Hz. The decrease, as shown in Figure 3.46, varies between 23-43 % depending on voltage levels and remaining pump chamber height. The same comparison is made for the valve influence, which amounts for 6.2-12.4 % of the flow rate reduction, but absolute values are within a relatively narrow range of 43-55 µl/min for 100 Hz (Figure 3.57). Gas capacitances like bubbles and cavitation, limit both the maximum flow rate and the achievable flow stability. Due to stable cavitation, forming gas bubbles, the flow rate dropped down to 65 % of the original flow until the bubble exits the pump within periods of $<$1 min. Adding an inline degasser, flow accuracy of $\pm$1.5 % over 5 h and $\pm$2.2 % over 10 h of operation (Figure 3.54) were accomplished. Without full cavitation, temperature was the main influence and led to accuracies of $\pm$0.15 % for decreased frequency and of $\pm$0.08 % for decreased voltage levels both at 2 h of operation (Figure 3.55).

As an outlook, the suggested optimizations towards maximum flow rate, energy efficiency and accuracy together with the high flow stability still need to be carried out. An extension of the model including temperature, and viscosity dependence would be therefore be helpful. The presented flow rate model provides the foundation for these optimizations. The understanding of flow rate influencing effects and their dynamic behavior not only helps to increase fluidic performance of micropumps, but also to improve reliability at longterm operation. Furthermore, the frequency dependent flow rate model enables accurate linearization for easier closed-loop control. Thus, adequate application specific design of liquid dosing systems with micropumps that fulfill all requirements becomes possible.

4 Reliability of micropump systems

According to the International Electrotechnical Commission (IEC), reliability is defined as „The ability of an item to perform a required function under given conditions for a given time interval“ (IEC 60050, 19-02-06). While performance describes the reaching of an absolute value of a requirement, reliability describes the time-dependent continuity of performance values. The main task of dosing systems can usually be reduced to a flow rate within a certain accuracy over a stated lifetime and failure probability, for example, an application requires the system to achieve 100 µl/min flow rate (performance) that needs to stay within an accuracy of ±10 % (reliability) over a lifetime of 20000 h (reliability) within a failure probability of less than 1 % (reliability). Therefore, the lifetime denotes the time interval, where all performance requirements have to stay within certain boundaries, constituting the accuracy band. Whenever the accuracy criteria is left, a failure is taking place. For certain applications, like insulin dosing, it is crucial to stay within accuracy limits. There are numerous inherent and external influences, where little is known about their dynamic working principles and effect magnitude on the flow (Figure 4.1). Therefore, the major influences that lead to flow rate variations were investigated in this chapter.

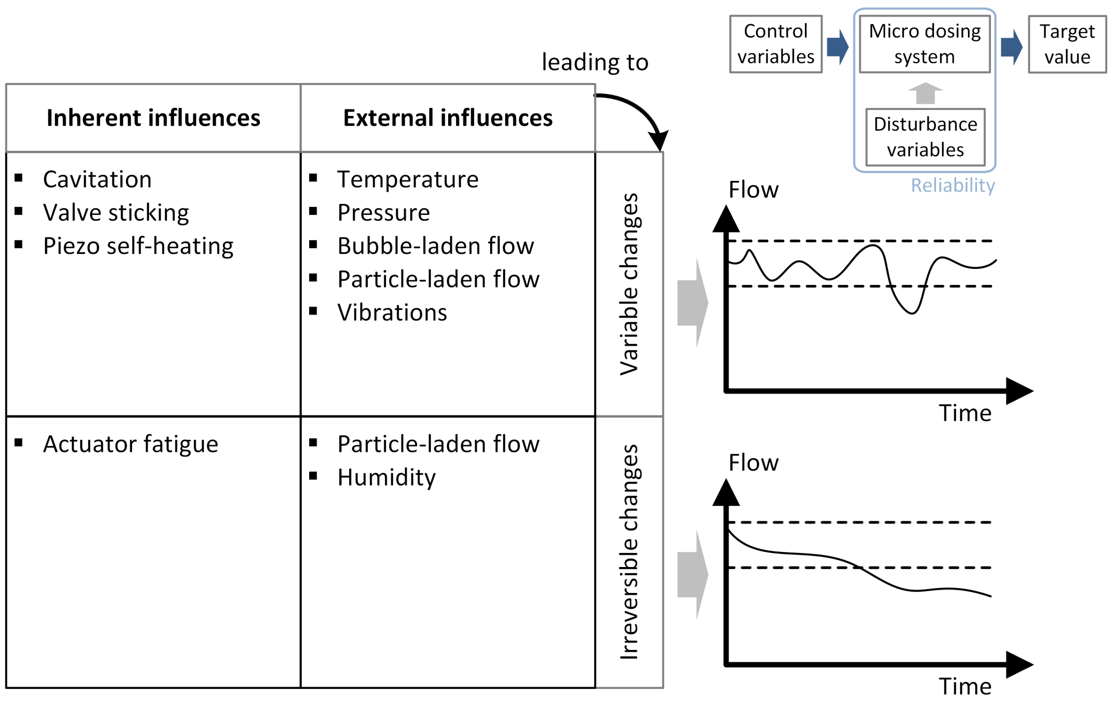

Figure 4.1: Reliability influences of micro dosing systems.

The root cause of flow rate variations are inherent influences, like cavitation, valve sticking or actuator fatigue and external influences, like variations of temperature and pressure, bubbles, particles or vibrations (Figure 4.1). These factors can lead to variable and irreversible changes. A simultaneous occurrence of

variations lead to a non-linear superposition of effects. The inherent influence of cavitation occurrence and its effect on performance and flow stability is already described in section 3.4. Actuator fatigue was investigated experimentally, by running longterm tests under different conditions. Inherent valve sticking was identified as a major issue of silicon flap valves with critical influence on flow stability. Guidelines to reduce sticking tendency by adaption of valve design is given. The consequences of temperature variations on the transient average flow rate was measured and evaluated by describing the impact of changing actuator zero-position, viscosity changes and piezoelectric expansion coefficients. The pressure dependence of micropump systems is mainly determined by the relative position and free displacement of the diaphragm. Therefore, the actuator stiffness was simulated and average and dynamic flow rate influence measured. For particle-laden flow, the failure locations, failure effects and critical particle characteristics were identified by supporting simulations and measurements.
The structure of this chapter follows the root causes of flow stability impairment, being inherent (section 4.1) and external (section 4.2) influences (Figure 4.1). Within these, the individual aspects of actuator fatigue (subsection 4.1.1), valve sticking (subsection 4.1.2), temperature dependence (subsection 4.2.1), pressure influence (subsection 4.2.2) and particle tolerance (subsection 4.2.3) are addressed.

4.1 Inherent flow influences

Inherent flow influences can appear under normal operation, meaning even if the driving and environmental operating conditions are within permissible limits. In this section, the dependencies and the magnitude of inherent effects are described. For the evaluation of the magnitude of flow rate change, the results from chapter 3 are needed. From experience, many different inherent effects are known. Two of the most important, being actuator fatigue and valve sticking, are investigated in individual sections. For a general overview, the known possible effects are described briefly. Here the effects are separated into reversible, meaning the ability of the influence to recover or vanish under operation, and irreversible effects.
As shown in section 3.4, cavitation is an inherent reversible effect that can influence the flow rate under certain conditions. Though, as it directly influences the function of the micropump and was integrated into the dynamic performance model of the micropump, it is located in the performance chapter and only referenced here: section 3.4 - paragraph 'Gas capacitance influence'.
A reversible inherent flow influencing effect is piezo self-heating [114, 89]. Due to dielectric hysteresis losses of the piezo, the actuator heats up and changes its deformation coefficient as well as its position relative to the pump chamber boundary (section 3.4). However, this effect only becomes significant for driving frequencies of several kHz and mainly with air. Pumping liquid beneath the diaphragm stabilizes its temperature and driving frequencies are usually far below several kHz, as the peak flow is reached at several hundred Hz for current micropumps. Minor irreversible mechanisms of piezo self-heating are depolarization and degradation through microcrack emergence [114].
Another reversible inherent effect is the actuator starting point with regard to the hysteresis. Both pressure hysteresis, but more important electrical hysteresis is responsible for varying starting points at same voltage levels. While the magnitude of pressure hysteresis is hardly an aspect for the reference pump type, electrical hysteresis was measured to cause a deviation of up to 30 % for the first pump cycle. Though, after the first cycle, the influence on the displacement falls below 5 % and vanishes after the second. Therefore, the influence has to be considered within a few strokes, but can be neglected for

continuous operation.
On the irreversible inherent side, one failure effect is the disconnection of a wire bond or any other electrical connection, for example due to vibration. Furthermore, humidity or leaking liquid may cause a shortcircuit at the piezo. High stresses may cause fractures of the flap, diaphragm (Figure 4.2) or piezo (Figure 4.3) or delaminate the adhesive. For electric fields above the specified limits or a temperature above the Curie temperature, depolarization of the piezo leads to reduced displacement efficiency. If inlet and outlet flow path feature an unwanted fluidic shortcircuit, pressure dependent leakage occurs. These are only the most common irreversible failure mechanisms and a full list needs to be obtained with a FMEA of each system individually to estimate the critical effects.

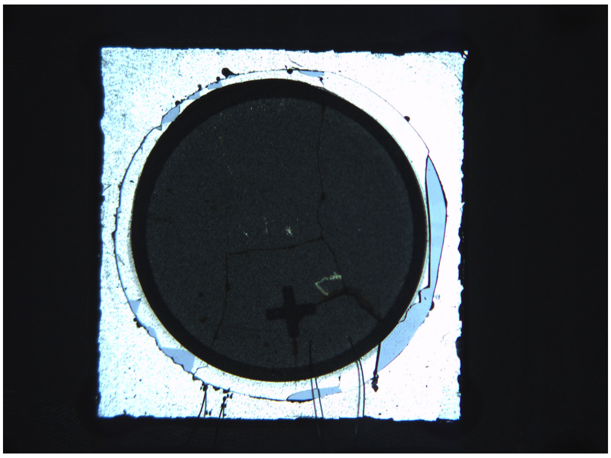

Figure 4.2: Photo of a diaphragm fracture.

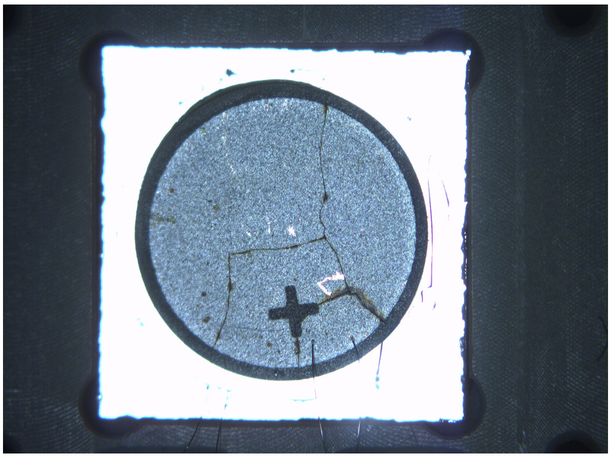

Figure 4.3: Photo of a piezo fracture.

4.1.1 Actuator fatigue

Actuator fatigue is the sum of all inherent variations of the actuator state. That includes changes of displacement per electric field or relative actuator position. Both effects will alter the flow rate, by mechanisms described in section 3.4. Fatigue tends to lead to irreversible changes, as internal and laminate material structure is affected. Therefore, the conditions that cause the major degradation, have to be well understood.

State of the art

The actuator consists of the piezo ceramic with its electrode layers, the diaphragm, which is attached to the pump body, and the adhesive, which connects the ceramic to the diaphragm. Fatigue may happen in all parts, but from literature and experience it is known to happen mainly at the piezo and the adhesive. In the piezo, mechanical and electrical degradation mechanisms are present. If stresses, particularly tensile stresses, exceed certain limits, microcracks may appear in the ceramic [115]. Especially in the instance of polarization switching, spontaneous cracking emerges [116]. Applying a signal with high slew rates induces high frequencies that may produce critical tensile stresses close to the resonance frequency or at a vibration overshoot [89]. Resulting cracks occur in a high dispersion and can hardly be detected by monitoring electrical resistance [117]. Once, microcracks emerged, the crack propagation is decisive for whether they grow to macrocracks through the whole ceramic. While cracks emerge more at tensile stress, cracks propagate faster under compressive than tensile stress [115]. Furthermore, an anisotropic

growth was observed, depending on the direction of the applied electric field [115]. While crack advance or arrest is a stochastic process [118], Lynch found that residual stresses at the domain boundaries are responsible as main crack propagation mechanism [116]. Microcracks lead to a distortion of the electrical field inside the ceramic [115, 119, 116], which reduces the possible displacement. In general, the crack fatigue mechanism strongly depends on the applied electric field [120, 121]. Suggested solutions to avoid cracks are to operate below the saturation level of a not fully polarized ceramic [116] and to stay below a certain mechanical strain to avoid irreversible damage [122]. Besides cracks, piezo fatigue occurs due to increased material hardness [123]. With increasing cycle number, the hardening rises due to domain switching. An initial degradation was observed, which was attributed to the relief of residual stresses from poling [124]. In combination of mechanical and electrical fatigue, the dielectric properties of the ceramic degrade with the number of cycles, because of the rearranging of domains away from the poling direction[125]. Pure electrical degradation takes place due to ionic migration, which increases the leakage current up to a total failure at a shortcircuit [126]. This mechanism can be detected by an increase of power consumption [126]. Main influences are humidity, porosity and the electrode material [127, 126].
The fatigue effects of adhesives were mainly investigated in the context of the full actuator laminate. Degradation of the adhesive involves mechanical as well as chemical mechanisms. Mechanical failure effects are either delamination or internal fracture. The chemical process of adhesive hardening of two compound epoxy resin is a stochastic thermodynamic process. It advances with time and temperature and depends on the mixing state of the resin. From the work of Gobert [128], we know that with increased hardening, inductivity and resistance decrease, while capacitance increases and resonance frequency remains constant. Following the hardening process recommendations of the producer seems to be good enough for practical stability but does not prevent subsequent changes of adhesive structure and rigidity. Actuator fatigue tests with a sinusoidal signal, performed by Wackerle [129] revealed that displacement variations may occur over time. Though, the displacement kept stable, after exposing the actuator to an additional 6 h at 130 °C after initial hardening and before operating load.

Research goal

The fatigue effects, know from the state of the art, do not lead to technically relevant degradation for modest signals and conditions. However, it is yet unknown, how the actuator would act in a typical micropump environment. From the experience of operating actuators with micropumps, actuator fatigue seems to occur in different magnitudes. This may be due to the challenging conditions of actuators in micropumps of high electric fields, rectangular signal or the touch down of the actuator against a pump boundary or pump fluid. Therefore these aspects need to be evaluated for micropump actuators to understand the influences and effect magnitudes of different fatigue mechanisms.

Methods

The main method to determine the actuator changes from the cyclic load was to measure the voltage or electric field dependent displacement of the actuator before and after the load. To determine the center displacement reliably, the line displacement with a lateral resolution of 2 µm was measured for each voltage step of 20 V. The average center displacement was calculated by averaging the centered 80 values, standing for a 40 µm distance of the 6.3 mm diaphragm. As the electric hysteresis of the piezo influences the measurement accuracy, only the second loop was used to evaluate the changes. Besides the averaging of multiple measurement points, the quasi-static measurement allows for a complete pressure equalization, which delivers an accurate and reliable measurement even if one valve is sticking.

From these measurements, two parameters can be extracted. First, the relative free static displacement is the difference between the lowest voltage (-60 V for MIKROAUG pump, -76 V for TUDOS pump) and the touch down of the actuator against the pump chamber boundary (kink in line) (Figure 4.4). Second, the displacement efficiency is the average displacement per applied voltage difference, extracted for the same range of free displacement (Figure 4.6).
The driving signal was controlled with an arbitrary wave form generator, amplified to high voltages with an extra amplifier (A). The environmental parameters of the lab were monitored and provided relatively stable conditions.

Results
For the evaluation of actuator fatigue both EMFT pump types (1.2) were stressed with different driving signals. Two effects were observed that change the effective displacement. Either the predeflection changes, which originates from the fabrication process to achieve a higher compression ratio. Or the displacement efficiency varies, described by an average displacement per applied electric field or voltage. At pure predeflection change (Figure 4.4) the actuator position, relative to the pump chamber boundary, is shifted. The hysteresis or the displacement efficiency can remain stable. The position shift can go in both directions and increase and decrease free displacement. In the case of altering displacement efficiency, two effects were observed. First, a linear change over the whole voltage range was observed, which either increases efficiency (Figure 4.5) or decreases efficiency by widening mainly the right hysteresis flank (rising voltage). Second, a bent displacement curve was measured, that so far only resulted in a decrease of efficiency (Figure 4.6).

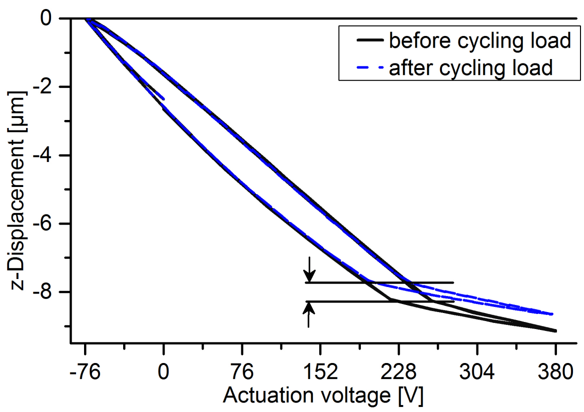

Figure 4.4: Example to a case of pure predeflection loss.

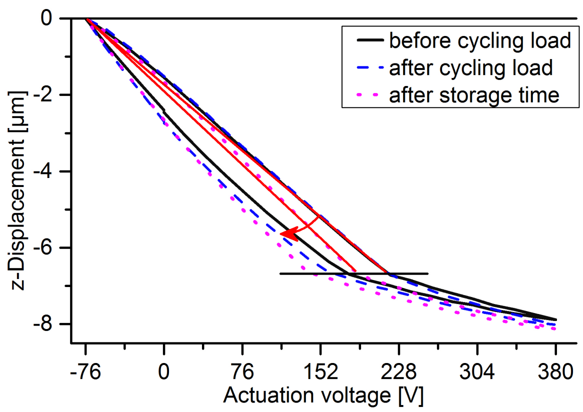

Figure 4.5: Example for a case of linear deflection efficiency loss.

To start with, the TUDOS pump type was stressed with different signals in air and water. Subsequently, the MIKROAUG pump was tested with water and the preferred rectangular signal for comparison. The standard procedure includes a static measurement before and after the cyclic load. The number of cycles was chosen as benchmark over pure time, because the domain switching in each cycle is the main fatigue mechanism.
The first set of TUDOS pumps was applied with the signal for highest fluidic performance in air, being a rectangular signal of -0.4|+2 kV/mm electric field strength and was strained for a little over 1 million cycles. The average loss of predeflection was 0.63 µm (Figure 4.7). The wave form of the signal was

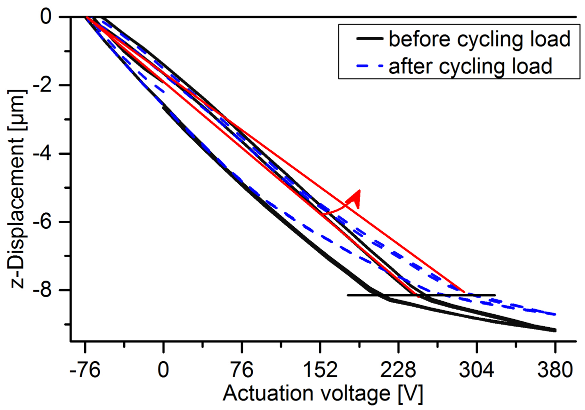

Figure 4.6: Example for a case of non-linear deflection efficiency loss.

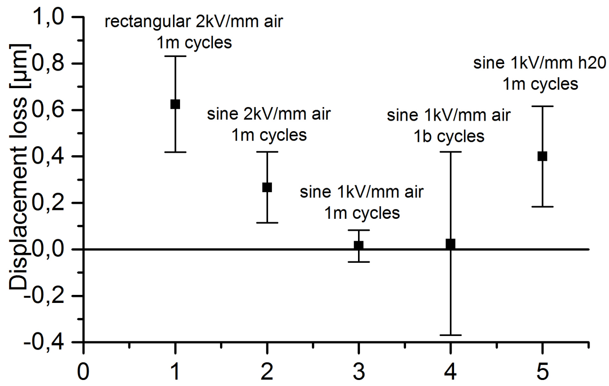

Figure 4.7: Predeflection loss for TUDOS pump type at different signals in air and water.

switched to sine to reduce maximum temporary stresses, resulting in an average predeflection loss of 0.27 µm (Figure 4.7). At a sine signal with 1 kV/mm positive electric field, both the electrically induced stresses were reduced and the mechanically induced stresses due to bending and the touch down of the actuator at the pump chamber boundary was avoided. This lead to a calculated average predeflection loss of 0.01 µm (Figure 4.7). With the sine signal, the predeflection did not change significantly over 1 million cycles. To test the long-term durability for this signal, the pumps were stressed for 1 billion cycles. Even though the calculated average predeflection loss of 0.02 µm is still low, the standard deviation almost six-folded with the highest single loss of 0.5 µm (Figure 4.7). As the objective are liquid dosing systems, the air tests were only run to ensure a reliable and simple test setup that provides the basic insights. Changing the setup to pump water, the average predeflection loss was 0.4 µm for a sine signal with -0.4|+1 kV/mm after 1 million cycles (Figure 4.7). The pumps were stored after the cyclic load and measured again after a few thousand hours to monitor any changes due to storage time. In general, the average changes were relatively low and seemed to decrease with time (Figure 4.8). Though the standard deviation of stored pumps after 1 billion cycles was relatively high.

The MIKROAUG pump type was tested with 8 samples with water and a rectangular signal of -0.4|+1 kV/mm over up to 6.3 million cycles. Despite a significant spread of data points, the predeflection loss seems to be increasing linearly with the number of cycles (Figure 4.9). While the predeflection reduction of the TUDOS pump type showed an average of 0.4 µm/million cycles at sine signal with water, the MIKROAUG pump exhibits an average of 0.7 µm/million cycles at rectangular signal. Though, despite the wave form, overall displacement of the MIKROAUG pump type is usually larger by a factor of 1.6 compared to the TUDOS pump type. Additionally, the MIKROAUG pumps tested in water showed a decrease in efficiency by widening the electrical hysteresis mainly on the right flank for increasing voltage.

Discussion

The displacement efficiency describes the displacement per voltage. If it changes, either the force generation (piezo) or the force transmission (adhesive) has to change. A linear increase of efficiency can either originate from an improved polarization of the piezo or a hardening of the adhesive that improves the force transmission. A linear decrease usually comes along with a widening of the electric hysteresis and can be attributed to the piezo. A nonlinear efficiency decrease, especially at higher electrical fields is most

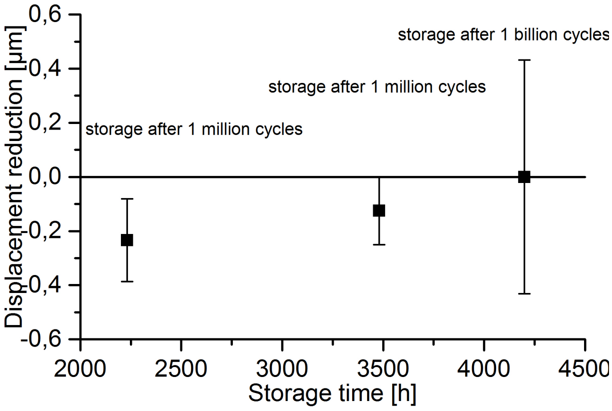

Figure 4.8: Influence of storage time after different cyclic load.

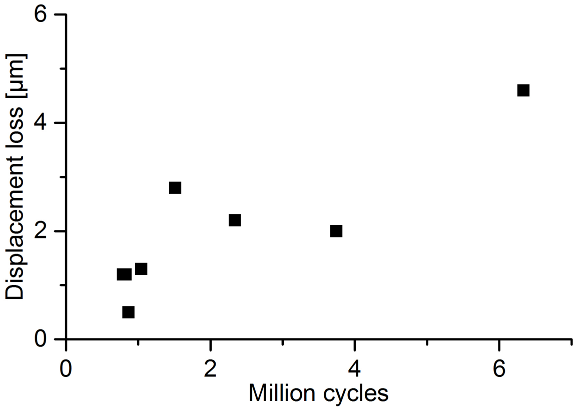

Figure 4.9: Distribution of MIKROAUG pump predeflection loss over number of cycles, driven by a rectangular signal pumping water.

likely an actual degradation of the piezo, as explained in the state of the art. The predeflection change can not be explained with a modified force generation or transmission, as the efficiency stays constant. Here, the relative position of the actuator and the pump chamber boundary varies. To achieve predeflection, the adhesive has to harden, while the piezo is in a shrinked state due to an applied positive electric field. After hardening and zeroing the electric field, the actuator predeflects. Measurements showed that this state can shift upward and downward due to cyclic load and storage time. The reason could be a lateral creeping of piezo position relative to the diaphragm, allowed by the adhesive due to the release of residual stresses. That means certain areas and connections within the adhesive get overstressed and disconnected, which leads to a loss in predeflection. In the new position the force transmission remains on the same level as before creeping. Thus, Young's modulus and force transmission stays constant. Therefore, the main fatigue mechanism most likely takes place in the adhesive and not the piezo. Despite touch down impact at 2 kV/mm or rectangular signal, the fatigue is limited to predeflection loss for the TUDOS pump type in air and water for all signals. Storage time increased predeflection on average. For the MIKROAUG pump type, the fatigue mechanisms are both predeflection loss and displacement efficiency loss. Only the predeflection loss is shown, as it is the performance limiting aspect and the pump chamber boundary is still reached. The magnitude of the predeflection loss and the additional efficiency loss can be explained by the higher deflections and therefore higher tensile stresses in the MIKROAUG pump type.

Degradation mechanisms follow the expected results in most cases, but measurements exhibit a high spread of results. This dispersion is caused by the technical spread of fabrication methods and the stochastic nature of piezo and adhesive fatigue mechanisms. Additionally, external conditions like temperature and humidity are yet neglected influences. Despite the possibility of avoiding certain operating conditions, the high deviations hardly allow for a systematic compensation of fatigue effects.

Conclusion

Fatigue mechanisms of piezo laminate actuators were investigated. Two main effects were identified, a change in predeflection and displacement efficiency. Both the adhesive layer and the piezo ceramic contribute to the fatigue effects. Though, the adhesive seems to be the main performance limiting aspects, especially for the MIKROAUG pump type if driven with water. Here, an average linear degradation of

0.7 µm/million cycles was measured. The TUDOS pump type shows less fatigue, but a clear dependence on the signal and its implications. While the softest signal (sine, 1 kV/mm, no touch down) shows minimal degradation, a rectangular signal of 2 kV/mm, including a touch down on the pump chamber, features the highest average degradation of 0.63 µm after 1 million cycles. Storage time has less influence and depends on the cyclic load before storage, but features a high spread from pump to pump, increasing with cycle count.

As an outlook, it would be interesting to see, whether the predeflection loss saturates eventually. Furthermore, to compensate for predeflection losses in micro dosing systems, a displacement sensor would enable the realtime adjustment of voltage levels.

4.1.2 Inherent valve sticking

Sticking, also referred to as stiction, of the valve is one of the most critical inherent failure and flow influencing effects for micropumps. Here, surface forces between the valve sealing lip and the flap prevent or disturb the valve from opening correctly. This changes the effectively moved volume of the pump and thus changes the flow rate. As the effect can even lead to a full stop of flow rate, it has to be seen as one of the most critical influences of current micropumps. Even though most influencing factors of sticking are known, it is hardly possible to predict its occurrence.

State of the art

Sticking in MEMS devices is a long known phenomenon and problem [130]. Responsible for this effect are forces between two surfaces. These interfacial forces can be of various nature, being capillary, van-der-Waals, electrostatic or chemical, like hydrogen bonding [130, 131]. The issue was most relevant for many MEMS devices and many studies and reviews were conducted to understand and solve it [132, 133, 134, 135]. The main differentiation was made between release sticking and in-use sticking. Release sticking takes place after a wet etching process, where capillary forces draw a flexible part, like a cantilever or diaphragm, towards another surface in the drying process. As a consequence high energy hydrophilic surface forces withstand the resilience of the part and keep it adhered [131]. In-use sticking takes place while under operation or in storage. Mastrangelo developed a method to quantify the sticking work [136]. In micropumps especially in-use sticking is an issue, but either emerges in the handling process before the first operation or occurs while under operation or subsequent storage. The closing reverse valve faces the internal pump chamber pressure, which presses the flap against the sealing lip area and facilitates the surface contact.

Two types of solutions to overcome release and in-use sticking are reported in literature, either physical or chemical modifications. Physical modifications confine themselves to the reduction of contact area, for example by roughening the surface structure, typically done by selective etching [133]. Surface reduction of up to a factor of 20 was reported [137]. The chemical approach alters the surface composition [138] by either changing the substrate surface, treat the silicon surface in NH4F or HF [139] or apply hydrocarbon or fluorocarbon-based self-assembled monolayers (SAMs) [140].

In the EMFT micropump, the issue of valve sticking appeared in various pump types. While the nature of the surface forces could not yet be identified with certainty, Gradl and Herz stated that probably a hydrophilic bond between the native oxide of the silicon surfaces is responsible for the valve sticking. Here the water from air humidity causes OH-groups to attach to the native silicon oxide. With two opponent surfaces of flap and sealing lip, hydrogen bridge bonds can form. This hypothesis was supported by experiments, where valves were heated up to 90 °C, causing the OH-groups to desorb from the oxide surface and valve sticking vanished subsequently. Further validated statements were made concerning the nature of sticking. A continuous operation reduces sticking, however storage time increases it. Valve opening pressures of up to 26 kPa were measured. Valve sticking emerged after some time of operation or storage, even if a pump did not exhibit sticking before. The valve leakage in reverse direction was independent from the valve opening pressure. After changing the fabrication process and the micropump design to achieve higher gas pressures, the valve sticking seemed to not be an issue for varying periods.

Research goal

During many measurements, valve sticking emerged as an issue for the current valve design, which is equivalent for the TUDOS and MIKROAUG pump type. The goal is to prove the occurrence and magnitude of valve sticking. Furthermore, the theoretic solutions from literature are evaluated together with valve simulations to suggest appropriate solutions to overcome flap valve sticking.

Methods

To eliminate the multitude of possible flow rate influences that are present in water, air measurements were chosen to evaluate valve sticking. As valve sticking occurs unpredictably, measurements over long periods of up to 2000 h and 2 billion cycles were evaluated for signs of valve sticking. The setup to measure the flow rate consisted of parallel driven pumps with the identical operation signal, while monitoring flow, operation voltage levels, temperature and humidity. For the evaluation of failure effects, static and dynamic center displacement and static valve opening pressure was measured subsequently.

Results

In order to systematically evaluate, if valve sticking is an issue in current EMFT pump types, a long-term test with air and parallely driven micropumps was set up. The valves of both EMFT pump types are identical and therefore comparable. TUDOS pumps were used to run the long-term tests of 1-2 billion cycles. 3 out of 10 pumps exhibited sudden flow jumps and were investigated in more detail. The flow course of three different pumps with sudden flow rate changes show the possible variation of pump characteristics (Figure 4.10). To exclude the possible influence of environmental parameters temperature, humidity and pressure, these were monitored and partially controlled with a climate chamber. The only significant correlation within the parameter variations was found for temperature (section 4.2.1). However, this effect is not strong enough to explain the sudden deviations in flow. Furthermore, positive and negative voltage levels were monitored and displayed a perfectly stable performance. The behavior of the main flow influencing parts, being actuator and valves, were investigated individually after the long-term test. Static and dynamic displacement showed stable values in the expected magnitude. But passive valve opening pressure displayed a initial opening pressure of 20 kPa (Figure 4.11 - black), which vanished in the second loop. After applying 10 kPa counter pressure at the outlet, which pushes the outlet flap towards the sealing lip area, the valve opening pressure returned with 17.5 kPa (Figure 4.11 - red). The valve opening pressure only shows the threshold pressure for the valve with the highest threshold, as the pressure is applied at the inlet of the pump and measured behind the outlet. The range of valve opening pressure, however is quite large. While most pumps show a passive valve opening pressure of <25 kPa, as in the long-term tests, individual pumps had opening pressures of up to 200 kPa, especially if driven with water before.

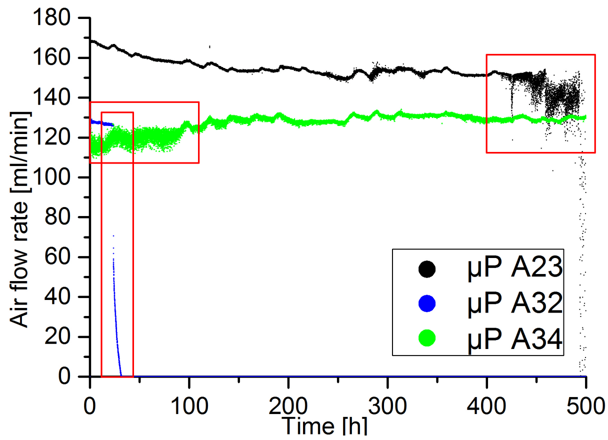

Figure 4.10: Course of air flow rate of three TUDOS pumps in long-term measurements of 500 h, showing sudden flow variations.

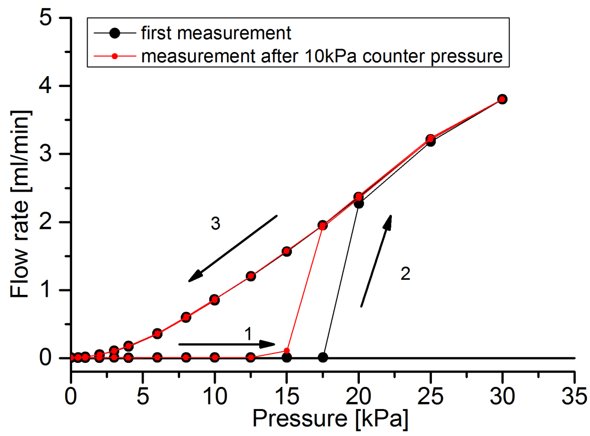

Figure 4.11: Typical passive valve opening pressure (A32) after the long-term test (black) and subsequently after applying 10 kPa counter pressure (red).

The conditions for water are different, because capillary forces at phase boundaries may increase valve opening pressures [92]. However, in the absence of bubbles, the effective valve opening force is higher due to the incompressible liquid. In the case of liquid dosing systems, when the fluidic path is still gas filled but not able to self-prime, initial sticking is the first main issue to overcome. For a filled path without bubbles, stable dosing becomes possible if additional other factors like cavitation (section 3.4) or particles (subsection 4.2.3) are avoided. Providing these conditions, stable dosing over 3 h for frequencies between 10-100 Hz was achieved (4.12). Thus, the pump did not show any signs of valve sticking during operation, but initial sticking after downtimes of several hours.

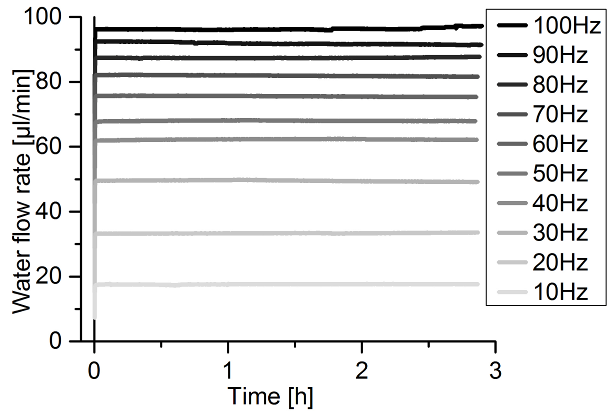

Figure 4.12: Stable water dosing conditions with -0.4|+0.1 kV/mm at a rectangular signal and varying frequencies (10-100 Hz).

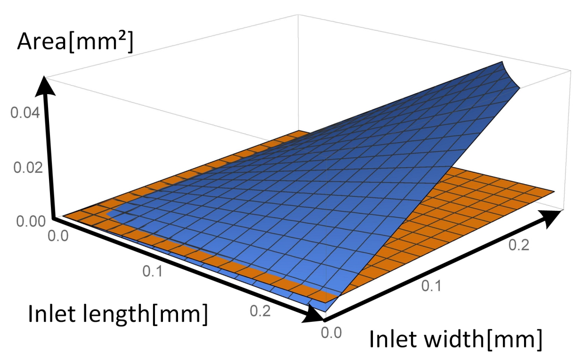

Figure 4.13: Valve sticking resistance indicators: pressure application area (blue) and contact area (orange) over valve inlet length and width.

For a reliable self-priming and start-stop-behavior, valve sticking needs to be prevented or its influence reduced to a negligible magnitude. Based on the concepts in literature, the most appropriate solutions are proposed. First, to reduce surface forces, the contact area $A_{contact}$ from the valve model (section 3.2) needs to be minimized:

$$A_{contact} = (w_i + w_s)\,(l_i + w_s) - l_i\,w_i \tag{4.1}$$

The other important factor is the effective opening force F_{open}:

$$F_{open} = p\,A_{pa} \tag{4.2}$$

, which depends on the pressure application area A_{pa}:

$$A_{pa} = l_i\,w_i \tag{4.3}$$

Combining both, a sticking resistance ratio is proposed:

$$r_{sticking} = \frac{A_{pa}}{A_{contact}} = \frac{l_i\,w_i}{(w_i + w_s)\,(l_i + w_s) - l_i\,w_i} \tag{4.4}$$

With increasing x_1, the contact area minimizes, while the effective opening force decreases as well. To maximize the sticking resistance ratio in Equ. 4.4 the inlet area should be as large as possible (x_1 minimal), optimally featuring a square inlet (Figure 4.13). Considering self-priming ability and bubble tolerance, the valve dead volume should be minimized as well. Therefore, the valve should feature a square flap with the maximum inlet pressure application area, if the flow performance is not critical. Because flow performance will drop due to a maximized flap capacitance, high valve flow resistance and increased reverse leakage due to high deformation (compare to 3.2).
Another option to improve valve sticking resistance, but avoiding a high flow performance loss, is by roughening the sealing lip surface. A reduction of surface area of up to a factor of 20 was reported [137]. This way, the sealing lip width can stay wider to decrease reverse leakage. Also the pressure application area can be reduced by increasing x_1 to provide large deflections of a narrow cantilever flap with low flow resistance. However, a reduction by a factor 20 would still keep valve sticking in the magnitude of possibly significant influence. With its changing magnitude and unpredictability, the reduction would need to be even larger. In addition, the mask design and process steps have to be adjusted significantly to implement selective etching on just the contact area between sealing lip and flap.
As a chemical modification, coatings are an option. Though, temperature levels in the subsequent process flow might yield challenges to biocompatibility and long-term stability. Therefore, rather a surface material change is suggested, where silicon nitride could replace the native silicon dioxide in the contact area. Silicon nitride features a lower hydrophilicity, which would reduce the surface forces. On the other hand, a reduction of hydrophilicity would lower the chances for a completely filled chamber, where bubbles might get trapped inside. These bubbles would take longer to dissolve if they can not be pumped out.

Discussion

Even though, the nature of the surface forces are not yet fully clear, it was shown that valve sticking is still an issue in EMFT micropumps. Sudden flow rate changes could be attributed to the sticking of valves in long-term measurements for 3 out of 10 pumps. The main problem with valve sticking is its unpredictable nature and effect magnitude. Valve sticking can appear as initial sticking, stabilize in operation or emerge after tens or hundreds of hours. It can lead up to a total failure with flow rates dropping to zero. The measured valve opening pressure mostly displayed levels below 25 kPa but reached up to 200 kPa. Initial sticking prevents self-priming and restart sticking frequently appears after hours of downtime after pump liquids. On the other hand, continuously stable operation without sticking was achieved by providing the right operating conditions. Both the unpredictability and the effect magnitude make it the most critical effect for micropump flow stability.

Therefore, a strategy to avoid sticking in micropumps is required for continuous reliable dosing. A roughening of the contact area seems to be the most promising approach of physical modifications. Thereby, the micropump performance is hardly affected and no narrow sealing lip edges increase the chance for fractures of the flap, as for contact area reduction. Within chemical modifications, changing the contact surface from native oxide to silicon nitride is promising, as surface forces can be reduced, while keeping a certain hydrophilicity. Through sufficient hydrophilicity, trapped bubbles can be prevented, while properly filling the pump chamber. The second best chemical choice are coatings, but processing was reported to be difficult and long-term stability is an issue if aggressive reagents are involved for cleaning purposes.

After all, valve sticking needs to be reduced to a level, where delayed valve opening behavior does not lead to significant flow rate influences. The accuracy budget of most applications is in the region of $\pm$5-20 % and temperature dependence and actuator fatigue already challenge the flow stability substantially.

Conclusion

Surface adhesion effects are a well known phenomena in micropumps. In current EMFT micropumps, the contact area between valve flap and sealing lip area are of high quality and planarity. This enables valve sticking in micropumps, where both contact areas are pressed against each other in every pump cycle. The magnitude of this sticking effect is so substantial that it may result in a total failure of the pump. Unfortunately, these pumps cannot be sorted out preliminary, as the effect is not predictable so far. The conclusion is that the effect magnitude has to be reduced by several orders of magnitude to reliably run accurate micro dosing systems. With the effect being known in literature since the 1990s, several avoidance methods were developed. After an evaluation, the proposed solutions are either a roughening of the contact area or replacing the native oxide surface with silicon nitride to reduce the surface forces themselves. Though, these changes require significant process changes and the effectiveness of the solutions have yet to be evaluated for flap valves.

4.2 External flow influences

The most important external influences for micro dosing systems are pressure levels, temperature, vibrations and particle or bubble laden flow. They affect the micropump component itself, but also other system components, such as particle filter, degasser and bubble remover, flow sensor or the general fluidic path.

The state of the art of bubble influence and bubble prevention is discussed in depth in section 3.4 (paragraph 'gas capacitance influence'). Depending on the flow stability requirements, bubbles often have to be prevented. Otherwise, temporary and even sustaining flow rate drops have to be faced.

Vibration from external sources can also affect the dosing stability of micropump systems. Besides shock events that may damage the integrity of the system and its connections, the dynamic valve and actuator behavior may be influenced by continuous vibrations in the region of related resonance frequencies. Thus, amplified valve leakage reduces the redirection efficiency or altered diaphragm oscillations may increase or decrease effective dynamic displacement and therefore the flow rate. From section 3.4, it is known that valve resonance frequencies are >1.2 kHz and actuator resonance frequencies are ~23 kHz. However, resonance frequencies vary depending on the load and stresses. Except for an application of oil lubrication at machine spindles [96], no other application is known to be exposed to vibrations in the relevant range. But even if vibrations occur, they need to be damped or decoupled from the micropumps, as their influence is hardly predictable or controllable. Furthermore, in the current state of EMFT micropumps, sticking could be increased by vibrations due to enforced contact between flap and sealing lip area.

4.2.1 Temperature dependence

Temperature is one of the major flow rate influencing effects for liquid dosing systems based on micropumps. This parameter already varies significantly during a day cycle due to climatic aspects, but is also affected by additional sources, like nearby machines or humans themselves. Furthermore, the micro dosing system itself can contribute to cooling due to evaporation or to heat generation and dissipation through losses at the piezo, sensors or pump driving electronics. For the tested micropump systems, though, the environmental temperature is the largest factor, mainly influencing liquid and actuator temperature.

State of the art

The influence of temperature on system performance includes many aspects. Askamp [141] investigated the effect of temperature on a micropump based pipetting system, which pumps air in order to move liquid. He fixed the driving signal and number of cycles and measured the dosed volumes, the changes of dynamic actuator displacement and air viscosity. The results showed flow rate variations of <3.5 % over a range of 30 K at dosing 1ml. However, the effects at pumping air are quite different and partially opposite from pumping water. For example, additional effects like pump chamber height depending damping increase to a relevant magnitude and the viscosity of water decreases with rising temperature, while air viscosity increases. Matsumoto et al. [142] even used this temperature dependency of liquids to build a pump that runs on this principle. Over the last 130 years, a multitude of models and correlations were proposed to describe the influence of temperature on liquid viscosity, which was summarized well by Seeton [143]. He mentions that the most referenced model is unfortunately often wrongly referred to. Furthermore, piezo self-heating is a significant aspect while pumping air [141], but far less important for water due to increased water cooling and in general lower frequencies. The change of piezo characteristics themselves mainly depend on the material composition [105].

Research goal

With the goal of high dosing stability, the influences of temperature on the system performance of liquid micropump systems need to be investigated and understood in order to reduce the influence systematically. Therefor the effect of temperature on liquid flow rate in general and with individual contributions of actuator and liquid need to be evaluated in order to alter the dependency by design or operation.

Methods

To measure the flow rate, a Coriolis flow meter was used (see Appendix A). This mass flow meter includes an integrated temperature sensor that was used to measure the temperature in the liquid at the outlet. A climate chamber (see Appendix A) was used for closed-loop control of the temperature at a constant humidity of 23 %. Even though the temperature changes of 4K were reached within minutes inside the

climate chamber, the whole micropump system needed 1.5 h to reach a steady state. The temperature dependence of the Coriolis flow sensor has to be taken into account as well.
The static displacement measurements to determine the free displacement above the pump chamber boundary were conducted with a profilometer (see Appendix A) inside a lab. As the profilometer could not be integrated in the climate chamber, the variations of lab temperature (~3 K) were utilized to measure the temperature influence of the actuator itself.

Results

The flow rate of a MIKROAUG pump is strongly dependent on the temperature and amount for an increase of 100 % at a change of 22 K between 12-34 °C for a driving frequency of 100 Hz with a rectangular signal and electric field levels of -0.4|+1.2 kV/mm (Figure 4.14). The dynamic change of flow rate seems to be split in two parts, first a very fast and high change of flow rate within minutes and second a slowly increasing flow change over 1.5 h (Figure 4.15). While the environmental temperate inside the climate chamber adapts to the 4 K-step within minutes, the liquid temperature was monitored as well, which only increases slowly (Figure 4.15). In order to evaluate the effect magnitude of potential influences, additional evaluations were done for the micropump actuator and the water viscosity. The valves should not be affected by a temperature change, as the flap is uniformly surrounded by native oxide, which leads to no significant bending stresses.
The free displacement of the actuator, relative to the pump chamber boundary, increases along with temperature (Figure 4.16). While temperature could only be varied about 3 K, multiple measurements were taken that indicate an exponential increase of free displacement with rising temperature (Figure 4.16). At a linearization, the effect amounts for 0.14 µm/K or about 1 %/K. The reasons for this effect are in the different thermal expansion coefficients $\alpha[T]$ of diaphragm and piezo material and in the varying piezoelectric properties. The dielectric properties of the ceramic itself would lead to a different displacement efficiency, but only changes about 0.05 %/K (d_{31}) for PIC255 and is even lower for PIC151 (TUDOS pump type) and can therefore be neglected. Thermal expansion, though leads to a length variation $\triangle L$, based on the initial length L_0, according to:

$$\triangle L = \alpha[T]\, L_0 \,\triangle T \tag{4.5}$$

Thermal expansion coefficient of silicon is $2.57{\times}10^{-6}K^{-1}$ [144] and of the piezo ceramic (PIC255) is between 4-8$\times 10^{-6}K^{-1}$ [105] leading to a relative factor of 1.5-3. This causes the actuator to change its relative position compared to the pump chamber boundary, as observed in the measurements. However, this effect only changes the flow rate if the dynamic displacement varies, which only takes place if the actuator touches the pump chamber boundary or if damping is changed significantly. In the current case, the actuator just about does not touch the boundary but faces strong viscous damping (3.4). Around 100 Hz, the flow rate is highly frequency dependent and a change in actuator zero-position significantly changes the effective dynamic stroke (Figure 4.18), as the damping increases towards the pump chamber boundary by the power of three. The dynamic displacement is then linearly proportional to the flow rate.
The dynamic viscosity of the liquid also depends on the temperature (Figure 4.17) and without the critical region can be described with [145]:

$$\mu = \mu_0[T] \times \mu_1[T, \rho] \tag{4.6}$$

with the density influence $\mu_1[T, \rho]$ the part of pure temperature dependence $\mu_0[T]$:

$$\mu_0[T] = \frac{100\sqrt{T}}{\sum_{i=0}^{3} \frac{H_i}{T^i}} \tag{4.7}$$

with experimentally determined coefficients H_i. Fluid flow through the shallow pump chamber mainly depends on wall and fluid friction (Hagen-Poiseuille - Equ. 3.13) and is proportional to dynamic viscosity: $q \sim \mu^{-1}$. With lower fluid flow resistance, the damping is reduced linearly, which reduces the damping by a constant factor. In the range between 12-34 °C the viscosity is reduced by 40 % which theoretically leads to a flow increase by a factor of 2.5. In terms of damping reduction this is equivalent to a shift of lower turning-point position of 1 µm and therefore an average, but non-linear change of 0.045 µm/K. The effect on the flow rate due to a shifted actuator position is according to the thermal expansion shift (Figure 4.18), but the effect due to the viscosity change is only about a third as high.

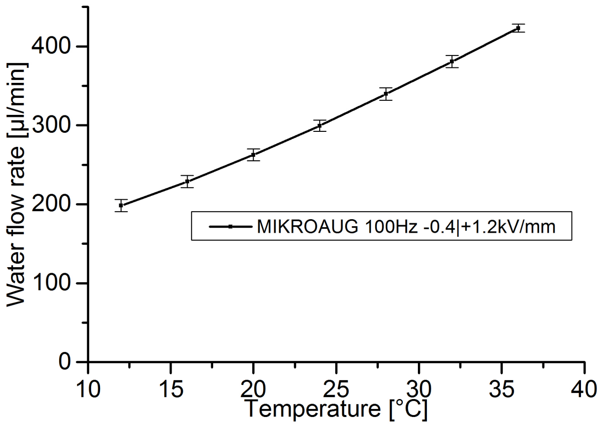

Figure 4.14: Temperature dependence of liquid flow rate of a MIKROAUG pump.

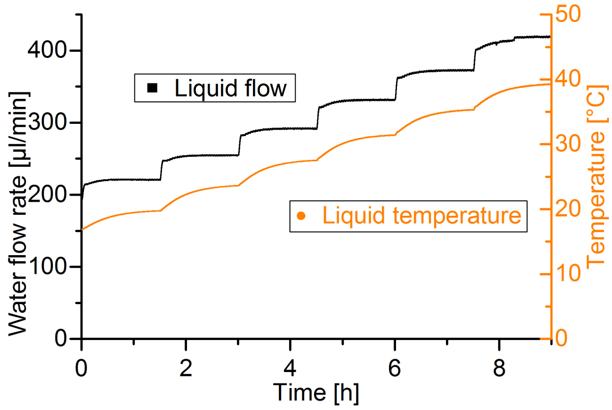

Figure 4.15: Transient flow course of one temperature cycle compared to the transient course of liquid temperature.

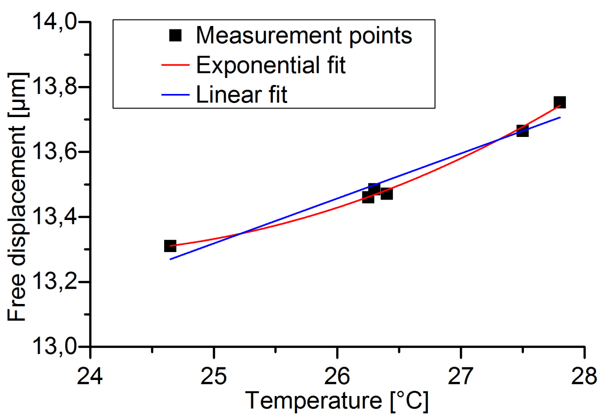

Figure 4.16: Measurement and two potential fit curves (linear and exponential) of temperature dependent free displacement.

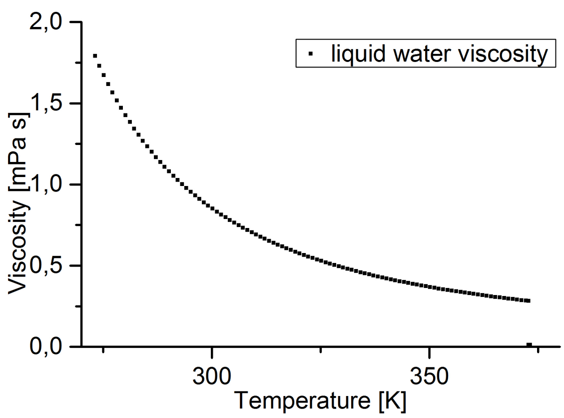

Figure 4.17: Temperature dependency of liquid water viscosity.

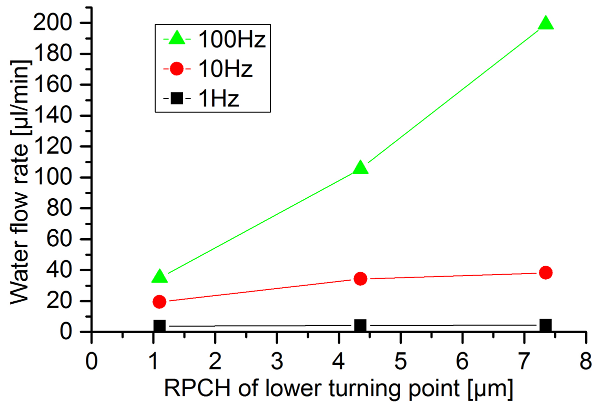

Figure 4.18: Remaining pump chamber height dependent flow at three different driving frequencies (1/10/100 Hz).

Discussion

The effect of temperature on the flow rate is highly frequency dependent, as it mainly correlates with pump dynamics due to an actually or equivalently shifted relative actuator position. Different thermal expansion coefficients of piezo and diaphragm amount for ~3/4 (0.14 µm/K) of the position shift and the viscosity effect was estimated to contribute ~1/4 (0.045 µm/K). However, the changes are not linear, but thermal expansion indicates an exponential increase of actuator position shift (Figure 4.16) and viscosity exhibits a declining increase along with increasing temperature (Figure 4.17). With the stronger thermal expansion effect, though, the resulting flow rate influence increases continually with rising temperature (Figure 4.14). This coherence can also be observed in the dynamic adjustment of the flow rate course. The temperature in the climate chamber adapts to a 4 K-step within minutes, the liquid temperature though only adapts within 1.5 h due to its high heat-absorption capacity (Figure 4.15). While the actuator temperature can adapt within minutes, a fast flow rate change of about 3/4 is followed by a slow flow rate change that correlates with the liquid temperature. Thereby, both effects can be separated quite well. While this is convenient for the measurement evaluation, it carries an issue if one wants to use temperature information for closed-loop flow control. Here, two measurements of temperature are needed, one close to the actuator diaphragm and one within the liquid in the pump chamber, in order to facilitate an accurate flow control. Besides indirect closed-loop flow control, the influence of temperature can be adjusted by design. A piezo material with a thermal expansion coefficient closer to the on of the diaphragm can be chosen. Or the pump chamber height or predeflection of the pump can be increased in order to reduce the effect of viscous damping on the dynamic displacement and therefore flow rate. If the pump is driven with lower frequencies, the temperature dependence also diminishes.

Conclusion

The effect of temperature on the flow rate of a micropump system was investigated. It was found that liquid viscosity contributes about 1/4 and thermal expansion about 3/4 to the effect of an actually or equivalently shifted actuator position relative to the pump chamber boundary. This results in a different damping factor and thus changes dynamic displacement and flow. To reduce the effect of temperature dependence, a few solutions are discussed that either change the main effect of actuator shift due to thermal expansion or reduce the influence of this effect by design or indirect closed-loop flow control.

The temperature dependence could also be used to maximize flow. If the actuator predeflection is limited by the process, a heating structure could be implemented in the silicon diaphragm to increase the standard predeflection under operation.

4.2.2 Pressure influence

Variations of pressure levels may affect the pump from various direction, being the inlet, the outlet or at the top the diaphragm. It usually has to be regarded in the design process, which is why most diaphragm models include the effect of uniformly distributed pressure at the diaphragm. In addition, the valve flow resistance depends on the pressure difference. One sources of pressure variations is the ambient pressure. However, it only alters the performance if the ambient pressure does not affect all ports of access simultaneously. In liquid dosing systems, the relative height of inlet reservoir and outlet point causes hydrostatic pressure at the pump. Other frequent pressure sources originate in the system environment. As a safety measure to stop free-flow, the inlet reservoir can feature a ongoing suction pressure. Excess or suction pressure may result from machine operating conditions at the system outlet.

State of the art

The pressure dependence of micro diaphragm pumps was obvious from the beginning and described with measurements for pumps with mechanical valves [54] and valveless pumps [146]. So far, this effect was mainly attributed to the diaphragm and its dependence was also integrated into static diaphragm models [83, 34] and is described by the stiffness parameter C_p (3.1). The pressure dependence was considered for the pump design, by assuming a working pressure and optimizing the displacement volume for this working point [34]. While this is a sensible approach for cases with constant working pressure, many applications feature variations in pressure conditions during operation. For a high dosing accuracy of continuous flow, the pump design should also consider the magnitude of possible time dependent variations. Furthermore, these variations may not only affect the diaphragm, but also free-flow and leakage flow through the valves. Furthermore, current pump dynamics require a transient contemplation of pressure changes to the pump and fluid paths.

Research goal

Due to the demand of high flow stability, the influence of pressure variations on the static and dynamic pressure dependence of diaphragm and valves needs to be investigated. The fluidic path between pump and pressure difference plays a decisive role to the pressure dynamics and has to be included in this evaluation.

Methods

For the outlet pressure dependent flow rate, a Coriolis flow sensor (see Appendix A) was used to measure the flow. The sensor features a high flow resistance due to its measurement principle. The sensor is placed between the pump outlet and a reservoir. The reservoir is half filled with water and pressurized by a pressure controller (see Appendix A). The different pressure steps of 10 kPa in the range of 0-200 kPa were applied for 75 s each and the whole loop was repeated 3 times.

Results

Depending on where the pressure variations are applied and what mechanism is dominant, the flow rate either decreases or increases. The relevant locations are the inlet, the outlet or at the top of the diaphragm affecting the diaphragm, the valves and or the dynamic pump operation. A static change of pressure difference between both sides of the diaphragm shifts the diaphragm position relative to the pump chamber boundary. The parameter describing this pressure sensitivity is C_p. In section 3.1, the 1D-value was measured for the MIKROAUG pump (0.078 µm/kPa) and compared to the model simulation (0.072 µm/kPa). The pressure sensitivity was evaluated with the actuator model (section 3.1) for different piezo geometries and diaphragm thicknesses (Figure 4.19) and for varying diaphragm radii (Figure 4.20). During a moving actuator, the pressure distribution beneath the diaphragm inside the pump chamber features the highest pressure gradient and overall pressure drop and in the fluidic path. Here, the valves work as pressure sinks. The pressure dependent static and dynamic valve behavior was discussed in section 3.2 and 3.4. It features quasi-static behavior in the relevant time scales and can lead to forward free-flow or reverse leakage flow.

Looking at the whole micropump in cyclic operation of supply and pump mode, more complex mechanisms influence the pressure dependence of the pump. With an effective change of relative diaphragm position compared to the remaining pump chamber height, the free displacement varies and the altered damping changes the transient behavior significantly (section 3.4).

If the inlet pressure is elevated compared to the outlet, the liquid will flow in with a higher velocity and lift up the diaphragm position in the supply mode compared to balanced pressure levels. The moving actuator introduces a pressure and volume sink inside the pump chamber. As long as the pressure difference between pump chamber (above the outlet valve) and behind the outlet valve is below 0, no flow will occur. Though, once the displacement slows down critically, free-flow through the outlet valve will take place, even if the actuator is still moving. After switching to pump mode the inlet valve closes and only opens once the chamber pressure falls below the inlet pressure. Roughly at this instance of pressure equilibrium, the diaphragm will stop moving. To summarize, inlet pressure increases the flow due to reduced damping and increased free displacement, but also leads to free-flow below a certain frequency.

At excess outlet pressure, also referred to as back pressure or counter pressure, the same valve opening conditions apply as for the inlet case. However, the lower turning point from pump to supply mode is shifted upwards by the outlet pressure. The upper turning point only depends on the inlet pressure, as the outlet valve is closed in reverse direction and the pressure can not reach the pump chamber. The relative displacement is reduced by outlet pressure, decreasing the flow. The initial up-shift of lower turning point lowers the RPCH-dependent damping and increases the potential frequency dependent flow rate. However, this effect can not compensate for the displacement loss (Figure 4.21). The flow rate continuously decreases with increasing outlet pressure at an average rate of 2 µl/min/kPa or an equivalent calculated rate of 2.3 µl/min/kPa if the sensor flow resistance is excluded. The theoretically calculated blocking pressure for the MIKROAUG pump type at electric field levels of -0.4|+1.2 kV/mm is 178 kPa. It needs to be pointed out that the Coriolis sensor introduces a high flow resistance after the pump outlet, separated by a flexible tube. This reduces the effective flow linearly with increasing flow rate. Without this flow resistance, a flow rate increase of ~15 % can be expected at ambient outlet pressure. The dynamic course of the flow rate change happens very fast within a few cycles and mainly depends on the equiliberation of the actuator position and the speed of the pressure controller to adjust to the new pressure level (Figure 4.22).

Besides system environment related pressure levels, variations in the natural environmental can affect the flow rate. According to the German weather services [147], the worldwide records for ambient pressure levels ranged from 87 kPa-108.5 kPa in two places of the world under extreme weather conditions. In Germany the extremes stayed between 95.4-106.1 kPa. However typical daily variations are in the range of 101.3±2 kPa. Now the ambient pressure can certainly affect the top of the diaphragm and depending on the system also inlet and outlet. In the worst case, the increased pressure would only access the top of the diaphragm, while keeping a constant ambient pressure at the inlet and outlet and having the actuator nearly touch the boundary. 2 kPa would amount for a down-shift of 0.15 µm of the upper turning point. At 100 Hz and nearly touching the pump chamber boundary, a 0.15 µm shift leads to flow rate change of 3.2 µl/min due to increased viscous damping (Figure 4.18). The additional reduction of free displacement due to chamber blocking would reduce the flow about 4.6 µl/min (section 3.4, Figure 4.21). Together, these typical maximum daily variations would result in a flow rate loss of 7.8 µl/min or 2.2 %.
The relative location of reservoir height compared to micropump and micropump compared to outlet (assumed ambient pressure) leads to a hydrostatic pressure, determined by Pascal's law:

$$p[h] = \rho g h \tag{4.8}$$

and depends on the density of the liquid ρ, the gravity g and the height difference h. For water of 21 °C and on earth's surface, a height difference of 1 m generates a pressure of 9.79 kPa. Typical height differences do not exceed 1 m, and are most often <10 cm for lab setups and neglectable for tightly packed implantable systems. The fill and thus pressure levels can vary due to operation or evaporation, but only cause a flow rate change of >1 % for <20 cm height difference.
Besides environmental pressure variations and changing reservoir fill levels, applications may feature additional pressure variations with higher values. This can be a constant suction inlet pressures to keep drugs inside the reservoir and prevent free-flow. Or rotating machines that are to be lubricated can build up pressures of up to several tens of kPa. Furthermore, partial clogging of the outlet will increase the outlet pressure and reduce the flow. The top of the diaphragm is typically only exposed to ambient pressure, but can be sealed of hermetically to keep a fixed pressure level. A fabrication introduced suction pressure is also able to up-shift the diaphragm for increased free displacement.

Discussion

The topic of pressure influence on micropump system flow faces various variation sources and flow rate changing mechanisms are numerous. Standard sources for pressure variations are ambient pressure due to weather conditions or height differences between reservoir, micropump and outlet. Though, more critical pressure sources arise from the application specific system setup, like reservoir pre-pressurization and conditions at the outlet-target, like body or machine pressure levels. The pressure affects the pump either by modifying the free displacement of the actuator, by different damping conditions, or by changing the valve efficiency with forward free-flow and reverse leakage. Detailed descriptions of the different mechanisms and the influence magnitude of certain pressure variations were given. Thus, allowing to take the pressure sensitivity of the actuator and the forward and reverse valve behavior into account for the design process. For the actuator, either its stiffness can be adjusted or the free displacement of the diaphragm can be limited. This limitation can be the touch down at the chamber boundary, which leads to stable flow rate, independent of the outlet pressure, until the lower turning point is shifted due to

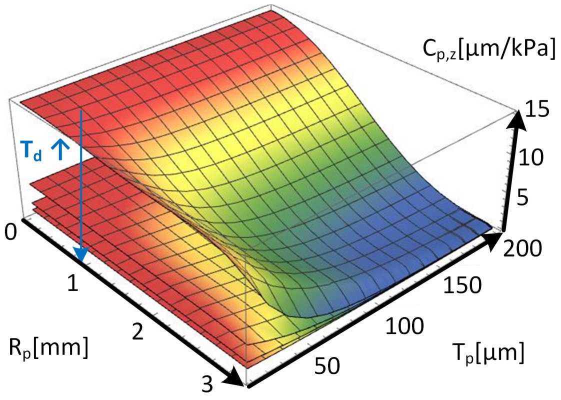

Figure 4.19: Displacement pressure sensitivity over piezo thickness and radius for varying diaphragm thickness (40/60/80/100 µm).

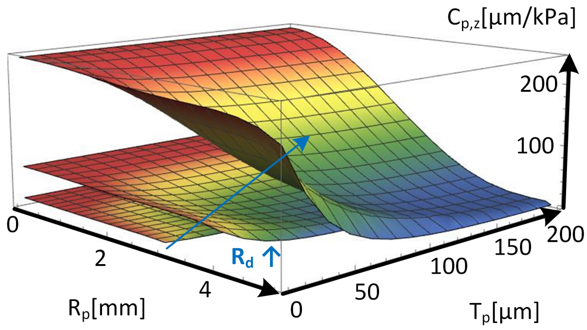

Figure 4.20: Displacement pressure sensitivity over piezo thickness and radius for varying diaphragm radius (3/4/5 mm).

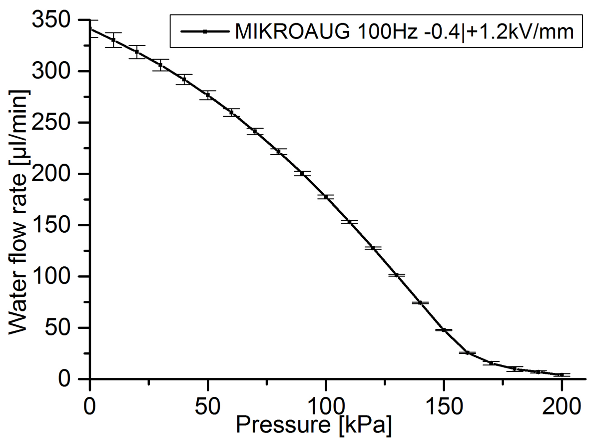

Figure 4.21: Outlet pressure dependence of liquid flow rate of the MIKROAUG pump.

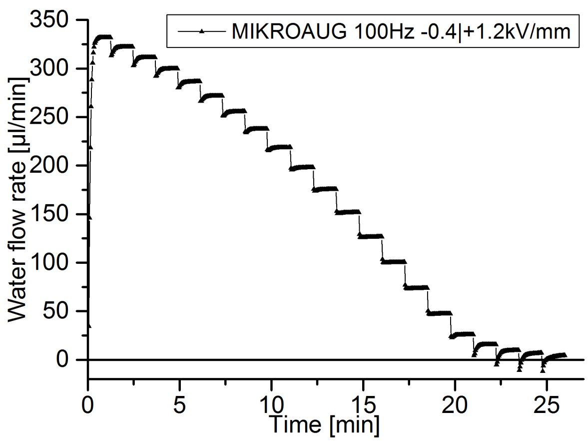

Figure 4.22: Transient flow course of one pressure cycle at decreasing outlet pressure levels.

increasing pressure. A double limiter was introduced by the company Debiotech, limiting the movement in both directions [36, 5]. However, all limitations introduce additional stress on the piezo ceramic and adhesive layer, which may lead to fatigue (section 4.1.1).

Besides changing the micropump design, a few guidelines for system setup and micropump operation can be given. One option arises for the driving signal of the pump. After switching modes, free-flow and leakage only occurs after a certain instance, when the diaphragm can not absorb the additional volume inside the pump chamber. This time period can either be reached by adjusting the frequency or the duty cycle time distribution. In general the duty cycle adaption offers more options on flow rate variability and can even be adapted to exceeding inlet or outlet pressure, if the information is available. On the system setup level, one option to prevent free-flow is to implement a free-flow-protection valve [77, 8]. Furthermore, the system should have equal inlet and outlet pressures. That means, either the height or inlet reservoir and system outlet should be equal or the reservoir can be custom pressurized to match the outlet. For example, if the system outlet faces the intra-body pressure, the inlet reservoir should have a pressure transmissible access to the body. If the pressure levels can be monitored, the driving frequency can be adjusted to keep the flow rate stable. The pressure sensors should be placed in the fluidic path outside of the pump, but close to the inlet and outlet, and close to the top of the diaphragm.

Conclusion

The pressure dependence of micropump system were investigated. The potential sources, points of application and effects of pressure variations were described. Due to superimposed mechanisms between actuator dynamics and valve behavior, it is difficult to predict the precise flow rate change. Example measurements of the transient adaption of flow rate due to pressure variations were conducted and the average flow rate change evaluated. Implementing a sensor at the outlet would allow for a compensation of the effect, if high pressure variations are to be expected in the system. Other aspects, like exceeding inlet pressure and a different range of frequencies can be estimated with the flow rate influencing effects model (section 3.4).

Options to improve the pressure tolerance were proposed. In the pump design, a stiffer actuator leads to lower frequency dependency, as well as a higher remaining pump chamber height. Single or double actuator limiter, restricting the displacement of the pump can lead to pressure independence in a certain range, but leads to reduced efficiency and increased fatigue. A duty cycle or frequency adaption can reduce free-flow and leakage and increase valve efficiency. Continuously equalizing inlet and outlet pressure levels in the system setup or implementing a free-flow-protection valve can reduce the effect of pressure variations. If the micropump system offers spare performance in an application, keeping the outlet above the inlet pressure, enables better flow controllability due to reduced free-flow. If flow accuracy is not a problem, a higher inlet pressure compared to the outlet, increases flow rate at the cost of a permanent base flow.

4.2.3 Particle laden flow

The influence of particle laden flow involves the particle tolerance of micropumps and possible solutions to increase particle tolerance or to prevent particle laden flow of changing the flow rate. In parts, in follows the publication 'Particle Tolerance of micro diaphragm pumps with low chamber heights and passive flap valves' [148].

In order to realize a micropump dosing system, not only performance but also reliability is of importance. 'Reliability also involves pumping during a longer time period, during which small particles or gas bubbles dissolved in the pumped liquid should not degrade device performance' [97]. The issue emerges mainly while pumping fluids that inherently contain particles like drugs, but also applies if particles cannot entirely be prevented during fabrication or handling. Therefore, the particle tolerance of micro diaphragm pumps with low pump chamber heights and passive flap valves was investigated. This research describes five failure mechanisms caused by different particle types in three locations of the pump. On the one side, analytical and FEM models were used to evaluate the geometric path through the pump and to facilitate the design of the pump's particle tolerance. On the other side, these models enabled the evaluation of the flow rate influence of particles and were supported by measurements. Furthermore, the criticality of different failure mechanisms was assessed. The results are the basis for an appropriate filter design and the adjustment of micropump particle tolerance to achieve reliable long-term operation.

State of the art

Some basic work on investigating the effects of particle laden flow through valveless nozzle-diffuser micropumps was done by Jang et al. [149], explaining the influence of particles on viscosity, the tendency of cavitation and agglomeration of particles. Even though check valves exhibit a particular sensitivity to clogging [97] and the risk of valve blocking [38] they are widely used due to their superior fluidic performance. Ezkerra et al. [150] and Goettsche et al. [151] both performed particle tolerance investigations on mechanical microvalves with moving parts. Ezkerra et al. investigated monolithically integrated cantilever check valves, observing particles only in the dead volume of the valve and hence not significantly changing the flow [150]. While investigating an active silicon membrane valve, Goettsche et al. found that the 'component most critical to particles in the case of membrane valves is the sealing rim under the membrane' [151]. There are approaches to improve the particle tolerance by including a filter upstream of the pump [5], or by changing the valve design [151, 152]. To overcome the bubble point of a filter that is placed upstream, a filter without bubble point was invented [153]. Dealing with passive flap valves with a narrow sealing rim and a diaphragm actuator with very low chamber heights, the performed studies can only partially be used to describe and improve particle tolerance of a micropump system.

Research goal

The goal is to understand the limits of particle tolerance and its failure mechanisms and to facilitate pump design by applying appropriate models. Thereby, save conditions for reliable operation are to be developed. Those solutions are to be found in micropump design, operation conditions and system setup including filter design.

Methods

The considered particle types are of different size, shape, material and rigidity, being plastic, magnetic, proteins and standard air particles. They can be applied at different volume concentrations. In order to achieve a defined concentration, a homogeneous distribution of the particles in the liquid is necessary. The fluid path from the reservoir to the tubing and the pump housing offers many locations for particle accumulation. To prevent this from happening, the solution in the reservoir is constantly being stirred, the tubing is kept short and the housing is designed with little non-moving dead volume. Furthermore, a high flow rate helps to keep the particles moving in the fluid. The experimental setup includes three measurement methods during operation and one subsequent destructive method. The real-time actuator displacement can be monitored by looking optically at the center of the actuator. The flow through the pump is measured with a gravimetric scale, to not contaminate more accurate in-line flow sensors. To measure the passive flow resistance a pressure can be applied at the inlet. After the active operation, the pump can be irreversibly opened by braking out the chamber and flaps. The inside of the pump can be investigated optically revealing the location of the accumulated particles.

To investigate the influence of adhering microparticles and specifically the influence of proteins on pump performance, 4 ml of eye liquid 'aqueous humor' from pigs was pumped in a cycle for 2 weeks. Each day, the whole 4 ml volume was pumped from one reservoir to another reservoir on a scale (compare to A) to measure the weight over time. For the next day, the reservoirs were changed.

The conductance of the porous filters was determined by measuring the static flow and pressure difference over the filter elements by applying pressure of up to 50 kPa with a pressure controller. Pressure sensors (compare A) were placed right before and behind the filter element.

Results

‚Particle tolerance' considers any significant interference of particles with the pump performance up to a total failure. The pump performance depends on the mechanic and fluidic behavior of the valve, the pump chamber and the actuator. Particles can cause an increase in flow resistance by partially or fully blocking the fluidic path. Particles can also impair mechanical movement of the flap valve or the actuator, changing either the characteristic pressure-flow dependence or the time-dependent displacement.

There are five known failure mechanisms caused by particles at three locations within the micropump (Table 4.1, Figure 4.23). First, the actuator displacement can be inhibited by a particle, located between the diaphragm and the shallow pump chamber. The critical particles are in size between the lowest remaining pump chamber height and the maximum height that passes through the valve. Second, the valve can be prevented from full closure of the flap on to the valve sealing lips. Hence, the leakage rate in opposite flow direction will result in reduced flow rate especially under influence of counter pressure [151, 38]. The critical size for this are particles of any size smaller than the maximum valve opening. Third, the valve cannot only be impeded but also stick under the presence of particles that tend to adhere to a silicon oxide surface. This effect can cause a blocking pressure of the valve that has to be overcome before opening. This either delays the time dependent flow into the chamber or even stops any pumping if the actuator cannot generate the necessary pressure. The opening pressure difference is theoretically limited (at the supply mode) by the difference between atmospheric pressure (101.3 kPa) and cavitation vapor pressure, being 2.3 kPa absolute for water at 20 °C. Fourth and fifth are based on the clogging of dead volume, located at the valve seat or the actuator chamber. The clogging leads to an increased flow resistance inside the pump chamber, which results in reduced flow and actuator velocity and increased cavitation tendency. The time to full clogging depends on the available space V_{dead} and the volumetric concentration of particles c_v in a fluid with flow rate Q and a filtering factor f_f that depends on the size distribution of the particles:

$$t_{clog} = \frac{V_{dead}}{f_f \, c_v \, Q} \tag{4.9}$$

Location	**Failure area**	**Failure mechanism**	**Critical particle features**
A	valve flap contact area	flap adherence: $R_{v,fw} \rightarrow \infty$	adhesion to SiO_2, softness
		flap blocking: $R_{v,rv} \downarrow$	size, rigidity
B	dead volume of valve and pump chamber	valve clogging: $R_{fl} \rightarrow \infty$	size, concentration
		chamber clogging: $R_{fl} \rightarrow \infty$	size, concentration, softness
C	actuator displacement volume	displacement reduction	size, rigidity

Table 4.1: Overview over particle failure areas, corresponding mechanisms and critical particle features.

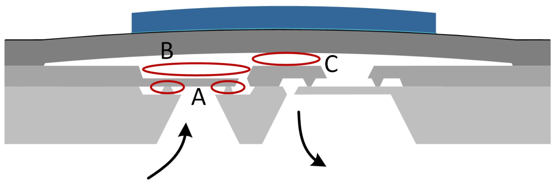

Figure 4.23: Particle failure locations in a micro diaphragm pump.

To evaluate the possibility of different failure mechanisms, the theoretic fluidic path of a particle was tracked. The failure mechanisms are mainly defined by the particle size, rigidity and adhesion tendency. With the analytical models of actuator (3.1, [34]) and valve (3.10, [90]) deformation, the size of potentially passing particles can be determined. For the present valve design and operating conditions, particles that are larger than ~10 µm are restrained from passing through (section 3.2). The pump chamber is defined by the initial fabrication height. The maximum and minimum position depend on the actuation voltages. In this case, the remaining center pump chamber height statically varies between 1 µm to 7.3 µm, implying a relative displacement of 6.3 µm at -75 |+175 V actuation voltage and ~5.2 µm relative dynamic displacement at 10 Hz. As it is known from section 3.4, the displacement reduction in dynamic operation mainly lifts up the lower turning point (pump → supply) due to higher viscous damping. As the inlet valve entrance is located 0.58 mm off the center and the outlet valve exit is located 0.68 mm off the center, the resulting maximum chamber heights are 95 % (6.95 µm) and 94 % (6.85 µm) of the center displacement.

To verify the hypothesis that particles of a certain size can pass the valve and enter or not enter the pump chamber, solutions with particle sizes of 1/2.7/5/7 µm were actively pumped with volumetric concentrations of 0.01 %. 1 µm and 2.7 µm particles easily passed the valve and pump chamber, but adhered to the SiO_2-surface, which reveals the flow pattern within the pump (Figure 4.24 and 4.26) and can also be observed at the outlet valve (Figure 4.25). 5 µm and 7 µm passed the valve, but agglomerated in the inlet dead volume (Figure 4.26) and were partially squished at the edge of the inlet rim (Figure 4.27). The relatively strong piezo actuator with a pressure ability of 178 kPa at a 6.3 mm chamber diameter is able to squash polystyrol particles, which leads to increased fluidic resistance inside the pump. The flow measurements confirmed this behavior, as there was no notable difference for 1 µm and 2.7 µm flow rates, but a total failure at the 5 µm (Figure 4.28) and an eventual drop at the 7 µm measurement (Figure 4.29). In these cases the geometric path along with the particle concentration defines the agglomeration velocity and the resulting flow resistance.

It was shown, that particles of certain sizes can enter different structures of the micropump and lead to clogging. The clogging usually leads to a gradually increasing flow resistance, but may also include sudden flow rate drops (Figure 4.28 and 4.29). The valve flap or the diaphragm can be blocked by particles, which significantly influences the flow rate. A particle can enter the inlet valve and gets clamped during the supply mode or a particle gets clamped in the outlet valve during pump mode. In the subsequent mode in both cases, the changed flow resistance of the reverse valve reduces the valve efficiency considerably. Depending on the position (between x_1 and x_2) of the clamped particle, the flap stays open and will lead to a certain pressure dependent flow (Figure 4.30) or an equivalent flow resistance (Figure 4.31). The flow resistance of the forward valve depends on the bending state, which changes with the pressure pulse. That results in a strong loss of valve efficiency for even small particles. The effective flow q_{eff} depends on

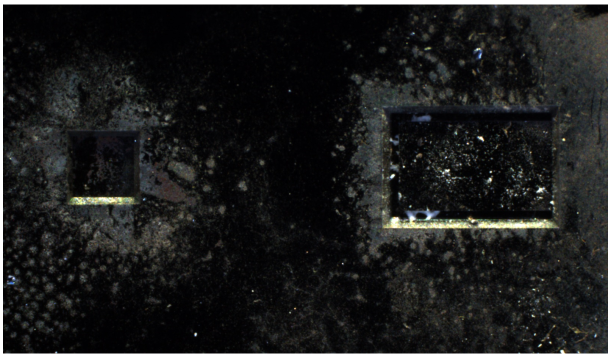

Figure 4.24: Adherence of 1 µm particles inside of the pump chamber.

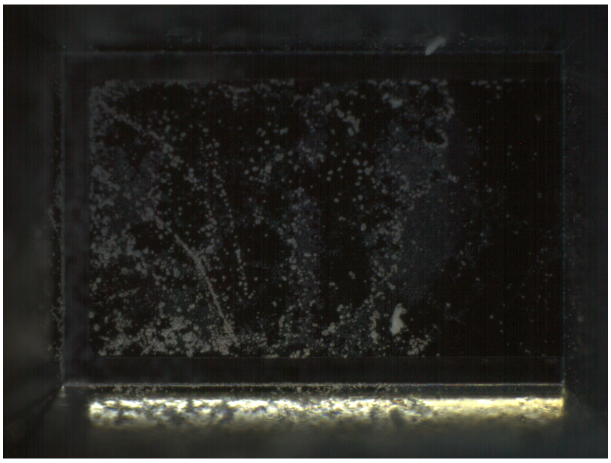

Figure 4.25: Adherence of 1 µm particles at the outlet valve flap, looked at from the outside.

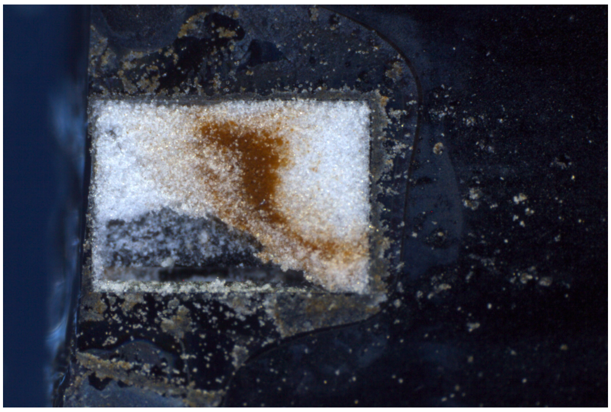

Figure 4.26: Agglomeration of 7 µm particles (white) at the inlet valve inside of the pump chamber and appearance of distributed 2.7 µm particles (brown).

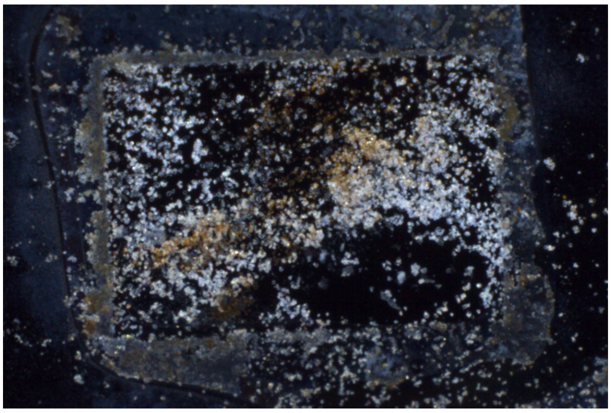

Figure 4.27: Squished 7 µm particles at the actuator diaphragm, opposite of the valve entrance.

the valve resistances according to Equ. 3.68 and contains a constant ($R^{-1}_{fl,blocked}$ - resistance of blocked valve) and a transient part ($R^{-1}_{v,fw}[t]$ - resistance of valve in forward direction):

$$q_{eff}[t] = \frac{\triangle p}{\left(R^{-1}_{fl,blocked} + R^{-1}_{v,fw}[t]\right)^{-1}} \tag{4.10}$$

If a particle blocks the diaphragm, two mechanisms occur. First, the relative dynamic displacement compared to the pump chamber height gets reduced. As shown in section 3.4, the free displacement strongly depend on the frequency. The absolute positions of lower and upper turning points can be measured (Figure 4.32) or calculated with the proposed model and define the displacement reduction by particles. However, once a particle blocks the lower turning point from reaching its natural equilibrium position, also the viscous damping coefficient of the pump chamber height dependent motion decreases (Figure 4.33). This leads to an up-shift of the upper turning point, as the actuator is accelerated in the beginning of the supply mode. Together with the influence of the reactive valve volume, the flow rate

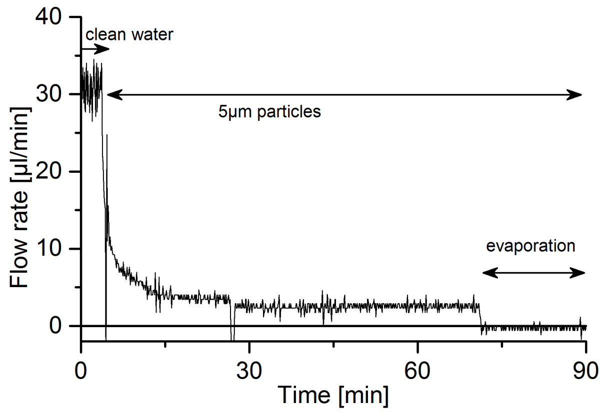

Figure 4.28: Flow rate course for 5 µm particle-laden flow of 0.01 % volume concentration.

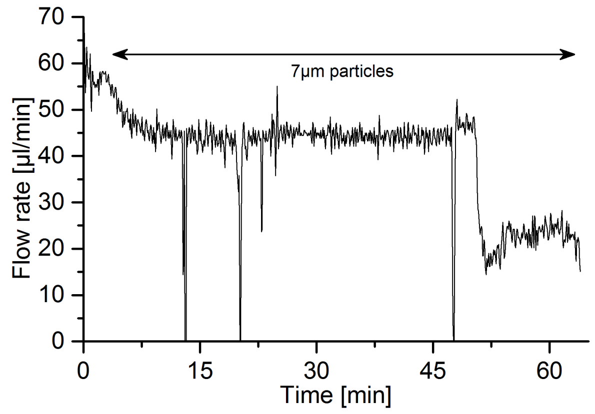

Figure 4.29: Flow rate course for 7 µm particle-laden flow of 0.01 % volume concentration.

reduction is frequency dependent but mainly defined by the loss of dynamic displacement.

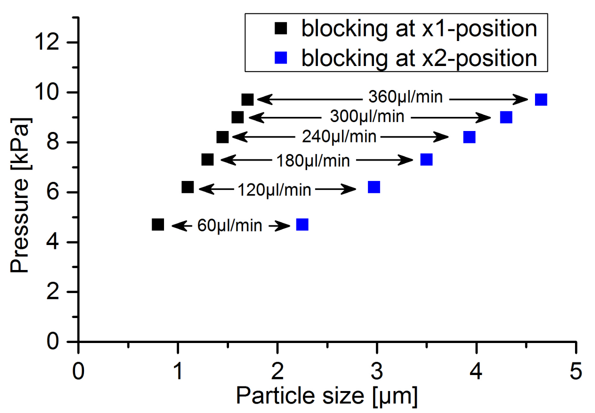

Figure 4.30: Range of particle sizes for valve positions between x_1 (black) and x_2 (blue) that cause the stated flow at the corresponding pressure difference over the valve.

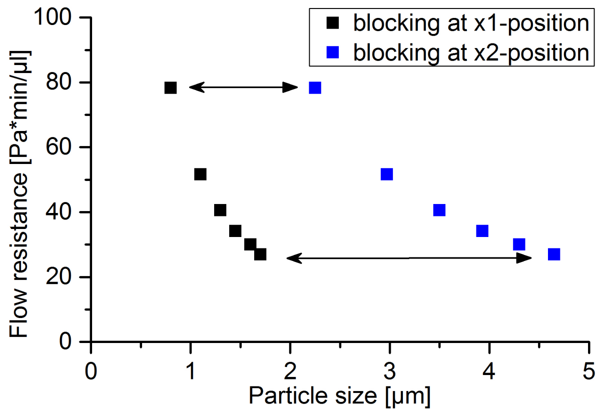

Figure 4.31: Resulting flow resistance for certain particle sizes at difference clamping positions at the valve between x_1(black) and x_2 (blue).

Microparticles that are smaller than the remaining pump chamber height can still cause clogging and valve blocking, but another effect is more critical. As the clogging time (Equ. 4.9) correlates with the volumetric concentration and the actually withhold number of particles, sub micron particles are less likely to fill the dead volume and lead to clogging. The effect of microparticles on valve blocking is also increasingly neglectable due to the non-linear pressure-flow curve (Figure 3.56). But, the adhesion of microparticles on the contact area of the flap valve is critical, as it can lead to valve adherence (compare to the natural sticking effect in subsection 4.1.2). In the case of particle caused valve sticking, the effect is based on a time and concentration dependent process concerning particles that tend to adhere to the silicon oxide surface of the contact area.

Proteins are a good example for microparticles that tend to stick to silicon oxide surfaces. To evaluate the effect of proteins on micropump performance, 4ml of aqueous humor was taken from pig eyes and pumped in a cycle for 2 weeks. Aqueous humor contains 600 kinds of proteins with sizes of up to 350 nm. The flow rate dropped to zero several times during the test, but always returned to pump, however with

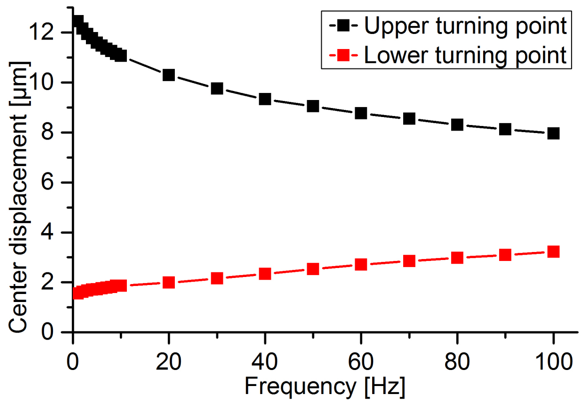

Figure 4.32: Measured frequency dependent change of turning points relative to the pump chamber boundary.

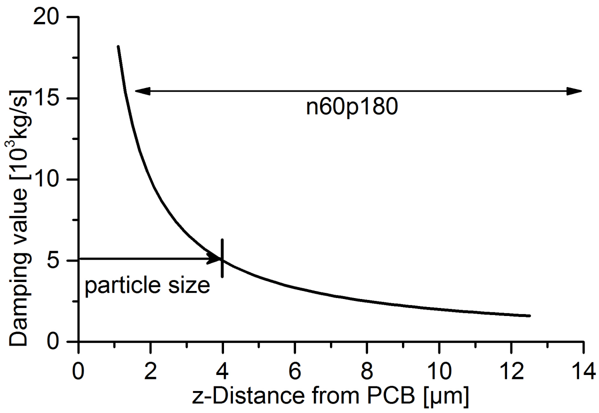

Figure 4.33: Effect of particle size on the resulting maximum viscous damping coefficient for clamped particles at the center position.

variations of up to -50 % compared to the maximum flow. After braking the pump and the flap open, agglomerations within the pump (Figure 4.34) and at the contact area of the flap valve (Figure 4.35) were observed.

For the evaluation of air-borne particles, a long-term test with four pumps and 2 µm filters pumped air for 5 months. No significant agglomerations or degradation were observed. According to [154] dry ambient European air has its main particle sizes between 3-800 nm. This indicates a tolerance towards the failure mechanism of flap adhesion and leads to reliable conditions due to the particle- and filter-sizes.

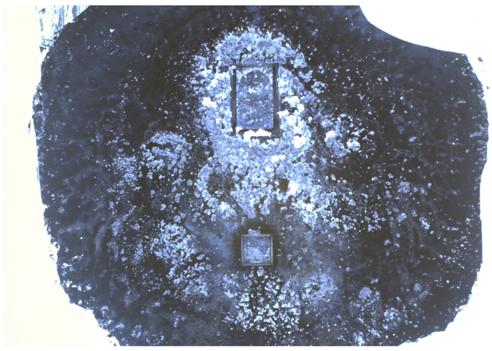

Figure 4.34: Protein agglomerations inside of the pump chamber.

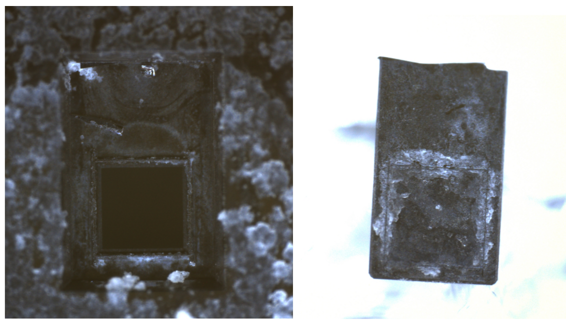

Figure 4.35: Adherence and induced sticking of proteins at the flap valve (seat - left, flap - right).

Particle tolerance can be a problem for certain applications, but there are solutions to increase the particle tolerance of the micropump and the micro dosing system. The micropump design can be changed regarding the lower turning point for the remaining pump chamber height (RPCH). The effect of particle size on flap blocking can be reduced by increasing x_1, resulting in a decrease of pressure application area. The higher the bending of both flaps, the higher the forward conductance and the lower the effect on the flow rate (Equ. 4.10). That would allow larger particle to block the valve as well, which however can be filtered with more ease.

If the particles are not an essential part of the pumping liquid, not like in blood or certain drugs, the obvious solution to limited particle tolerance is prefiltration of the liquid or including a particle filter.

Prefiltration is the best solution, but poses the threat of leaving particles in the fluidic path of the dosing system that originate from the fabrication and assembly process or that are generated while operating.
The use of in-line filters is a widely spread and accepted solution, but brings along new considerations and issues. First, the choice of filter type is important. Porous filters are pressure resistant up to several hundreds of kPa, have a low package space requirement and can be easily integrated in housings. Membrane filters on the other hand feature low flow resistance per pore size due to small channel length, but have a lower burst pressure and often a larger package size.
Second, the maximum pore size has to be determined. To prevent all failure mechanisms, all particles would have to be excluded from entering the pump. However, a decreasing pore radius R_{pore} comes along with lower conductance and depends on the number of parallel pores N_{pores} of length l_{pore}:

$$\text{Conductance} \propto \frac{N_{pores}}{2R_{pore}\, l_{pore}} \tag{4.11}$$

The filter's bubble point is the critical pressure between liquid and gas and increases with decreasing pore radius:

$$\triangle p_{bubble} = \frac{2\,\sigma_{12}\, cos\,\theta}{R_{pore}} \tag{4.12}$$

with the surface energy between liquid and gas σ_{12}, the wetting angle between solid and liquid θ.
If the valve sticking by adhered particles and agglomeration inside the chamber, caused by particles of sizes <RPCH, pose no reliability issue, the pore size of the filter can be chosen to match the RPCH. Otherwise, these microparticles have to be filtered with an in-line filter.
Third, while the filter reduces the initial performance, a clogging of the filter affects the flow accuracy unpredictably.
Fourth, to limit the influence on the flow accuracy, a regular exchange of the filter can be chosen. Though, this should come along with a two-stage filter concept, where a main filter and a safety filter is integrated in to the pump. The latter prevents failure due to particles from the exchange of the main filter.
In order to select appropriate filters, the conductance of porous filters was measured. Due to different wetting angles between solid and liquid and production influenced pore size distribution, the conductance of PEEK, titanium and stainless steel was compared for otherwise identical filter area and declared pore size (Figure 4.36). PEEK shows the lowest conductance, but provides endurance against many chemicals. Therefore, the influence of pore size (Figure 4.37) and filter area (Figure 4.38) on the conductance of PEEK filters was also investigated. The pore size measurement indicates the R_{pore}^{-1}-dependence, while the area should have a linear dependence.

Discussion

Particles can cause valve sticking, blocking and clogging, as well as pump chamber clogging and actuator blocking. These five failure mechanisms are caused by particles of different size, concentration, rigidity and adherence tendency to the pump surfaces. With selected analytical and FEM models, the geometry of the fluidic path inside the pump can be evaluated and was verified by measurements.
Clogging depends on the volumetric concentration and the size of particles. This failure effect only affects the flow rate significantly, once the dead volume is filled with particles. This can be in front of the valve entry, in the valve dead volume inside the pump or in the pump chamber dead volume. The most critical

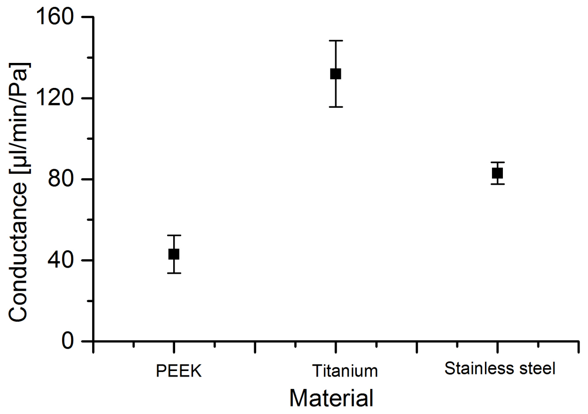

Figure 4.36: Influence of filter material of porous filters on conductance with otherwise same area and pore size.

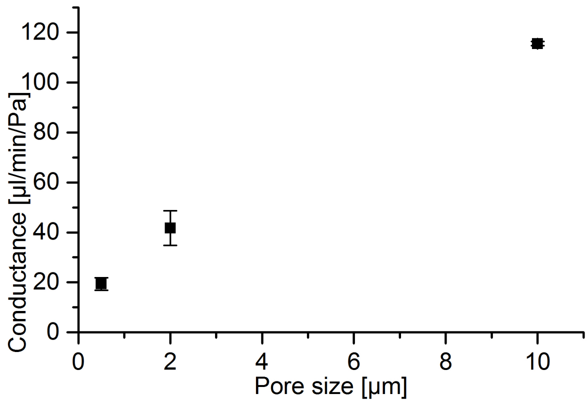

Figure 4.37: Influence of increasing pore size on conductance of PEEK filters.

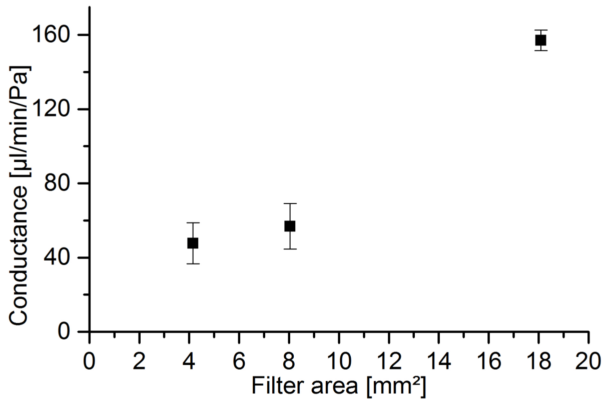

Figure 4.38: Influence of increasing filter area on conductance of PEEK filters.

particles can enter the pump chamber, but are too large to pass and get squished, if soft enough. Thereby, the entry only needs few particles to strongly increase the inlet flow resistance. Therefore, particles larger than the remaining pump chamber height (RPCH) should be filtered before the valve. Thereby actuator blocking is also prevented, which would directly decrease the flow rate.

Valve blocking displays a more complicated issue, as every size of blocked particles directly decreases the valve efficiency. Only the effect magnitude can be reduced by limiting the allowed particle size that enter the valve through filtration. In addition, the increase of valve inlet position x_1 reduces the potential effect of particles size on flow rate influence. Furthermore, the concentration is an important aspect for valve blocking, as the chance of clamping a particle depends on it. Here, the reduction of sealing lip width and perimeter can help to lower the change of blocking.

For microparticles in the liquid that tend to adhere to the inner pump surface, the solution approaches are limited. If the microparticles are part of the liquids purpose, like in drugs, the valve has to be designed for high sticking resistance (section 4.1.2). The pump chamber should provide enough dead volume for agglomerations. An ultimate solution is to alter the inner surface to prevent adhesion. If the microparticles are not part of the desired purpose, they can be prefiltered or in-line filtered. However, to minimize the initial and continuous effect of filter and filter-clogging, the filter surface area should be as

large as possible. The exchange of filter units has to be considered as well, by design and maintenance schedule.
A safety filter is of practical importance for all systems, as low amounts of particles, emerged from handling, assembly and operation, can be withhold. Prefiltration should be applied wherever possible to avoid flow rate influences and the additional filter component. Constructional particle sinks in front of the filter can also help to reduce the amounts of particles that need to be filtered. If an application cannot reach the reliability requirements due to the valve issues, a valveless nozzle/diffuser micropump with lower fluidic performance and efficiency might be an appropriate alternative.

Conclusion
It was understood and described what kind of failure mechanisms occur at different locations in the pump and which particle properties contributed to the failures. Suitable analytical models, describing the geometric path through the pump, were evaluated for this cause. By considering different types of particles, being plastic, magnetic, proteins and standard air particles, it was possible to explain the criticality of the different failure effects. The adherence of the flap valve can lead to a complete failure of the pump and is within the most critical mechanisms. As many influences, like surface forces and charges, are involved, this mechanism cannot be modeled appropriately and has to be tested for every new fluid. However, if the adherence poses no obvious problem, the overall particle tolerance and flow rate influence can be adjusted by pump design, operating voltages, and by implementing an upstream in-line filter with an appropriate pore size.

5 Liquid flow control solutions

In order to meet all micro dosing system requirements, both performance and reliability have to be addressed. Understanding the dynamic behavior of both aspects allows for an aligned design of system architecture and its components. However, many design goals feature competing optimization directions. Only by correctly balancing all requirements, suitable open-loop flow control solutions can be found for different applications. Open-loop flow control is usually easier and cheaper to implement than closed-loop flow control, where additional sensors and computing capacity are required. In return, closed-loop flow control is able to provide good flow stability at a high performance level and increased safety. Therefore, the potential of both solution categories was evaluated in this chapter.

For open-loop flow control, an overview of the main influencing parameters is given for the key characteristics of micropump systems. Furthermore, the competing design directions were worked out. Together, they lead to a proposed design process to balance different goals of performance and reliability. Where this process does not yield a sufficient result, but performance demands alone can be met, closed-loop flow control provides solutions. Direct measurement of the target value flow or indirect measurement of flow influencing parameters, like temperature, constitute the basis for an autonomously adapting system. For this cause, the sensor technologies 'differential pressure based flow sensors' and 'thermal calorimetric flow sensors' are evaluated for their capability to accurately measure pulsatile or continuous micropump flow. In addition, system integration aspects regarding the flow pulsatility, realizable control modes and system robustness were addressed for the combination of sensors and micropumps.

This chapter contains the considerations of open-loop flow control (section 5.1) and is followed by the evaluation of closed-loop flow control (section 5.2).

5.1 Design balance for open-loop flow control

To meet all requirements with an open-loop flow control system is challenging due to a multitude of performance and reliability demands on the one side and due to numerous degrees of freedom regarding the system design (Figure 5.1) on the other side. While the necessary system functions are predefined, the design process and all decisions for system parameters are free to make. In this section, the aspects for the design of open-loop flow control systems are described. That includes the degrees of freedom for the design of the core fluidic functions, its different optimization goals, the evaluation of opposing design directions and the process to find the right design balance to meet all requirements.

This section aggregates the investigations of performance (Ch. 3) and reliability (Ch. 4) chapters. The approaches for micropump and system-level design are reviewed in section 1.1 and section 1.3.

Research goal

The goal for this section is to impart the main influencing parameters of different performance and reliability requirements, identify major competing design directions and to provide a process to balance between different critical goals. Thereby, the degrees of freedom for the design of micropump based dosing systems are to be exploited to meet all requirements in open-loop flow control.

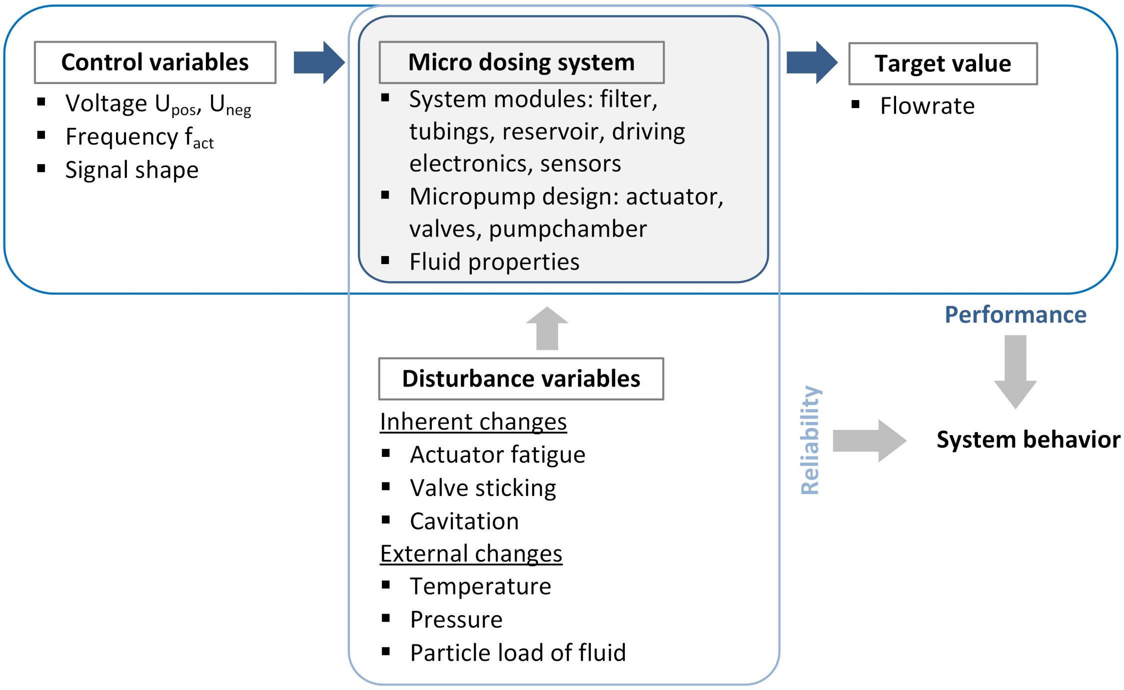

Figure 5.1: Performance and reliability behavior of micro dosing systems.

Overview of influencing parameters

In order to understand the degrees of freedom, the involved system parameters are listed first. The liquid properties (Figure 5.2) are often not part of the design space, as they are usually predefined by the application. Though, they influence the reachable system characteristics and have to be regarded. The critical factors of the liquid are its pressure, temperature, density, viscosity and its concentration of solved gas, floating bubbles and particles.

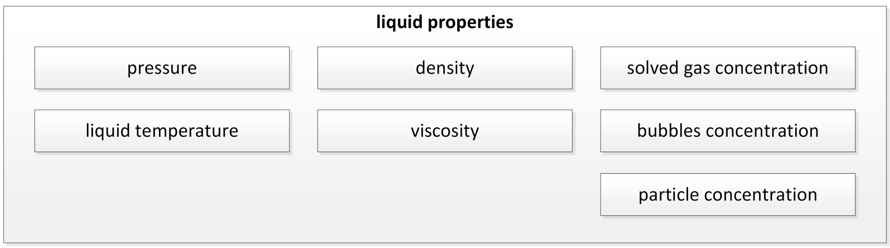

Figure 5.2: Most relevant properties of liquids.

Besides the predefined liquid properties, the fluidic performance behavior depends on the selectable geometric and material parameters (Figure 5.3) and the adjustable control variables (Figure 5.1). The reliability behavior depends on the disturbance variables, being inherent or external influences.

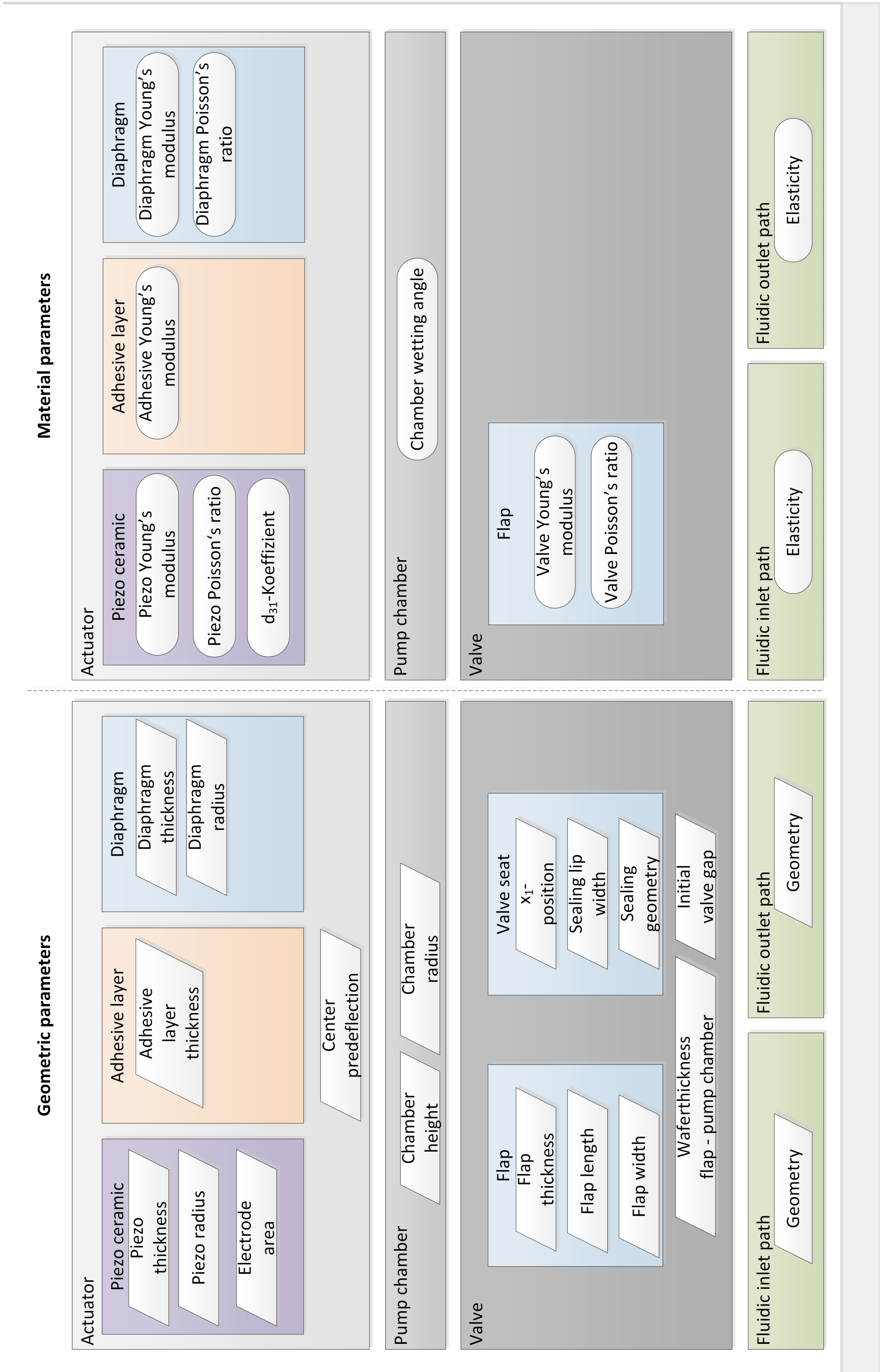

Figure 5.3: Geometric and material key parameters of fluidically active parts.

Optimization of key requirements

From the multitude of influencing parameters, certain key characteristics, like dynamic actuator motion, valve behavior or pulsatility damping can be derived. By themselves, many of these aspects were investigated in chapter 3 and 4. In this paragraph, the dominant influences of key requirement goals are identified and dependencies summarized. Both the knowledge from simulations and measurements were used to conduct this analysis.

The boxes with round angles indicate key requirements, boxes with sharp angles denote dominant key aspects. Dashed lines are used, whenever the influence only occurs under mentioned specific conditions.

Flow rate The flow rate or often a range of flow rate is the primary goal of a micro dosing systems, as all fluidic related tasks can be reduced to it. If a certain volume is to be delivered, a time interval can be assigned, if a pressure level needs to be stabilized, the flow rate is the means to compensate for variations. Many other requirements are influenced or directly depend on it. For example, the energy consumption is usually referred to relative to the dosing task. The influences on the frequency dependent flow rate were investigated in section 3.4. The static displacement together with the liquid pressure ability and resistive damping determines the dynamic displacement (Figure 5.4). In return, the actually flown liquid is defined by the effect of gas capacitances that delay the time dependent flow. Valve loss effects, like the reactive valve volume affect the redirection efficiency of the valves and changes initial resistive damping along with the remaining pump chamber height (RPCH). The fluidic characteristics of inlet and outlet path can change the dynamic behavior of a micropump and can be described with a network of resistances, capacitances and inertances.

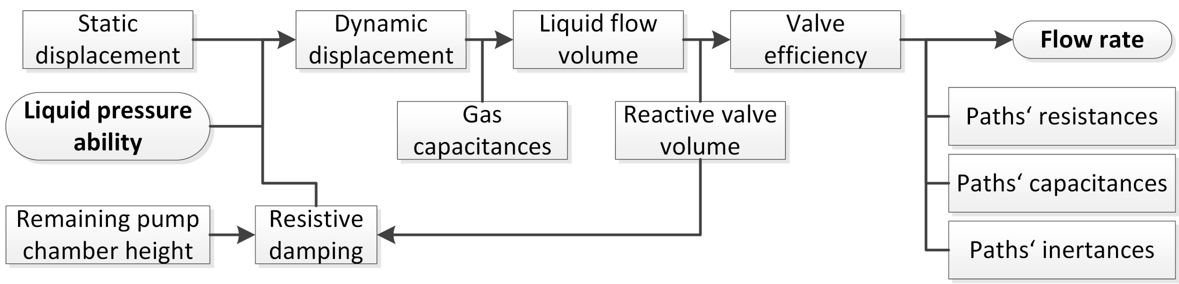

Figure 5.4: Flow rate influences.

Liquid pressure ability The liquid pressure ability describes the maximum pressure that can be generated by the actuator. Based on the actuator model, it depends on the one hand on the pressure sensitivity of the actuator and on the other hand on the achieved displacement (Figure 5.5). The actuator geometry and material properties define the actuator stiffness and the displacement due to an applied electric field. The diaphragm annulus determines the flexibility of the actuator to a large extent. The liquid pressure ability is important to overcome clogging or other flow resistances in the fluidic outlet path. The higher the liquid pressure ability, the lower is the influence of damping and the faster the actuator can reach its static displacement. This decreases the frequency-dependency of the flow rate and changes the peak-flow rate at the peak frequency. Furthermore, it defines the ability to generate cavitation and its intensity. A minimum liquid pressure ability of 97 kPa is necessary to produce vapor cavitation in water at 21 °C.

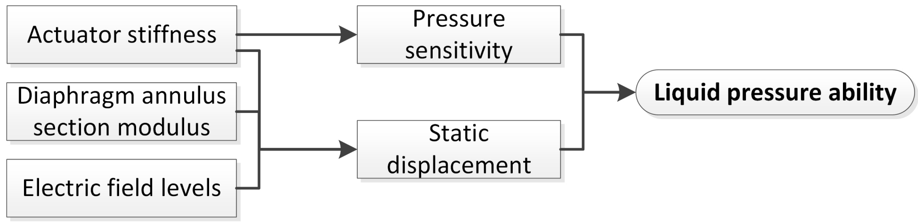

Figure 5.5: Liquid pressure ability influences.

Gas pressure ability The gas pressure ability describes the maximum excess and suction pressures that can be generated with gas. It is defined by the compression ratio between displacement volume and dead volume in equilibrium (Figure 5.6). In equilibrium, the gas pressure reduces the static displacement due to the actuator's pressure sensitivity and thereby increases the dead volume. A minimum dead volume in equilibrium means, the actuator barely touches the pump chamber boundary. In a practical use case, either the inlet or outlet is to be evacuated or pressurized. Then, valve leakage reduces the gas pressure ability until an equilibrium is reached after each cycle.

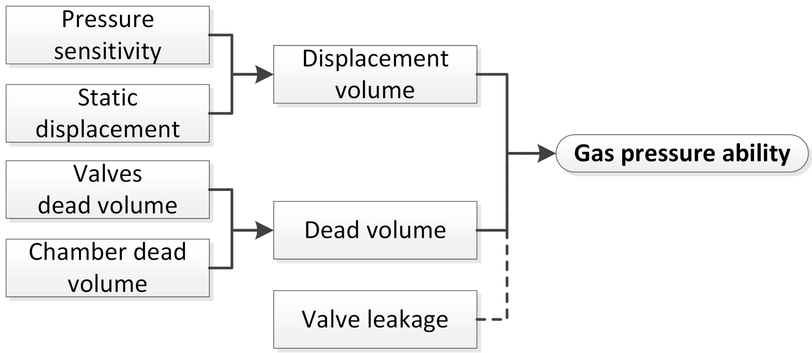

Figure 5.6: Gas pressure ability influences.

Self-priming ability The self priming ability directly depends on the gas pressure ability (Figure 5.7). The generated suction pressure has to be lower than a system related inlet pressure in order to prime the inlet path. Here, the valve leakage effect has to be included into considerations. In addition, the bubble tolerance is relevant for self-priming, in case the pump chamber does not fill itself properly or a bubble is part of the priming liquid.

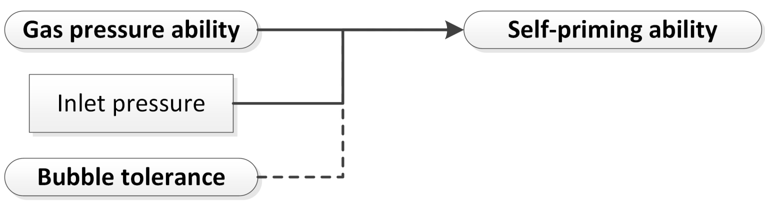

Figure 5.7: Self-priming ability influences.

Energy efficiency, energy consumption, battery runtime The energy efficiency is a key characteristic for the electric requirements of the system. It depends on the electric-electric conversion efficiency, executed by the driving electronics and the electric-fluidic conversion efficiency, executed by the micropump (Figure 5.8). The energy efficiency, again, defines the energy consumption and relates to the actually used fluidic performance. Together with the battery capacity, the battery runtime is determined. While electric-electric conversion efficiency lies between 20-95 %, electric-fluidic conversion efficiency is usually smaller than 10 % and often below 1 % (section 3.1 and 3.4).

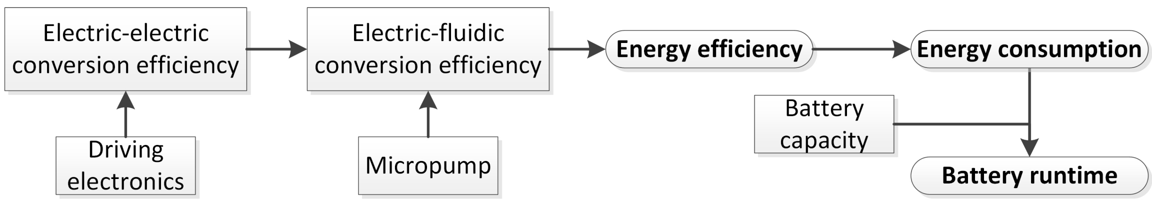

Figure 5.8: Energy efficiency influences.

Accuracy & lifetime The key requirement flow rate accuracy summarizes all deviations caused by inherent or external disturbance variables (Figure 5.9). If the specified accuracy limits are exceeded, a failure occurs. Depending on the system definition, if a failure is only temporary, either the lifetime ends by definition or the error is accounted to the failure probability. This definition is important and can be illustrated at the example of a drug delivery system, where an over- or underdosing beyond the accuracy limits could be fatal. Besides estimable variations from inherent effects or defined ranges of external influences, stochastic failure effects like a defect of driving electronics pose a remaining failure probability.

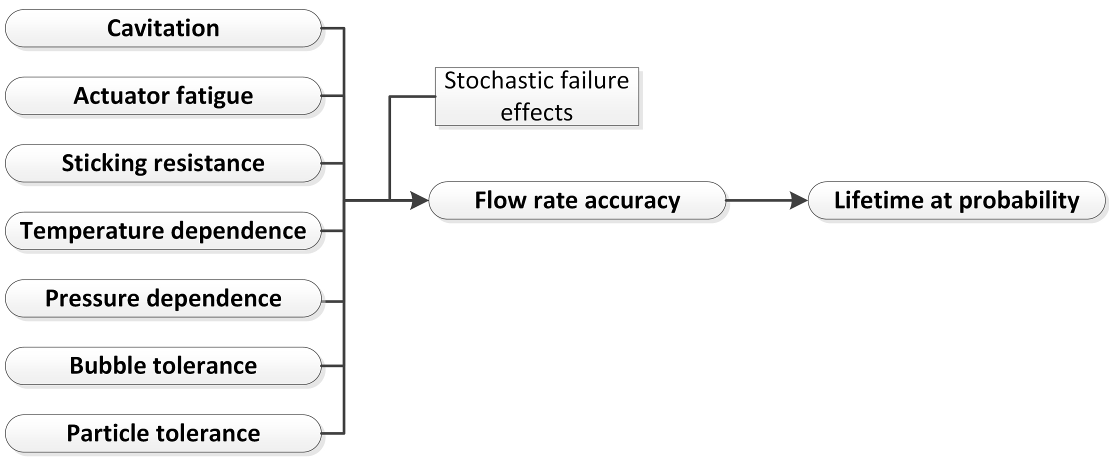

Figure 5.9: Accuracy and lifetime influences.

Cavitation Cavitation can occur, if the liquid pressure ability is greater than the vapor pressure and emerges earlier with a high slew rate of the signal and strong resistive damping (Figure 5.10). If the concentration of solved gas is high enough, stable cavitation can generate bubbles. These bubbles have to pumped out of the micropump, which decreases the flow and may produce a dead time at the system outlet, if not resolved or removed. Thus, cavitation is able to directly change the flow performance and flow accuracy. The effect is integrated in the flow rate influencing model in section 3.4.

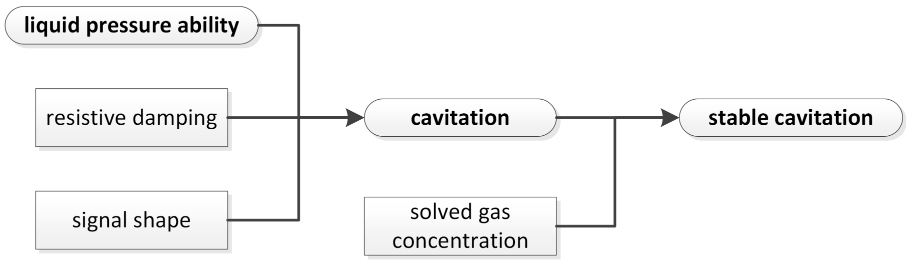

Figure 5.10: Cavitation influences.

Actuator fatigue Actuator fatigue may produce irreversible performance variations in both directions and exhibits two main characteristics (section 4.1.1). One changes the actuator zero-position, which in return changes the dynamic displacement through varied resistive damping and ultimately the flow rate (Figure 5.11). The other, less frequent effect, changes the deflection per applied voltage, which changes both the flow rate and the pressure ability. The main influence is mechanical stress through bending, touch down at the chamber boundary, dynamic pressure from the fluid and induced excitation frequencies. Together with the number of cycles to stress the actuator, the overall fatigue is determined. While a changing zero-position is most likely attributable to the adhesive layer, a changing displacement efficiency can be caused by the adhesive layer or the piezo.

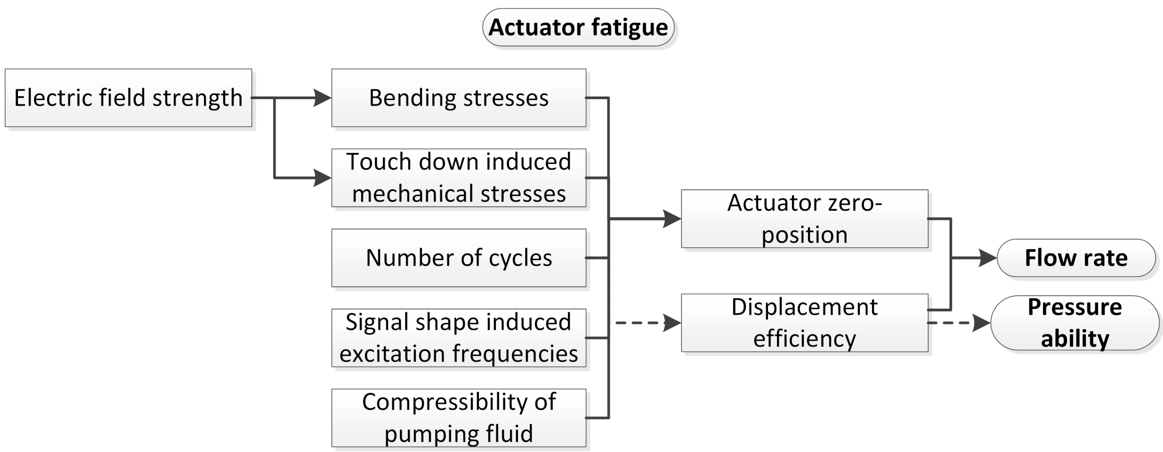

Figure 5.11: Actuator fatigue influences.

Sticking resistance Inherent valve sticking can lead to a partial reduction or total stop of flow rate (section 4.1.2). The effect can emerge while in storage or under operation, though for perfectly filled liquid pumps, storage sticking is more likely and critical. The valve's sticking resistance depends on the competing opening and adhesion forces (Figure 5.12). The adhesion forces of natural sticking depends on the valve contact area. Previous studies indicate water or humidity induced hydrogen bonds between attached OH^{-}-groups at the silicon oxide surfaces. Additional capillary forces at the two phase boundary between liquid and gas or particle adhesion can increase the adhesion forces. The opening forces depend on the liquid pressure ability if the pump is perfectly filled with water and on the gas pressure ability if the pump is filled with air. Together with the pressure application area the opening forces are defined.

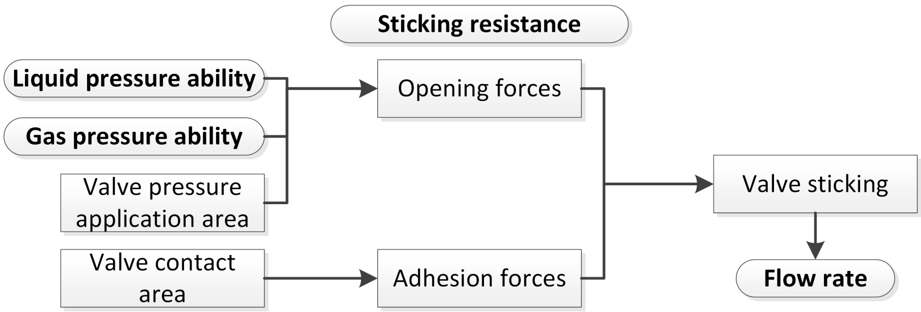

Figure 5.12: Sticking resistance influences.

Temperature dependence The temperature strongly affects the performance of liquid micro diaphragm pump systems through a change in dynamic displacement (section 4.2.1). Temperature variations cause a change of dielectric properties of the piezo, but this strongly depends on the used material and is negligible for the investigated ceramics (Figure 5.13). Due to different thermal expansion coefficients of piezo and silicon diaphragm, the actuator zero-position increases with rising temperature for this material combination. Together with a decreasing water viscosity for rising temperature, the flow resistance decreases. Overall a strong and almost linear increase of flow rate was measured for rising temperature levels. However, the time scales of flow adaption due to ambient temperature changes are considerably different for the individual effects.

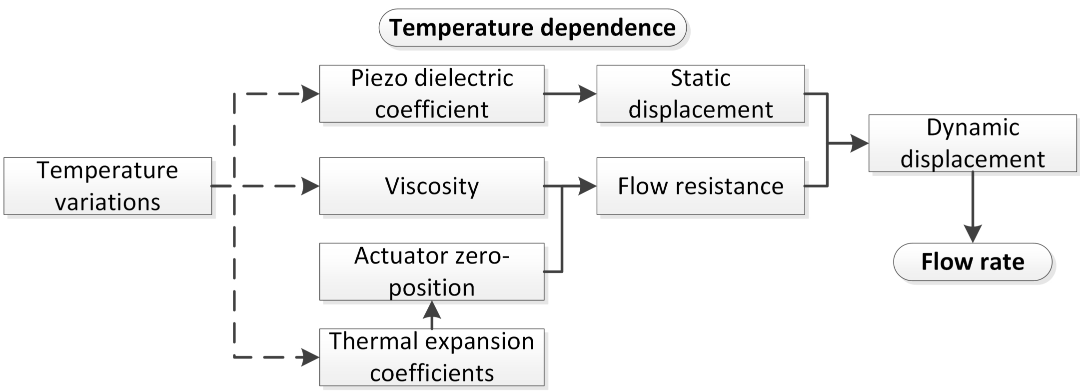

Figure 5.13: Temperature dependence influences.

Pressure dependence The pressure dependence of micro diaphragm pumps is mainly determined by the actuator, but also by valves and pump chamber (section 4.2.2). A pressure increase at the outlet, which is the most common case, increases the lower turning point of the actuator, equivalent to an decrease of ambient pressure level (Figure 5.14). That decreases the viscous damping, but cannot compensate the loss of effective displacement and effectively leads to a roughly linear flow rate reduction. The pressure sensitivity of the actuator defines the quantitative change of displacement. If an excess pressure difference between inlet and outlet occurs, the liquid only faces forward valve and chamber resistances and leads to free-flow.

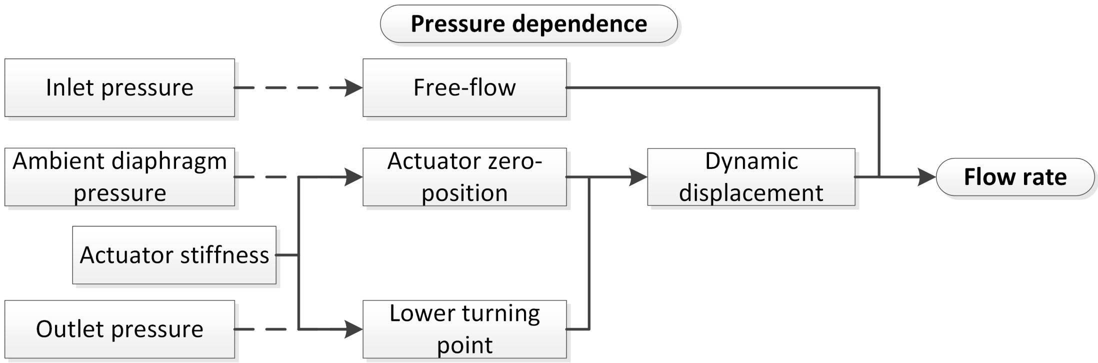

Figure 5.14: Pressure dependence influences.

Particle tolerance Particle tolerance covers the influence of certain particle types and concentrations on the flow rate of a micropump system (section 5.15). Particles affect the particle filter and the fluidic path through the micropump. All failure effects reduce the flow rate, one way or another (Figure 5.15). The clogging speed of valve or pump chamber depends on the available dead volume and the particle volume concentration of particles that cannot pass an obstacle. Adhering particles can cause valve sticking, which also depends on the sticking resistance of the valve. For particles that can theoretically pass the valve, valve blocking may occur, clamping a particle for one or more cycles and reducing the valve's redirection efficiency. Particles that can enter the pump chamber, but are larger than the remaining pump chamber height of the lower turning point, can, depending on their rigidity, either get squished or block the displacement.

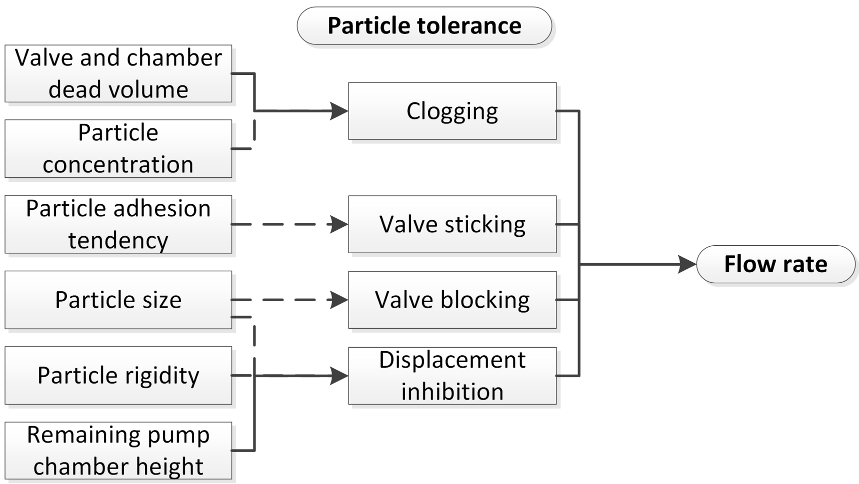

Figure 5.15: Particle tolerance influences.

Bubble tolerance Bubble tolerance defines the ability of the micropump system to deal with bubbles. While bubbles need to be avoided if high flow accuracy is required, bubble tolerance can be important for the self-priming ability. The gas pressure ability determines the available pressure to move bubbles through the inlet valve and to push them out through the outlet valve (Figure 5.16). External pressure levels and valve relief-pressure at inlet and outlet add up on the required gas pressure ability. If the gas bubble can be moved through the pump, the actually flow liquid each cycles is reduced by capacitive damping. Thus, the flow rate is reduced, while gas bubbles remain inside the pump. The systems dead time of flow depends on the bubble volume and the current flow rate.

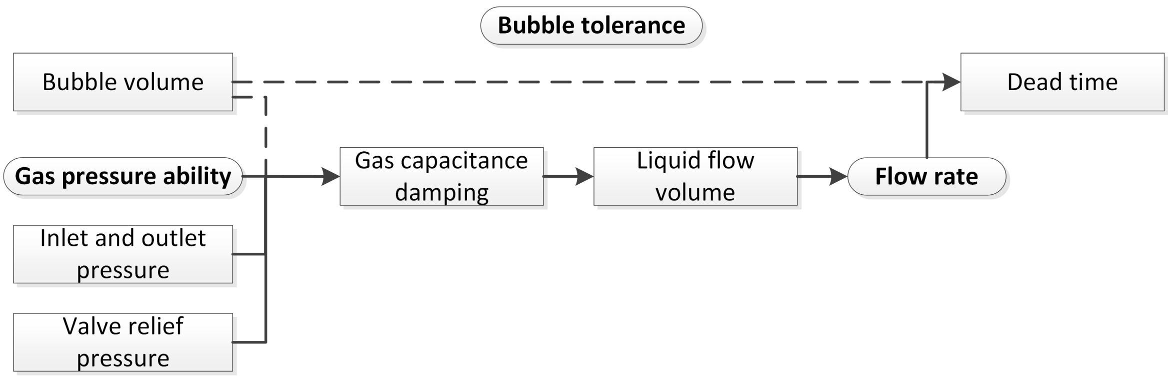

Figure 5.16: Bubble tolerance influences.

Competing design directions

The complex interactions of different performance and reliability characteristics exhibit many competing design directions. To provide the foundation for an appropriate design process, the competing key parameters of the system and their influence on different requirement goals are described here. Namely, these are the remaining pump chamber height, the actuator stiffness, the diaphragm radius, the valve bending and the valve sealing lip width.

Remaining pump chamber height The remaining pump chamber height (RPCH) is one of the most critical system parameters, as it has a strong impact on the flow rate, the gas pressure ability, self-priming ability, bubble tolerance, particle tolerance and the actuator fatigue. The flow rate strongly depends on the RPCH due to viscous squeeze film damping (section 3.4). The lower the RPCH, the lower the flow rate, but the higher the gas pressure ability due to reduced chamber dead volume (section 3.3). The gas pressure ability, again, correlates with the self-priming ability and the bubble tolerance. Furthermore, the RPCH defines the particle tolerance of the pump chamber, for non adhering particles. As a micropump parameter it is defined as the distance between pump chamber boundary and actuator displacement. Usually, the RPCH is referred to the minimum distance to the center displacement of the lower turning, but in special cases, the transient central RPCH or the radius dependent RPCH is used. The RPCH can be adjusted by the fabricated pump chamber height, the predeflection of the actuator and the turning points of displacement. However, the adjustable predeflection is limited. Therefore, either a minimum fabricated pump chamber height is necessary for full displacement or the static and dynamic displacement may have to be reduced by lowering the positive voltage level. A third option is to let the actuator touch the boundary in static displacement, but barely touch it under dynamic operation, where the relative displacement is reduced (section 3.4). If the actuator touches the pump chamber boundary during cyclic operation, actuator fatigue can reduce the displacement over time (subsection 4.1.1). If the degradation is within accuracy boundaries over the lifetime, this operation mode is a fourth option. For the definition of the fabricated pump chamber height, one has to consider that about one third of the cylindrical chamber volume will be part of the displacement volume, while the other two thirds will increase the dead volume. A balance between flow performance and required gas pressure ability is usually the key to a optimized robust pump.

Actuator stiffness The actuator stiffness is an important characteristic for liquid and gas pressure ability, flow rate, cavitation and pressure sensitivity. Though, it is a difficult characteristic to optimize, as its influence on the requirement goals depends on many additional design parameters and system conditions. With increasing stiffness, the liquid pressure ability rises. Thus, gas pressure ability, self-priming ability and bubble tolerance increase as well. While the displacement volume decreases with rising stiffness, the flow rate does not necessarily do so. Due to the high resistive damping of the actuator in the pump chamber, the dynamic displacement depends on the actuator force, which is described by the liquid pressure ability (section 3.4). An increased stiffness features less frequency dependency of the flow rate and thereby a higher flow linearity. Up to a certain point, increased stiffness can lead to higher peak flows, which can be evaluated with the model, provided in section 3.4. Another important flow rate influencing aspect is cavitation (section 3.4). With increasing stiffness, the liquid pressure ability soon rises above the vapor pressure, where cavitation may occur. That affects both flow rate performance and stability and is described in section 3.4. The pressure sensitivity also correlates with the actuator stiffness, which is relevant for the pressure dependence of the micropump. To change the actuator stiffness, mainly the piezo thickness T_p and the diaphragm thickness T_d are important. T_p increases the voltage, but provides higher actuation force. An increasingT_d lowers the conversion efficiency and should only be increased to cope with limiting stresses (section 3.1). The diaphragm radius R_d has to be chosen along general system performance criteria (section 3.1). An optimized ratio $\frac{R_p}{R_d}$ of piezo radius R_p compared to R_d usually stays between 80-95 % for maximum yield of displacement volume and pressure ability.

These considerations leave three options regarding the design of actuator stiffness. The first option is to keep the liquid pressure ability below the vapor pressure to avoid cavitation for certainty, while optimizing for displacement volume. This leads to high flow rate efficiency at low frequencies, due to usually low voltages and high displacement per voltage. But it also leads to a low peak flow if the RPCH is kept low and exhibits a large pressure sensitivity. The relatively large displacement, though, provides the option to increase the fabricated pump chamber height to reduce viscous damping, while maintaining self-priming ability and bubble tolerance.

The second option is to design high actuator stiffness, for high pressure ability and low pressure sensitivity. Cavitation can be avoided with a sine wave up to a certain frequency. Or the pump is driven under cavitation conditions, but stable cavitation is avoided or its flow rate influencing effects reduced by an in-line degasser (section 3.4). The frequency still has to be limited to avoid super cavitation, where the vapor cavitation bubble cannot fully collapse but increases over a number of cycles. To benefit from the high liquid pressure ability, but to avoid cavitation at the same time, the signal shape and duty cycle can be modified. The supply mode can be given a lower slew rate to avoid cavitation or a longer time share of the cycle to have the cavitation bubble implode before mode switching. The pump mode can apply the fully voltage in a rectangular signal for maximum liquid performance. This mode has the advantage of higher liquid pressure ability. If optimized well, the peak flow can be higher than for option one, especially at low pump chamber heights.

The third option uses an actuator design as option two, but limits the operating voltages to decrease the pressure ability below cavitation possibility. Thereby, the displacement volume is lower than the first two options, but provides a higher flow rate linearity with increasing frequency and a potentially higher peak flow frequency. In addition, its pressure sensitivity is lower. If a clogging event occurs, where high pressure ability is needed, it can be generated during the pump mode by applying a higher voltage together with a low supply slew rate.

Diaphragm radius The diaphragm radius R_d defines the performance class for micropumps (section 3.1). Most important, it determines the minimum dosing volume at constant voltage levels and the flow rate range over the displacement volume at a certain working pressure (Figure 3.12). While displacement volume increases, liquid pressure ability decreases with rising radius (Figure 3.14). The liquid pressure ability can be adjusted by increasing actuator stiffness over T_d and T_p, but the available fluidic performance (displacement volume $\times$ liquid pressure ability) increases with rising R_d (Figure 3.15). Therefore the diaphragm radius should always be chosen as large as the required system size ($\sim R_d$, electronics size at voltage levels), costs ($\sim T_p$, piezo volume) and voltage levels (breakdown voltage gas) allow.

Valve bending The valve bending mainly influences the flow rate and particle tolerance. For the flow rate, forward flow resistance, forward reactive valve volume, reverse leakage and reverse reactive valve volume are most important. For particle tolerance, the particle blocking is determined by the valve bending. With thinner flap thickness and larger pressure application area, the bending increases, which decreases the forward flow resistance. On the other hand, the reactive valve volume increases, as well as the reverse leakage and the reverse reactive valve volume due to flap deflection. However, in pumps with low chamber heights, the valve resistance is small compared to the pump chamber (section 3.4). Therefore, the valve bending should be reduced with decreasing RPCHs. Additionally, the flow rate influence of valve particle blocking increases with smaller x_1-position (= larger pressure application area) and larger particles can block the valve with increased bending.

Valve sealing lip width The valve sealing lip width has an impact on reverse leakage, sticking resistance, particle tolerance and valve reliability. The higher the lip width, the lower the leakage flow, due to a higher flow resistance of the gap. Together with the sealing extent, the lip width determines the contact area, which, in return, defines the potential sticking force. A smaller sealing lip width also decreases the chance for particles to get clamped under the flap, as they are missing a sufficient contact area. With very thin sealing lips, though, the contact pressure is focused on a small area, which can lead to cracks at the flap for high liquid pressures.

Design process to balance performance vs. reliability

With the multitude of performance and reliability requirements, the determination of the design process order is not straight forward and includes iterative aspects. Therefore, a relatively generic design approach was developed to facilitate the design of micropump based dosing systems (Figure 5.17). It includes the most important performance and reliability requirements.

Like for the actuator alone, the micropump system design starts with the definition of the diaphragm radius, which determines the performance class and size of the micropump. The flow rate range and the minimum stroke volume at constant voltage levels is the main influencing aspect for R_d. Additional

restrictions like size dimensions, limitations for the driving signal, like voltage levels and frequency or external conditions, should to be considered at this point and initially set.
The requirements of liquid pressure ability and pressure sensitivity that influence the cavitation tendency, confine the allowed design space with a minimum actuator stiffness. Within this design space the actuator geometry can be optimized towards the most relevant requirements, being peak flow rate, energy efficiency and accuracy aspects. The flow rate optimization correlates with the displacement volume optimization up to certain point, but diverges eventually, as the actuator stiffness is involved over the dynamic motion damping. The optimization of accuracy aspects due to external variations, like pressure dependence or temperature dependence, depend on their tolerable limits on the one side and their range of variation on the other. The reached initial design of the actuator can change after following the subsequent process steps and iteratively adapting certain design aspects.
From flow rate, pressure ability and particle tolerance requirements the valve bending can be determined by the parameters of maximum fluidic pressure, pressure application area and flap geometry. The pressure application should always use the full flap width and maximum x_2-position with safety margins of ~25 µm or whatever the process allows. Only the x_1-position is variable. In the following step, the required sticking resistance and valve reverse leakage defines the contact area and pressure application area over sealing geometry (circular, rectangular), x_1-position and the sealing lip width.
The required gas pressure ability to achieve self-priming ability and bubble tolerance can be determined with the system conditions, pump geometry and surface hydrophilicity. With the knowledge of static displacement volume and actuator stiffness, the maximum dead volume for valve and pump chamber can be estimated. Together with accuracy requirements (actuator fatigue, particle tolerance, temperature dependence), the remaining pump chamber height can be determined. This parameter again defines the necessary fabricated pump chamber height at adjustable predeflection.
Now all parameters to calculate frequency dependent dynamic displacement, liquid flow volume and valve efficiency are given and the estimated frequency dependent flow rate can be determined. Subsequently, achievable accuracy, energy efficiency, energy consumption and estimated battery runtime can be calculated.
Due to complex dependencies, some major iteration steps are indicated for the process, that focus on the competing design directions actuator stiffness, valve bending, remaining pump chamber height and the effect of valve efficiency on the dynamic displacement (Figure 5.17). In the indicated stages of the design process, the need of important components, like degasser, bubble remover, filter and sensor and their design restrictions are defined.
After the process was conducted once, some requirements might not yet be met. Therefore, budgets of goals that exceed their requirements have to be identified. These budgets can be used to improve the other requirements until a match is found and secondary characteristics are optimized.
Due to the multitude of influencing parameters and model inaccuracies within a few percent, an open-loop calibration of the system might be necessary. With the defined range of external influences and knowledge about inherent influences, like fatigue, the achievable accuracy can be determined. If the combined influences exceed the allowed accuracy, a probability calculation of the parallel appearance of influences can be performed. This probability can be compared to the allowed failure probability at the lifetime. If no solution can be found by balancing performance and reliability, but performance requirements alone can be reached, closed-loop flow control provides a solution (following section 5.2).

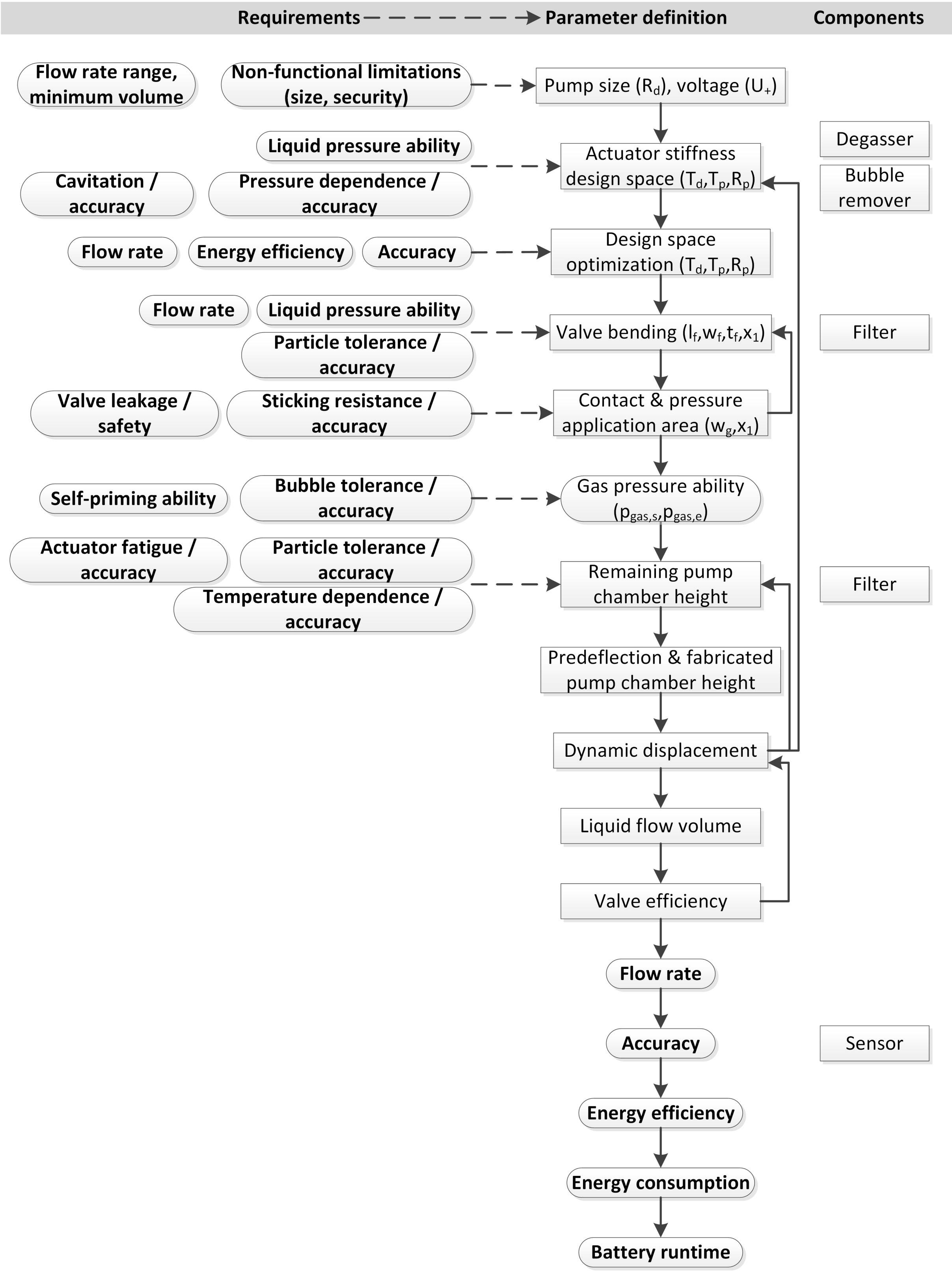

Figure 5.17: Design process to balance performance and reliability requirements.

Discussion

In order to design micropump based dosing systems in open-loop control, the system has to be designed specifically to the application's requirements. The design aspects involve performance and reliability requirements. The overview of influencing parameters provides information about the degrees of freedom of the system. For the key requirements, the strongest influences were depicted. However, the focus was set on geometric optimization that barely considers the mentioned material properties.

The range of utilizable materials is often limited due to the fabrication technologies, required to produce microtechnical structures. Often, silicon is the main bulk material, produced with semiconductor manufacturing technologies. For the piezo ceramic and the adhesive layer, more choices of material classes are available, but usually one is dominant due to advantageous properties. Epoxy resin is chosen for its high Young's modulus and hard PZT ceramic was selected for its high lateral deformation (d_{31}) in combination with high force generation. Yet, optimizing the material parameters would certainly provide a benefit and displays potential for future investigations. Several parameters are already included in the analytical and FEM models, but others, like the adhesive, would have to be added.

The main competing design directions are crucial to understand in order to predict the consequences of design changes. This is especially important, as the design process is relatively complex and yields many interdependencies. Therefore, iterations are necessary at the crucial design aspects to balance different requirements. Even though, the models cover a huge part of the system design space, some aspects, like the surface and geometry dependent bubble tolerance, are not well described or interconnected. A numeric evaluation of the models is often necessary, because analytical solutions cannot be found, even with powerful tools like Mathematica or MatLab. Therefore, many parts were interconnected numerically to allow for an estimation of high level requirements from a set of individual parameters.

Conclusion

In this section, the results from system architecture, performance and reliability were summarized in order to enable the application specific design of micropump based dosing systems. The goal is usually to design a system that can be open-loop controlled, because disturbance influences are minimized and the system behavior is well understood and predictable. For that, an overview of the system parameters was given. The main influences of the key requirements was described and competing design directions discussed. Last but not least, a generic design process for a target-oriented and efficient system design was proposed. This process includes the relevant system parameters to achieve the most important requirements. That way, performance and reliability goals can be balanced to enable a new application. The final goal would be a program, where requirements and system conditions, like fluid properties, external conditions or other restrictions can be set and a final design will be generated. This section provides a step towards this goal.

If, however, the balancing of performance and reliability requirements does not lead to a sufficient solution to meet all requirements, a closed-loop flow control can be implemented. That way, the design focus can be set to performance optimization, while neglecting most reliability influences. The options and methods to set up a closed-loop flow control system will be investigated in the subsequent section.

5.2 Closed-loop flow control

Closed-loop flow control uses information from sensors to adapt the system behavior by changing its control variables (Figure 5.18). The involved steps are always measure, plan and act. To measure, sensors are needed that provide accurate and robust readouts as an electronic signal. In order to plan the change, a model of the dynamic system behavior is required. That way, the defined action leads to an aligned adaption of control variables that cause the desired change of the target value. The extracted sensor information can either directly be the target value flow rate, or indirectly measure major influences on the system behavior, being system parameters (displacement, fluid properties) or environmental parameters (temperature, pressure).

Indirect closed-loop control

Indirect system or environmental sensors offer less information about the target value than a direct measurement. However, in some application cases, a indirect sensor might be sufficient for the required accuracy and may be cheaper and easier to integrate into the system. This integration may address the hardware integration or the software integration. The advantages may reduce development effort and system manufacturing price.

The most useful options for indirect system sensors are the measurement of the micropump actuator or the outlet valve status. Information about the transient displacement, relative to the pump chamber boundary, gives information about the actually displaced volume. Though, as described in section 3.4, this value is not equivalent to the flow rate, as gas capacitances and valve efficiency reduce the effective flow rate. Though, the flow rate can be estimated, if the system runs without bubbles and cavitation and is safe from interfering particles. Options to integrate a deflection sensor is by implementing piezo self-sensing through the driving piezo or an additional piezo sensing layer [155, 156], though the relative position is difficult to obtain. Other options may look at the relative pump chamber position through implementing a capacitance between boundary and diaphragm. The outlet valve position would be able to offer direct effective flow information with some constraints. If a particle is clamped or the flap movement is partly determined by inertia, the valve position does not correlate with the effective flow.

For environmental parameters, temperature, pressure and flow resistance are best applicable. From subsection 4.2.1, the strong temperature dependence of micropump flow is known, which affects the diaphragm and the liquid. Therefore, two sensors are recommended, one measuring the liquid temperature, the other the ambient temperature. In cases of high pressure variations (subsection 4.2.2), pressure sensors should be placed in the fluidic path close to the pump inlet and outlet and above the diaphragm to measure the ambient pressure. If bubbles cannot be avoided from passing through the pump or being generated occasionally, a bubble detector should be placed in the fluidic outlet path. In combination with a bubble remover behind it, the system can increase the flow rate for the period in which the bubble gets separated in the bubble remover. In cases of high particle concentrations, the clogging of filters can be measured, which correlates with its flow resistance. That way, the control variables can be adjusted to compensate the lower flow rate or a notification for a filter exchange can be generated.

Direct closed-loop control

The direct measurement of flow features the highest information and safety for a system and allows for the accurate control of the flow rate. Suitable sensor technologies and control methods are researched in the following paragraphs, which contains the publication of the Sensor-Journal [98].

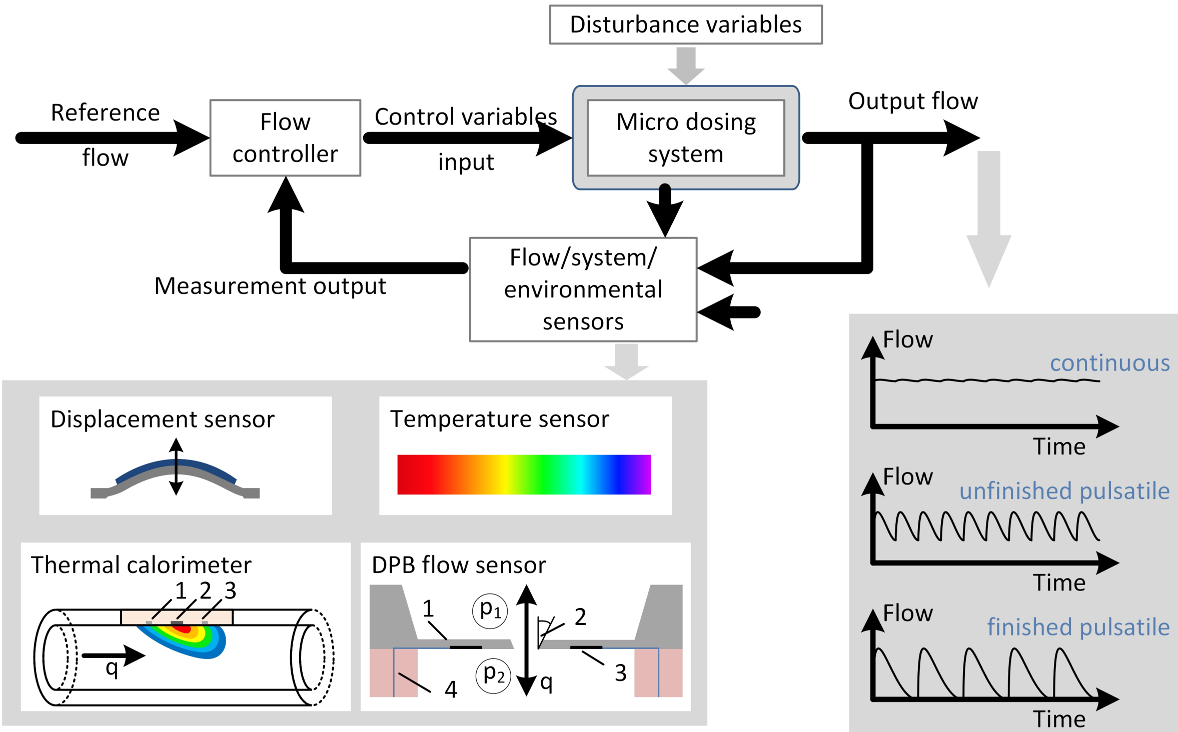

Figure 5.18: Closed-loop liquid flow control.

Abstract
With the combination of micropumps and flow sensors, highly accurate and secure closed-loop controlled micro dosing systems for liquids are possible. Implementing a single stroke based control mode with piezoelectrically driven micro diaphragm pumps can provide a solution for dosing of volumes down to nano liters or variable average flow rates in the range of nl/min to µl/min. However, sensor technologies feature a yet undetermined accuracy for measuring highly pulsatile micropump flow. Two miniaturizable in-line sensor types providing electrical readout - differential pressure based flow sensors and thermal calorimetric flow sensors - are evaluated for their suitability of combining them with mircopumps. Single stroke based calibration of the sensors was carried out with a new method, comparing displacement volumes and sensor flow volumes. Limitations of accuracy and performance for single stroke based flow control are described. Results showed that besides particle robustness of sensors, controlling resistive and capacitive damping are key aspects for setting up reproducible and reliable liquid dosing systems. Depending on the required average flow or defined volume, dosing systems with an accuracy of better than 5 % for the differential pressure based sensor and better than 6.5 % for the thermal calorimeter were achieved.

Introduction
The field of micropump research is by now about 30 years old and started with Smits' patent on a silicon micropump 1984 [30] and the publications of van Lintel in 1987 [32] and Smits in 1989 [31]. Since then, many review papers described different actuation and valve technologies, pump concepts and potential applications mainly in medical devices but also in analysis systems, biological research and other areas [50, 29, 2, 38, 3, 95, 94, 157].

However, compared to the potential, not many applications have yet been realized. This may be due to the challenging requirements in performance, efficiency, costs and reliability for most applications [3, 94]. Summarizing the applications' main requirements of performance and reliability, the challenge lies in creating a stable flow or dose a precise amount of volume with micropumps. Many influences such as gas capacitances [97, 35, 158], particles [97, 158, 148, 5], pressure [33, 34], temperature [142], piezo actuator fatigue [159], etc. have to be controlled in order to achieve high dosing accuracy. These obstacles were already evident in an early phase of micropump research, which lead to the combination and integration of microfluidic flow sensors in the relevant range of nl/min to ml/min. Various flow sensor principles have since been established and used for combination with micropumps: thermal anemometers [160, 161, 162], differential pressure sensing [163, 164, 165, 166], time-of-flight pressure sensing [167], ultrasonic transducers [168], optical [166, 169, 170] or capacitive [96] flank monitoring, capacitive [8] or impedance based [171] volume monitoring, Coriolis force [172], hotwire [173] and fluid drag force on cantilevers [63, 174]. The flow monitoring methods were in part used to investigate micropump behavior and in part connected to a control unit in order to build closed-loop controlled systems to improve dosing accuracy. However, little insight on transient flow sensor accuracy at pulsatile flows was gained. Besides direct flow measurement, other sensors were incorporated into the devices and setups in order to measure secondary influences like pump chamber pressure [173, 175, 176] and diaphragm deflection [175, 177] or environmental influences. Of course, these types of sensors, measuring only influence aspects of possible flow rate changes, have limited validity for flow determination. However, even though the real-time flow is the desired information for a safe closed-loop controlled system, there may be cases where accuracy requirements can be addressed with an environmental or deflection sensor, that is often cheaper due to a higher level of development, less complexity or higher volumes.

The overall goal is to establish accurate micro dosing systems with high performance and variability of flow to enable applications such as insulin dosing [176] or oil lubrication [96]. For high system accuracy, the goal is to combine micropumps with flow sensing technologies. However, the pulsatility of micropump flow is a challenge for sensors and dynamic accuracy limited.

The specific goal is to evaluate sensor accuracy at pulsatile flow and to combine sensor and micropump to establish single stroke based flow control. Therefore, calibration measurements with two suitable sensor technologies were performed - differential pressure based flow sensors and thermal calorimetric flow sensors - with a new method, where displacement volumes are compared to flow volumes. Sensor robustness and influence of resistive and capacitive damping was assessed to combine these sensor technologies with micro diaphragm pumps. For a broad applicability of the control mode, limitations of accuracy and performance were determined for the single stroke based flow control mode.

Within the Introduction, a review of working principle and state of the art of the three main categories for this paper is provided, being the micropump, the sensor technologies and flow control modes. In paragraph 'Materials and methods', parameters and fabrication methods of pumps and sensors and calibration methods are explained. In the 'Results' paragraph, the influence of resistive and capacitive damping, single stroke calibration of sensor technologies and limitation of accuracy and performance for the single stroke based flow control is described. Sensor accuracy and system performance limitations is discussed in the following paragraph, together with an outlook on future investigations. The research is summarized with the achieved accuracy and main conclusions.

Micro diaphragm pump The type of micropumps addressed in this article feature a micro diaphragm actuator and passive valves. Various actuation principles are plausible, like electrostatic, magnetic or piezoelectric [95]. However, for diaphragms in the range of mm, the piezoelectric actuation delivers the highest forces. For passive valves, the most common are mechanical check valves like flaps and membranes or non-mechanical nozzle-diffuser valves, while the former provide higher flow directing efficiency [95]. The cross-section of the used micropump is shown in Figure 5.19. The working principle can be separated into the two phases supply and pump mode. In the supply mode, suction pressure is generated by the up-moving diaphragm leading to inlet flow. In the pump mode, the fluid is pushed out through the outlet valve by excess pressure generated by the downward moving diaphragm. This behavior causes the pulsatile flow behavior at the pump outlet. A rectangular driving signal allows for the highest fluidic performance with increasing frequency, displayed in Figure 5.20, because the fluid is moved in the smallest possible time.

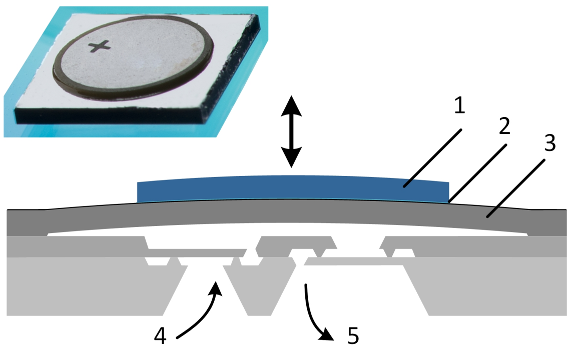

Figure 5.19: Micropump and its cross-section: (1) piezo; (2) adhesive; (3) actuation diaphragm; (4) inlet valve; and (5) outlet valve.

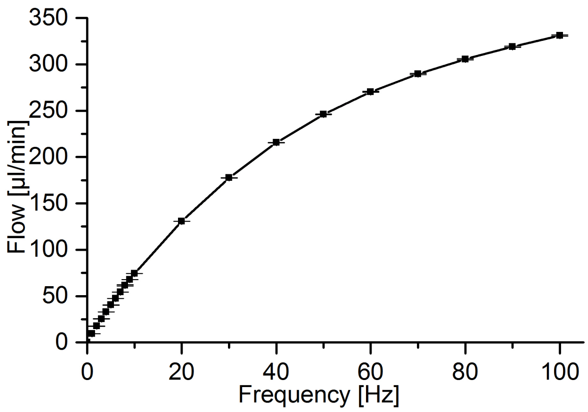

Figure 5.20: Micropump flow rate over frequency of pump as described in methods or section 3.4.

Miniaturizable in-line flow sensor technologies In order to create accurate closed-loop controlled micro dosing systems, the sensors have to fulfill a number of requirements. The sensors need to be placeable in-line of the fluidic path and provide electronically readable real-time flow information. The feasible miniaturized size should be comparable to the micropump to maintain the size advantage on a system level. Most important, the sensor needs to be able to measure the highly pulsatile transient micropump flow correctly. The pulsatility of micro diaphragm pump flow leads to high changing velocities of flow rate in a wide range of flow and is a challenge for sensors. A high sensor velocity, being the time between a flow step and the correct sensor signal, is necessary and is summarized for different microflow sensing technologies in Table 5.1. Meeting the other basic requirements of dimensions, in-line placement and electronic readout, the differential pressure based (DPB) and the thermal flow sensing principles were selected and their state of the art to accurately measure the pulsatile flow reviewed.

Differential pressure based (DPB) flow sensor This type of flow sensor uses a differential pressure between two points in the fluidic path while knowing the flow resistance to calculate the flow. In general, a flow resistance limits the fluidic performance of the system and should therefore be minimized. However, reducing the flow resistance and therefore the pressure drop also reduces the exploitable signal for the sensor. Using very sensitive pressure sensors can compensate that theoretically up to a lower limit, but makes the system vulnerable to flow misinterpretation due to pressure variations from external

Sensor principle	**Measurement velocity**
Optical/capacitive flank monitoring	0.4 ms [178]
Differential pressure based	<1 ms [166]
Thermal calorimeter	40 ms [179]
Thermal TOF (time-of-flight)	6–25 ms [180]
Coriolis	50–200 ms [181]
Gravimetric scale	<2 s [182]

Table 5.1: Sensor principle and their measurement velocity.

influences. An equilibrium, where externally induced noise and sensor zero stability are in the same order of magnitude should be chosen. Pressure sensors in Wheatstone-bridge configurations provide minimized dependence on temperature.

The most important characteristic for pulsatile flow measurement is the sensor velocity. For flow sensors with piezoresistive solid state pressure sensors, the main constraint for flow sensor velocity is the mechanical response time. As shown in Figure 5.21, using a diaphragm based differential pressure sensor with a central orifice as flow restriction simplifies the fabrication of such a sensor significantly, and allows for an almost temperature independent flow sensor at large orifices compared to diaphragm thickness. This was patented in 1997 [183] and described by Richter et al. [166]. The authors described the basic principle of the sensor, the influence of orifice diameter, temperature and viscosity on the static behavior, the blocking effect of gas bubbles and some basic considerations on the dynamic behavior with response time and signal validity if used with micropumps.

Depending on the ratio α between orifice diameter and diaphragm thickness, the influence of viscous friction and therefore viscosity and temperature influence changes. The transition from dominating viscous friction at a ratio of $\alpha <<1$ (Hagen–Poiseuille) to dominating inertia effects with $\alpha >>1$ (Torricelli) and a state in between with $\alpha = 1$ (Hagenbach correction), where diameter and thickness are in the same order of magnitude, can be described by different laws mentioned in brackets [166]. While Hagen–Poiseuille and Torricelli match the static calibration curves well for respected geometries, the intermediate state proves to be less accurate and a certain temperature hence viscosity dependency was observed [166]. Unfortunately, the geometries needed for the investigation of dynamic micropump behavior together with externally induced noise levels feature ratios of a little over one and cannot be fitted very well with the laws.

A FEM study of transient flow through the sensor in the state of the art showed, that velocity profiles behave quasi-static up to harmonic frequencies of 10 kHz [166]. Furthermore an experimental study was carried out, where a steady flow was modulated with a harmonic flow profile in order to investigate the accuracy of accumulated sensor flow compared to scale flow for frequencies up to 1 kHz [166]. This study showed increasing deviations for rising frequencies, hence rising flow rate alteration speed, up to roughly 11 % underestimation of flow at 1 kHz. Due to the setup of an elevated modulated flow, the noisy regimes of the sensor close to zero flow were avoided. The investigations on the dynamic behavior also show contradictory results for a 100 Hz driving frequency. While average flow of sensor signal and reference scale show an underestimation of flow, comparing it to an FEM-simulations showed almost no phase shift but an overestimation around the peak flow.

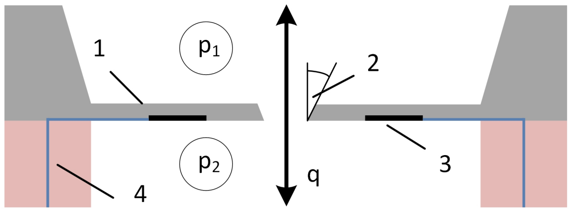

Figure 5.21: Principle of pressure sensor based flow sensor: (1) silicon diaphragm; (2) orifice cone angle; (3) piezoresistors; and (4) conducting gasket.

Thermal flow sensors Thermal flow meters, where local heating of the fluid is used, are the most common sensors to monitor microflow. They are based on three different configurations, which are heat loss at hotwires, microthermotransfer based calorimeter and thermal TOF (time-of-flight) [180, 184]. While some measure the mass flow and others measure the flow velocity, all are sensitive to thermal properties of the fluid. Thermal transduction principles are thermoresistive, thermoelectric, thermoelectronic or frequency analog [184]. While calorimeter, as depicted in Figure 5.22, are composed of one heater and at least two temperature sensors (one upstream and one downstream), they are driven in a steady state of heater power. Based on the temperature difference and the heater power consumption the current flow rate can be determined [185]. For thermal TOF sensors, the time difference between heat pulse generation and temperature peak detection at the sensor is a measure of flow velocity. While calorimeter are better suited for flows with faster thermal diffusion than convection, the thermal TOF principle brings advantages at higher flow velocities [160]. The thermal conduction between heater and thermosensors should be minimized by reducing thermal capacity and using isolating materials. Using freely suspended nitride channels [186] or removing bulk substrate behind the sensing elements [180] are measures to achieve this. For the measurement of pulsatile flow, the calorimetric principle is more suitable due to a constant and higher readout-frequency compared to the exponentially increasing flight times and decreasing accuracy for declining flows rates at TOF sensors. Therefore, low flow pulses can be monitored more accurately with calorimeters. In order to increase sensor velocity the distance between heater and sensor could be reduced. However, this stands in contrast to the sensitivity [185] as the solid-state heat transfer disturbs the temperature sensor, limiting both calorimeters and TOF sensors. Except for one combination of thermal TOF and a micropump [187], mainly calorimetric flow sensors were used for combination with micropumps [161, 162, 187, 64]. Woitschach et al. mentioned significantly rising deviations for increasing flow rates due to the pulsatility of the micropump without going into detail explaining those [162]. Except for the latter, no investigations about the dynamic accuracy of calorimetric flow sensors are known to the authors.

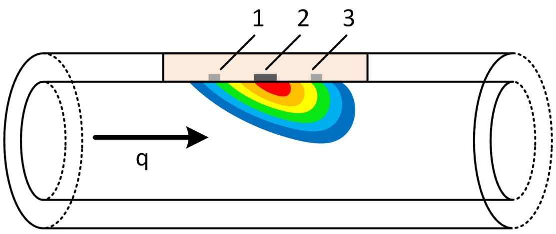

Figure 5.22: Principle of thermal flow sensor: (1,3) temperature sensor; and (2) heater.

Flow control methods To start with, the system setup sets the foundation for a reliable and accurate dosing system. In Figure 5.23, a generic setup for microfluidic dosing systems is shown. Besides the reservoirs, the system can consist of a degasser, filter, pump with driving unit, pressure smoothing elements (PSEs) and a flow sensor. The degasser has two purposes, first to remove passing bubbles and second to degas the liquid so that remaining bubbles in the fluidic path are dissolved after several minutes of operation. An alternative method to provide an initially bubble free fluidic path is deploying the CO2-priming method as described in [82]. Little variations in inner cross section diameter supports this strategy. The filter prevents particles from entering sensitive structures. In the pump, particles can lead to valve leakage or stroke obstruction, for sensors, clogging is the most critical issue. The micropump needs driving electronics to provide adjustable voltage levels and signal shapes with frequencies up to several kHz. Depending on the desired control mode, different PSEs need to be implemented. The flow sensor provides the basis for accurate flow control and can be used for additional safety as bubble detector. The real output flow rate can only be measured behind the pump, as leakage may occur at the interconnections of the pump to the fluidic path. Therefore, the preferred location is after the pump and close to the outlet. For investigation purposes, it is recommended to place two sensors, one before and one behind the pump, to compare both signals. For maximum performance, as little flow resistance as possible is to be installed, mainly concerning filter and flow sensor. A free-flow protection valve and a flow sensor for leakage detection with lower flow range offer additional safety.

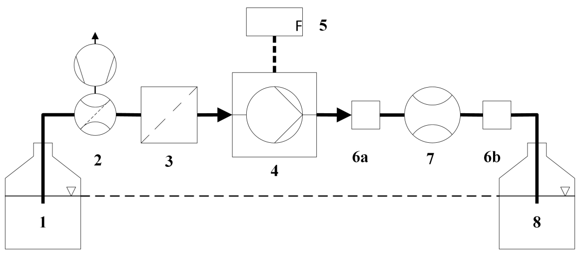

Figure 5.23: Generic liquid dosing system setup for stable continuous flow: (1) reservoir; (2) in-line degasser; (3) filter; (4) micropump; (5) electronic driver; (6a,b) pressure smoothing element (PSE); (7) flow sensor; and (8) outlet reservoir.

Materials and methods

One of the main advantages of micro diaphragm pumps is the high range of flow rate that can be adjusted by changing the driving signal. To ensure a high accuracy while combining micropump and flow sensor, three different modes of operation are possible. The first provides a steady flow for the sensor, where static calibration curves are valid. To achieve such a stable flow with a micropump, a carefully designed damping needs to be implemented. The range of driving frequencies to stay within small boundaries of flow variation, however are quite small. By exceeding these frequency boundaries, the pulsatility of the flow will increase, leading to the second mode. Transient dynamic accuracy of DPB and calorimetric sensors however is also limited, mainly undetermined and no model for a transient correction is known. This leads to the third imaginable operating mode, where fully completed single strokes of pulsatile flow are measured. This mode offers certain advantages. The minimal volumes of each stroke that can be dosed can be adjusted by the voltage levels and the average flow can be adjusted in a wider range until reaching the cut-off frequency. Furthermore, the accuracy for these single strokes can be measured and calibrated for a pump-sensor combination. For a wide frequency range, the capacitive damping has to be minimized. Therefore, between pump and sensor, gas capacitive damping needs to be prevented, as shown in paragraph 'Capacitive and resistive fluidic damping' and elastic capacitive damping needs to be minimized, as described in paragraph 'Transient single stroke measurement'.

Materials and equipment Table 5.2 shows an overview of the used materials and equipment. It also states whether it was fabricated or if it is commercially available. Design parameters and fabrication processes for micropumps and DPB flow sensors are described subsequently.

Materials and equipment	**Manufacturer model**
Silicon micropumps	Fraunhofer EMFT [8, 11]
Differential pressure based (DPB) flow sensor	Fraunhofer EMFT [166]
Thermal flow sensor	Sensirion LPG10-0500
Coriolis mass flow meter	Bronkhorst miniCORI-Flow
Gravimetric scale	Sartorius 225S
Frequency generator	Agilent 33120A
High voltage amplifier	Piezomechanik SVR 150/3
Pressure controller	Mensor CPC3000
Surface topography measurement	FRT 300 µm sensor
Analog readout device	NI I/O-Box 6211

Table 5.2: Material and equipment overview.

<u>Silicon micropump</u>

The key parameters of the silicon micropump, with its cross-section sketched in Figure 5.19, are shown in Table 5.3. The process to fabricate the micropump is as follows: the pump consists of three wafers, two for the valve and one for the actuator including the pump chamber, as indicated in Figure 5.19. The monocrystalline silicon wafers start with mask layers of silicon nitride and silicon oxide. After lithography and DRIE etch masking, the main structuring is done by KOH etching. A two-step etching process allows for different structuring depths of the valve wafers. After removing remaining mask layers, thermal oxidation allows for the silicon fusion bond in order to join first the two valve wafers and subsequently the actuation wafer. To reduce the diaphragm thickness, grinding and polishing is used. A sputtered aluminum layer provides the contact for the adhered piezo disc from manufacturer PI. The piezo is attached to the diaphragm according to a fabrication method that is also referred to as initial deflection method [52] to achieve a higher compression ratio by applying an initial deflection combined with low pump chamber height. The pump is adhered to a fluidic adapter that connects to the flow sensors by use of stiff PEEK capillaries.

<u>Differential pressure based (DPB) flow sensor</u>

For the manufacturing of the DPB flow sensor, a bi-directional 5 psi differential pressure sensor for liquids was chosen, providing a response time of 1 ms. The chosen sensor type was of the Honeywell 24 PC Series, while the Sensortechnics/FirstSensor RPOP005D6A presents a slightly less accurate alternative. A central orifice was lasered into the sensor diaphragm, using a 355 nm UV laser in pulsed mode at 20 kHz and 2 W for 1 s and a circular oscillation pattern. Diameters and respective maximum flow rates at the

Actuator					Pump chamber height
Diaphragm thickness	**Diaphragm diameter**	**Piezo thickness**	**Piezo diameter**	**Piezo type**	
40 µm	6.6 mm	150 µm	5.6 mm	PIC255	3 µm
Valves					
Flap length	**Flap width**	**Flap thickness**	**Valve seat length (cubic)**	**Seal lip width**	
800 µm	480 µm	15 µm	380 µm	6 µm	

Table 5.3: Micropump key parameters.

maximum pressure of the sensors are displayed in Table 5.4. The cone angle, originating in the lasering process, results in a direction dependent flow number μ. The nozzle diameter is always the larger one, leading to a nozzle like flow profile if pressure is applied at this side of the diaphragm. That anisotropy can either be avoided by use of DRIE etching or enhanced and used to measure leakage flow with higher sensitivity.

Pressure sensors are naturally very sensitive to internal or externally induced stress, leading to measurably changing zero-flow offset values. That is why, besides calibration measurements, an additional zero-offset recording has to take place once the sensor is installed in the final setup. For flow calculation, this new zero-offset value has to be the reference value for signal values as if it was the zero-offset value of the calibration measurement. The offset values were individually evaluated before each measurement and exhibit a standard deviation of 3.6 µl/min.

Label	Pressure range	Repeatability & hysteresis	Nozzle diameter	Diffuser diameter	Max. nozzle flow	Max. diffuser flow
DPB65µ	5 psi = 34.5 kPa at 110 mV	±52 Pa or ±0.17 mV	65 µm	60 µm	270 µl/min	260 µl/min
DPB50µ	5 psi = 34.5 kPa at 110 mV	±52 Pa or ±0.17 mV	50 µm	45 µm	165 µl/min	158 µl/min

Table 5.4: Differential pressure based (DPB) sensor key parameters.

Measurement methods Table 5.5 shows the overview over the methods used for measurements and data processing. For Methods (a) and (b), the setup structure is sketched in Figure 5.24. The medium for all measurements was DI water. The carbon dioxide priming method [82] is used to ensure a bubble free fluidic path between reservoir and outlet and was applied for all measurements.

Static calibration of flow sensors

The static calibration of the flow sensors was done with the measurement setup shown in Figure 5.24a. The water reservoir (b) is set under air pressure, controlled by a pressure regulator (a). The readout of the flow sensors (2/3) are compared to a reference flow sensor (4) placed downstream. The pressure was increased until the maximum sensor range had been reached. Three full cycles of pressure increase and decrease were conducted in each direction. The OriginPro (v9.1G, OriginLab Corporation, Northampton,

Method	Measurement of
(a) Static calibration of flow sensors	Static reference flow vs. sensor voltage
(b) Dynamic calibration of flow sensors	Stroke volume vs. sensor voltage vs. average reference flow

Table 5.5: Measurement methods overview.

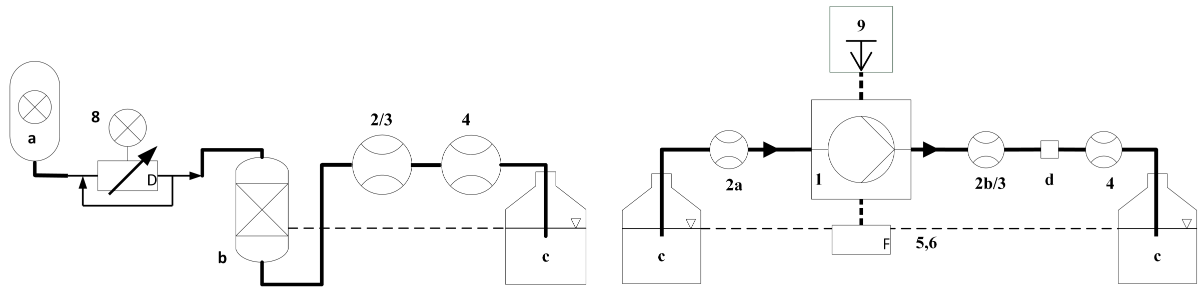

Figure 5.24: Measurement setups for: (a) static calibration; and (b) single stroke calibration (Table 5.5). Description numbers refer to Table 5.2. Additionally: a: pressure source; b: pressured reservoir; c: reservoir; and d: pressure smoothing element (PSE).

MA, USA) curve "ExpDec2" was fitted to the experimental results and used to calculate the dynamic flow.

Single stroke calibration method

The measurement setup in Figure 5.24b for the dynamic calibration method consists of a micropump and at least two flow sensors. For the DPB sensor, one was located right before the pump (2a) and one behind (2b). For the thermal calorimeter, only one was placed behind the pump (3). The elastic capacitive damping was minimized by using stiff capillaries and short distances between pump and sensor. The average flow was monitored by the reference flow meter (4). The actuator deflection was measured at the diaphragm center by a profilometer (9) with 4 kHz scanning frequency.

The procedure to acquire one calibration point includes a fully finished pump cycle at a pump driving frequency of 0.5 Hz, providing 1 s each for supply and pump mode. The voltage levels were varied between 200 V and −60 V in 20 V-steps, depending on the sensor range.

The calibration compares two volumes, one is the integrated flow volume of the flow sensor, the other is the calculated stroke volume of the actuator deflection. To calculate the stroke volume of each cycle, the center point deflection is multiplied by a factor representing the volume per deflection:

$$V_{disp} = \triangle z \, \frac{\pi \int_a^b x \, y[x] \, dx}{z_{line\,center}} \tag{5.1}$$

the volume per deflection is constant within the full deflection range of the micropump. The measured relative line displacement of the actuator, as shown in Figure 5.25, is used to calculate this ratio by integrating the line fit over half a revolution after shifting the line center to $x = 0$.

Results

The achievable system accuracy depends on the sensor accuracy, the time between measuring deviations

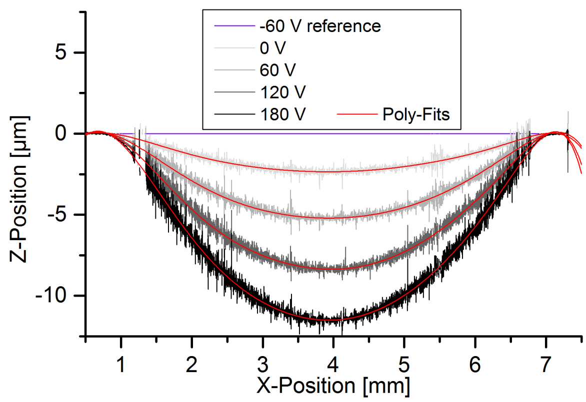

Figure 5.25: Line-displacement of actuator for stroke volume determination.

and adjusting the flow and the adjustment accuracy. The task of dosing systems lies either in generating a certain average flow or dosing a defined volume. Micro diaphragm pumps always generate pulsatile flow. The systems outlet flow characteristic can be fully pulsatile, meaning the flow always reaches zero each cycle, continuous, by implementing tailored pressure smoothing elements (PSE), or in a state in between. To work with the single stroke based flow control, the sensor is placed before the optional main PSE. The influence of capacitive and resistive damping on flow pulsatility is evaluated in paragraph 'Capacitive and resistive fluidic damping'. The ability of DPB and thermal flow sensors to measure the transient single stroke micropump flow is investigated in paragraph 'Transient single stroke measurement', followed by describing the influence of these results on single stroke based closed-loop control.

Capacitive and resistive fluidic damping Resistive fluidic damping depends on the flow resistance between actuator and the whole fluidic path. Resistive damping reduces flow velocity and prolongs the flow, which reduces the maximum driving frequency, where flow pulses are fully finished.

Capacitive fluidic damping in general has the same smoothing effect on a flow pulse as resistive damping, but stores the pressure in a capacitance. Such a capacitance can be a bubble within the fluidic path or an elastic element. Decoupling the actuator from a high fluidic resistance or fluid inertia by using a capacitance, increases the maximum driving frequency at fully finished flow pulses but reduces the stroke volume due to the counter pressure at the charged capacitance. During the time of the supply mode, the capacitance pressure is transformed to outlet flow. In a correct configuration, this can increase maximum flow, while smoothing it.

However, it is very difficult to implement a reproducible capacitive damping if different sized bubbles may occur in the fluidic path, which is why gas bubbles need to be avoided. Capacitive damping in general can never completely be avoided, as even stiff solid-state bodies such as capillaries or other housing parts exhibit a certain elasticity. Elastic capacitive damping though can be better controlled by specific design. To investigate the magnitude of gas capacitive and elastic capacitive damping on the flow, a perfectly filled fluidic path with as little elastic damping as possible was set up together with a DPB flow sensor. The elastic damping between pump and sensor lead to finished flow pulses after 200 ms, driven at 1 Hz (Figure 5.26). At 10 Hz, leaving 50 ms for the pump mode and 100 ms for the whole cycle, the pulse was not able to finish completely. After introducing a bubble in between pump and sensor, the flow was measured at 5 Hz meaning the pump stroke is limited to 100 ms, the full cycle to 200 ms. At pure elastic

damping, the charged capacitance only results in minor deviations of flow curves, while strong smoothing occurs at gas capacitive damping.
Pressure smoothing elements (PSEs) allow for tailored capacitive elastic damping. Options for implementation are elastic solid-state elements like diaphragms, chambers or tubes. Here, PSEs can be designed easily with available models of basic geometries and materials. Materials should exhibit low permeability for gases as longer operation downtimes of several hours or days may lead to evaporation through thin plastic structures or diffusive materials like silicone, leaving bubbles in the fluidic path behind.

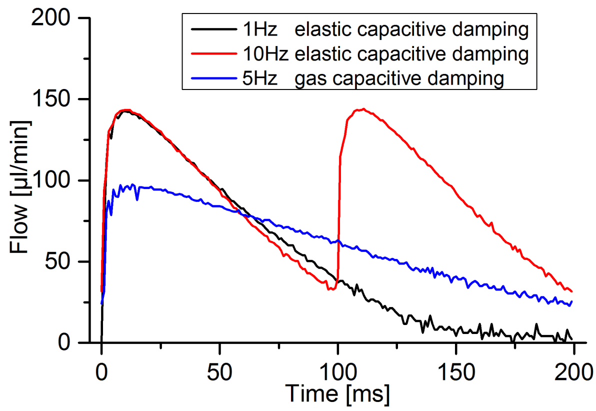

Figure 5.26: Influence of elastic and gas capacitive damping on the flow.

Transient single stroke measurement To measure the transient flow of the fluidic step response of a rectangular driving signal accurately and in full range is a challenge for sensors due to high flow rate changing rates. The introduced sensor technologies - differential pressure based flow sensors and thermal calorimeter - are the fastest in-line measurement methods while providing electrical readout that were identified with sensor velocities of 1 ms for the DPB sensor and 40 ms for the thermal sensor.
Static calibration measurements with the same reference flow sensor were taken out to establish comparable flow values and to describe the achievable accuracy in static operation. For the DPB sensor a bi-directional static calibration curve was recorded (Figure 5.27). The high steepness of the curve close to zero indicates low sensitivity. This leads to a high inaccuracy for low flow rates, but increasing accuracy for rising flow. The direct static calibration curve with sensor signal over flow cannot be determined independently, as the program output directly shows flow values. However, from the literature, it is known that an exponential curve is to be expected for thermal calorimeter [180]. This correspond to the increasing deviations with rising flow rates as observable in Figure 5.28. The sensor behaves bi-directional, which is only indicated for a short range in the diagram.
For the determination of sensor accuracy of pulsatile flow, the micropump was used to generate flow pulses of different height and volume by increasing the absolute voltage difference, according to the 'Single Stroke Calibration Method'. The DPB sensor was addressed with the pump's full voltage amplitude of 260 V. The thermal sensor was addressed with a maximum of 90 V. The actuator velocity peak is always reached within 1 ms. Comparing the sensor signal to the actuator velocity, as depicted in Figure 5.29, a delay of 8–14 ms from actuator to flow signal peak occurs, depending on the voltage level and for a perfectly filled fluidic path. The thermal sensor reaches its flow peaks at relatively stable 20 ms (Figure 5.30). DPB flow finishes after 150–200 ms, while calorimetric flow finishes after 100–150 ms.

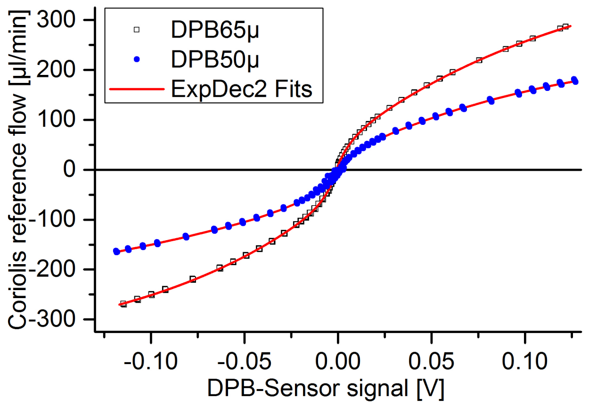

Figure 5.27: Bi-directional calibration curves including mathematical fit-functions.

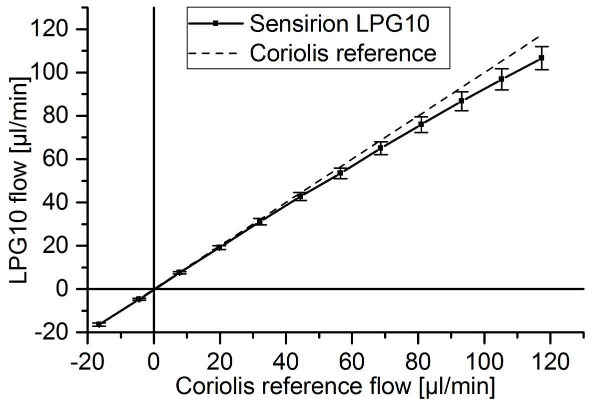

Figure 5.28: Static calibration of thermal calorimeter (LPG10) against Coriolis flow meter.

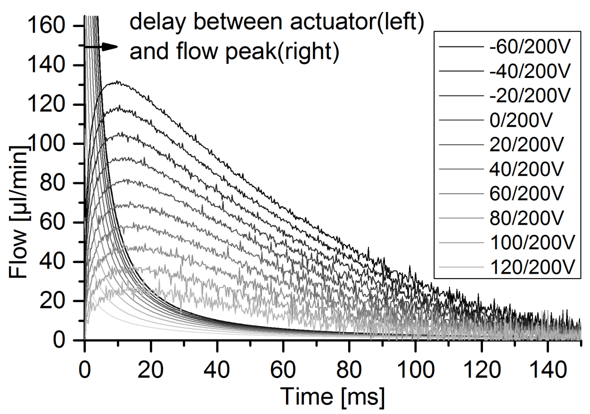

Figure 5.29: The actuator velocity (derivative of displacement Hill-fit-curves of Figure 5.31) and the DPB50µ sensor flow compared for the pump mode.

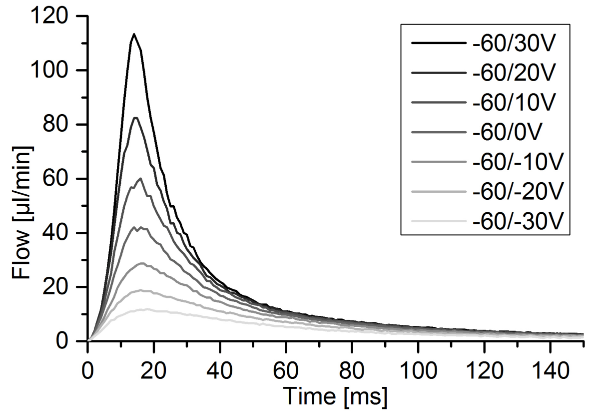

Figure 5.30: Dynamic flow pulses for rising voltage levels.

For the determination of average flow and flow volumes, the accumulated flow is calculated for each pump stroke. The time course of the stroke volume and the integrated sensor flow are compared and depicted in Figure 5.31 for the DPB50µ sensor and in Figure 5.32 for the thermal sensor. While the actuator signal can be calculated for the whole measured spectrum, the DPB sensor's flow signal becomes too noisy to be evaluated for pulses with peak flows below 25 µl/min for sensors with maximum flow rates of −165 µl/min. With full-scale flow of 120 µl/min of the thermal sensor combined with high accuracy at low flow rates, lower pulses down to can be measured.

Stroke volume and sensor flow volume are compared at 500 ms, when the actuator is static and all pressure capacitances are equalized, hence no more liquid is flowing. For the two DPB sensors, deviations between the two volumes are shown in Figure 5.33. For voltage differences below 80 V, the signal was too noisy to evaluate. The sensors underestimate the flow up to voltage differences of 120 V, after that an overestimation of flow stabilizes at roughly 4–5 %. The thermal flow sensor was subject to much higher flow rate changing rates. Stroke and flow volume are compared in Figure 5.34 and show a general overestimation of flow between 2–6.5 %.

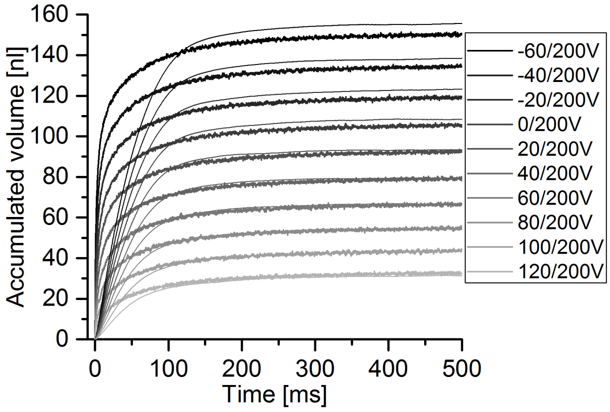

Figure 5.31: Comparison of accumulated stroke volume (noisier signal) and DPB50µ sensor flow.

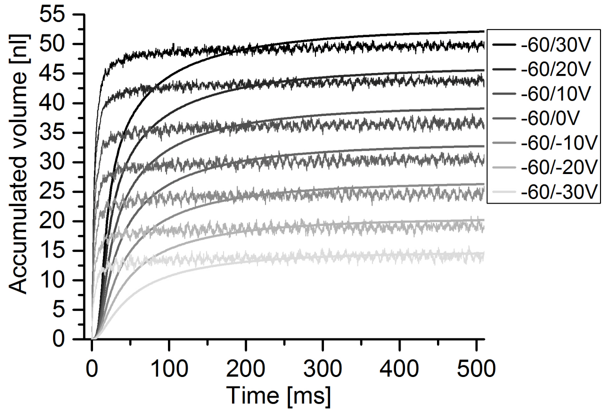

Figure 5.32: Comparison of accumulated stroke volume (noisier signal) and LPG10 sensor flow.

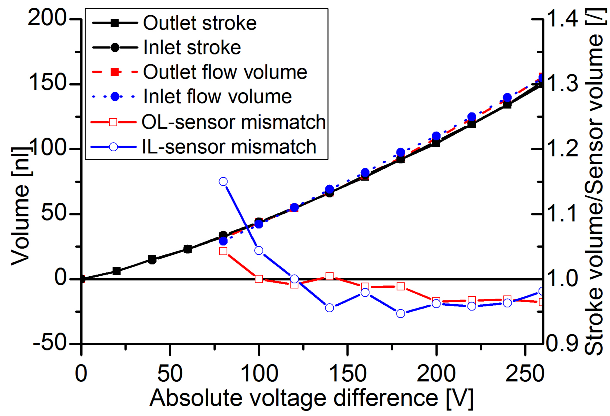

Figure 5.33: Accumulated volume for stroke (y-error: 0.09–0.19 nl) and flow (y-error: 1.79–2.26 nl) at 500 ms and the mismatch factor between both.

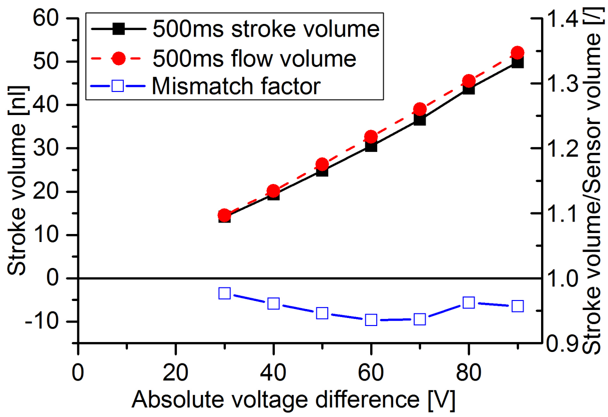

Figure 5.34: Comparison of stroke volume and sensor volume (y-error: 0.32–0.57 nl) at 500 ms for the thermal flow sensor.

Single stroke based flow control mode Applying the single stroke based control mode has certain limitations for performance and accuracy. The volume of one pump stroke is mainly limited by the maximum electric field that can be applied to the piezo and is typically between −0.4 kV/mm and +2 kV/mm. That is −60|+300 V for a piezo thickness of 150 µm. However, the actuator touches the pump chamber boundary at 200 V, which gives the practical limit. Before defining the maximum frequency, the main limiting factors on a minimal setup are described briefly. The outlet path starts with the actuation diaphragm and the outlet valve within the pump followed by a minimized elastic capacitive damping element, an in-line flow sensor and an outlet tube. The whole outlet path exhibits a certain fluidic resistance, significantly increased by the DPB sensor compared to the thermal sensor. The actuation displacement flow is mainly determined by the resistance and the charged pressure at the elastic capacitance between pump and sensor. The flow through the sensor is further damped compared to the displacement flow due to the capacitance but effectively finishes at the same time as the actuator. The final sensor readout is additionally smoothed and delayed by the sensor velocity. To define the maximum driving frequency of the pump to stay within fully finished flow pulses, all these time delays have to be considered. If one wants the actuator to balance itself out to fully static, the maximum frequency is:

$$f_{max,static} = \left[2\left(t_{disp,static} + t_{sensor-velocity}\right)\right]^{-1} \tag{5.2}$$

For maximum performance at a certain elastic capacitive damping (leading to a flow delay $t_{capacitive-delay}$ at the sensor), only the measured flow needs to return to zero within a full cycle. That means the actuator is switched from pump to supply mode, while still moving downwards. In this case, the maximum frequency $f_{max,dyn}$ for single stroke based control is limited to:

$$f_{max,dyn} = \left[t_{disp,dyn} + t_{capacitive-delay} + t_{sensor-velocity} + t_{processing}\right]^{-1} \tag{5.3}$$

While the processing time $t_{processing}$ can be done in the supply mode for the static scenario, it has to be added to Equ. 5.2 for real-time flow control. A stiff pressure-insensitive actuator increases the performance by achieving higher stroke volume at outlet pressure. If a continuous flow is desired, a PSE can be placed after the sensor. The benefit lies in establishing a continuous flow while maintaining the pump cycle based closed-loop control. This also decreases the maximum flow range needed for the sensor, which therefore increases sensitivity, as the ratio between both is limited. The limitations of achievable accuracy depend on the adjustment accuracy and the sensor accuracy. The sensor can measure each stroke with a certain accuracy (acc) and precision (prec). The sensor's accuracy and precision is stroke volume dependent. With rising stroke numbers $N_{strokes}$ for the dosing task, the precision influence gets smaller. The total accuracy acc_{total} of the stroke adjustment only plays a role for the last stroke, as it can be set according to the accumulated flow volume before. The total accuracy for each dosing task is therefore:

$$acc_{total,dosing}\,[\mathrm{nl}] = \pm\left(\sum acc_{sensor}[\triangle U] + \frac{prec_{sensor}[\triangle U]}{N_{strokes}} + acc_{total,adjustment}\right) \tag{5.4}$$

Discussion

Sensor accuracy at pulsed flow The goal was to evaluate sensor accuracy of micropump generated pulsatile flow. In general, these pulses exhibit a steep flow increase within a few milliseconds (Figures 5.29 and 5.30), followed by a flow decline within tens or hundreds of milliseconds. With increasing absolute voltage difference, the flow pulses show a higher peak flow but similar overall times to reach zero flow. While the investigated sensor technologies are subject to misinterpretation of fast changing flow rates, that effect is diminished, as there is always a rising and a falling flank.

The DPB sensors uniformly showed higher inaccuracy with decreasing flow pulse heights (Figure 5.33). Below 80 V, the signal was not clearly evaluable, as it was within signal noise. One difficulty of this technology is the choice of pressure range and flow restriction. While a low flow restriction (high orifice diameter) leads to inertia dominated flow with less temperature dependence, the sensor range has to be small enough to measure the full range of the maximum desired flow pulse. However, this leads to a high sensitivity and high signal noise due to environmental influences. Due to the steep static calibration curve close to the offset value, little changes in voltage mean a high difference in flow. Combined with the sensor noise very low flow rates might not be detected but results in high errors. For flow pulses generated with more than 120 V, a stabilizing deviation of roughly 5 % is observable. Not all sources of errors are known yet. One already mentioned is an offset shift between calibration and individual measurement.

Sources of misinterpretation might be in fast changing flows, where pressure difference does not match the static calibration of actual flow and temperature difference between calibration and measurement. Another error case is the partial clogging of the sensor orifice, which is not easily detectable, because it just compresses the calibration curve, overestimating the actual flow. Due to the fast response time of below 1 ms, the sensor velocity plays a subordinate role in smoothing the signal. This is a major advantage of this sensor type and makes it suitable to investigate highly pulsatile micropump flow.
For the thermal calorimeter, the achieved accuracy of integrated flow over a full pulse was within 6.5 %. The static calibration of the thermal calorimeter shows the highest flow precision at zero flow and decreases with rising flow due to an exponential shaped flow over sensor signal (Figure 5.28). Therefore, lower pulses with respect to maximum flow can be measured compared to the DPB sensor. However, the sensor speed of 40 ms [179] is lower than the 1 ms of the DPB flow sensor, which leads to reaching the flow peak at around 20 ms compared to 8–14 ms for similar elastic damping and despite lower resistance (Figure 5.30). Heat transfer from liquid to the temperature sensors combined with surrounding thermal mass not only results in the slower sensor velocity, but also reduces the measured peak flow. For rising flow an underestimation and for decreasing flows an overestimation of flow is to be expected. The overall flow overestimation indicated a higher impact of the slower changing decreasing pulse flank. The microthermotransfer principle also allows for higher tube diameters and provides a more robust system with less chance of clogging through bubbles or particles. For a wider flow range combined with high sensitivity for leakage flow detection a specific design or additional sensors can be considered.

Flow control modes To employ the single stroke based flow control on a system level, not only sensor accuracy is critical, but also fluidic performance, efficiency and stroke adjustment accuracy. While the DPB sensor includes a significant additional fluidic resistance in the outlet path with its orifice, the thermal sensor allows for larger tube diameters. The time for finishing the flow pulse across the sensor will decrease for the thermal sensor, the maximum driving frequency to stay in the finished single stroke mode will increase compared to the DPB sensor. As described in paragraph 'Single stroke based flow control mode', for higher frequencies it is recommended to just have finished flow pulses at the sensor after a full cycle, not at the actuator. However, having unfinished movement of the actuation diaphragm will result in a higher temperature dependence, hence lower stroke volume adjustment accuracy. Additionally the efficiency decreases, because the actuator switches to supply mode before the full deflection is finished. To sum up, higher fluidic performance comes along with lower adjustment accuracy and lower efficiency. By smoothing the pulsatile micropump flow with large capacitances (PSEs), holding multiple stroke volumes with low pressure changes, a continuous flow rate can achieved. Sensors with lower velocity can be employed behind the PSEs to measure continuous flow. A range of flow rate with a high accuracy can be chosen, being low flow rates for thermal calorimeters or high flows for DPB based sensors. Another advantage over transient pulsatile measurements is the potential direct use of the output parameter for control purposes requiring no or less further processing. However, implementing PSEs for minimal damping for a certain flow rate is challenging. Changing the frequency will result in more pulsatility and less accuracy. At the single stroke based control mode, a higher range of driving frequency can be employed with defined accuracy limits. Dosing defined volumes with several strokes can be done with a very high accuracy by adjusting the stroke volume after each cycle, leaving only the sensor accuracy and the last adjusted stroke as main sources for deviations (compare to Equ. 5.4). In general, capacitive damping has a big impact on flow, which is why it has to be limited to elastic capacitive damping by avoiding gas bubbles.

Future investigations While capacitive damping plays a strong role in flow performance for microfluidic systems, there is little existing literature about designing elastic capacitances of defined magnitude of influence. Mechanical models for different shapes like tubes or diaphragms should be adapted to provide information about their dynamic capacitive behavior with fluid pressure. Thereby, continuous flow control with the sensor placed behind the smoothing element might achieve higher accuracy or even a wider range of frequency with a variable PSE. Single stroke based control mode on the other hand would profit from enabling continuous flow in minimal space requirement. A dynamic sensor calibration method that is able to correct changing flow rates would of course be most desirable and enable an accurate flow control over the full frequency range of micropumps.

Conclusion

Micro dosing systems based on micropumps are able to accurately deliver defined volumes of liquid down to nano liters or average flow rates in the range of nl/min to µl/min. Inherent system or micropump fatigue together with variable changes of environmental parameters, however, influence performance stability and reproducibility. Combining micro diaphragm pumps with flow sensors enables accurate closed-loop controlled systems.

In this section, two sensor technologies were evaluated for their ability to measure the highly pulsatile micropump flow to be employed for single stroke based flow control: differential pressure based (DPB) sensors and thermal calorimetric flow sensors. Depending on the required average flow or defined volume, dosing systems with an accuracy of better than 5 % for the differential pressure based sensor and better than 6.5 % for the thermal calorimeter were achieved. A method was developed that enables calibration of single stroke flow pulses by comparing displacement volume with sensor volume. Limitations of accuracy and performance at combining these sensors with micropumps for the single stroke based flow control were given. DPB flow sensors exhibit a sensor velocity of 1 ms that results in peak-flow detection after 8–14 ms. However, orifices of 50–65 µm produce significant fluidic resistance, which prolongs the flow and reduced maximum frequencies for single stroke based flow control to 5–6 Hz. Furthermore, a trade-off between particle robustness and temperature dependence versus signal to noise ratio regarding their orifice diameter has to be taken into account. By contrast, thermal flow sensors display higher fluidic performance up to 6–10 Hz maximum frequency and higher particle robustness due to a larger tube diameter and good sensing range combined with high sensitivity. Because of the sensor velocity of 40 ms, the flow peak is only reached after 20 ms.

Enhancing sensor velocity for thermal calorimeter or finding transient calibration methods for both technologies are desirable goals to enable stable, accurate operation up to higher pump frequencies. Alternatively, providing design guidelines of implementing pressure smoothing elements for smoothed flow also enables higher flows with accurate measurement, but provide little flow variability.

6 Summary

6.1 Conclusion

Micropump based liquid dosing systems have a variety of potential applications. However, each application features a different set of performance and reliability requirements. In order to meet all goals of new micro dosing systems, an application specific system design is usually necessary. In this work, an approach to design micropump based liquid dosing systems is presented. The process to define the system architecture is based on the requirements and includes the selection of functional components, the design of specific core components, as well as the choice of operating strategies and the challenges of system integration. Within this framework of system architecture, the emphasis lies on investigating the performance and reliability aspects of micropump systems. With a combination of measurements as well as new analytical and numerical models, the major influences of flow performance and flow stability were identified and can be simulated. However, performance and reliability aspects often display competing design directions. Therefore, the major influences of the most relevant requirements are given, together with a generic balancing process to deal with these opposing design issues in open-loop flow control. For the case that flow stability goals cannot be met at the same time as flow performance goals, the combination of micropumps and direct or indirect flow sensing for closed-loop flow control is evaluated. The system architecture with its operating conditions provides the foundation for a reliable dosing system.
The proposed design process to regard the most important aspects is described in chapter 2 and starts with the evaluation of the requirements. The most relevant performance goals are flow rate, liquid and gas pressure ability, self-priming ability, energy consumption and battery runtime, flow characteristics, size and costs. Reliability can be summarized as accuracy of performance over the specified lifetime within a certain failure probability. For liquid dosing systems it includes the tolerance of variations of external influences like temperature, pressure, vibration, particles or bubbles. Before designing the individual components, the composition of functional components has to be chosen with care, as it determines the basic working principles of the device. The system behavior depends on the design and driving signal, but is influenced by internal and external disturbance variables. Operating conditions, like preparation procedures or control of certain conditions, were defined to improve flow characteristics. A challenging part of system design is the implementation of the desired architecture. Therefore, some of the major obstacles and their interdependencies are described.
The performance of liquid dosing system is determined by its driving unit the micropump actuator in combination with the connected fluidic network. For increased gas pressure ability, necessary for self-priming ability and bubble tolerance, micropump of the state of the art feature reduced pump chamber height of a few micrometers. This change in geometry caused a squeeze film effect with strong viscous damping that changed the pump dynamics significantly and made existing models inaccurate. In chapter 3, the most important performance characteristics of micropump systems were therefore investigated and new analytical as well as numerical models were developed to provide simulation tools for pump design. An existing static actuator model [34] was adapted and validated to evaluate novel performance aspects, like stress limitations, the relevance of diaphragm and piezo geometry on displacement volume and pressure

ability, efficiency calculation and cost considerations. While the static and dynamic deflection of the valve can be modeled analytically, the dependence of fluid friction on complex geometry does not allow for a simple purely analytical model to describe the flow rate through the valve. Therefore, an extensively parametrized FEM based fluid-structure-interaction (FSI) model was developed in COMSOL in order to allow for a fast adaption of valve geometry and flow evaluation. Considering the whole micropump with external conditions, the excess and suction gas pressure abilities were investigated. Theoretical evaluations of pressure abilities were compared to experimental investigations in order to figure out the practical influence of valve leakage. To understand the flow rate influencing effects of micropumps for liquids are not only important to accurately design the fluidic performance, but it also constitutes the foundation to estimate the influence of disturbance variables. Therefore, all major flow influencing effects were investigated. These are liquid resistive damping, cavitation based gaseous capacitive damping and reactive valve volumes. Analytical models were developed that are able to describe and predict the transient actuator displacement, derive the frequency dependent displacement and estimate the valve loss effect in order to determine the flow rate performance of micropumps. In addition, a new oscillator model is able to simulate the inception of cavitation and the time course of both actuator and liquid. The individual effect models were combined into a single-cycle based, frequency dependent, flow rate model, validated for frequencies of up to 100 Hz.

The reliability or flow stability of micro dosing systems, investigated in chapter 4, is challenged by many disturbance variables. These can be inherently present or externally induced. Inherent influences like cavitation, actuator fatigue and valve sticking mainly depend on handling and driving conditions and all feature high statistical variance in appearance. Due to their poorly predictable nature, they should be avoided or reduced below significant influence, where possible. The impact and criticality of these effects were investigated and potential approaches to solve the issues were given. External influences like temperature, pressure, particle-laden flow, bubbles and vibration mainly depend on the environment of the application an can therefore hardly be avoided. The strategy to reduce the influence in these cases is by changing the systems design parameters, like for example the actuator stiffness for pressure dependence. Temperature, pressure and particle laden flow were investigated and evaluated with supporting models to identify the key factors to adjust their sensitivity. All disturbance variables cause flow variations and therefore affect the flow stability of an open-loop controlled system. Leaving the specified accuracy band even though only temporarily, like due to temperature variations, would mean a failure that has to be avoided in certain applications.

Due to the multitude and effect magnitude of disturbance variables as well as competing design directions, it is challenging for many applications to meet all performance and reliability requirements over the specified lifetime. Therefore, the two approaches open- and closed-loop flow control solutions are presented in chapter 5. With a design balancing process, an efficient way to enable open-loop flow control systems, is proposed. It builds upon the given overview of main influences of the most critical characteristics and deals with the analyzed competing design directions. As a result, different goals can be weighed according to their importance, for example pump chamber height can be designed towards higher bubble tolerance or flow rate or the actuator can feature higher pressure ability or lower cavitation tendency. In some cases, inherent effects cannot be ruled out or disturbance variables are too high to meet the reliability goals at the same time as the performance goals. For example, the required flow rate can be achieved, but external effects like temperature variations are too high to stay within the specified accuracy band for the flow rate. If the performance goals alone can theoretically be met, a closed-loop flow control can

enable these applications. However, such systems are accompanied by higher costs due to the additional component and increased data processing demands. For closed-loop flow control, the sensor technologies have to be chosen carefully, regarding the required flow control mode and flow characteristics. Highly pulsatile micropump flow with high gradients of flow change are difficult to measure accurately with flow sensing technologies in microfluidics or lead to additional issues. Even though, damping of the flow behind the micropump is possible, it comes along with performance changes and potentially reduces the flow rate variability if a certain flow smoothness is to be achieved. These issues were evaluated for a suitable selection of flow sensing technology and flow control mode.
To summarize the achievements, solutions for the design of micropump based dosing systems in open- or closed-loop flow control are presented, following a requirements based design approach. This displays progress towards the goal of an adaptable micropump based dosing systems platform that can meet the requirements of many different applications.

6.2 Outlook

With the goal to realize as many different micro dosing applications as possible, a number of topics and issues still have to be addressed. Among these are the system design approach with performance and reliability, the development of functional components, general micro integration technologies as well as accurate, reliable and cheap producibility of the whole micro dosing system platform.
The quality of the system design process essentially depends on the quality of the individual models themselves. The model to calculate the gas pressure ability should be expanded by the identified quantitative influence of gas leakage. This aspect is important for self-priming ability and bubble tolerance, where usually the pump is filled with gas only. In addition, the bubble tolerance strongly depends on the filling of the pump chamber with liquid. This in turn depends a lot on the wettability of the solid surface by the liquid and the pump chamber geometry. To find the exact limitations of required gas pressure ability for certain conditions would allow for a more aligned pump design with increased remaining pump chamber height for lower viscous damping and thus higher fluidic performance.
The novel model, describing the flow rate influencing effects of micro diaphragm pumps is able to describe the dynamic pump behavior in a wide range of driving and environmental conditions. It is the foundation to estimate the influence height of disturbance values, i.e. the flow stability. Even though, the major effects and dynamics of pressure, temperature and viscosity were identified and estimated, they are not yet integrated as models. Integrating these submodels into the system behavior model would allow for an automatically computed solution with less iterations for the system design.
The pure size of particles can be dealt with by appropriate design of pump and filters. However, the particle adhesion tendency has to be reassessed with each new combination of involved surfaces, geometry, actuation forces and liquids.
Due to the poor predictability of valve sticking, a production method has to be found to avoid it. As the process might also change the surface of the whole micropump chamber, attention has to be paid to the surface wettability, regarding bubble tolerance.
If the design balancing process does not yield a solution, but performance demands alone can be met, closed-loop flow control provides an alternative solution. Indirect and direct flow sensing are the basis for closed-loop flow control. Accurate indirect flow control can only be employed if the expected disturbance values and their range of variations are well known. Furthermore, it is only beneficial, if the used sensing

technology and its integration is much easier and cheaper than using direct flow sensing. Otherwise, direct electrically readable microfluidic flow sensing technologies provide more information and safety for closed-loop flow control. While the control modes 'fully finished pulsatile flow' and 'continuous flow' can be measured and controlled well with current sensing technologies, 'unfinished pulsatile flow' still features unknown accuracy. Sensing technologies should be investigated and developed towards measuring high flow changing gradients accurately. The thermal anemometer currently seems to provide the best trade-off between measuring accuracy, sensitivity, robustness, miniaturization and flow resistance. Combinations of different sensing technologies, like thermal time-of-flight and calorimeters have the potential to increase measurement accuracy over a wider flow range.

The proposed deployment of functional components are important for a reliable operation of dosing systems. They display fluidic elements that can be abstracted as networks of fluidic inertances, resistances and capacitances. The influence of these networks on the micropump system performance is often secondary, but can be calculated by integrating them into the models. However, besides the influence on the system, many components, like degassers, bubble removers, flow sensors, flow capillaries and interconnection systems, are often not yet in a desired development state. Often they cannot provide the required size, reliability or usability. While small degassing chambers are commercially available, they require an additional vacuum supply, which makes the system non-portable and a micropump dosing platform would profit immensely from a miniaturized and autonomous degasser. Passive bubble remover need improvements regarding long-term stability and the ability to filter even small bubbles at a low pressure drop. In general, little results in standardization of microfluidic components and systems have yet been achieved, but first approaches are visible.

System integration aspects of microfluidic systems spread over a huge spectrum, from electronic circuits, sensor integration, pulsatility damping, fluidic connections, hermeticity to free-flow protection. For these challenges, different semiconductor fabrication processes, micro machining, adhesion techniques as well as layer deposition need to be implemented and appropriate testing methods introduced. Besides the main goal of miniaturization, reliability and cheap producibility are the important requirements. System integration technologies and general system design has to be consistent with feasible production technologies. The fabrication of single components and their assembly to systems reveal great challenges. Critical system parameters need to be manufactured accurately with little deviations or post-processing calibrations methods need to be established for compensation. Standardized processes should be chosen and the automation of the whole production needs to be enhanced.

Due to complex products and expensive manufacturing, the development times of microsystems are often long and feature great costs. On the other hand they often provide the opportunity of cheap mass production due to little material demands and batch processing. Therefore, the first application of a new technology is often the most challenging one, because development and industrialization require large investments. That limits the range of first applications to high value, high volume or low technical demands. Thus, before a broad micropump dosing platform can be established, the focus should lie on few potential entry applications that comply with these conditions. After this step, the platform can be expanded with additional components and other applications can be targeted more easily. The development will then probably go towards more reliable systems, smaller sizes at similar performance and more intelligent functions. Thus, cognitive systems that autonomously calculate decisions based on sensor data can be realized for improved flow influence prediction, automatic flow rate adaption, failure and maintenance prediction as well as automatic transmission of relevant information to the user.

A Measurement equipment

The variety of measurements required a large number of equipment, summarized in Table A.1. There, the equipment type, the manufacturer model and where applicable the range and accuracy are denoted. The equipment is segmented into general equipment, sensor technologies and devices for environmental control. The measurement methods of how the equipment is used is described in the individual sections under 'Methods'.

Equipment type	Manufacturer model	Range	Accuracy
General equipment			
Frequency generator	Agilent 33120A		
High voltage amplifier	Piezomechanik SVR 500		
Analog readout device	NI I/O-Box 6211		
Sensor technologies			
Differential pressure based (DPB) flow sensor (lq)	Fraunhofer EMFT	section 5.2	
Thermal calorimeter flow sensor (lq)	Sensirion LPG10-0500	0.24-120 $\frac{\mu l}{min}$	±5 %MV‖±0.2 %FS
Thermal calorimeter flow sensor (lq)	Bronkhorst µ-Flow L01	6.6-333 $\frac{\mu l}{min}$	±2 %FS
Coriolis mass flow meter (lq) + temperature & density sensors	Bronkhorst miniCORI-Flow M12	1.6-500 $\frac{\mu l}{min}$	±0.2 %MV
Gravimetric micro scale (lq)	Sartorius 225S	8.2 mg-220 g	±0.1 mg
Thermal calorimeter flow sensor (g)	Bronkhorst EL-Flow F-100C	0.014-0.7 $\frac{ml}{min}$	±0.5 %MV±0.7 FS
Displacement measurement	FRT Profilometer 300 µm	0-300 µm	±0.1 µm
Temperature measurement (lq/g)	testo 175 T3 datalogger + T-type sensors	-200|1000 °C	±0.5 °C
Pressure sensors	SensorTechnics CTE8000	0-100 kPa	±1 kPa
Pressure sensors	Honeywell 26PCCFA6D	±15 psi = 103 kPa	±1 kPa
Environmental control			
Pressure controller	WIKA Mensor CPC3000	-0.5|2 kPa	0.1 Pa
Pressure controller	DRUCK DPI510	0-10 kPa	1 Pa
Temperature & humidity control in climate chamber	ThermoTEC ESPEC Platinous J	-40|100 °C 20-98 %r.F.	

Table A.1: Measurement equipment with type, model, range and sensitivity.

The two most common sensors for average flow rate measurements are the Coriolis mass flow meter and the gravimetric scale. The in-line Coriolis sensor provides very good accuracy and an unmatched range (Figure A.1), but features a temperature dependent high pressure drop (Figure A.2), which has to be accounted for. The scale is a general flow sensing alternative for special liquids. Usually in-line sensors are only calibrated for very few liquids, including DI water. In addition, a contamination of the in-line flow sensors with particles, proteins or critical fluids can be avoided with a scale. Here, simply the collecting container has to be exchanged. The scale can provide high flow accuracy for long measurement times (Figure A.3). But, evaporation is a critical influence, that can be reduced with an evaporation trap for settling times of >10min (Figure A.4, measurement done by S. Kibler). Overall, the long setup and measurement times leave this sensing type effortful and unpractical and should only be employed if no alternative sensor can be used.

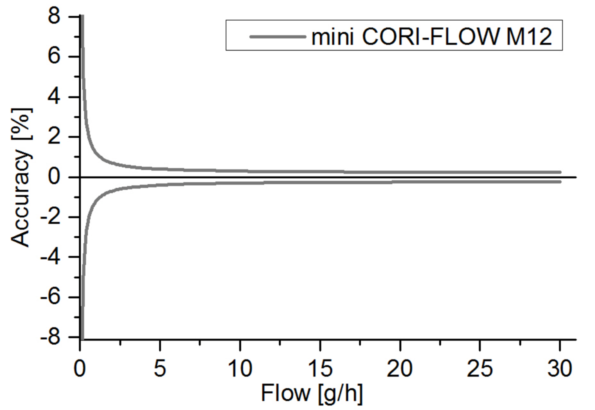

Figure A.1: Flow dependent accuracy of Coriolis mass flow meter.

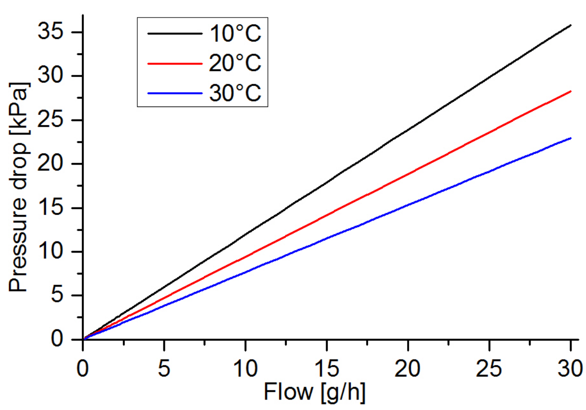

Figure A.2: Temperature and flow dependent pressure drop of Coriolis mass flow meter.

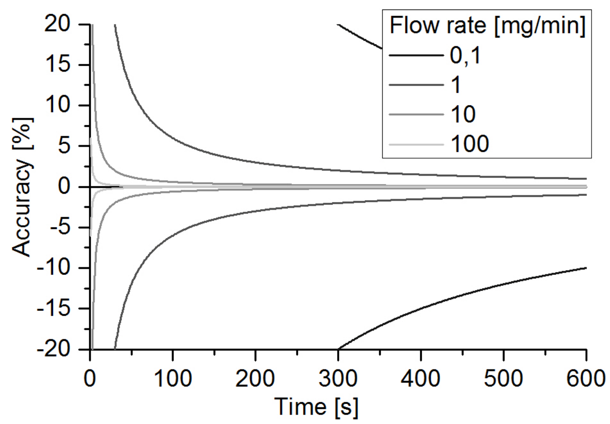

Figure A.3: Time dependent accuracy of gravimetric micro scale.

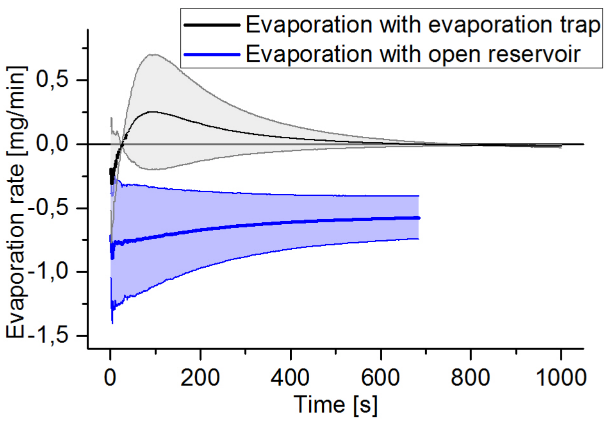

Figure A.4: Time dependent influence of evaporation with open reservoir and evaporation trap, three measurements each, accuracy band describes the standard deviation [measurement done by S. Kibler].

List of Publications

[i] C. Jenke, S. Kager, M. Richter, and C. Kutter, "Flow rate influencing effects of micropumps," *Sensors Actuators A Phys.* (2018), https://doi.org/10.1016/j.sna.2018.04.025.

[ii] C. Jenke, J. P. Rubio, S. Kibler, J. Häfner, M. Richter, and C. Kutter, "The Combination of Micro Diaphragm Pumps and Flow Sensors for Single Stroke Based Liquid Flow Control," *sensors*, vol. 17, no. 755, pp. 1–19, 2017, https://doi.org/10.3390/s17040755.

[iii] M. Richter, C. Jenke, S. Röhl, C. Kutter, Fraunhofer Society for the Advancement of Applied Research, „Mobile Device For Determining A Component In Ambient Air", Patent application, 2017.

[iv] C. W. Jenke, T. Muster, M. Richter, and C. Kutter, "Particle Tolerance of micro diaphragm pumps with low chamber heights and passive flap valves," in Proc. *MikroSystemTechnik Kongress '15*, Karlsruhe, 2015, p. 4.

[v] C. Jenke, M. Köhn, M. Wackerle, C. Kutter, and M. Richter, "Dynamic Behavior of a Piezoelectric Micropump Actuator," in Proc. *2nd Int. Conf. Micro Fluid. Handl. Syst.*, Freiburg, 2014, pp. 61–64.

[vi] C. Jenke, S. Kibler, Y. Gao, A. Hollot, T. Neuhann, B. Kirchhof, B. Montag, and M. Geiger, "Optimization of a Piezoelectric Micropump Actuator for Medical Application in Glaucoma and Phthisis Therapy," in Proc. *14th Int. Conf. New Actuators*, Bremen, Germany, 2014, pp. 165–168.

List of Symbols

$\alpha[T]$	thermal expansion coefficient
α_f	flow profile based flow coefficient
$\ddot{z}$	second derivative of deformation in z-direction
$\ddot{z}_{AF}$	second derivative of CMM-model displacement in z-direction
δ_E	big signal square correction factor
$\dot{z}$	first derivative of deformation in z-direction
$\dot{z}_{AF}$	first derivative of CMM-model displacement in z-direction
η_{ef}	electric-fluidic conversion efficiency
η_{eV}	electric-volumetric conversion efficiency
η_{valve}	valve redirection efficiency
$\hat{z}$	normalized eigenvector
$\hat{z}_i$	SMM-model normalized eigenvectors
κ	isentropic exponent
λ	general eigenvalue
$\lambda_{1,2}$	eigenvalues of CMM-model
μ	dynamic viscosity
$\mu_0[T]$	part of pure temperature dependence of dynamic viscosity
$\mu_1[T,\rho]$	part of temperature and density dependence of dynamic viscosity
μ_{disp}	reduction factor of static to dynamic displacement per stroke
ν	poisson's ratio
ω_0	angular frequency
ρ	density
ρ_{PZT}	density of PZT ceramic
$\rho_{silicon}$	density of silicon
$\rho_{silicon}$	density of water
σ	tensile stresses in radial direction

σ_{12}	surface energy between liquid and gas
$\sum acc_{sensor}$	sum of sensor accuracy influences
$\sum V_{losses}$	sum of valve efficiency losses
θ	wetting angle between solid and liquid
$\triangle L$	absolute length difference
$\triangle p_{bubble}$	bubble point of single pore
$\triangle T$	absolute temperature difference
ε_0	vacuum permittivity
ε_r	material permittivity
A	general constant
a, b, c, d	SMM-model eigenvalue solutions
$A_{1,2}$	CMM-model constants
$A_{contact}$	valve contact area
A_d	onesided circular surface area of the diaphragm
A_e	electrode area
A_{flow}	valve cross sectional area of flow
A_o	orifice area
A_{pa}	pressure application area
A_p	onesided circular surface area of piezo
$acc_{total,adjustment}$	total accuracy of adjustment for next pump cycles
$acc_{total,dosing}$	total dosing accuracy with probability calculation
C	capacitance of a capacitor
C_E	volumetric-electrical coupling coefficient
C_{flap}	fluidic capacitance of flap valve
c_L	isothermal compressibility
C_p	fluidic capacitance
c_v	volumetric concentration of particles in a fluid
D	damping factor matrix of SMM-model
d_{AF}	damping factor of CMM-model

d_{amp}	CMM-model damping factor amplitude
d_A	internal actuator damping factor
d_{exp}	CMM-model damping factor exponent
d_e	electrode distance of plate condensator
d_F	fluidic resistive damping factor
D_L	Lehr's damping ratio
d_{shift}	CMM-model damping factor shift
E	Young's modulus
e	Euler's number
E_{neg}	negative electric field strength
E_{pos}	positive electric field strength
E_z	electric field in z-direction
f	frequency
f, g, h, j	SMM-model normalized eigenvector elements
f_f	filtering factor
f_H	Hill fit function
$f_{max,dyn}$	maximum driving frequency for the sensor to get back to zero within one full cycle
$f_{max,static}$	maximum driving frequency to reach fully finished flow pulses in each mode (pump and supply)
F_{max}	initial maximum force
F_{open}	valve opening force
G_i	SMM-model constants
h	height
H_i	experimental coefficient of dynamic viscosity dependence
h_{pch}	fabricated pump chamber height
I_y	axial area moment of inertia, bending around y-axes
K	spring constant matrix of SMM-model
k_{AF}	spring constant between actuator diaphragm and liquid
k_A	spring constant of actuator

L_0	initial length
l_c	channel length
l_f	valve flap length
l_i	inlet length
l_{pore}	length of filter pores
L_{tube}	tube length
M	masses matrix of SMM
M	torque
m_{AF}	sum of actuator and liquid masses
m_A	mass of actuator
M_{coeff}	SMM-model general solution coefficients matrix
m_F	mass of fluid
n	Hill fit function exponent
N_{pore}	number of filter pores
$N_{strokes}$	number of strokes
p	pressure
p_{in}	inlet pressure
$p_{max,air}$	maximum achievable excess pressure, relative to ambient pressure
p_{max}	maximum pressure ability
$p_{min,air}$	maximum suction pressure relative to ambient pressure = minimum absolute air pressure
p_{out}	outlet pressure
$p_{v,setup}$	pressure difference at single valve measurement setup
p_w	working pressure
$prec_{sensor}$	sensor precision with probability distribution
Q	flow rate
q	flow
q_{eff}	effective flow
Q_{max}	maximum achievable flow rate
$q_{v,setup}$	measured flow at single valve measurement setup

q_v	effective flow through valve
R_d	diaphragm radius
$R_{fl,blocked}$	fluidic resistance at a blocked valve
R_{fl}	fluidic resistance
R_{pore}	filter pore radius
R_p	piezo radius
$R_{ref,setup}$	fluidic resistance of measurement setup
$r_{sticking}$	sticking resistance ratio
r_{tube}	inner tube radius
$R_{v,fw}$	static resistance of valve in forward direction
$R_{v,rv}$	static resistance of valve in reverse direction
T	temperature
t	time
$t_{capacitive-delay}$	time for the flow at the sensor to get back to zero
t_{clog}	time till clogging limit reached
$t_{closure}$	time after mode switching till flap closes the valve
$t_{disp,dyn}$	time for the actuator displacement to finish the flow pulse
$t_{disp,static}$	time to reach fully finished flow pulses
T_d	diaphragm thickness
t_f	valve flap thickness
t_{p1}	pump mode starting time
t_{p2}	pump mode end time
$t_{processing}$	required time to process the flow sensor data and calculating the next cycle voltage levels
T_p	piezo thickness
t_{s1}	supply mode starting time
t_{s2}	supply mode end time
$t_{sensor-velocity}$	time for the sensor to reach the correct signal after a flow step
U	voltage
U_n	negative voltage level

U_p	positive voltage level
$V_{dead,chamber}$	dead volume of valve chamber
$V_{dead,valves}$	dead volume of valve in pump chamber direction
V_{disp}	displacement volume
v_d	stroke volume per center displacement
V_{end}	pump internal volume at actuator end position
$V_{expanded}$	SMM-model affected liquid volume at pressure expansion
$V^{(1)\,in}_{flap,cap}$	reactive valve volume loss through inflow at outlet in phase 1
$V^{(1)\,out}_{flap,cap}$	reactive valve volume loss through outflow at inlet in phase 1
$V_{flow,in}$	actually flown volume into the pump
$V_{flow,out}$	actually flown volume out of the pump
V_{flow}	actually flown volume across pump boundary
$V_{in,inlet}$	inflow through pump inlet
$V_{in,outlet}$	inflow through pump outlet
$V_{out,intlet}$	outflow through pump inlet
$V_{out,outlet}$	outflow through pump outlet
$V^{(1)\,in}_{phaseshift}$	phase shift leakage loss through inflow at outlet in phase 1
$V^{(1)\,out}_{phaseshift}$	phase shift leakage loss through outflow at inlet in phase 1
V_p	volume of piezo ceramic
$V^{(2)\,in}_{R,fl}$	static resistance leakage loss through inflow at outlet in phase 2
$V^{(2)\,out}_{R,fl}$	static resistance leakage loss through outflow at inlet in phase 2
V_{start}	pump internal volume at actuator starting position
$V_{stroke,dyn}$	dynamic stroke volume
$V_{stroke,static}$	static stroke volume
V_{stroke}	stroke volume = displacement volume per cycle (assuming pump mode = supply mode)
W_C	energy of capacitor
w_c	channel width
W_f	fluidic work
w_f	valve flap width

w_i	square valve inlet width
w_s	valve sealing lip width
x_1	inlet beginning position
x_2	inlet end position
z_0	initial displacement at starting position
z_{AF}	center diaphragm displacement of CMM-model in z-direction
z_A	actuator displacement in z-direction
z_{creep}	creep actuator displacement due to the piezo
z_c	channel height
z_F	fluid movement of SMM-model in z-direction
$z_{linecenter}$	line center displacement in z-direction
z_p	pump mode displacement
z_{stroke}	displacement of one mode stroke
z_s	supply mode displacement

List of Figures

List of Tables

Bibliography

[1] N.-T. Nguyen and S. T. Wereley, *Fundamentals and Applications of Microfluidics.* Boston - London: Artech House, 2002.

[2] D. J. Laser and J. G. Santiago, "A review of micropumps," *J. Micromechanics Microengineering*, vol. 14, no. 6, pp. R35–R64, 2004.

[3] A. Nisar, N. Afzulpurkar, B. Mahaisavariya, and A. Tuantranont, "MEMS-based micropumps in drug delivery and biomedical applications," *Sensors Actuators B Chem.*, vol. 130, no. 2, pp. 917–942, 2008.

[4] Yole Dévelopment (B. Roussel, S. Clerc), "From Technologies to Market, Microfluidic Applications 2015," Tech. Rep., 2015.

[5] D. Maillefer, H. van Lintel, G. Rey-Memet, and R. Hirschi, "A HIGH-PERFORMANCE SILICON MICROPUMP FOR AN IMPLANTABLE DRUG DELIVERY SYSTEM," in *Proc. Twelfth IEEE Int. Conf. Micro Electro Mech. Syst. (MEMS '99)*, Orlando, FL, USA, 1999, pp. 541–546.

[6] R. Yang, M. Zhang, and T.-J. Tarn, "Dynamic Modeling and Control of a Micro-needle Integrated Piezoelectric Micro-pump for Diabetes Care," in *2006 Sixth IEEE Conf. Nanotechnol.*, Cincinnati, OH, USA, 2006, pp. 146–149.

[7] G. Liu, C. Shen, Z. Yang, X. Cai, and H. Zhang, "A disposable piezoelectric micropump with high performance for closed-loop insulin therapy system," *Sensors Actuators A Phys.*, vol. 163, no. 1, pp. 291–296, 2010. [Online]. Available: http://dx.doi.org/10.1016/j.sna.2010.06.030

[8] M. Richter, M. Wackerle, S. Kibler, M. Biehl, O. Zeiter, J. Nuffer, and R. Halter, "Miniaturized drug delivery system TUDOS with accurate metering of microliter volumes," in *Proc. AMA Conf. 2013*, Nürnberg, Germany, 2013, pp. 420–425.

[9] W. L. Rohr, A. J. Dextradeur, and D. D. Konieczynski, "Closed-loop drug delivery system," Patent US 7108680, 6 Mar., 2002.

[10] A. Doll, M. Heinrichs, F. Goldschmidtboeing, H. Schrag, U. T. Hopt, and P. Woias, "A high performance bidirectional micropump for a novel artificial sphincter system," *Sensors Actuators A Phys.*, vol. 130-131, pp. 445–453, 2006.

[11] C. Jenke, S. Kibler, Y. Gao, A. Hollot, T. Neuhann, B. Kirchhof, B. Montag, and M. Geiger, "Optimization of a Piezoelectric Micropump Actuator for Medical Application in Glaucoma and Phthisis Therapy," in *Proc. 14th Int. Conf. New Actuators*, Bremen, Germany, 2014, pp. 165–168.

[12] P.-A. Auroux, D. Iossifidis, D. R. Reyes, and A. Manz, "Micro Total Analysis Systems. 2 . Analytical Standard Operations and Applications," *Anal. Chem.*, vol. 74, pp. 2637–2652, 2002.

[13] D. R. Reyes, D. Iossifidis, P.-a. Auroux, and A. Manz, "Micro Total Analysis Systems. 1. Introduction, Theory, and Technology," in *Anal. Chem.*, 2002, vol. 74, pp. 2623–2636.

[14] A. T. Woolley, D. Hadley, P. Landre, A. J. DeMello, R. A. Mathies, and M. A. Northrup, "Functional Integration of PCR Amplification and Capillary Electrophoresis in a Microfabricated DNA Analysis Device electrophoresis (CE) chips have been successfully coupled," *Anal. Chem.*, vol. 68, pp. 4081–4086, 1996.

[15] J. Khandurina, T. E. McKnight, S. C. Jacobson, L. C. Waters, R. S. Foote, and J. M. Ramsey, "Integrated System for Rapid PCR-Based DNA Analysis in Microfluidic Devices," *Anal. Chem.*, vol. 72, pp. 2995–3000, 2017.

[16] B. H. van der Schoot, S. Jeanneret, A. van den Berg, and N. F. de Rooij, "A silicon integrated miniature chemical analysis system," *Sensors Actuators B Chem.*, vol. 6, pp. 57–60, 1992.

[17] D. Mark, S. Haeberle, G. Roth, F. Von Stetten, and R. Zengerle, *Microfluidic Lab-on-a-Chip Platforms: Requirements, Characteristics and Applications.* Dordrecht: Springer Netherlands, 2010, pp. 305–376. [Online]. Available: https://doi.org/10.1007/978-90-481-9029-4{_}17

[18] T.-h. Wang and D. Ph, "From the Guest Editors Transforming Microfluidics into Laboratory Automation," *J. Assoc. Lab. Autom.*, vol. 15, no. 3, pp. A15–A16, 2010. [Online]. Available: http://dx.doi.org/10.1016/j.jala.2010.03.002

[19] K. S. Elvira, X. C. i. Solvas, R. C. R. Wootton, and A. J. DeMello, "The past, present and potential for microfluidic reactor technology in chemical synthesis," *Nat. Chem.*, vol. 5, pp. 905–915, 2013.

[20] E. Kjeang, N. Djilali, and D. Sinton, "Microfluidic fuel cells : A review," *J. Power Sources*, vol. 186, pp. 353–369, 2009.

[21] T. Zhang and Q.-m. Wang, "Performance of miniaturized direct methanol fuel cell (DMFC) devices using micropump for fuel delivery," *J. Power Sources*, vol. 158, pp. 169–176, 2006.

[22] V. Singhal and S. V. Garimella, "Induction electrohydrodynamics micropump for high heat flux cooling," *Sensors Actuators A Phys.*, vol. 134, pp. 650–659, 2007.

[23] H. K. Ma, B. R. Hou, H. Y. Wu, C. Y. Lin, J. J. Gao, M. C. Kou, and C. M. Co, "Development and application of a diaphragm micro-pump with piezoelectric device," *Microsyst. Technol.*, vol. 14, pp. 1001–1007, 2007.

[24] R. S. Shawgo, A. C. R. Grayson, Y. Li, and M. J. Cima, "BioMEMS for drug delivery," *Curr. Opin. Solid State Mater. Sci.*, vol. 6, pp. 329–334, 2002.

[25] E. N. Wang, L. Zhang, L. Jiang, J.-M. Koo, J. G. Maveety, E. A. Sanchez, K. E. Goodson, and T. W. Kenny, "Micromachined Jets for Liquid Impingement Cooling of VLSI Chips," *J. Microelectromechanical Syst.*, vol. 13, no. 5, pp. 833–842, 2004.

[26] L. Zhang, J.-m. Koo, L. Jiang, M. Asheghi, K. E. Goodson, A. Member, J. G. Santiago, and T. W. Kenny, "Measurements and Modeling of Two-Phase Flow in Microchannels With Nearly Constant Heat Flux Boundary Conditions," *J. Microelectromechanical Syst.*, vol. 11, no. 1, pp. 12–19, 2002.

[27] B. D. Iverson and S. V. Garimella, "Recent advances in microscale pumping technologies: A review and evaluation," *Microfluid. Nanofluidics*, vol. 5, pp. 145–174, 2008.

[28] M. Richter, M. Wackerle, and S. Kibler, "TECHNOLOGY AND APPLICATIONS OF MICRODOSING SYSTEMS," in *Proc. of MIDEM*, vol. 41, no. 4, Ljubljana, 2011, pp. 253–256.

[29] N.-T. Nguyen, X. Huang, and T. K. Chuan, "MEMS-Micropump: A Review," *Trans. ASME*, vol. 124, pp. 384–392, 2002.

[30] J. Smits, "Micropompe Piézoélectrique," Patent NL 19830002860, 15 Aug, 1984.

[31] J. G. Smits, "Piezoelectric Micropump with Three Valves Working Peristaltically," *Sensors and Actuators*, vol. A21-A23, pp. 203–206, 1990.

[32] H. T. G. van Lintel, F. van de Pol, and S. Bouwstra, "A Piezoelectric Micropump Based On Micromachining Of Silicon," *Sensors and Actuators*, vol. 15, pp. 153–167, 1988.

[33] R. Zengerle and M. Richter, "Simulation of microfluidic systems," *J. Micromechanics Microengineering*, vol. 4, pp. 192–204, 1994.

[34] M. Herz, D. Horsch, G. Wachutka, T. C. Lueth, and M. Richter, "Design of ideal circular bending actuators for high performance micropumps," *Sensors Actuators A Phys.*, vol. 163, pp. 231–239, 2010. [Online]. Available: http://dx.doi.org/10.1016/j.sna.2010.05.018

[35] M. Richter, R. Linnemann, and P. Woias, "Robust design of gas and liquid micropumps," *Sensors Actuators A Phys.*, vol. 68, pp. 480–486, 1998.

[36] H. van Lintel, "Micropump Having A Constant Output," Patent US 5085562, 4 Apr., 1990.

[37] H. V. Lintel, P. Poscio, and F. Nefttel, "PIEZOELECTRIC MICROPUMP HAVING ACTUATION ELECTRODES AND STOPPER MEMBERS," 1998.

[38] P. Woias, "Micropumps - past, progress and future prospects," *Sensors Actuators B Chem.*, vol. 105, pp. 28–38, 2005.

[39] T. Higuchi, K. Suzumori, and S. Tadokoro, *Next-Generation Actuators Leading Breackthroughs*. London: Springer, 2010.

[40] G. Biancuzzi, T. Lemke, P. Woias, O. Ruthmann, H. J. Schrag, B. Vodermayer, T. Schmid, and F. Goldschmidtboeing, "An Efficient Low-voltage Micropump For An Implantable Sphincter System," pp. 2360–2363, 2009.

[41] J. Judy, T. Tamagawa, and D. Polla, "Surface-machined micromechanical membrane pump," in *Proc. IEEE Micro Electro Mech. Syst. '91*, 1991, pp. 182–186.

[42] R. Zengerle, A. Richter, and H. Sandmaier, "A Micro Membrane Pump With Electrostatic Actuation," in *Proc. Micro Electro Mech. Syst. '92*, Travemünde, Germany, 1992, pp. 19–24.

[43] F. C. M. van de Pol, H. T. G. van Lintel, M. Elwenspoek, and J. H. J. Fluitman, "A Thermopneumatic Micropump Based on Micro-engineering Techniques," *Sensors and Actuators*, vol. A21-A23, pp. 198–202, 1990.

[44] W. Y. Sim, H. J. Yoon, O. C. Jeong, and S. S. Yang, "A phase change type of micropump with aluminium flap valves," *J. Micromechanics Microengineering*, vol. 13, pp. 286–294, 2003.

[45] S. Böhm, W. Olthuis, and P. Bergveld, "A plastic micropump constructed with conventional techniques and materials," *Sensors Actuators A Phys.*, vol. 77, pp. 223–228, 1999.

[46] W. Benard, H. Kahn, A. Heuer, and M. Huff, "A titanium-nickel shape-memory alloy actuated micropump," in *Proc. Int. Solid State Sensors Actuators Conf. (Transducers '97)*, 1997, pp. 361–364.

[47] C. Zhan, T. Lo, L. Liu, and T. Peihsin, "A silicon membrane micropump with integrated bimetallic actuator," *Chinese J. Electron.*, vol. 5, no. 2, pp. 33–35, 1996.

[48] S. Guo, T. Fukuda, K. Kosuge, F. Arai, K. Oguro, and M. Negoro, "Micro catheter system with active guide wire," in *Proc. IEEE Int. Conf. Robot. Autom.*, 1995, pp. 79–84.

[49] K. W. Oh and C. H. Ahn, "A review of microvalves," *J. Micromechanics Microengineering*, vol. 16, pp. R13–R39, 2006.

[50] S. Shoji and M. Esashi, "Microflow devices and systems," *J. Micromechanics Microengineering*, vol. 4, pp. 157–171, 1994.

[51] A. K. Au, H. Lai, B. R. Utela, and A. Folch, "Microvalves and Micropumps for BioMEMS," *Micromachines 2011*, vol. 2, pp. 179–220, 2011.

[52] M. Richter, M. Wackerle, and M. Herz, "Method for Manufacturing a Bending Transducer, a Micro Pump and a Micro Valve, Micro Pump and Micro Valve," Patent WO 2011/107162, 5 Mar., 2010.

[53] S. Hansen, "Membrane Pump With Stretchable Pump Membrane," Patent US 6948918 B2, 25 Sep., 2003.

[54] R. Zengerle, J. Ulrich, S. Kluge, M. Richter, and A. Richter, "A bidirectional silicon micropump," *Sensors Actuators A Phys.*, vol. 50, pp. 81–86, 1995.

[55] W. V. D. Wiingaart, H. Anderson, P. Enoksson, K. Noren, and G. Stemme, "The First Self-Priming And Bi-Directional Valve-less Diffuser Micropump For Both Liquid And Gas," in *Thirteen. Annu. Int. Conf. Micro Electro Mech. Syst.*, 2000, pp. 674–679.

[56] M. A. Saaman, "Micropump avoiding microcavitation," Patent EP 0568902, 27 Apr., 1993.

[57] N.-c. Tsai and C.-y. Sue, "Review of MEMS-based drug delivery and dosing systems," *Sensors Actuators A Phys.*, vol. 134, pp. 555–564, 2007.

[58] J. Kan, K. Tang, G. Liu, G. Zhu, and C. Shao, "Development of serial-connection piezoelectric pumps," *Sensors Actuators A Phys.*, vol. 144, pp. 321–327, 2008.

[59] A. Ullmann, "The piezoelectric valve-less pump-performance," *Sensors Actuators A Phys.*, vol. 69, pp. 97–105, 1998.

[60] B. H. van der Schoot, S. Jeanneret, A. van den Berg, and N. F. de Rooij, "Modular setup for a miniaturized chemical analysis system," *Sensors Actuators B Chem.*, vol. 15-16, pp. 211–213, 1993.

[61] C. Zhang, D. Xing, and Y. Li, "Micropumps, microvalves, and micromixers within PCR microfluidic chips : Advances and trends," *Biotechnol. Adv.*, vol. 25, pp. 483–514, 2007.

[62] R. H. Liu, J. Yang, R. Lenigk, J. Bonanno, and P. Grodzinski, "Self-Contained, Fully Integrated Biochip for Sample Preparation, Polymerase Chain Reaction Amplification, and DNA Microarray Detection," *Anal. Chem.*, vol. 76, pp. 1824–1831, 2004.

[63] V. Gass, B. H. van der Schoot, S. Jeanneret, and N. F. de Rooij, "Integrated flow-regulated silicon micropump," *Sensors Actuators A Phys.*, vol. 43, pp. 335–338, 1994.

[64] N. T. Nguyen, S. Schubert, S. Richter, and W. Dötzel, "Hybrid-assembled micro dosing system using silicon-based micropump / valve and mass flow sensor," *Sensors Actuators A Phys.*, vol. 69, pp. 85–91, 1998.

[65] Q. Cui, C. Liu, and X. F. Zha, "Study on a piezoelectric micropump for the controlled drug delivery system," *Microfluid. Nanofluidics*, vol. 3, pp. 377–390, 2007.

[66] M. Herz, "Optimierung der Förderrate einer piezoelektrischen Hochleistungs-Mikropumpe," Ph.D. thesis, Technical University Munich, Munich, Germany, 2011.

[67] D. D. Meng and C.-j. Kim, "Micropumping of liquid by directional growth and selective venting of gas bubbles," *Lab Chip*, vol. 8, pp. 958–968, 2008.

[68] K. Hosokawa, T. Fujii, and I. Endo, "Handling of picoliter liquid samples in a poly(dimethylsiloxane)-based microfluidic device," *Anal. Chem.*, vol. 71, pp. 4781–4785, 1999.

[69] Z. Yang, S. Matsumoto, and R. Maeda, "A prototype of ultrasonic micro-degassing device for portable dialysis system," *Sensors Actuators A Phys.*, vol. 95, pp. 274–280, 2002.

[70] D. D. Meng, J. Kim, and C. J. Kim, "A degassing plate with hydrophobic bubble capture and distributed venting for microfluidic devices," *J. Micromechanics Microengineering*, vol. 16, pp. 419–424, 2006.

[71] M. W. Jornitz, "Filter Construction and Design," in *Adv. Biochem. Eng.*, 2006, vol. 98, pp. 105–123.

[72] R. E. Madsen, "Filter Validation," in *Adv. Biochem. Eng.*, 2006, vol. 98, pp. 125–141.

[73] M. Alberti, L. Meixner, A. Rückerl, M. Eder, H. Endres, and K. Bock, "'Sensor-filter' - Intelligent micro filter system in foil technology," *Sensors Actuators A Phys.*, pp. 1–7, 2013. [Online]. Available: http://dx.doi.org/10.1016/j.sna.2013.01.015

[74] R. Meyknecht, "Miropump And Method For The Production Thereof," Patent EP 1700036, 20 Dec., 2004.

[75] V. Lintel and Y. S. Leungki, "Micromachined Filter For A Micropump," Patent US 5997263 A, 10 Feb., 1997.

[76] P. C. Lord, C. K. Nason, D. Y. Yap, S. D. Das, and R. J. Lebel, "Implantable Medication Delivery Device," Patent US 2006/0122578, 20 May, 2003.

[77] M. Richter and J. Krukow, "Pump Arrangement Comprising a Safety Valve," Patent US 2010/0290935, 23 Nov., 2007.

[78] H. Gensler, R. Sheybani, P.-y. Li, R. L. Mann, and E. Meng, "An implantable MEMS micropump system for drug delivery in small animals," *Biomed Microdevices*, vol. 14, pp. 483–496, 2012.

[79] S. Z. Razzacki, P. K. Thwar, M. Yang, V. M. Ugaz, and M. A. Burns, "Integrated microsystems for controlled drug delivery," *Adv. Drug Deliv. Rev.*, vol. 56, pp. 185–198, 2004.

[80] V. K. Sharma, "The Future Is Wireless: Advances in Wireless Diagnostic and Therapeutic Technologies in Gastroenterology," *Gastroenterology*, vol. 137, no. 2, pp. 434–439, 2009. [Online]. Available: http://dx.doi.org/10.1053/j.gastro.2009.06.029

[81] T. S. Lammerink, M. Elwenspoek, and J. H. J. Fluitman, "Integrated micro-liquid dosing system," in *Proc. IEEE Micro Electro Mech. Syst. '93*, Florida, FL, US, 1993, pp. 254–259.

[82] R. Zengerle, M. Leitner, S. Kluge, and A. Richter, "Carbon Dioxide Priming of Micro Liquid Systems," in *Proc. IEEE Micro Electro Mech. Syst. '95*, Amsterdam, The Netherlands, 1995, pp. 340–343.

[83] S. A. N. Prasad, Q. Gallas, S. Horowitz, B. Homeijer, B. V. Sankar, L. N. Cattafesta, and M. Sheplak, "Analytical Electroacoustic Model of a Piezoelectric Composite Circular Plate," *AIAA*, vol. 44, no. 10, 2006.

[84] S. A. N. Prasad, "Two-Port Electroacoustic Model Of A Piezoelectric Composite Circular Plate," M.S. thesis, University of Florida, FL, US, 2002.

[85] M.-h. B. Company, S. Timoshenko, and S. Woinowsky-Krieger, *Theory of Plates and Shells*. McGraw-Hill Book Company, 1897.

[86] M. Deshpande and L. Saggere, "An analytical model and working equations for static deflections of a circular multi-layered diaphragm-type piezoelectric actuator," *Sensors Actuators A Phys.*, vol. 136, pp. 673–689, 2007.

[87] C. Mo, R. Wright, W. S. Slaughter, and W. W. Clark, "Behaviour of a unimorph circular piezoelectric actuator," *SMARTMATERIALS Struct.*, vol. 15, pp. 1094–1102, 2006.

[88] M. Papila, M. Sheplak, and L. N. Cattafesta, "Optimization of clamped circular piezoelectric composite actuators," *Sensors Actuators A Phys.*, vol. 147, pp. 310–323, 2008.

[89] K. Uchino, "Materials Issues In Design And Performance Of Piezoelectric Actuators: An Overview," *Acta mater*, vol. 46, no. 11, pp. 3745–3753, 1998.

[90] J. Ulrich and R. Zengerle, "Static and dynamic flow simulation of a KOH-etched microvalve using the finite-element method," *Sensors Actuators A Phys.*, vol. 53, pp. 379–385, 1996.

[91] D. Horsch, "Untersuchung des struktur-. und fluidmechanischen Verhaltens einer piezoelektrisch angetriebenen Mikromembranpumpe," Diploma Thesis, Technical University Munich, Munich, Germany, 2009.

[92] M. Richter, "Modellierung und experimentelle Charakterisierung von Mikrofluidsystemen und deren Komponenten," Ph.D. thesis, Universität der Bundeswehr München, Munich, Germany, 1998.

[93] C. Jenke, S. Kager, M. Richter, and C. Kutter, "Flow rate influencing effects of micropumps," *Sensors Actuators A Phys.*, apr 2018. [Online]. Available: https://doi.org/10.1016/j.sna.2018.04.025

[94] F. Abhari, H. Jaafar, and N. A. Md Yunus, *A comprehensive study of micropumps technologies*, 2012, vol. 7, no. 10.

[95] F. Amirouche, Y. Zhou, and T. Johnson, "Current micropump technologies and their biomedical applications," *Microsyst. Technol.*, vol. 15, pp. 647–666, 2009.

[96] S. Kibler, L. Hassan, M. Richter, and C. Kutter, "Feedback Controlled Microdosing System for Nanoliter per Second Dosing Rates Using a Capacitive Phase Boundary Time-of-Flight Flow Sensor," in *Proc. 2nd Int. Conf. Micro Fluid. Handl. Syst.*, 2014, pp. 92–95.

[97] W. V. D. Wijngaart, H. Anderson, P. Enoksson, K. Noren, and G. Stemme, "The First Self-Priming And Bi-Directional Valve-less Diffuser Micropump For Both Liquid And Gas," in *Thirteen. Annu. Int. Conf. Micro Electro Mech. Syst.*, 2000, pp. 674–679.

[98] C. Jenke, J. Pallejà Rubio, S. Kibler, J. Häfner, M. Richter, and C. Kutter, "The Combination of Micro Diaphragm Pumps and Flow Sensors for Single Stroke Based Liquid Flow Control," *Sensors*, vol. 17, no. 4, p. 755, apr 2017. [Online]. Available: https://doi.org/10.3390/s17040755

[99] R. Pratap, S. Mohite, and A. K. Pandey, "Squeeze Film Effects in MEMS Devices," *J. Indian Inst. Sci.*, vol. 87, pp. 75–94, 2007.

[100] C. Jenke, M. Köhn, M. Wackerle, C. Kutter, and M. Richter, "Dynamic Behavior of a Piezoelectric Micropump Actuator," in *Proc. 2nd Int. Conf. Micro Fluid. Handl. Syst.*, Freiburg, 2014, pp. 61–64.

[101] L. T. Gomes, "Effect of damping and relaxed clamping on a new vibration theory of piezoelectric diaphragms," *Sensors Actuators A Phys.*, vol. 169, pp. 12–17, 2011. [Online]. Available: http://dx.doi.org/10.1016/j.sna.2011.04.005

[102] X. He, W. Xu, N. Lin, B. B. Uzoejinwa, and Z. Deng, "Dynamics modeling and vibration analysis of a piezoelectric diaphragm applied in valveless micropump," *J. Sound Vib.*, vol. 405, pp. 133–143, 2017. [Online]. Available: http://dx.doi.org/10.1016/j.jsv.2017.05.025

[103] T. X. Dinh and Y. Ogami, "A dynamic model of valveless micropumps with a fluid damping effect," *J. Micromechanics Microengineering*, vol. 21, no. 11, 2011.

[104] S. Singh, N. Kumar, D. George, and A. K. Sen, "Analytical modeling, simulations and experimental studies of a PZT actuated planar valveless PDMS micropump," *Sensors Actuators, A Phys.*, vol. 225, pp. 81–94, 2015. [Online]. Available: http://dx.doi.org/10.1016/j.sna.2015.02.012

[105] Physik Instrumente, "Catalogue: PI Piezoelectric actuators," [Downloaded: 13 October 2017]. [Online]. Available: https://www.piceramic.de/de/?type=5600{&}downloadUid=1389{&}downloadFileUid=1259

[106] P. H. Schweitzer and V. G. Szebehely, "Gas Evolution in Liquids and Cavitation," *J. Appl. Phys.*, vol. 21, pp. 1218–1224, 1950.

[107] C. E. Brennen, *Cavitation and Bubble Dynamics*. Cambridge University Press, 1995. [Online]. Available: https://authors.library.caltech.edu/25017/

[108] T. Gerlach and H. Wurmus, "Working principle and performance of the dynamic micropump," *Sensors Actuators A Phys.*, vol. 50, pp. 135–140, 1995.

[109] A. Olsson, P. Enoksson, G. Stemme, and E. Stemme, "An Improved Valveless Pump Fabricated Using Deep Reactive Ion Etching," in *IEEE*, 1996, pp. 479–484.

[110] K. Opitz, E. Schlücker, and O. Schade, "Cavitation in Reciprocating Positive Displacement Pumps," in *Proc. Twenty-Seventh Int. Pump Users Symp.*, Houston, Texas, US, 2011, pp. 27–33.

[111] A. Chandrasekaran and M. Packirisamy, "Experimental investigation of cavitation behavior in valveless micropumps," *J. Micromechanics Microengineering*, vol. 22, no. 125019, pp. 1–15, 2012.

[112] I. Eames, A. Azarbadegan, and M. Zangeneh, "Analytical Model of Valveless Micropumps," *J. Microelectromechanical Syst.*, vol. 18, no. 4, pp. 878–883, 2009.

[113] L. Mercury and Y. Tardy, "Negative pressure of stretched liquid water. Geochemistry of soil capillaries," *Geochim. Cosmochim. Acta*, vol. 65, no. 20, pp. 3391–3408, 2001.

[114] M. Alguero, F. Guiu, and M. J. Reece, "Degradation of PZT-4D hard piezoceramics under moderate heating," *J. Eur. Ceram. Soc.*, vol. 20, pp. 2705–2711, 2000.

[115] H. Wang and R. N. Singh, "Crack propagation in piezoelectric ceramics : Effects of applied electric fields," *J. Appl. Phys.*, vol. 81, no. 11, pp. 7471–7479, 1997.

[116] C. S. Lynch, "Fracture Of Ferroelectric And Relaxor Electro-Ceramics: Influence Of Electric Field," *Acta mater*, vol. 46, no. 2, pp. 599–608, 1998.

[117] J.-H. Koh, S.-J. Jeong, M.-S. Ha, and J.-S. Song, "Electric field induced fracture mechanism and aging of piezoelectric behavior in Pb(MgNb)O_3 - Pb(ZrTi)O_3 multilayer ceramic actuators," *Ceram. Int.*, vol. 30, pp. 1863–1867, 2004.

[118] J. Shieh, J. E. Huber, and N. A. Fleck, "Fatigue crack growth in ferroelectrics under electrical loading," *J. Eur. Ceram. Soc.*, vol. 26, pp. 95–109, 2006.

[119] M. Okayasu, K. Sato, and M. Mizuno, "Influence of domain orientation on the mechanical properties of lead zirconate titanate piezoelectric ceramics," *J. Eur. Ceram. Soc.*, vol. 31, pp. 141–150, 2011.

[120] J. Nuffer, D. C. Lupascu, and J. Ro, "Damage Evolution In Ferroelectric PZT Induced By Bipolar Electric Cycling," *Acta mater*, vol. 48, pp. 3783–3794, 2000.

[121] J. M. Calderon-Moreno and M. Popa, "Stress dependence of reversible and irreversible domain switching in PZT during cyclic loading," *Mater. Sci. Eng.*, vol. 336, pp. 124–128, 2002.

[122] H. Weitzing, G. A. Schneider, J. Steffens, M. Hammer, and M. J. Hoffmann, "Cyclic Fatigue Due to Electric Loading in Ferroelectric Ceramics," *J. Eur. Ceram. Soc.*, vol. 19, pp. 1333–1337, 1999.

[123] M. Okayasu, G. Ozeki, and M. Mizuno, "Fatigue failure characteristics of lead zirconate titanate piezoelectric ceramics," *J. Eur. Ceram. Soc.*, vol. 30, pp. 713–725, 2010.

[124] D. Wang, Y. Fotinich, and G. P. Carman, "Influence of temperature on the electromechanical and fatigue behavior of piezoelectric ceramics," *J. Appl. Phys.*, vol. 83, no. 10, pp. 5342–5350, 1998.

[125] W.-P. Tai and S.-H. Kim, "Relationship between cyclic loading and degradation of piezoelectric properties in Pb(Zr,Ti)O_3 ceramics," *Mater. Sci. Eng.*, vol. 38, pp. 182–185, 1996.

[126] D. Zheng, J. Swingler, and P. Weaver, "Current leakage and transients in ferroelectric ceramics under high humidity conditions," *Sensors Actuators A Phys.*, vol. 158, pp. 106–111, 2010.

[127] I. P. Lipscomb, P. M. Weaver, J. Swingler, and J. W. Mcbride, "The effect of relative humidity , temperature and electrical field on leakage currents in piezo-ceramic actuators under dc bias," *Sensors Actuators A Phys.*, vol. 151, pp. 179–186, 2009.

[128] C. Gobert, "Aufstellung von Qualitätskriterien für piezoelektrische getriebene Biegewandler durch Impedanzmessung Vorgehensweise," Tech. Rep., 2003.

[129] M. Wackerle and M. Richter, "IMPUM IV Final Report v1.1," Tech. Rep., 2011.

[130] A. L. Hartzell, M. G. da Silva, and H. R. Shea, *MEMS Reliability.* Springer, 2011.

[131] W. R. Ashurst, C. Carraro, R. Maboudian, and W. Frey, "Wafer level anti-stiction coatings for MEMS," *Sensors Actuators A Phys.*, vol. 104, pp. 213–221, 2003.

[132] N. Tas, T. Sonnenberg, H. Jansen, R. Legtenberg, and M. Elwenspoek, "Stiction in surface micromachining," *J. Micromechanics Microengineering*, vol. 6, pp. 385–397, 1996.

[133] K. Komvopoulos, "Surface engineering and microtribology for microeleetromechanical systems," *Wear*, vol. 200, pp. 305–327, 1996.

[134] R. Maboudian and R. T. Howe, "Critical Review : Adhesion in surface micromechanical structures," *J. Vac. Sci. Tchnology B*, vol. 15, no. 1, pp. 1–20, 1997. [Online]. Available: http://dx.doi.org/10.1116/1.589247

[135] D. Boer and T. M. Mayer, "Tribology of MEMS," *MRS Bull.*, no. April, pp. 302–304, 2001.

[136] C. H. Mastrangelo, "Adhesion-related failure mechanisms in micromechanical devices," *Tribol. Lett.*, vol. 3, pp. 223–238, 1997.

[137] Y. Yee, K. Chun, J. D. Lee, and C.-J. Kim, "Polysilicon surface-modification technique to reduce sticking of microstructures," *Sensors Actuators A Phys.*, vol. 52, pp. 145–150, 1996.

[138] W. R. Ashurst, C. Yau, C. Carraro, C. Lee, G. J. Kluth, R. T. Howe, and R. Maboudian, "Alkene based monolayer ® lms as anti-stiction coatings for polysilicon MEMS," *Sensors Actuators A Phys.*, vol. 91, pp. 239–248, 2001.

[139] M. R. Houston, R. T. Howe, and R. Maboudian, "Effect of hydrogen termination on the work of adhesion between rough polycrystalline silicon surfaces," *J. Appl. Phys.*, vol. 81, pp. 3474–3483, 1997.

[140] U. Srinivasan, M. R. Houston, R. T. Howe, and R. Maboudian, "Self-Assembled Fluorocarbon Films For Enhanced Stiction Reduction," in *Proc. Int. Conf. Solid-State Sensors Actuators (Transducers '97)*, Chicago, 1997, pp. 1399–1402.

[141] N. Askamp, "Erfassung der Einflüsse auf die Dosiergenauigkeit einer Mikromembranpumpe in der Luftpolsterpipettierung," B.S. Thesis, Hochschule München, Munich, Germany, 2010.

[142] S. Matsumoto, A. Klein, A. Schroth, and R. Maeda, "Micropump based on temperature dependence of liquid viscosity," in *Proc. SPIE 3242, Smart Electron. MEMS*, vol. 3242, 1997, pp. 364–371.

[143] C. J. Seeton, "Viscosity - temperature correlation for liquids," *Tribol. Lett.*, vol. 22, no. 1, pp. 67–78, 2006.

[144] H. Watanabe, N. Yamada, and M. Okaji, "Linear Thermal Expansion Coefficient of Silicon from 293 to 1000 K," *Int. J. Thermophys.*, vol. 25, no. 1, pp. 221–236, 2004.

[145] IAPWS: International Association for the Properties of Water and Steam, "Revised Release on the IAPS Formulation 1985 for the Viscosity of Ordinary Water Substance," [Accessed: 01 December 2017], 1997. [Online]. Available: http://www.iapws.org/relguide/visc.pdf

[146] S. Chandika, R. Asokan, and K. C. K. Vijayakumar, "Flow characteristics of the diffuser / nozzle micropump - A state space approach," *Flow Meas. Instrum.*, vol. 28, pp. 28–34, 2012. [Online]. Available: http://dx.doi.org/10.1016/j.flowmeasinst.2012.06.003

[147] DWD: German Weather Service, "Weather Records," [Accessed: 07 November 2017], Tech. Rep., 2017. [Online]. Available: https://www.dwd.de/SharedDocs/broschueren/DE/presse/wetterrekorde.pdf?{_}{_}blob=publicationFile{&}v=11

[148] C. W. Jenke, T. Muster, M. Richter, and C. Kutter, "Particle Tolerance of micro diaphragm pumps with low chamber heights and passive flap valves," in *Proc. MikroSystemTechnik Kongress '15*, Karlsruhe, 2015, p. 4.

[149] L.-S. Jang, C. J. Morris, N. R. Sharma, R. L. Bardell, and F. K. Forster, "Transport Of Particle-Laden Fluids Through Fixed-Valve Micropumps," in *Proc. 1999 ASME Int. Mech. Eng. Congr. Expo.*, Nashville, Tennessee, 1999.

[150] A. Ezkerra, L. J. Fernández, K. Mayora, and J. M. Ruano-López, "SU8 diaphragm micropump with monolithically integrated cantilever check valves," *Lab Chip*, vol. 11, pp. 3320–3325, 2011.

[151] T. Goettsche, J. Kohnle, M. Willmann, H. Ernst, S. Spieth, R. Tischler, S. Messner, R. Zengerle, and H. Sandmaier, "Novel approaches to particle tolerant valves for use in drug delivery systems," *Sensors Actuators A Phys.*, vol. 118, pp. 70–77, 2005.

[152] E. Chappel, "Microfluidic valve having improved tolerance to particles," Patent WO 2014136090, 7 Mar., 2013.

[153] M. Herz, M. Richter, and M. Sutter, "Pump having a filter arrangement," Patent WO 2010102961, 5 Mar., 2010.

[154] W. Birmili, A. Wiedensohler, J. Heintzenberg, and K. Lehmann, "Atmospheric particle number size distribution in central Europe: Statistical relations to air masses and meterorology," *J. Geophys. Res.*, vol. 106, no. D23, pp. 32 005–32 018, 2001. [Online]. Available: http://dx.doi.org/10.1029/2000JD000220

[155] W. W. Law, W.-h. Liao, and J. Huang, "Vibration control of structures with self-sensing piezoelectric actuators," *Smart Mater. Struct.*, vol. 12, pp. 720–730, 2003.

[156] E. Grasso, N. Totaro, H. Janocha, and D. Naso, "Piezoelectric self sensing actuators for high voltage excitation," *Smart Mater. Struct.*, vol. 22, no. 065018, p. 13, 2013.

[157] P. Gravesen, J. Branebjerg, and O. S. Jensen, "Microfluidics-a review," *J. Micromechanics Microengineering*, vol. 3, no. 4, pp. 168–182, 1993. [Online]. Available: http://stacks.iop.org/0960-1317/3/i=4/a=002?key=crossref.b937fbfa327ffcb4bee296d7459f34fc

[158] H. Andersson, W. V. D. Wijngaart, P. Nilsson, W. van der Wijngaart, P. Nilsson, P. Enoksson, and G. Stemme, "A valve-less diffuser micropump for microfluidic analytical systems," *Sensors Actuators B Chem.*, vol. 72, no. 3, pp. 259–265, 2001.

[159] D. C. Lupascu, A. Glazounov, and H.-j. Kleebe, "Microstructural modifications of ferroelectric lead zirconate titanate ceramics due to bipolar electric fatigue," vol. 22, pp. 2133–2142, 2002.

[160] M. Elwenspoek, T. S. J. Lammerink, R. Miyakei, and J. H. J. Fluitman, "Towards integrated microliquid handling systems," *J. Micromechanics Microengineering*, vol. 4, pp. 227–245, 1994.

[161] N.-T. Nguyen, A. H. Meng, J. Black, and R. M. White, "Integrated flow sensor for in situ measurement and control of acoustic streaming in flexural plate wave micropumps," *Sensors Actuators A Phys.*, vol. 79, pp. 115–121, 2000.

[162] O. Woitschach, C. Sosna, and W. Lang, "A New Generation of a Regulated Micropump for Medical Applications," in *Proc. Ninth IEEE Sensors Conf. (SENSORS 2010)*, Waikoloa, HI, USA, 2010, pp. 2472–2477.

[163] K. D. Patel, M. S. Bartsch, M. H. McCrink, J. S. Olsen, B. P. Mosier, and R. W. Crocker, "Electrokinetic pumping of liquid propellants for small satellite microthruster applications," *Sensors Actuators B Chem.*, vol. 132, pp. 461–470, 2008.

[164] L. Chen, Y. Liu, L. Sun, D. Qu, and J. Min, "Intelligent Control of Piezoelectric Micropump Based on MEMS Flow Sensor," in *Proc. 2010 IEEE/RSJ Int. Conf. Intell. Robot. Syst.*, Taipei, Taiwan, 2010, pp. 3055–3060.

[165] Y. Fouillet, O. Fuchs, S. Maubert, M. Cochet, F. Baleras, C. Chabrol, N. David, and R. Campagnolo, "A Silicon Micropump with on-chip Flow Meter," *Procedia Eng.*, vol. 47, pp. 314–317, 2012. [Online]. Available: http://dx.doi.org/10.1016/j.proeng.2012.09.146

[166] M. Richter, M. Wackerle, P. Woias, and B. Hillerich, "A novel flow sensor with high time resolution based on differential pressure principle," in *Proc. 12th IEEE Int. Conf. Micro Electro Mech. Syst. '99*, Orlando, FL, USA, 1999, pp. 118–123.

[167] P.-C. Huang, M.-H. Wang, M.-K. Chen, and L.-S. Jang, "Experimental analysis of time-phase-shift flow sensing based on a piezoelectric peristaltic micropump," *J. Phys. D. Appl. Phys.*, vol. 49, p. 175402, 2016. [Online]. Available: http://dx.doi.org/10.1088/0022-3727/49/17/175402

[168] M. Wang and J. Chen, "A high-precision gravity intravenous infusion rate meter using CMUT arrays," in *Proc. 2009 IEEE Int. Ultrason. Symp.*, Rome, Italy, 2009, pp. 1355–1358.

[169] J. Ni, B. Wang, S. Chang, and Q. Lin, "An integrated planar magnetic micropump," *Microelectron. Eng.*, vol. 117, pp. 35–40, 2014. [Online]. Available: http://dx.doi.org/10.1016/j.mee.2013.11.014

[170] A. T. Al-Halhouli, S. Demming, A. Dietzel, and S. Büttgenbach, "Design, Fabrication, and Characterization of a Continuous Flow Micropump System," *J. Therm. Sci. Eng. Appl.*, vol. 8, no. 021006, pp. 1–6, 2016.

[171] S. Böhm, B. Timmer, W. Olthuis, and P. Bergveld, “A closed-loop controlled electrochemically actuated micro-dosing system,” *J. Micromechanics Microengineering*, vol. 10, pp. 498–504, 2000.

[172] J. Haneveld, T. S. J. Lammerink, M. Dijkstra, H. Droogendijk, M. J. D. Boer, and R. J. Wiegerink, “Highly Sensitive Micro Coriolis Mass Flow Sensor,” in *Proc. 21th IEEE Int. Conf. Micro Electro Mech. Syst. ’08*, no. 1, Tucson, AZ, USA, 2008, pp. 920–923.

[173] T. X. Dinh, V. T. Dau, S. Sugiyama, and P. H. Pham, “Fluidic device with pumping and sensing functions for precise flow control,” *Sensors Actuators B Chem.*, vol. 150, pp. 819–824, 2010. [Online]. Available: http://dx.doi.org/10.1016/j.snb.2010.08.009

[174] V. Lien and F. Vollmer, “Microfluidic flow rate detection based on integrated optical fiber cantilever,” *Lab Chip*, vol. 7, pp. 1352–1356, 2007.

[175] O. Fuchs, Y. Fouillet, S. Maubert, M. Cochet, C. Chabrol, N. David, X. Médal, and R. Campagnolo, “A novel volumetric silicon micropump with integrated sensors,” *Microelectron. Eng.*, vol. 97, pp. 375–378, 2012. [Online]. Available: http://dx.doi.org/10.1016/j.mee.2012.04.036

[176] D. Dumont-fillon, H. Tahriou, C. Conan, and E. Chappel, “Insulin Micropump with Embedded Pressure Sensors for Failure Detection and Delivery of Accurate Monitoring,” *micromachines*, vol. 5, pp. 1161–1172, 2014.

[177] Z. Zhang, J. Kan, G. Cheng, H. Wang, and Y. Jiang, “A piezoelectric micropump with an integrated sensor based on space-division multiplexing,” *Sensors Actuators A Phys.*, vol. 203, pp. 29–36, 2013. [Online]. Available: http://dx.doi.org/10.1016/j.sna.2013.08.027

[178] R. Zengerle, W. Geiger, M. Richter, J. Ulrich, S. Kluge, and A. Richter, “Transient measurements on miniaturized diaphragm pumps in microfluid systems,” *Sensors Actuators A Phys.*, vol. 46-47, pp. 557–561, 1995.

[179] Sensirion, “LPG10 Liquid Flow Sensor (Preliminary Datasheet),” [Accessed: 23 December 2016]. [Online]. Available: https://www.sensirion.com/lpg10/

[180] M. Ashauer, H. Glosch, F. Hedrich, N. Hey, H. Sandmaier, and W. Lang, “Thermal flow sensor for liquids and gases based on combinations of two principles,” *Sensors Actuators A Phys.*, vol. 73, pp. 7–13, 1999.

[181] Bronkhorst, “mini CORI-FLOW Datasheet M12-M14,” [Accessed: 20 December 2016]. [Online]. Available: https://www.bronkhorst.com/getmedia/b4567f31-bb12-4480-8d06-dbc353d91c79/mini-cori-flow-us

[182] Sartorius, “Cubis MSA225S Datasheet,” [Accessed: 23 December 2016]. [Online]. Available: https://www.sartorius.com/{_}ui/images/h10/h2c/8836071489566.pdf

[183] M. Richter, “Proportioner / Flow sensor,” Patent WO 98/48328 - DE 19758462, 22 Apr., 1998.

[184] J. T. W. Kuo, L. Yu, and E. Meng, “Micromachined Thermal Flow Sensors - A Review,” *micromachines*, vol. 3, pp. 550–573, 2012.

[185] T. S. J. Lammerink, N. R. Tas, M. Elwenspoek, and J. H. J. Flultman, “Micro-liquid flow sensor,” *Sensors Actuators A Phys.*, vol. 37-38, pp. 45–50, 1993.

[186] M. Dijkstra, M. J. D. Boer, J. W. Berenschot, T. S. J. Lammerink, R. J. Wiegerink, and M. Elwenspoek, "Miniaturized thermal flow sensor with planar-integrated sensor structures on semicircular surface channels," *Sensors Actuators A Phys.*, vol. 143, pp. 1–6, 2008.

[187] M. Richter, A. Prak, J. Naundorf, M. Eberl, H. Leeuwis, P. Woias, and A. Steckenborn, "A Chemical Microanalysis System as a Microfluid System Demonstrator," in *Proc. 9th Int. Conf. Solid-State Sensors Actuators*, Chicago, IL, USA, 1997, pp. 303–306.

Acknowledgment

This thesis was created during my work as research associate at the Fraunhofer Research Institution for Microsystems and Solid State Technologies in Munich.

I would like to thank everyone who helped to realize this thesis, in particular:

Prof. Dr. rer. nat. Christoph Kutter for the constantly motivating and constructive supervision, taking the time for valuable discussions and helping with guiding decisions.

Prof. Dr.-Ing Roland Zengerle for being the second examiner, devoting time to deal with my thesis and motivating by being an expert on the research field.

Prof. Dr. rer. nat. Georg Düsberg for heading the examination committee.

Dr.-Ing. Martin Richter for leading the Micro Dosing Systems department, helpful scientific discussions and providing me with the freedom to conduct my research.

M.Sc. Christian Engst, not only for the constant moral support but also for always being a good partner for discussions about the scientific approach.

All colleagues and students of the Micro Dosing Systems department for the help and great collaboration, especially:
Dr.-Ing. Sebastian Kibler,
Dipl.-Phys. Martin Wackerle,
M.Sc. Ying Gao,
M.Sc. Simone Kager,
M.Sc. Jaume Pallejà Rubio.

Last but not least my private thanks go to my wife, son, brother and parents for making this thesis possible.